

https://dspace.org/

Assessment of face area hangingwall stability in a hard rock bord and pillar mine

Matsobane, Jeane Mokgadi

2021
https://hdl.handle.net/10539/33349

Downloaded from a DSpace repository. https://dspace.org/

School of Mining Engineering



UNIVERSITY OF THE
WITWATERSRAND,
JOHANNESBURG

ASSESSMENT OF FACE AREA HANGINGWALL STABILITY IN A HARD ROCK BORD AND PILLAR MINE

Jeane Mokgadi Matsobane

A research report submitted to the Faculty of Engineering and the Built Environment, University of the Witwatersrand, Johannesburg, in partial fulfilment of the requirements for the degree of Master of Science in Engineering.

Johannesburg, 2020

DECLARATION

I declare that this report is my own, unaided work. I have read the University Policy on Plagiarism and hereby confirm that no plagiarism exists in this report. I also confirm that there is no copying nor is there any copyright infringement. I willingly submit to any investigation in this regard by the School of Mining Engineering and I undertake to abide by the decision of any such investigation.



23 August 2021

Signature of Candidate

Date

ABSTRACT

The aim of this project was to establish guidelines for TARP team members to assist with issuing support recommendations. To this end, ground conditions that may be intersected within the unsupported face area were assessed. The assessment included evaluation of behaviour of the ground conditions at various panel spans and advances per blast, and evaluations of the influence of the last line of support.

The results show that the effectiveness of the last line of support is influenced by keyblock dimensions, in particular the perimeter exposure of these blocks in the hangingwall. A reduction in span and advance per blast were found to be beneficial in reducing the height of the potential falls of ground. This is important where there are shallow dipping discontinuities, as the analysis showed the main failure of the front line of support to be insufficient bolt length in these situations.

In general, the current support system is sufficient for a 10 m span in normal ground conditions (with only steeply inclined joints), and where parting planes are parallel to the strata. However, a reduction in span and face advance is appropriate whenever a pothole is approached or where there are shallow dipping discontinuities.

Shear zones need to be supported, with good areal support, as soon as practically possible after exposure. The smallest practical span is recommended for these structures. The orientation of the shear zone, zone thickness and the presence of other discontinuities intersecting the shear zone, will determine the advance per blast.

ACKNOWLEDGMENTS

I wish to express my gratitude and appreciation to the following people and organisations for their support in this project:

My supervisors Mr Z Thebethe for his assistance with the project proposal and Professor B Watson for his patience, invaluable guidance, insight and support towards completing the project.

Sibanye Stillwater management for providing me with resources to complete the project.

OHMS representatives for their patience and prompt response on JBlock queries and technical support

Bathopele rock engineering team with much needed commitment with keeping the department afloat during the completion of the project.

Bathopele MRM team for their assistance with geology, survey and Microstation^{tm} related queries.

TABLE OF CONTENTS

DECLARATION I

ABSTRACT II

ACKNOWLEDGMENTS IV

LIST OF TABLES X

LIST OF FIGURES XIII

LIST OF ABBREVIATIONS XXI

1 INTRODUCTION 1

1.1 Mine Background 2

1.2 Project Background 11

1.3 Research Motivation 13

1.4 Definition of the Problem 16

1.4.1 Original design at Sibanye Stillwater's bord and pillar operations 16

1.4.2 Current design at Sibanye Stillwater's bord and pillar operations 19

1.5 Research Objectives 24

1.6 Research Methodology 24

1.7 Chapter Summary 25

2 DESIGN CONSIDERATIONS 26

2.1 Clarity of Design Objectives and Existing Constraints 29

2.2 Description and Trends of FOGs in the Face Area at Bathopele . 30

2.2.1 FOG trends in GCDs 30

2.2.2 FOG trends in terms of failure mechanism, bord width, TARP classification and TARP triggers 39

2.2.3 Discussion on the FOG trends 47

2.2.4 The effectiveness of the last row of support 55

2.2.5 Summary of the FOG analysis 59

2.3 Applicable Methods of Analysis 60

2.3.1 JBlock 62

2.3.2 Unwedge 64

2.4 Chapter Summary 70

3 DATA COLLECTION AND PROCESSING 72

3.1 Details of the Excavation to be Assessed 72

3.1 Orientation, Persistence and Shear Strength Properties of the Discontinuities 76

3.1.1 Data on hangingwall layers 76

3.1.2 Joint data collection 78

3.1.3 Joint data processing 81

3.2 Support Units Details 88

3.3 Chapter Summary 89

4 MODELLING SET-UP AND RESULTS 90

4.1 Assessment of Ground Conditions Using the Modified Stability Graph 93

4.2 Assessment of Ground Conditions Using JBlock 110

4.2.1 JBlock set-up and input parameters 110

4.2.2 JBlock results 113

4.3 The Influence of Reduction in Span for Ground Conditions with Low Angled Structures 134

4.4 The Influence of Reduction in Advance per Blast for Ground Conditions with Low Angled Structures 138

4.5 Assessment Using Unwedge 142

4.6 Calculation of Vertical Tensile Zone 146

5 ANALYSIS AND DISCUSSION OF RESULTS 149

6 TARP GUIDELINES 164

6.1 Overall Ground Conditions 164

6.2 Potholes, Slumps and Reef Rolls 168

6.3 Vertically Inclined Shear Zones 174

6.4 Shallow Dipping Structures 178

7 CONCLUSIONS 193

8 REFERENCES LIST 197

A. Bathopele Fall of Ground Database (Bathopele Mine, 2019) 209

B. Bathopele Geology Legend 215

C. Mapping Data 216

C.1 A log of the scanlines 216

C.2 Data of mapped discontinuities 217

D. Support product information 230

D.1 Laboratory Uniaxial Tensile Strength test certificate for 18mm rebar230

D.2 Laboratory test certificate for 18mm rebar washer 231

D.3 Underground pull tests information on the 18mm bolts and results 232

E. Q' system and N' tables (Barton, 2015) 233

E.1 Selection of joint roughness and joint alteration for calculation on N' 233

E.2 Graphs and equations used in calculating A and C factor and α, respectively (Hutchinson & Diederichs, 1996) 234

E.3 Graph used in establishing the B factor (Hutchinson & Diederichs, 1996) 235

F. Frequency plots of dimensions of keyblocks for shallow dipping structures from JBlock models 236

G. Location of FOGs of plan view from FOG reports 244

G.1 FOGs that resulted from shallow dipping structures striking obliquely and near-parallel to mining direction..... 244

G.2 FOGs that resulted from shallow dipping structures near-perpendicular to mining direction..... 246

LIST OF TABLES

Table 2-1. Comparison between the various GCDs 38

Table 2-2. FOG Volume per TARP classification 43

Table 2-3. FOG occurrence in terms of bord span 44

Table 2-4. Comparison of FOG dimensions with respect to bord span 45

Table 2-5. Fall out thickness for a specific bord span range for FOGs that were caused by shallow dipping structures 55

Table 3-1. Position of parting planes as observed from borehole inspections. 78

Table 3-2. Summarised joint properties. 85

Table 3-3. Values used to calculate friction angle. 88

Table 4-1. Position of parting planes as observed from borehole inspections. 91

Table 4-2. Ground conditions considered during the project and their references. 92

Table 4-3. Calculation of joint volume from joint spacing and rock mass classification data 94

Table 4-4. Calculation for factor B 96

Table 4-5. N' Calculation results for slickensided low angled joints. 96

Table 4-6. N' Calculation results for low angled joints with serpentinite infill only. 97

Table 4-7. Calculation results for hydraulic radius for different mining span and length of panels..... 100
Table 4-8. Input parameters and values used in JBlock modelling. 111
Table 4-9 Support failure results from JBlock for normal ground conditions. 119
Table 4-10. Summary of failure mode and failed support for ground conditions with a parting plane..... 123
Table 4-11. Height, volume, face area and distance from the face of the keyblocks that resulted in support failure (large face area for blocks with FOT less than 1.2 m). 124
Table 4-12. Ground conditions considered during the project and their references..... 125
Table 4-13. Summary of failure mode and failed support for ground conditions with low angled structures..... 126
Table 4-14. Unwedge results for potential wedges. 145
Table 4-15. Calculation results of VTZ at different depths below surface and mining span..... 148
Table 5-1. A summary of results, with shallow dipping structures ranked from the least favourable to favourable..... 151
Table 5-2. Thickness and depth for FOGs involving chromitite stringers. ... 155
Table 6-1. TARP Guidelines for ground conditions A, B and J. 165
Table 6-2. TARP Guidelines and recommendations for shallow dipping structures. 166

Table 6-3. TARP Guidelines and recommendations for shallow dipping structures. 167
Table 6-4. Support resistance calculation parameters and values for calculation of FOS calculation for 1.6 m resin bolts. 173
Table 6-5. Support resistance calculation parameters and values for calculation of FOS for 3 m resin bolts. 184
Table D-1. Underground pull test information on encapsulated length and hole diameter (Gieling, 2018) 232
Table D-2. Underground pull test results on the 18mm bolts (Gieling, 2018) 232

LIST OF FIGURES

Figure 1-1. Map showing the location of Bathopele mine in relation to major towns (Fourie, 2020) 4

Figure 1-2. Stratigraphy surrounding the UG2 reef 5

Figure 1-3. Example of the underground workings on plan view, showing the orientations and dimensions of the bords and pillars at 179 m depth below surface 6

Figure 1-4. A summary of approved TARP system at Sibanye Stillwater (after Sibanda, 2019a) 8

Figure 1-5. Plan view of typical layout at Bathopele - not to scale 11

Figure 1-6. Fall of ground accidents at Bathopele - location analysis (Sibanda, 2018) 14

Figure 1-7. Stability of beams - long excavations (Stacey & Swart, 2001) 18

Figure 1-8. Hydraulic radius concept (Hutchinson & Diederichs, 1996) 20

Figure 2-1. Engineering design wheel by Stacey (2005, as cited in Stacey, 2009) 27

Figure 2-2. Plan view of the GCDs at Bathopele 32

Figure 2-3. Major geological anomalies at Bathopele 33

Figure 2-4. Percentage of FOGs per mining district within the face area 34

Figure 2-5. Plan view of Bathopele mine showing the mined-out and unmined portion of the two main districts 35

Figure 2-6. The rate of FOGs per 100 000 m² per GCD 36
Figure 2-7. Fallout thickness frequency for the different GCDs 38
Figure 2-8. FOG boundaries for the FOGs that occurred in the face area 41
Figure 2-9. FOG percentage per TARP classification 42
Figure 2-10. A plan view of a mined-out area showing a –various shallow dipping structures that remained stable upon intersection prior to support installation. 46
Figure 2-11. Plan view and section view of a FOG that occurred from a serpentinised fault zone (van Rensburg, 2007)..... 47
Figure 2-12. FOG from the Hex River fault zone (Sibanda, 2012) 47
Figure 2-13. Various structural patterns (Stillborg, 1994:47)..... 49
Figure 2-14. A photo of a FOG that resulted from unravelling of Iron-Rich Replacement Pegmatoids (Gloster, 2016) 50
Figure 2-15. Photo of FOG that resulted from multiple shallow dipping structures and vertical joints (Dube, 2015)..... 51
Figure 2-16. Photo of FOG that resulted from chromitite parting, vertical joints and water (Matsobane, 2016b). 51
Figure 2-17. Zone of influence associated with stope face in a shallow mining environment (Daehnke, Roberts & Squelch, 2002)..... 52
Figure 2-18. Unsupported model (Watson & Gerber, 2018) 54
Figure 2-19. Long section of a FOG that was bounded by a single shallow dipping fault and a vertical pegmatite vein, showing zero influence of the last line of support (van Rooyen, 2011). 56

Figure 2-20. A schematic illustration of the load distribution into the rock as a result of rockbolt pre-tensioning (Stillborg, 1994: 43) 58
Figure 2-21. JBlock flow chart (Kotze, 2012) 63
Figure 2-22. Various wedge shapes depicted on plan view 66
Figure 2-23. Bathopele geology legend 67
Figure 2-24. Wedges that failed under the action of gravity 68
Figure 2-25. Examples of stereonet plots for an unstable and stable wedge (Hudson & Harrison, 1997) 69
Figure 3-1. Plan view of the western side of Central shaft showing sections where mapping was done. 73
Figure 3-2. Plan view of Bathopele Mine showing the area where the investigation was done and major geological structures. 74
Figure 3-3. Various face area possibilities with respect to mining direction. . 75
Figure 3-4. Position of triplets as observed from borehole inspections. 78
Figure 3-5. A plan view of Central shaft sections showing geology mapped by the geology department. 80
Figure 3-6. Stereographic pole contour plot of mapped discontinuities. 84
Figure 3-7. Mapped joints on plan as established from scanline mapping. ... 86
Figure 3-8. Correction for joint spacing error (Nezomba, 2012). 87
Figure 3-9. Central shaft panel classification distribution for 2018-2019 Oct (Sephaphathi, 2019). 89
Figure 4-1. Hydraulic radius parameters. 98
Figure 4-2. Hydraulic radius versus the long span of the panel. 101

Figure 4-3. A plot of the calculated N' and hydraulic radius (After Hutchinson & Diederichs, 1996). 102
Figure 4-4. Assessment of "F" ground conditions using stability graph method showing the major influence of joint wall conditions and size of excavation (After Hutchinson & Diederichs, 1996). 104
Figure 4-5. A demonstration of the influence of dip direction of low angled structures on the calculation of α. 107
Figure 4-6. Illustration of the limitation of the Modified Stability Graph in terms of position of pervasive structures in a mining excavation. 109
Figure 4-7. Excavation file in JBlock. 112
Figure 4-8. Support parameters and values used in JBlock. 112
Figure 4-9. Clamping stress correlation. 113
Figure 4-10. Demonstration of the meaning of face distance results from JBlock. 114
Figure 4-11. JBlock results for normal ground conditions with FOT at 1.3 m. 116
Figure 4-12. Frequency of keyblocks plotted against distance from the face for normal ground conditions. 117
Figure 4-13. Height and maximum edge of keyblocks plotted against distance from the face. 118
Figure 4-14. Frequency plot of keyblocks versus distance from the face for ground conditions with a parting plane. 121
Figure 4-15. Support failure plot for ground conditions with parting plane. . 121

Figure 4-16. Distribution plots of the dimensions of the keyblocks with ground conditions with a parting plane. 122
Figure 4-17. Frequency plot of the height of the keyblocks of low angled structures (excluding JS4). 127
Figure 4-18. Keyblocks that resulted in support failure for ground conditions with low angled structures. 128
Figure 4-19. A plot of all the keyblocks with ground conditions with low angled structures. 129
Figure 4-20. Dimensions of the keyblocks with joint set 4 (R1) included in the model. 130
Figure 4-21. Frequency plots of dimensions of ground conditions with low angled ramp structures (excluding R1). 131
Figure 4-22. Plot of face distance versus height of keyblocks for JS4. 133
Figure 4-23. Plot of face distance versus height of keyblocks for ramp structure with 294° dip direction. 133
Figure 4-24. Number of bolts too short per 2000 m² mined at different bord span. 136
Figure 4-25. Face distance versus height of keyblocks for JS4 at 8m span. 137
Figure 4-26. Face distance versus height of keyblocks for JS4 at 6m span 137
Figure 4-27. Percentage of bolts too short for 2m and 3m advance at 10m span. 139

Figure 4-28. Percentage of bolts too short for 2m and 3m advance at 8m span. 139
Figure 4-29. Number of bolts too short per 2000 m² mined at different bord span. 140
Figure 4-30. JBlock results for JS4 with reduced advance per blast. 141
Figure 4-31. A stereonet plot of the major near-vertical joints sets and low angled structures. 144
Figure 5-1. Central shaft 10w panel 4 FOG within the face area (Macebele, 2019). 154
Figure 5-2. East shaft 8E P4 FOG plan (Bathopele Survey dept., 2013). ... 158
Figure 5-3. K6 large FOG plan and photo (K6, 2018). 161
Figure 5-4. Pegmatite vein with serpentinite infill/coating on the sides. 163
Figure 6-1. Position of chromitite layers with respect to the main seam for a typical reef roll or slumps. 172
Figure 6-2. Factor of safety versus tributary area for 1.6m resin bolts. 173
Figure 6-3. Plan view of location of an FOG due to shear zone and a photo of where the shear zone unravelled (Matsobane, 2017). 175
Figure 6-4. Selection of shotcrete thickness (Stacey, 2001). 177
Figure 6-5. FOG that occurred from a vertically inclined shear zone at Central shaft strike 5W bord 5 (Matsobane, 2016d). 177
Figure 6-6. A shear zone that was successfully mined through at Central shaft strike 11W bord 5. 178
Figure 6-7. JBlock results for normal ground conditions with FOT at 1.3m. 180

Figure 6-8. Frequency plots of dimensions of ground conditions with low angled ramp structures (excluding R1). 181
Figure 6-9. Recommended guidelines for addressing shallow dipping structures. 183
Figure 6-10. Factor of safety versus tributary area for 3m bolts for 2.6m fallout thickness. 184
Figure 6-11. Nomogram for determining effective length of bolts and determining the point at which the bolts become ineffective (After Carstens, 2013). 185
Figure 6-12. Strategic application of reducing panel span for dealing with shallow dipping structures. 187
Figure 6-13. An example of an excel tool that can be used to determine support requirements for rectangular wedges. 189
Figure 6-14. An example of an excel tool that can be used to determine support requirements for tapered wedges. 190
Figure F-1. Frequency plots of dimensions of keyblocks for shallow dipping structure with 0° dip direction at 6 m to 9 m span from JBlock models 237
Figure F-3. Frequency plots of dimensions of keyblocks for shallow dipping structure with 24° dip direction at 6 m to 9 m span from JBlock models 238
Figure F-4. Frequency plots of dimensions of keyblocks for shallow dipping structure with 114° dip direction at 6 m to 9 m span from JBlock models ... 239
Figure F-5. Frequency plots of dimensions of keyblocks for shallow dipping structure with 180° dip direction at 6 m to 9 m span from JBlock models ... 240

Figure F-6. Frequency plots of dimensions of keyblocks for shallow dipping structure with 204° dip direction at 6 m to 9 m span from JBlock models ... 241
Figure F-7. Frequency plots of dimensions of keyblocks for shallow dipping structure with 294° dip direction at 6 m to 9 m span from JBlock models ... 242
Figure F-8. Frequency plots of dimensions of keyblocks for shallow dipping structure with 199° (JS4/R1) dip direction at 6 m to 9 m span from JBlock models 243

LIST OF ABBREVIATIONS

BIC: Bushveld igneous complex

COP: Code of practice

EEE: Early entry examination

ERF: Effective Radius Factor

FLAC3D: Fast Lagrangian Analysis of Continua in 3 Dimensions

FOG or FOGs: Fall of ground or falls of ground

FOS: Factor of safety

GCD: Ground Control District

GPR: Ground Penetrating Radar

HR: Hydraulic radius

HSE: Health, safety and environment

HW: Hangingwall

IRUP: Iron-Rich Ultramafic Replacements Pegmatoids

LHD: Load-haul-dump vehicle

OHMS: Open House Management Solutions

RMC: Rock mass classification

RMR: Rock mass rating

SIMRAC: Safety in Mines Research Advisory Committee

TARP: Trigger Action Response Programme

UCS: Uniaxial Compressive strength

UDEC: Universal Distinct Element Code

UG2: Upper group number two seam

VTZ: Vertical tensile zone

1 INTRODUCTION

The two traditional strategies that have been adopted in the mining industry to manage hangingwall hazards are preventative and control strategies. Preventative strategies focus on development of new and more effective support systems by studying dynamics of rock behaviour surrounding mine excavations. Control strategies are focused on allowing the failure to occur in a controlled manner while simultaneously attempting to improve the competency of mine personnel through training (Peake & Ashworth, 1996). The aim of this research in a broader sense was to establish a preventative strategy for addressing falls of ground (FOGs) in the face area.

Godden (2010) argues that control strategies such as the Trigger Action Response Program (TARP) and related risk management tools are subjective, relying too heavily on human interventions and the will to make changes. Non-compliance to TARP system across mining operations confirms Godden's statement. The changes must be made as and when they are required despite the inevitability of production pressures. Support systems should be used to reduce risk to minimum achievable levels (Godden, 2010).

There have been several FOGs in the face area following inspections and issuance of support recommendations by TARP response teams. Currently it is the responsibility of the TARP response team member to assess ground conditions, conclude on the stability of the excavation being assessed and

issue support recommendations. There are presently no documented guidelines for addressing TARP triggers to TARP response teams.

Literature indicates that excavation geometry is key to stability of mine excavations (Budavari, 1983, Milne, 1997, Jager & Ryder, 1999, Watson, 2004, Hoek, 2006, Murphy et al, 2016). The effective strength of the rock mass on the periphery of an excavation is dependent on the size of the excavation because the size influences the volume of exposed rock and associated discontinuities (Jager & Ryder, 1999). Bord width is the only dimension that has been designed using rock engineering principles and design methods thus far at Bathopele. As a first step in establishing guidelines to addressing TARP triggers, hangingwall behaviour must be understood within the face area taking into account the entire unsupported surface area of the hangingwall. It was therefore the purpose of this study to assess the hangingwall stability within the face area for various ground conditions at different excavation geometries at Bathopele mine.

1.1 Mine Background

Bathopele mine is a shallow, fully mechanized and trackless bord and pillar operation in the Bushveld Igneous Complex (BIC). The location of the mine in relation to major towns is shown in Figure 1-1. Two sets of decline shafts are used to access the orebody, namely Central and East shaft. The Mine is

currently operating between 76 m and 470 m below surface. The shallowest areas mined on reef are approximately 36 m below surface. Depth of mining will reach 510 m below surface. Bathopele is one of Sibanye Stillwater's six bord and pillar operations in Rustenburg. The Upper Group 2 (UG2) chromitite reef is exploited at Bathopele either through dual seam or single seam mining cuts. A dual seam cut includes the UG2 (i.e. main seam) and the leader seam, which is mined together in a single cut. The single seam cut consists only of the UG2. A stratigraphic column showing the hangingwall and footwall rocks of the seam at Bathopele is provided in Figure 1-2.

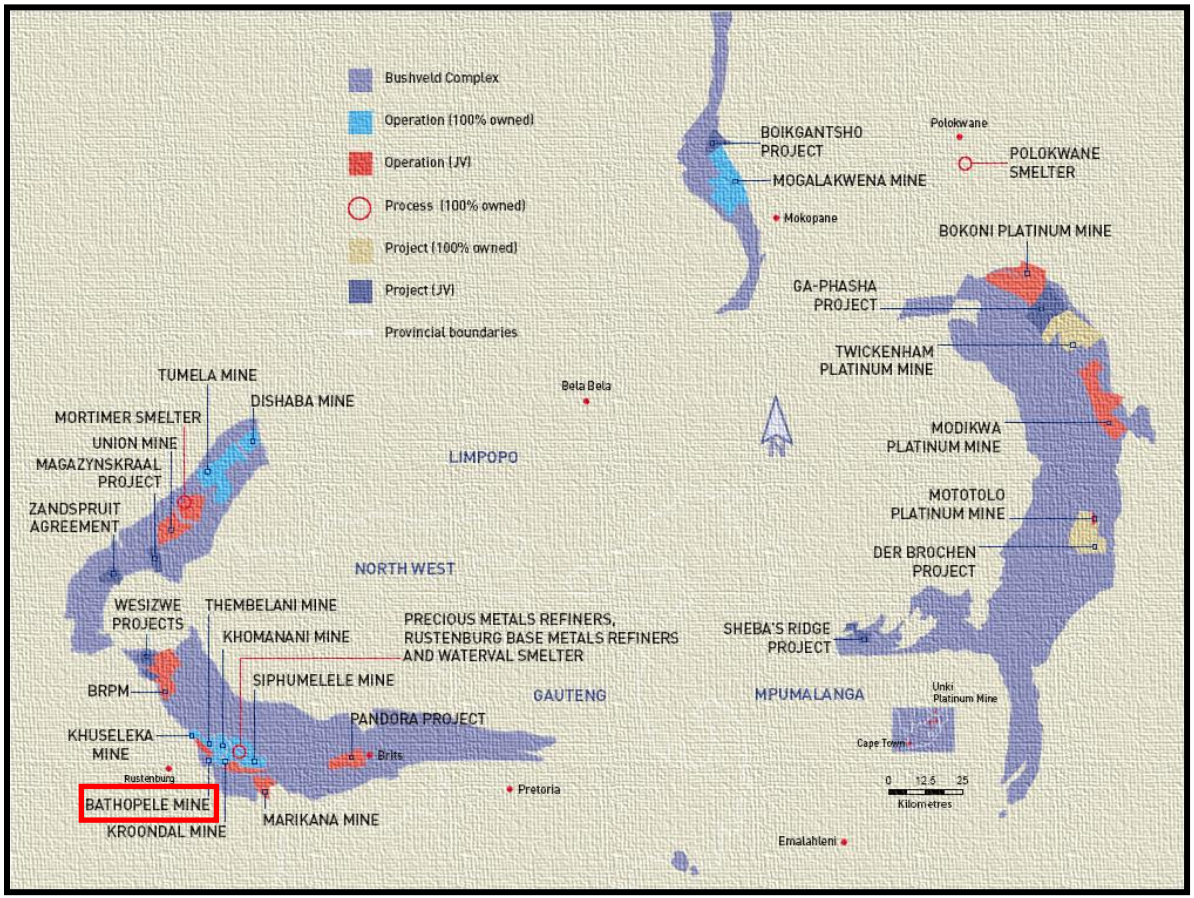

Figure 1-1. Map showing the location of Bathopele mine in relation to major towns (Fourie, 2020)

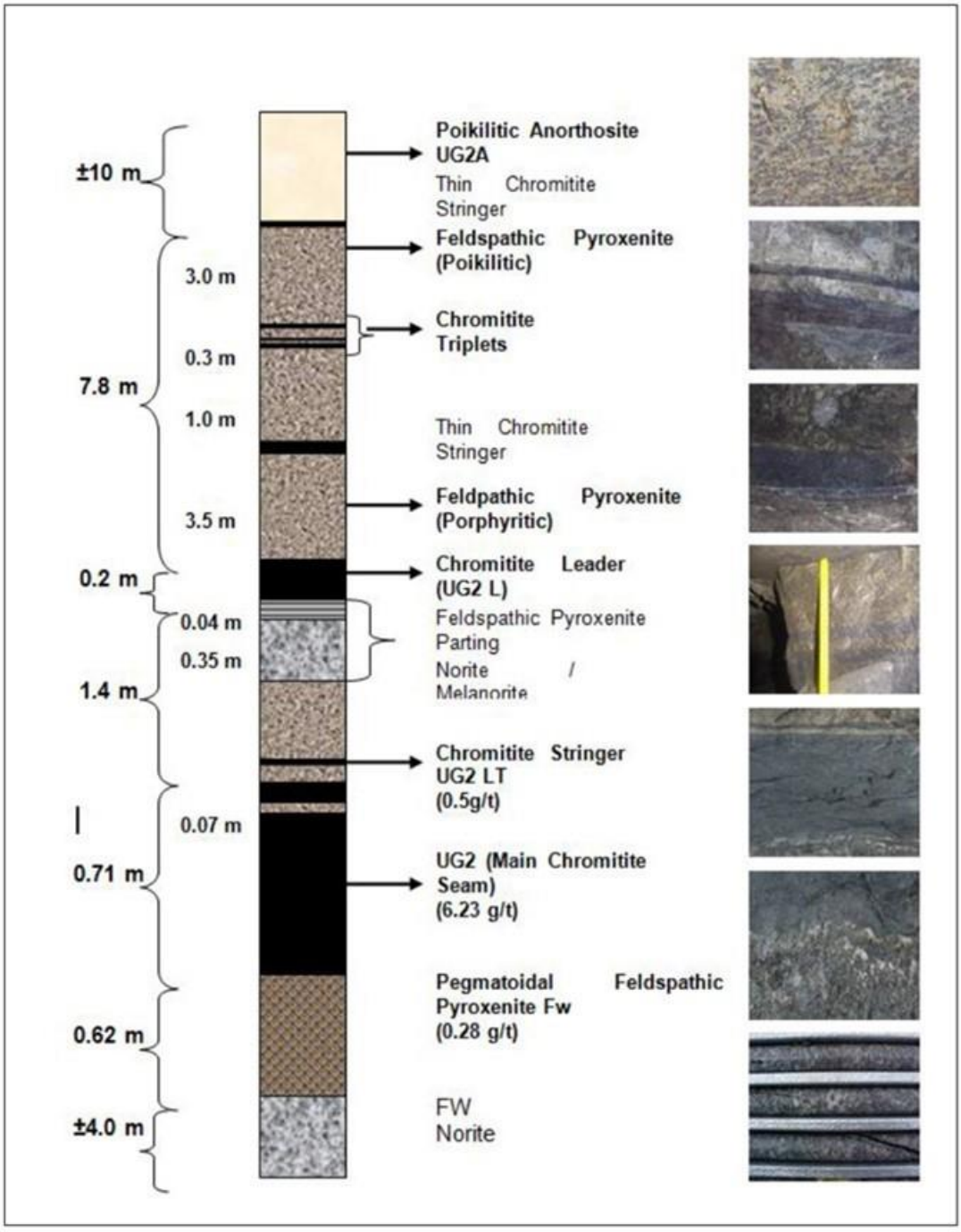

Figure 1-2. Stratigraphy surrounding the UG2 reef

The layout consists of 10 m bords with pillars that vary in size according to depth. The 10 m is both on strike and dip and it is the maximum allowable span for bords (Figure 1-3). The Mine's support design is based on the Voussoir beam theory where the objective of the primary support is to reinforce a 1.3 m high beam.

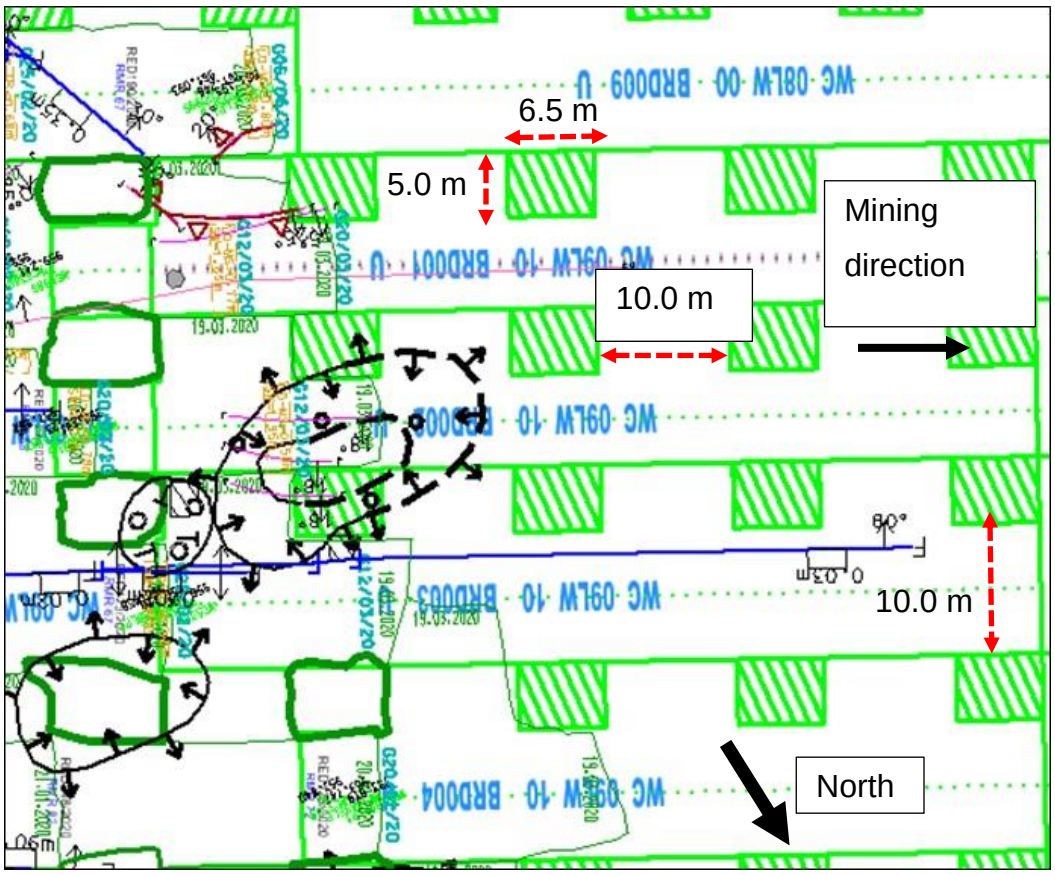

Figure 1-3. Example of the underground workings on plan view, showing the orientations and dimensions of the bords and pillars at 179 m depth below surface

The primary support is often compromised by ground conditions that deviate from normal. Anomalous ground conditions are addressed according to the

Company's TARP procedure. TARP is a hazard identification and treatment system and it is an integral part of Early Entry Examination (EEE) for prevention of FOGs.

A summary of the TARP system at Sibanye is provided in Figure 1-4. The figure shows the TARP procedure, the TARP triggers and the participants. TARP classification refers to a rating of a bord depending on the trigger present. A bord is rated according to the highest trigger if more than one trigger is present. TARP 3 classification is higher than TARP 1 classification. TARP 3 triggers require higher level of expertise in terms of support recommendations.

A TARP 2 classification can either be T2 or TP2. T2 means that a workplace has been stopped due to exposure of a TARP 2 trigger by blasting and the mining crew is awaiting support recommendations from a TARP 2 response team. The classification is changed to TP2 only after support recommendations have been issued. The same applies to TARP 3 classification.

T1 conditions refer to normal ground conditions. Mine standards and procedures apply for T1 classification. The triggers for the different classifications are provided on the far right in Figure 1-4.

TRIGGER ACTION RESPONSE PLAN - TARP

Steps	Action
1	Identify hazard or trigger
2	Rate each trigger and rate workplace according to the highest trigger if more than one trigger is present
3	Notify the relevant response team depending on the TARP rating of the workplace.
4	The response team must outline the remedial action to be taken and the duration / location / extent of such remedial action. The workplace must be classified as "TP2 or TP3" whilst the remedial action is taking place.
5	Reclassify workplace accordingly when the remedial action has been implemented or ground conditions change.

TARP level	Authority
1	Holder of at least a Competent A Certificate of Competence.
2	Shift Supervisor or Legally Appointed Mine Overseer
3	Strata Control Officer or Legally appointed Mine Manager /Unit Manager Mining or Rock Engineer or Vice President

TARP Class	Action	Trigger
T1	Normal mining as Standards and Procedures demand	• Brow <1m • Prominent joint, veins dipping ≥ 60°
T2	Request "TARP 2" Team intervention after Barricading.	• Brow >1m and <2.5m • Prominent geological features (dykes, faults, shears) dipping ≥ 60 • Abnormal change in reef contact e.g. a steep roll or reef displaced by other geological features. This includes reef left in the hanging wall (RIH) • Blocky ground, wedges and key blocks in the hanging wall
T3	Request "TARP 3" Team intervention after Barricading.	• Brow > 2.5m • Water from the hanging wall • Prominent flat dipping feature < 60° to horizontal. • Dome or Slump feature present or suspected • FOG (Irrespective of size) • Tensile cracks visible in h/wall • Abnormal support failure • Abnormal pillar scaling/failure • Dust sifting from hanging wall. • An increase in audible rock fracturing. Also referred to as the rock "talking". • At least two TARP 2 triggers that have the potential to interact and/or intersect
TP2/ TP3	The team continue as normal but with instructions until bord is classified back to T1/T2.	• The visiting "T2" or "T3" team that issued instructions shall stipulate under which conditions the working place shall return to "T1" or "T2" status.

Figure 1-4. A summary of approved TARP system at Sibanye Stillwater (after Sibanda, 2019a)

It has been concluded from observations during underground inspections, accident investigations and short-term planning sessions that the success of TARP lies in:

i. The ability of the mining team to identify FOG hazards during EEE,
ii. The notification of the relevant response team and the timeous response thereof, and,
iii. Compliance by the mining team to the support recommendations issued by the response team.

In addition, the response team must be able to fully assess the hazard in order to issue appropriate support recommendations, and the mining team must be able to carry out the support recommendations in a safe manner. The aforementioned activities are primarily carried in the newly exposed face area after blast.

Figure 1-5 shows a digital plan view of the layout and mined out area at Bathopele. For the purpose of this study, the definitions of the different locations within a bord are divided as follows and also shown in Figure 1-5. **The primary focus of this research is the face area:**

i. **Face area:** the area between the face and the last row of support.

ii. **Intermediate area**: the area between the last row of support up to approximately 50 m from the face. The area is inclusive of the second to third last split from the face depending on the pillar sizes in the section. The area forms part of the travelling way and most services are within this area e.g. boomer boxes. Entry examination procedure requires inspection to be done within this area. Services departments are required to inspect bords up to at least 2 splits behind the face. Therefore, the area receives much attention and has significant traffic in terms of people and machinery.

iii. **Back area**: This is the area beyond 50 m. *Current sweepings* are done in this area. These types of sweepings are done between the 2-year historic line and the current tip position line in active sections and sections that have reached the boundary (Potgieter, 2017, A. Beyl 2020, pers. Comm., 9 May). Active sections refer to sections in which blasting takes place.

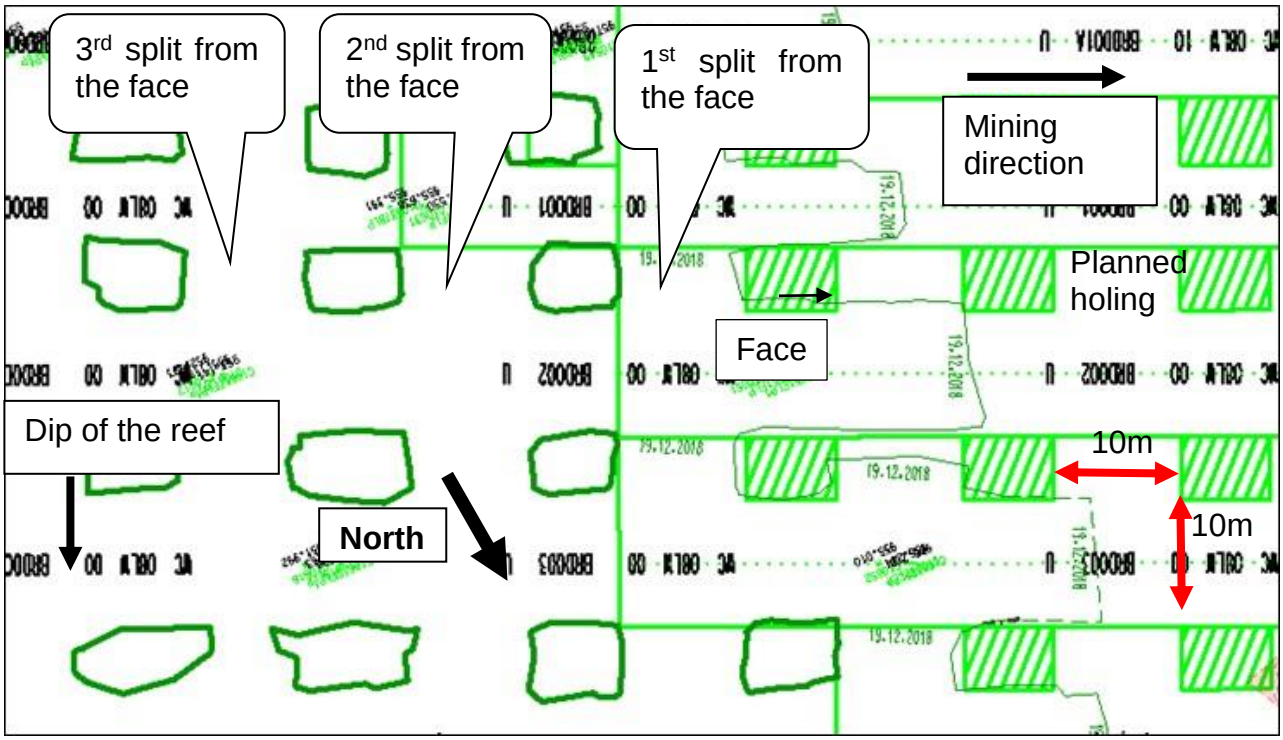

Figure 1-5. Plan view of typical layout at Bathopele - not to scale

1.2 Project Background

Ground Control Districts (GCDs) at Bathopele mine have been established and are specified in the Code of Practice (COP) to Combat Rockfall and Rockburst Hazards. The mine layout is designed according to the COP requirements for each GCD. The minimum support required for each GCD has also been specified in the Ground Control District and Associated Bord and Pillar Support Standard i.e. the support standard.

The maximum distance between the last line of support and the face after the blast is specified as 4.5 m in the support standard (Sibanda, 2019b). However, the distance applies to all ground conditions i.e. the maximum allowable unsupported span in the mining direction for various GCDs at Bathopele is not specified. Furthermore, the 4.5 m is based on the maximum advance per blast achievable production wise and is not based on rock engineering design. It is common practice to reduce advance per blast by 35 % in unfavourable ground conditions but the practice is based on mine personnel experience with the ground conditions. The degree to which the ground conditions are unfavourable is thus subjective.

Support strategies specific to the various GCDs are for known ground conditions within known locations of the mine. Such known ground conditions include those of major fault zones. Although the strategies exist, TARP system is beneficial in ensuring that the strategies are implemented. Ground conditions tend to vary within major geological structures and TARP thus ensures that each workplace is treated on its own merit. It would also be uneconomical to implement generic support strategies for all geological features that may present a FOG risk such as reef rolls and domes in random areas. TARP is therefore also beneficial in addressing such non-pervasive FOG hazards.

A limitation of the current GCD standard and TARP system is therefore an unusual intersection of the FOG hazards (i.e. TARP triggers) within one blast

in the 4.5 m unsupported area. A decision needs to be made on whether to support or abandon the excavation, and rock engineering guidelines are required in making the decision. Currently at Bathopele mine it is the responsibility of the TARP response team member to assess ground conditions, conclude on the stability of the excavation being assessed and issue support recommendations accordingly. That is, there are currently no documented guidelines for addressing TARP triggers to TARP response teams. This study was aimed at addressing this shortcoming.

1.3 Research Motivation

TARP is applied primarily in the face area of mine excavations. The majority of FOGs at Bathopele and Kroondal operations occur in the face area as indicated in Figure 1-6, with 80 % of the FOGs having occurred in the face area at Bathopele since inception (Sibanda, 2018). Additionally, there have been several FOGs in the face area following inspections and provision of support recommendations by TARP response teams (Gloster, 2016, Matsobane, 2016a, Mukwevho, 2018). Multiple FOGs have been investigated that occurred in the face area which occurred whilst there was no mining activity in the panels. Other FOGs have occurred whilst the panels are stopped for inspection by a member of the rock engineering department or relevant response TARP member (Van Rooyen, 2002, Louw, 2007, Matsobane, 2017, Matsobane 2016b).

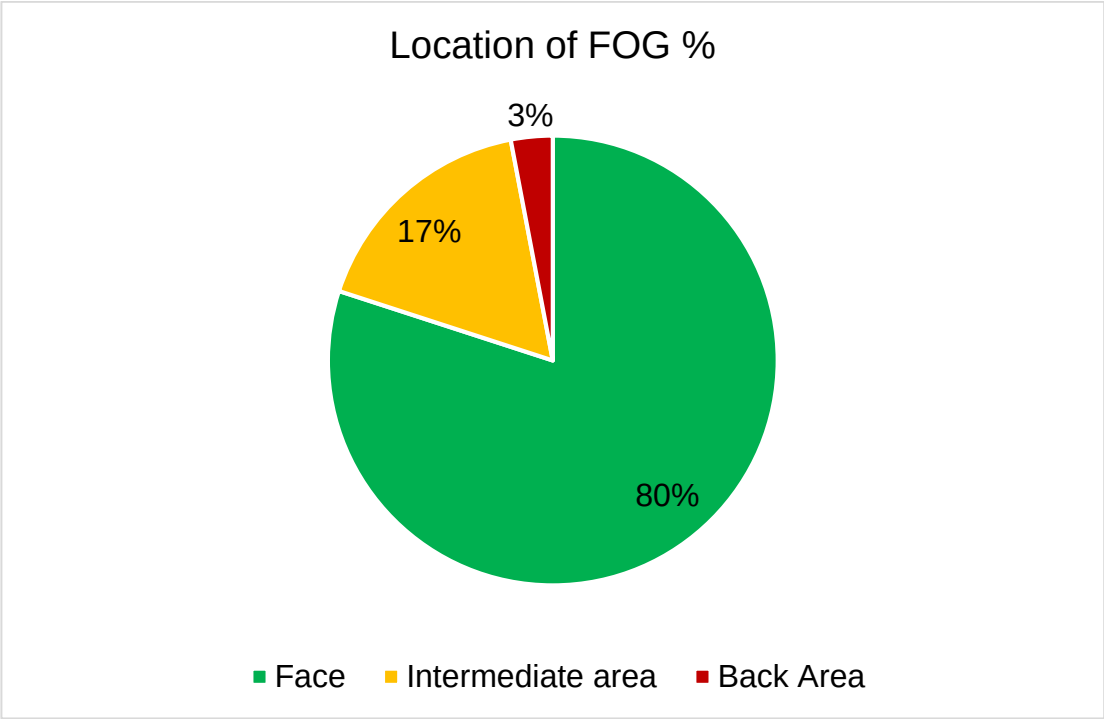

Figure 1-6. Fall of ground accidents at Bathopele - location analysis (Sibanda, 2018)

Examples of FOGs that occurred within the face area following an inspection by a member of the rock engineering department are discussed below to illustrate the challenge with TARP:

i. Hangingwall unravelled from a shallow dipping fault, vertical joints and a shear zone at Bathopele at strike 3w bord 3 Central shaft in 2016. The FOG occurred in the unsupported face area and failed some of the bolts installed in the last line of support. A support recommendation to install longer bolts and apply 50 mm shotcrete was issued on the 25th of

February 2016 and the FOG occurred on the 16th of March 2016. The recommendation also required the bord span to be reduced to 6 m and the advance per blast to be reduced from 3 m to 2 m. Support recommendations were yet to be carried out when the FOG occurred. It was concluded at the time that the water within the rockmass caused rapid deterioration that resulted in the FOG. Bord width was 7.6 m (Matsobane, 2016a).

ii. A gravity induced FOG occurred at Kroondal K6 shaft in 2018. The FOG boundaries were a shallow dipping fault, 2 pegmatite veins and a chromitite stringer. The bord width was 10.5 m. Secondary support in the form of long anchors was planned for the bord, but had not yet been installed when the FOG occurred (Mukwevho, 2018).

In both FOG instances, it had not been determined whether it was safe to enter the bords to install the supports. The current shortcoming with the TARP system is that TARP response team members currently rely on observations and site experience in deciding whether or not it is safe to enter the excavation for the purpose of support installation. Documented guidelines that stem from the understanding of the factors that drive instability would assist TARP members in addressing TARP triggers.

The FOGs highlighted above could have occurred during cleaning operations, support installation or entry examination processes, resulting in loss of life. The FOGs could also have resulted in loss of machinery and equipment. A reduction of bord width from 10 m to 6 m locks a significant amount of ground and may not have been necessary if the rock behaviour had been better understood. Load-haul-dump vehicles (LHDs) operate under unsupported areas during cleaning operations. The observed risk may be better reduced if the support was installed closer to the face. It is imperative to understand the behaviour of the rock mass within the face area of a bord.

1.4 Definition of the Problem

1.4.1 Original design at Sibanye Stillwater's bord and pillar operations

The original design for bord widths at Bathopele by Johnson and Noble (2002) was based on two methods, namely:

i. Safety in Mines Research Advisory Committee (SIMRAC) span design chart after York (1998) for angles of joints and friction angle (as cited in Johnson & Noble, 2002), and;

ii. the Voussoir beam graph for maximum stable span at various beam thicknesses and rockmass moduli.

The recommended mining span was 12 m for normal ground conditions. Allowable maximum distance between the last line of support and the face was not specified in the report. The limitation of the Voussoir beam graph (Figure 1-7) is that it only considers the strength of the rock and the dip of the strata in establishing the maximum unstable span for a given beam thickness. Shallow dipping features are therefore not taken into account when using the method. Murphy, et al. (2016) also highlighted similar limitations of the Voussoir arch methodology. The importance of timeous identification of areas with poor ground conditions and low angle joints was emphasized by Johnson and Noble (2002). The reduction in mining span to 6 m was recommended for those areas, without any geotechnical justification. It was stated in the report that 3D modelling was done using Elfen to confirm a bord width of 12 m in normal ground conditions, however the modelling results could not be found.

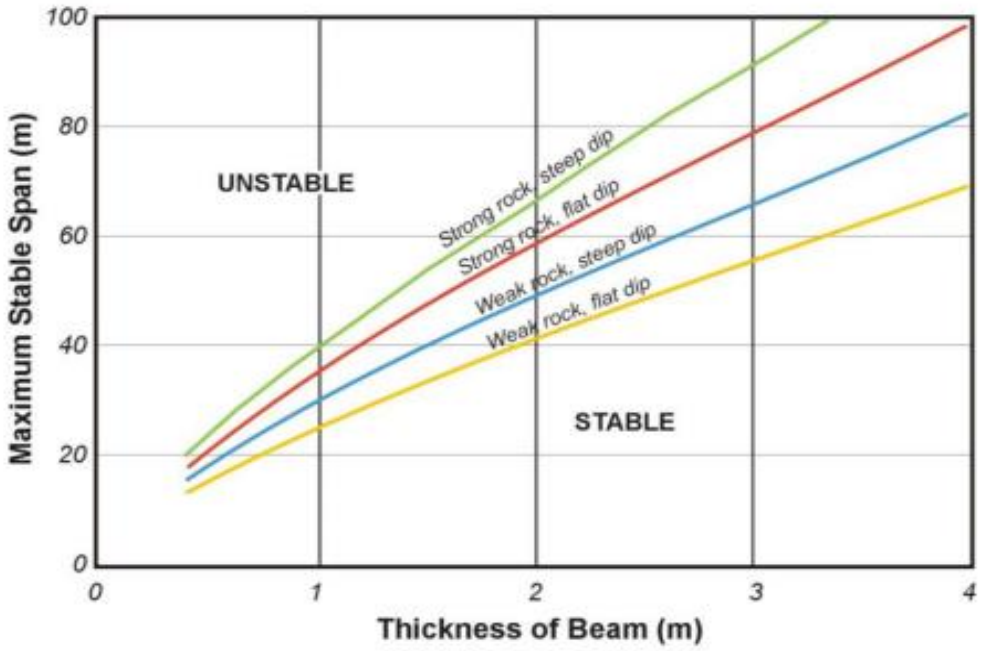

Figure 1-7. Stability of beams - long excavations (Stacey & Swart, 2001)

The original support design for Kroondal bord and pillar operations in 2010 (Aquarius Platinum (SA) (Pty) Ltd, 2016) was based on modelling results obtained from Itasca's Universal Distinct Element Code (UDEC) software. The design documents were compiled by Godden (2010). These documents also did not differentiate maximum unstable hangingwall surface areas for various ground conditions. Thus, the designs did not address the effectiveness of the last line of support for either the Bathopele or Kroondal operations.

1.4.2 Current design at Sibanye Stillwater's bord and pillar operations

Currently the design for Kroondal operations and Bathopele is based on two assessment methods:

i. The bord widths are designed based on the Modified stability graph method by Potvin (1988) as discussed by Hutchinson and Diederichs (1996). The design is based on a database that was collected over many years.

ii. UDEC was used to determine the thickness of a self-supporting beam at a given span in both the absence and presence of shallow dipping structures. Chromitite partings were included in the model. The positions of the chromitite partings were those observed under normal ground conditions (Matsobane, 2019).

The Modified Stability Graph is one of the several empirical design methods that take into account unsupported span based on Rock Mass Classification (RMC). Other methods are Rock Mass Rating (RMR) and Q charts (Hutchinson & Diederichs, 1996). According to Hutchinson and Diederichs (1996), the RMR and Q charts were developed for tunnels in which the long span is assumed to be infinite and hence they consider only the critical span, which is the short span. The stability graph method takes into account the hydraulic radius (HR) and ground conditions to determine stable unsupported span. The rock mass

conditions are quantified using the modified stability number (N'). The stability number is determined from the modified rock quality index (Q'), which is calculated from Barton's Q-rating equation by discounting the last quotient, i.e. the non-geological components. The hydraulic radius is calculated by dividing the area of interest by its perimeter (Hutchinson & Diederichs, 1996). A graphical representation of hydraulic radius is provided in Figure 1-8.

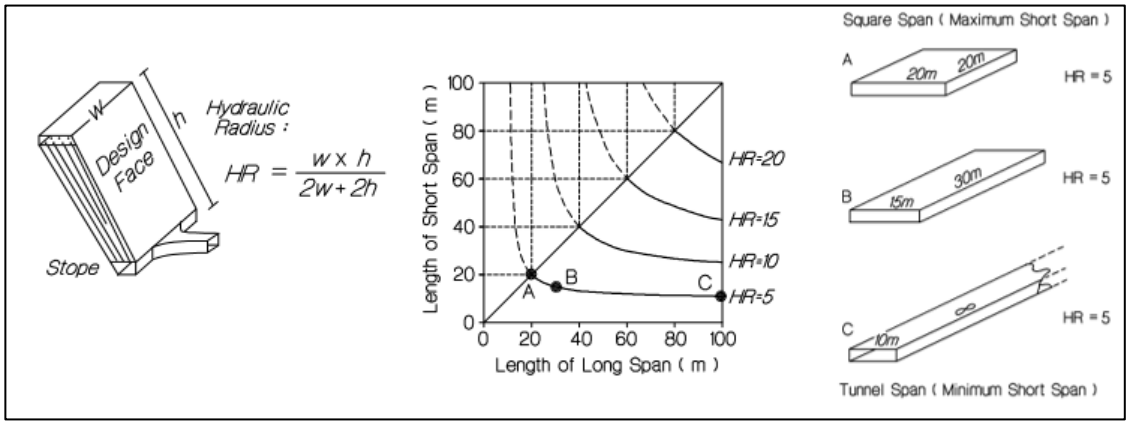

Figure 1-8. Hydraulic radius concept (Hutchinson & Diederichs, 1996)

An infinitely long tunnel was assumed for Bathopele and Kroondal bord and pillar operations (Sibanda, 2018). Murphy & et al (2016) also assumed an infinitely long bord in their assessments of stable unsupported span when using the stability graph method. An infinitely long tunnel will have a hydraulic radius

of approximately half the width of the bord (Hutchinson & Diederichs, 1996). Stability increases if the short span is kept constant and the long span is reduced due to increased confinement and rigidity provided by extra two abutments (Hutchinson & Diederichs, 1996). The analysis does not account for bord intersections.

Intersections can however be accounted for in the design by quantifying the surface geometry using Effective Radius Factor (ERF) method. ERF method was developed for complex geometry whereby deformation can be determined at any point along the excavation. The influence of abutments, pillars and brows is taken into account in the calculation of ERF developed by Milne (1996) (as cited in Andrews & Barsanti, 2008). A program written by P Lunder can be used to calculate ERF values (Milne, 1997). ERF contours can be mapped from the computed values and areas of concern can be viewed with variation in mining steps and excavation geometry. The calculated ERF value can be plotted on the Stability graph instead of HR to determine areas that fall within the stable, unstable or transition zone (Machuca, et al., 2015).

Although hydraulic radius accounts for the combined influence of size and shape of excavation stability, it is still compared against a value determined through RMC as mentioned above. RMC systems are only applicable to the conditions in which they were developed, and should not be used outside of this database. Case in point, Murphy et al (2016) states that Barton's Q system

is suited to analysing stability of hangingwall with jointed rock mass and shallow dipping structures such as low angled joints and ramp faults. The hangingwall should contain one or more prominent joint sets of uniform dip and dip direction (Murphy, et al., 2016). In other words, the RMC does not cover some of the ground conditions at the Mine. According to Esterhuizen (2014), the bord widths at Two Rivers Platinum Mine range between 6 m and 12 m depending on the rock mass rating. There was a spate of FOGs at the Mine and they were reduced through strategies non-related to RMC (Esterhuizen, 2014).

Even though RMC has its limitations, the influence of shallow dipping structures on stability can be assessed using the stability graph method as illustrated by Murphy et al (2016). However, it has only been used for the design of the overall layout for various GCDs, and UDEC modelling was done to assess the influence of shallow dipping structures.

The UDEC program that was used for the design is a two-dimensional (2-D) modelling program. The effect of face advance could not be properly investigated. Le Bron and Piper (2015) investigated 9 m and 6 m spans using Flac3D (Itasca, 2017). The aim of the exercise was to determine hangingwall behaviour strictly in the presence of shallow dipping structures. The results indicated that opening will occur along 45° joints, independent of the span, if the joints daylighted in the hanging wall. Additionally, separation occurred immediately along the joint after a 2 m advance from the joint intersection.

Therefore, 1 m advance per blast was recommended for such conditions, with immediate installation of long anchors. The model was worst-case, based on the entire hangingwall being cut by 45° dipping joints. In addition, the model was not calibrated by rock laboratory testing or geotechnical mapping (Le Bron & Piper, 2015). The model results do not agree with field observations and a 1 m advance is yet to be recommended by a TARP team at Bathopele.

Open House Management Solutions (OHMS) performed a sensitivity analysis of key block formation to variations in shallow dipping joint set properties and effectiveness of primary support for Bathopele. The probabilistic design tool JBlock was used for the exercise. Only 9 m bords, mining in one direction, were investigated (Gouvea, 2013). The maximum stable unsupported surface area of a bord was also not considered, although it is possible for JBlock to analyse such situations. JBlock only considers keyblock types of failure, but the advantage of this analysis is that different mining layouts can be compared. The excavation modelled in JBlock represents the area mined or hangingwall exposed and the influence of the installed support (Joughin, et al., 2012). OHMS recommended that more geotechnical data should be collected for future JBlock analysis.

In summary, the design at Bathopele thus far considered only the bord width. The bord widths are designed for regional ground conditions for each GCD. Anomalous ground conditions in random areas are addressed on a case-by-

case basis using the TARP system. The influence of advance per blast was considered only once for a single TARP trigger. The effectiveness of the last line of support has not been investigated. Furthermore, the modelling results were never calibrated against field observations. And data collection as recommended by Groundwork and OHMS was never done. The current design does not properly address the influences of reducing the bord span, face advance and the effectiveness of the last line of support.

1.5 Research Objectives

Shortcomings of the current COP, support design and TARP with regards to hangingwall behaviour within the face area have been discussed at length in the preceding sections. The aim of this study is to address the shortcoming by assessing the hangingwall stability in the face area at Bathopele mine through:

i. Evaluating problematic ground conditions at different bord dimensions using appropriate methods,
ii. Determining the effectiveness of the last line of support, and
iii. Establishing guidelines for TARP members to ensure informed support recommendations are issued.

1.6 Research Methodology

In summary, the following steps were followed in completing this research:

i. The FOGs that have been reported and investigated at Bathopele that occurred within the face area as captured in the FOG database were analysed
ii. Failure mechanisms involved in the FOGs were established
iii. Appropriate methods to evaluate such failure mechanisms were investigated
iv. Data required to correctly use such methods was established. The data was then collected and processed.
v. Face areas were assessed using numerical models
vi. The results from the assessment were validated using actual FOGs

1.7 Chapter Summary

The shortcomings of the TARP procedure and the GCD standard in addressing FOG hazard in the face area were presented in this chapter which are the motivation for this project. The FOGs that have occurred within the face area provide proof of the shortcomings, and were briefly discussed. The objectives and a summary of the research methodology were also highlighted. The issue of stable unsupported spans must be considered a design issue. Therefore, the following chapter is about understanding the behaviour of the rock mass within the face area.

2 DESIGN CONSIDERATIONS

The subject of this study is related to excavation design and hence this chapter is about the design process applicable to rock engineering. Such engineering design has been addressed by Bieniawski (1991, 1992) (as cited in Stacey, 2004). Bieniawski's design methodology is comprised of six design principles.

i. Design principle 1: Clarity of design objectives and functional requirements
ii. Design principle 2: Minimum uncertainty of geological conditions
iii. Design principle 3: Simplicity of design components
iv. Design principle 4: State of the art practice
v. Design principle 5: Optimization
vi. Design principle 6: Constructability (Stacey, 2004)

The six principles can be linked to the engineering design methodology provided in Figure 2-1 developed by Stacey (2005, as cited by Stacey 2009). It can be noted from the design wheel (Figure 2-1) that the design process is made up of two main components which are: defining the design and executing the design. Essentially, the design cannot be executed if the design has not been properly defined and hence the importance of this chapter for this project.

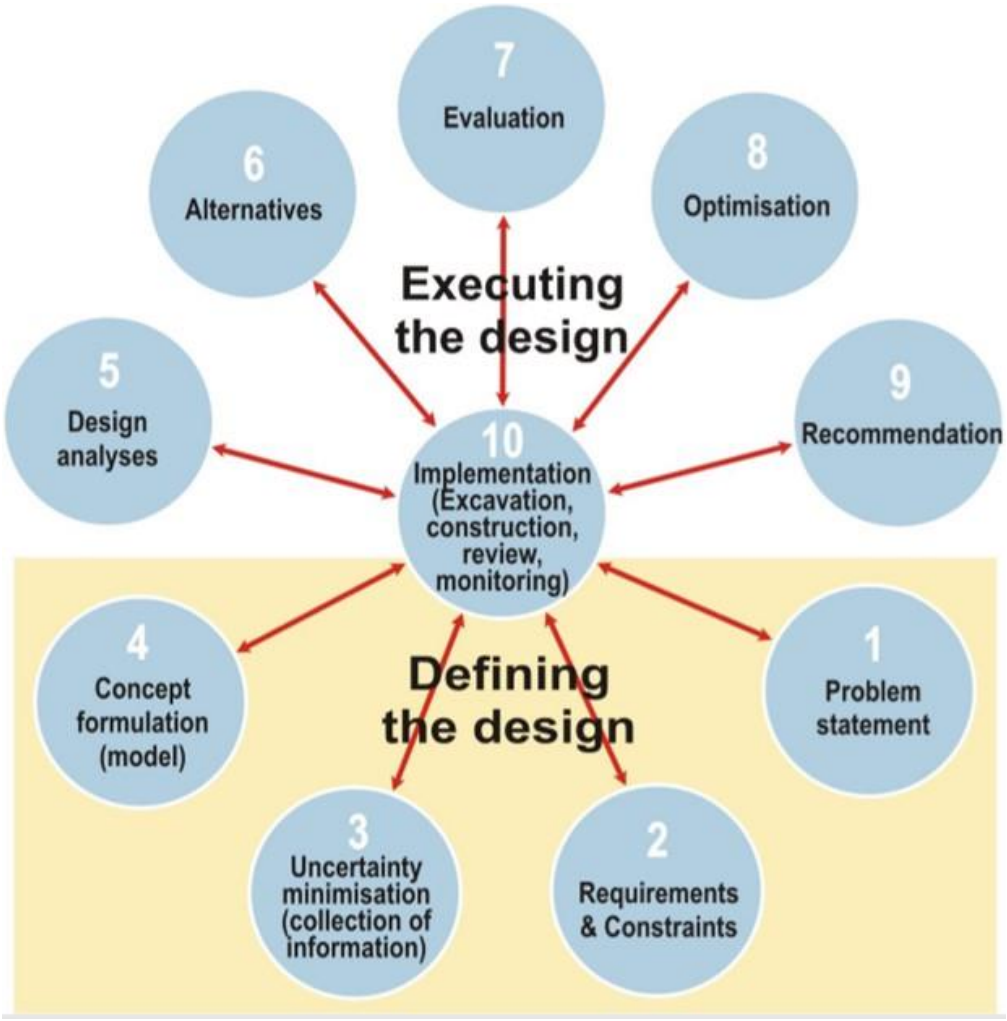

Figure 2-1. Engineering design wheel by Stacey (2005, as cited in Stacey, 2009)

The design wheel principles applicable to this research are:

i. **Definition of the problem and consideration of existing constraints:** this has been discussed at length in Chapter 1.

ii. **Understanding of the likely mechanisms of failure:** This ensures that the correct design/failure criteria are used in the design, ensuring a correct and valid design. The tools that may be used to assess the hangingwall stability are only tools to assess a problem that already exists (Stacey, 2009). The issue of the FOGs within the face area has been raised. Some examples of those FOGs have been given, but a detailed analysis of the rock mass behaviour/condition causing those FOGs has not been done. There is a risk of conducting the wrong analyses if failure mechanisms are not understood. The focus of this chapter will therefore be a study on the FOGs that have already occurred.

iii. **Minimization of uncertainty by collecting relevant and sufficient data:** As mentioned in Section 1.4, collection of geotechnical data has been recommended because of the insufficient data used in some of the previous design work.

The six design principles and the engineering design are used as a checklist. This chapter describes the necessary research using Bieniawski's six design principles (as cited in Stacey, 2004).

2.1 Clarity of Design Objectives and Existing Constraints

The motivation for this study is that there have been uncontrolled rockfalls in the face area that were not anticipated and as such, had the potential for loss of life and/or equipment. One of the reasons for the surprise FOGs was that TARP members did not have comprehensive guidelines to address the FOG hazards. This shortcoming existed even with the design documents, GCD with its associated support standards, and the TARP procedure.

Some of the constraints to consider are related to multiple factors affecting rockmass behaviour, FOG data available at Bathopele and published material on bord and pillar mining in hard rock conditions. This research assesses ground conditions that have resulted in FOGs in relation to bord dimensions and the last row of support. There are several other factors that affect excavation stability as discussed by Palmström (1995) that are not evaluated in this project.

One of the constraints of the study is that only the FOGs that have been reported and investigated are considered. There may have been other FOGs that have not been investigated, which could limit model validity. The quality and the type of data captured may also be a restriction. For instance, the FOG database for the Kroondal operations has very limited data compared to that of

Bathopele. Furthermore, capturing of FOG data only started years after mining commenced.

Finally, it is noteworthy that published material for hard rock behaviour in bord and pillar operations is sparse. The majority of the research is on pillar design, and very little on bord behaviour. Significantly more articles have been published on bord behaviour in coal mining.

2.2 Description and Trends of FOGs in the Face Area at Bathopele

The FOG database for FOGs that have occurred in the face area at Bathopele is provided in Appendix A. The database was studied in order to understand the failure mechanisms of the FOGs within the face area. The readily available information on the database was sorted in terms of relevance. Other information missing from the database had to then be gathered from the FOG reports and/or digital plans. The FOG reports are available on the Company's intranet. Some reports are missing, some are password protected, some lack details and some have not been plotted on plan and location of FOG is not specified in the report. Conclusions on the FOG boundaries and span could not be made from either the database or the reports where details were lacking.

2.2.1 FOG trends in GCDs

The analysis of the FOG database started on a regional basis by considering the trend in terms of GCDs. There are eight GCDs for Bathopele and Kroondal

operations as specified in the GCD standard. From the eight GCDs, six have been identified at Bathopele as shown in Figure 2-2 and the GCDs are as follows:

i. **GCD A:** Multiple low angled structures and water
ii. **GCD B:** Transition zone from GCD A and D, multiple faults with fair-ground conditions
iii. **GCD D:** Major fault zones (i.e. the Hex River fault zone and the Dednam fault zone)
iv. **GCD E:** Single seam mining with leader seam >1.3 m above main seam
v. **GCD F:** Dual seam mining with leader seam <1.3 m above main seam
vi. **GCD G:** potential for water influx with aquifer on triplets horizon, undermining of Hex River and areas shallower than 100 m below surface.

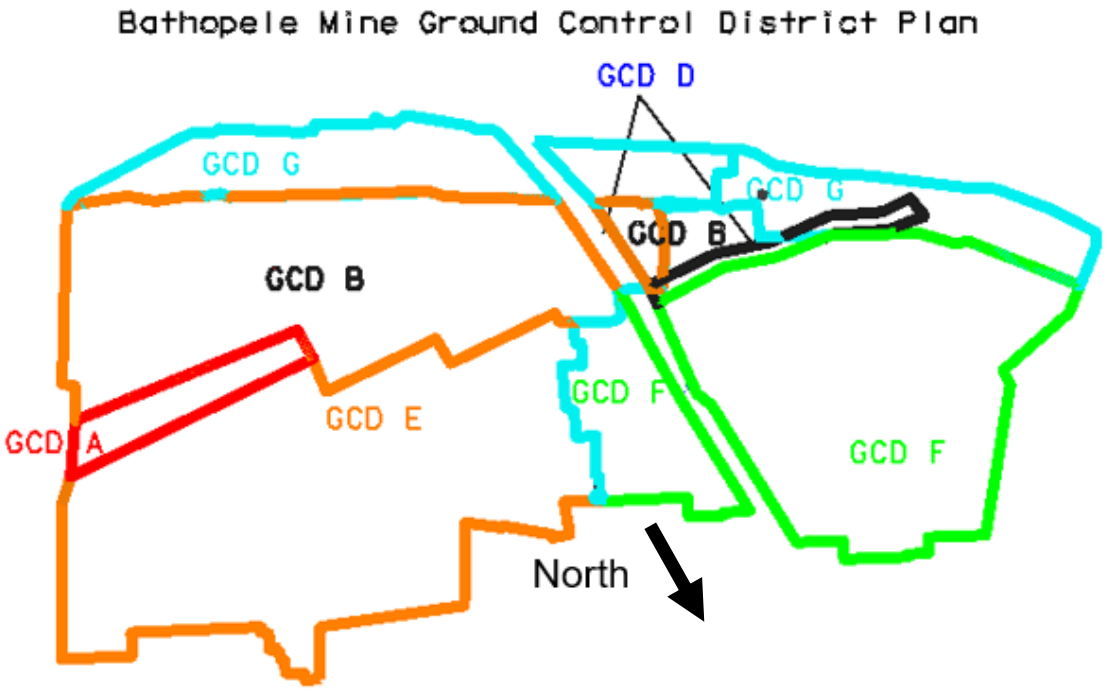

Figure 2-2. Plan view of the GCDs at Bathopele

The GCDs at Bathopele have changed recently with the amalgamation of the standards of the bord and pillar operations within Sibanye. The GCDs in the FOG database have been adopted to the new standard for the first time with this project. Initially GCDs A and B did not exist and therefore the FOG data for those GCDs is under GCD E and F. To make sense of the GCDs, a plan view of the geology is provided in Figure 2-3. The legend for interpretation of geological structures depicted on plan is provided in Appendix B.

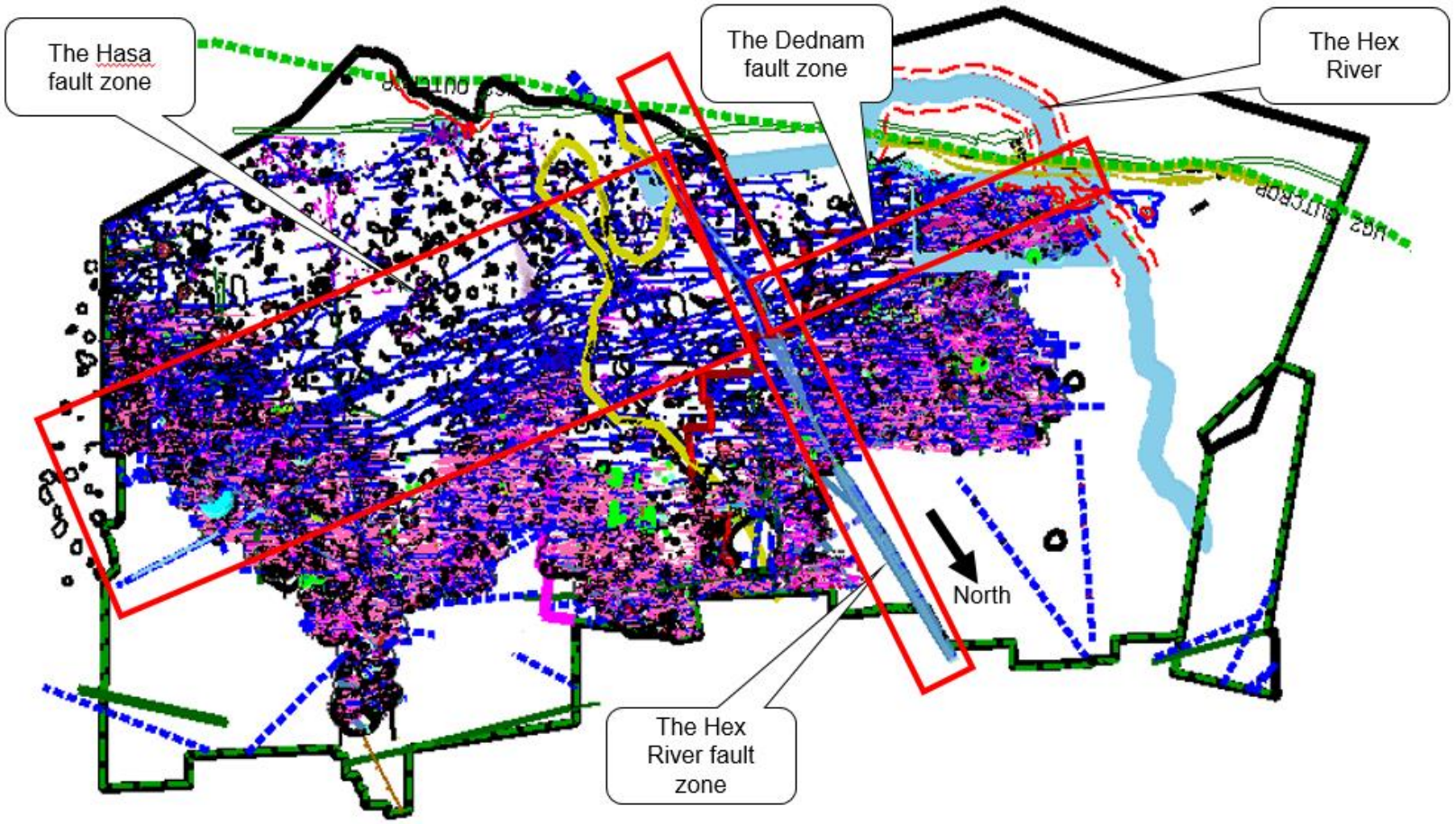

Figure 2-3. Major geological anomalies at Bathopele

Processing of the FOG data within the face area reveal that the majority of the FOGs occurred within the single seam district (GCD E) as shown on Figure 2-4. It appears that the single seam district is comparatively a high-risk environment from the analysis, but it is not; because most ground has been mined on single seam at Bathopele (Figure 2-5). The normalised data for rate of FOGs per 100 000 m^2 in Figure 2-6 shows that GCD F (dual seam mining district) is actually of a slightly higher risk.

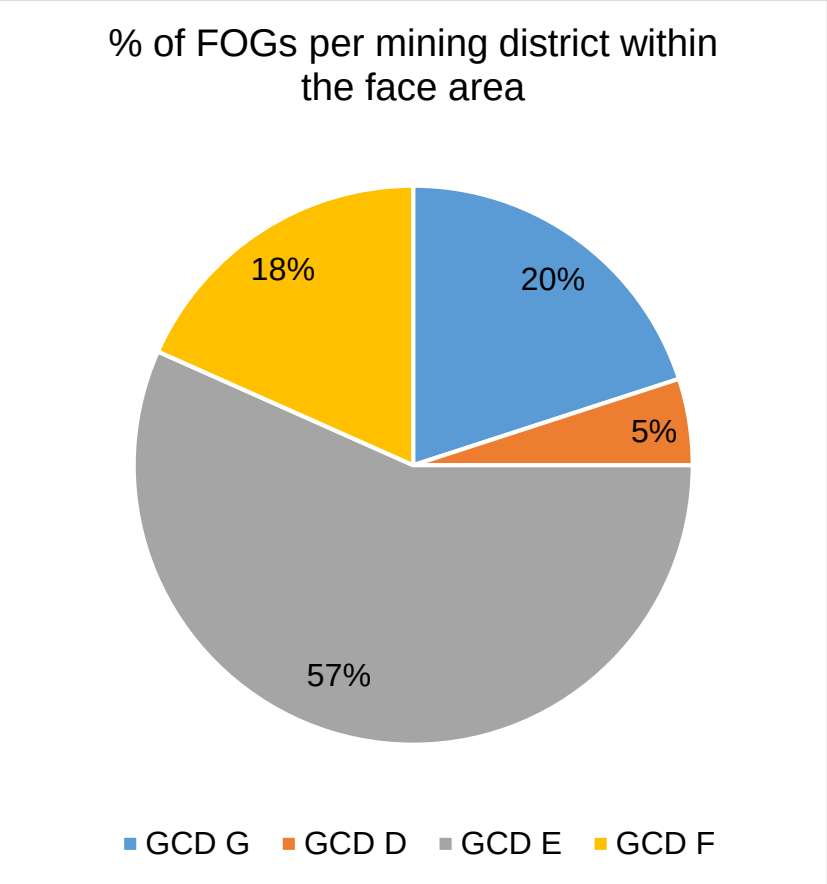

Figure 2-4. Percentage of FOGs per mining district within the face area

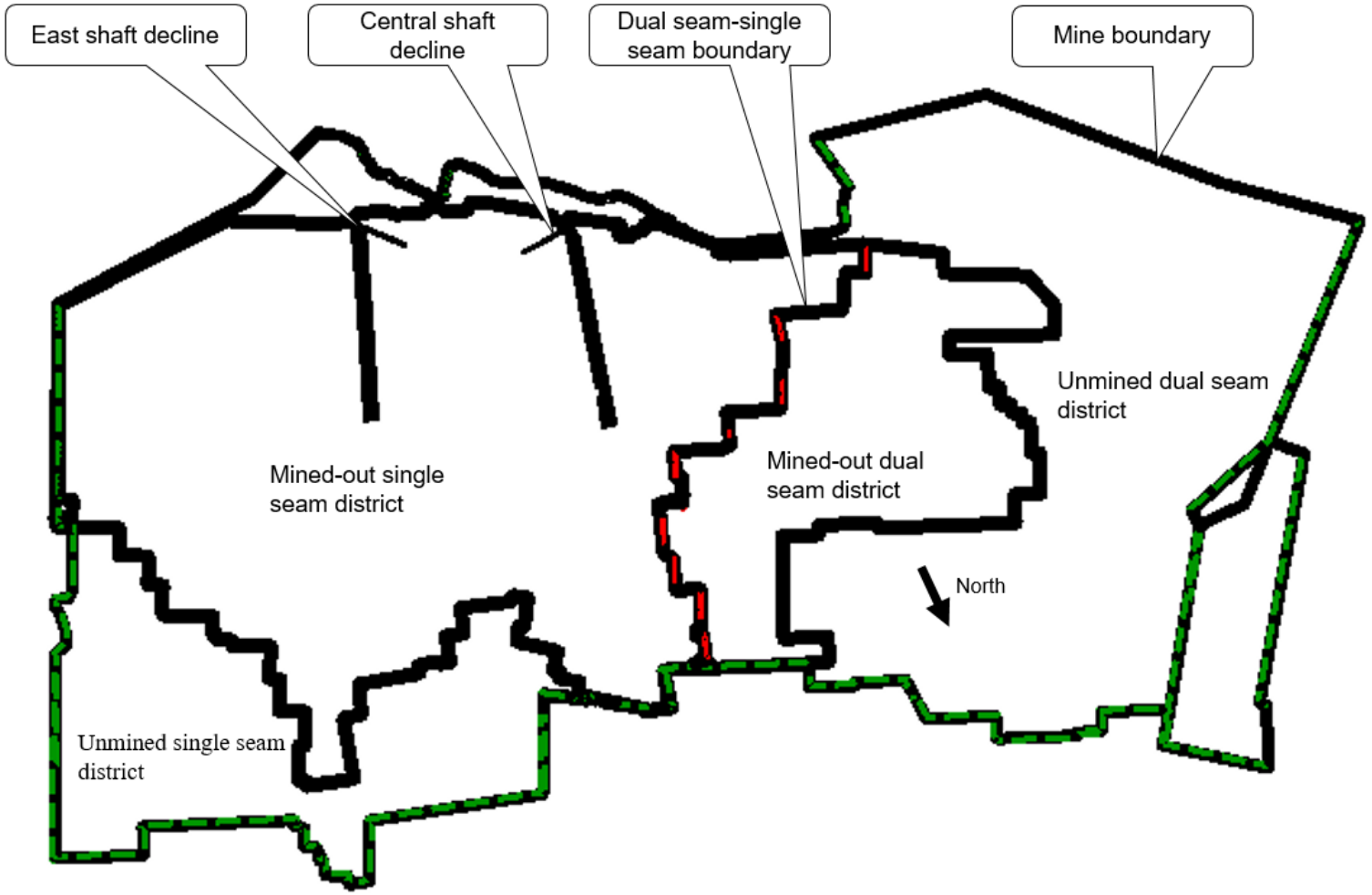

Figure 2-5. Plan view of Bathopele mine showing the mined-out and unmined portion of the two main districts

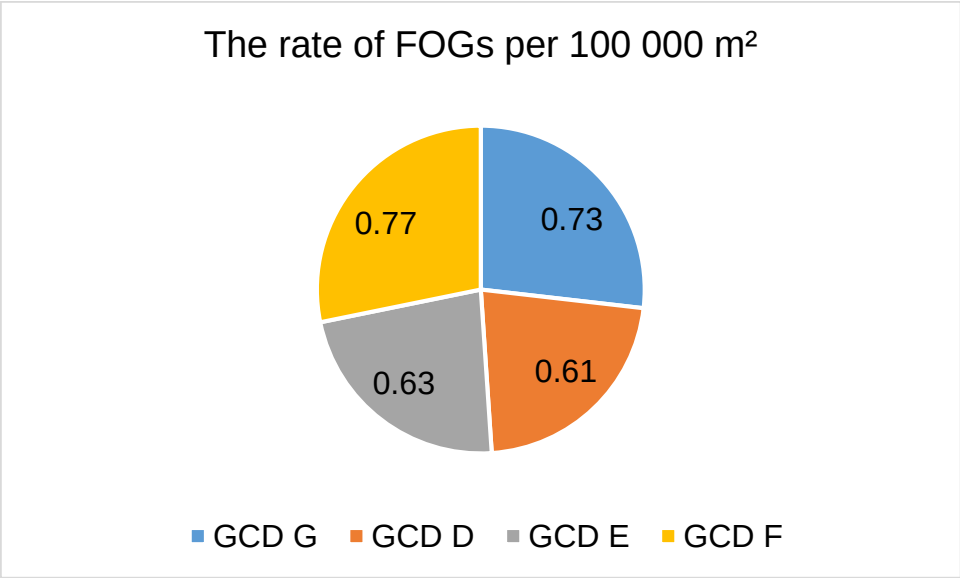

Figure 2-6. The rate of FOGs per 100 000 m² per GCD

What differentiates the single seam and dual seam district is the presence of a chrome stringer ±20 cm above the main seam in single seam GCD and the leader seam at ≤1.3 m above the main seam in dual seam GCD. The chrome stringer is a hazard in single seam GCD if hangingwall is not mined up to the stringer. The leader seam is a hazard in dual seam if hangingwall is not mined on top contact of the leader seam. The two partings therefore present a similar risk. However, the chrome stringer in GCD E above the main seam has been observed to be less competent than the top contact of the leader seam.

The leader seam is a hazard in single seam GCD in potholes and slumps, and, the doublets and triplets are a hazard for dual seam GCD in potholes and slumps. The leader seam was one of the FOG boundaries in five out of fifteen FOGs that involved a hangingwall layer in single seam district. Triplets and

doublets were one of the FOG boundaries in four out of five FOGs in the dual seam district. This is in spite of the fact that the leader seam is at 1.4 m above the hangingwall in single seam GCD and the doublets and triplets are at 3.5 m and 4.5 m above the hangingwall, respectively, in dual seam GCD. The point is, triplets present a much higher risk because they contain cavities and carry water in some areas. It should be noted from the FOG database (Appendix A) that out of the four FOGs in the dual seam district involving the hangingwall layer, two were also affected by water. In addition, it should be noted that a relatively large portion of the remaining ground at Bathopele will be on dual seam (Figure 2-5). The remaining bord and pillar operations within Sibanye are on dual seam. Therefore, the area of concern should be the dual seam district (GCD F).

In terms of TARP classification (Figure 1-4) and panel span, there is little difference between the GCDs as shown in Table 2-1. Figure 2-7 does however show that the FOGs with the largest Fallout Thickness (FOT) occurred in GCD E (single seam GCD). The maximum FOT recorded in GCD F is 2m.

Table 2-1. Comparison between the various GCDs

GCD	% of FOG occurrence in the GCD	Depth range	TARP classification	Mining direction	Span range
GCD G	20%	<100 m	Varies	Varies	6-9m, with significant missing data
GCD D	5%	Varies	TP2 and TP3	Varies	4,2-7,2 m
GCD E	57%	Varies	Varies	Varies	5,6-9,8 m
GCD F	18%	Varies	Varies	Varies	4,7-9,2 m

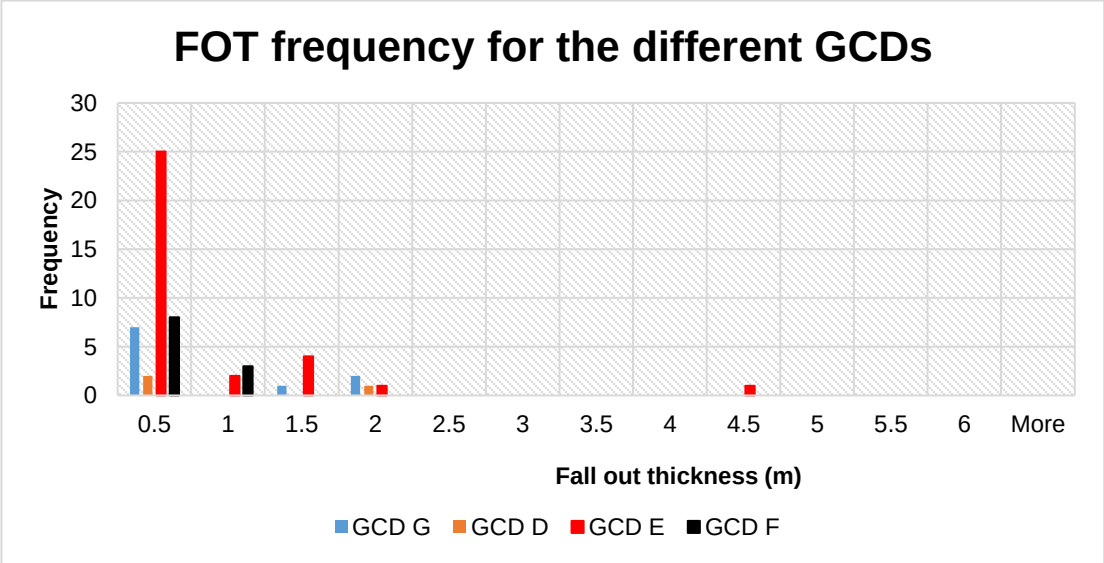

Figure 2-7. Fallout thickness frequency for the different GCDs

2.2.2 FOG trends in terms of failure mechanism, bord width, TARP classification and TARP triggers

The following findings were determined from the FOG database:

i. The FOGs occurred during different mining activities, barring, support installation, face preparation, face drilling, loading and when there was no activity in the panels. None of the activities appear to be predominant except that very large falls seem to have occurred during periods of no activity in the panels.

ii. Surface planes were geological features for all the FOGs. Blasting fractures were mentioned in 13% of the FOGs. Stress fractures are not mentioned in any of the FOG reports. The FOGs were therefore **gravity driven**, irrespective of the activity, which is expected for a shallow mining operation such as Bathopele.

iii. All known geological TARP hazards appear to have contributed to instability as shown in Figure 2-8. Joints were one of the major release surfaces, accounting for 85 % of the FOGs. However, it must be noted that the joint dip angles were not described and could either be vertical or low angled. The same applies to shears, faults, dykes and veins. The 35 % of the shallow dipping structures could either be joints, faults, shears or dykes.

iv. Hangingwall (HW) parting planes include chromitite stratum such as the chrome stringer above the UG2, the leader seam, doublets, triplets, top reef contact or any other parting plane that dips at less than 15°. The HW layers have been discussed in Section 2.2.1. All the FOGs that involved hangingwall stratification had a FOT of less than 1 m, irrespective of bord span. It must be noted that mining has been successfully done in areas where parting planes are positioned at less than 1 m above the hangingwall without any instability. Bathopele mining lease area is plagued with reef rolls and potholes. A lot of bords have successfully been mined through potholes and reef rolls. Seemingly, certain conditions have to exist for the partings to fail. Note that FOGs with higher FOT occurred on shallow-dipping features that cut through the strata.

v. FOG percentage per TARP classification is evenly distributed between TP2 and TP3 as indicated in Figure 2-9. The FOG boundaries that caused FOGs in T1 panels were joints, top reef contacts and blast fractures.

vi. The largest FOGs in terms of volume were recorded in TP3 panels as shown in Table 2-2. A shallow dipping structure was one of the FOG boundaries for such large FOGs. All the FOGs with FOT larger than 1 m involved a shallow dipping structure that cut through the strata.

vii. Surprisingly, there is no information regarding the distance of permanent support from the face when the FOGs occurred. The FOG report templates have changed over the years but this information was never included. There is a column in the FOG database to capture this information but the information was never captured.

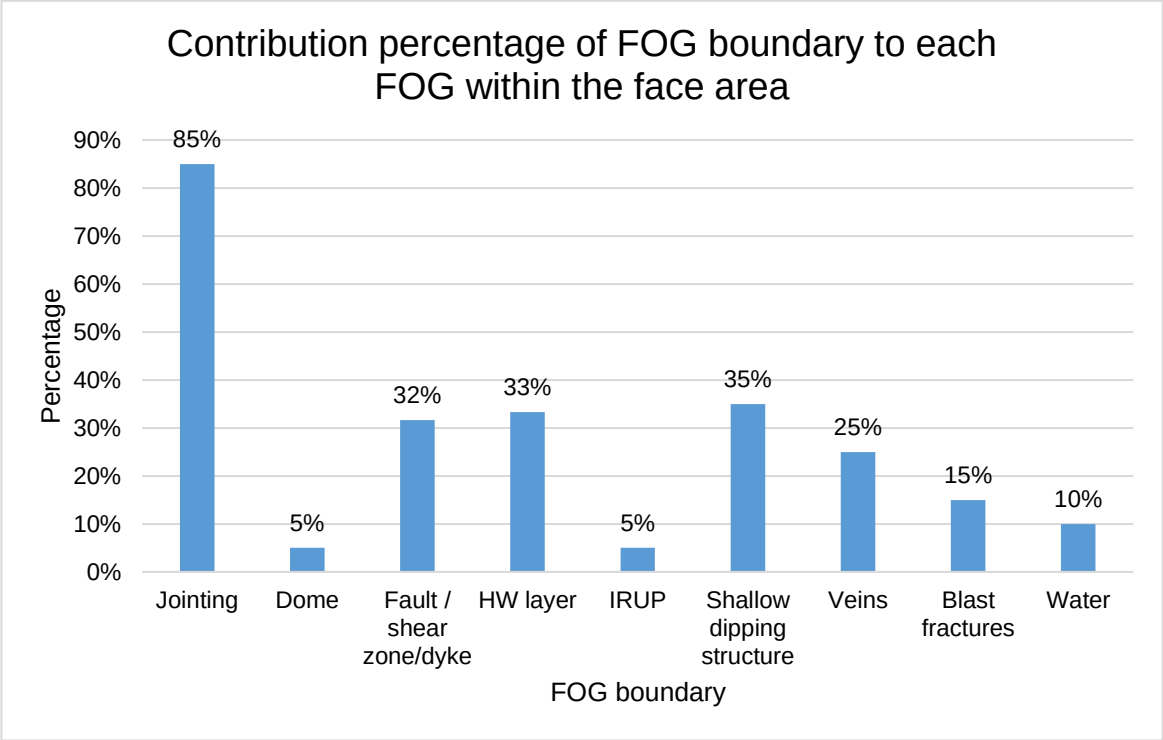

Figure 2-8. FOG boundaries for the FOGs that occurred in the face area

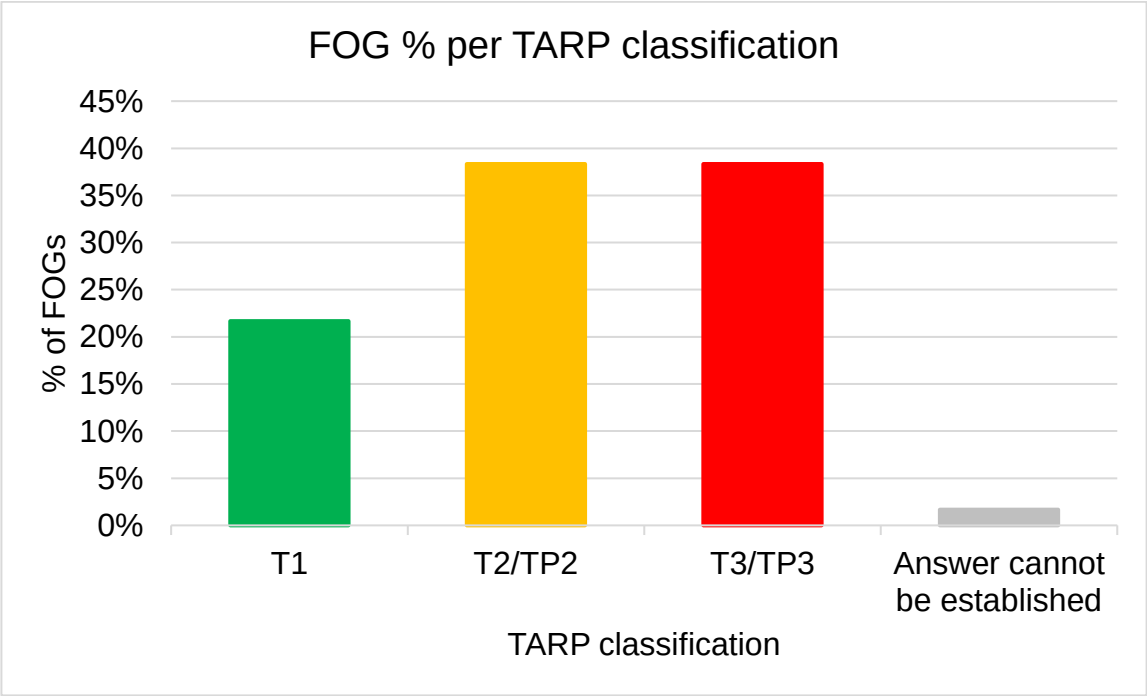

Figure 2-9. FOG percentage per TARP classification

Table 2-2. FOG Volume per TARP classification

TARP Classification	T3/TP3	T2/TP2	T1
FOG volume (m^3)	0.0030	0.0007	0.0003
	0.0032	0.0008	0.0018
	0.0700	0.0050	0.0020
	0.0770	0.0086	0.0040
	0.1680	0.0090	0.0044
	0.1730	0.0240	0.0060
	0.5775	0.0274	0.0140
	4.8069	0.0945	0.0300
	11.7600	0.2400	0.0383
	21.4500	1.1900	0.1325
	26.8640	1.2600	0.1680
	30.0000	1.8000	0.3240
	30.0000	1.8000	0.3402
	31.2000	2.0720	0.4050
	84.5000	2.8800	0.6900
	90.0000	6.0000	1.2500
	441.0000	12.1730	3.8063
		15.0000	

Further processing of the FOG data was done and the results are given in Table 2-3 and Table 2-4. Although there is a significant amount of data missing with regards to the span at the time of the FOG, it would appear that span does not always play a major role in stability. The FOG database shows that cases of FOGs where shallow dipping structures were one of the FOG planes occurred in the bords where mining span was between 5.8 m and 9.4 m. Figure 2-10 shows plan view of bords that were successfully mined through shallow dipping structures without instability, and at different mining span. A possible reason

for successfully mining through these structures could be that they were timeously treated according to TARP procedure. A FOG causal analysis that was done recently showed that failure to identify hazards and non-compliance were contributing factors 100% and 92% of the time, respectively (Sibanda, 2019c). However, there could be other factors that contributed to stability of the hangingwall through the structures depicted in Figure 2-10.

The FOG database shows that a highly weathered zone in a <6 m span, as shown in Figure 2-11 was unstable and failed even through it was addressed as per TARP procedure, similar to the FOGs that involved shallow dipping structures as discussed in Section 1.3. A photo of a highly weathered zone is provided in Figure 2-12. Therefore, the nature of the FOG hazard/s present and perhaps, the treatment of the hazard, may have a stronger correlation to stability than span.

Table 2-3. FOG occurrence in terms of bord span

Span range	Instances of FOG occurrence
4 m - 6 m	17%
6.1 m - 7 m	18%
7.1 m - 8 m	10%
8.1 m - 9 m	20%
9.1 m - (>10 m)	10%
Missing answer	25%

Table 2-4. Comparison of FOG dimensions with respect to bord span

Span range		4m-6m	6,1 m-7 m	7,1 m-8 m	8,1 m-9 m	9,1 m-(>10 m)	Comment
FOG length (m)	Minimum	0.300	0.100	0.480	0.150	0.330	The 6 m was in 4,5 m re-raise, involving a 45° joint, chromitite parting and vertical veins
	Maximum	6.000	4.000	10.000	14.000	5.000	
	Average	1.853	1.392	4.396	3.605	1.630	
FOG width (m)	Minimum	0.200	0.050	0.380	0.070	0.110	The 4,7 m was the final dimension from reportedly 2 FOGs that occurred in the same area
	Maximum	4.700	2.900	6.500	7.000	3.000	
	Average	1.560	0.750	2.336	2.072	0.960	
FOG FOT (m)	Minimum	0.050	0.040	0.150	0.050	0.050	The 2 m was in the Hex River fault zone which in this case was a highly weathered zone
	Maximum	2.000	0.900	1.600	4.500	2.000	
	Average	0.538	0.338	0.750	0.682	0.487	

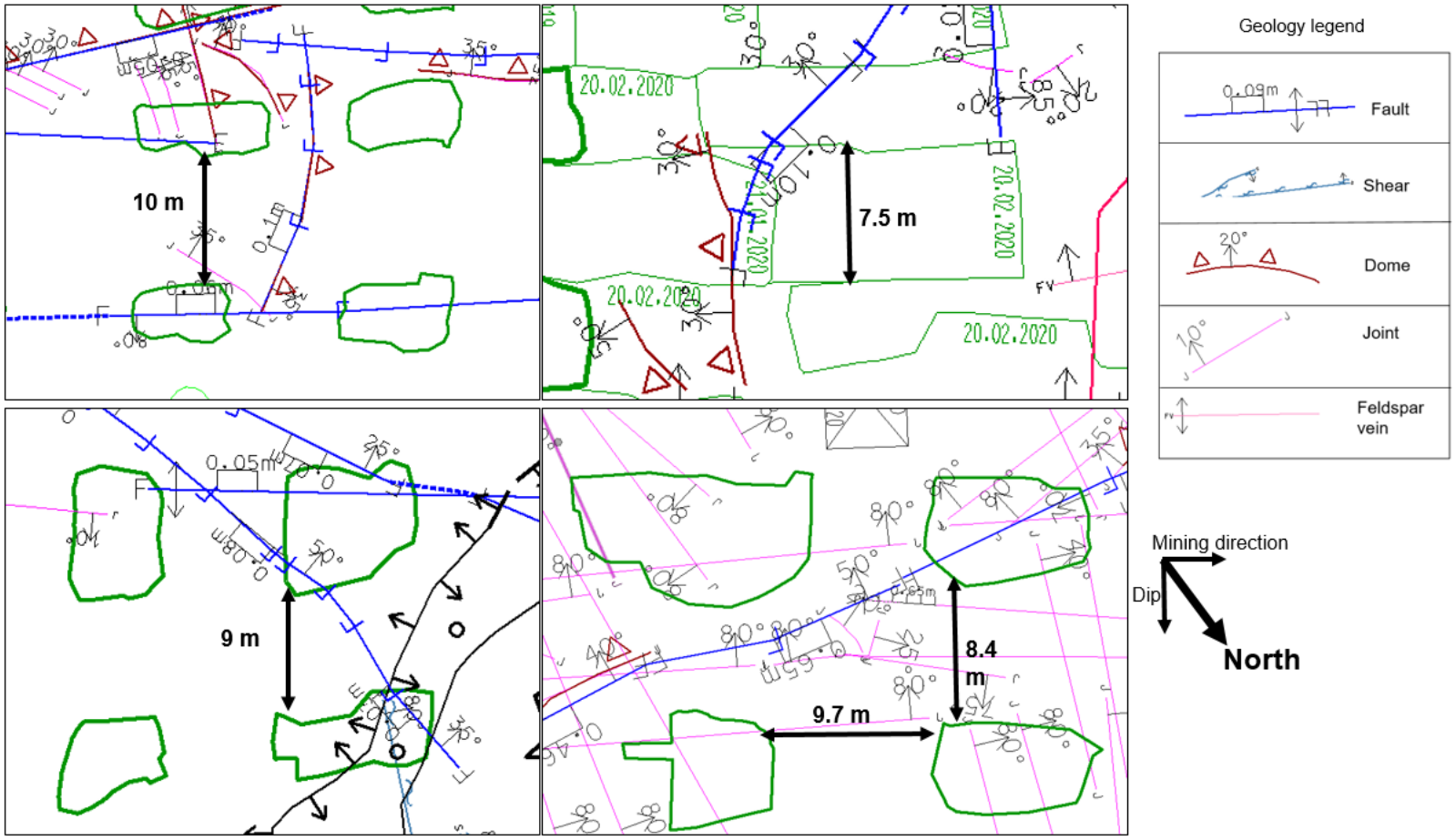

Figure 2-10. A plan view of a mined-out area showing a –various shallow dipping structures that remained stable upon intersection prior to support installation.

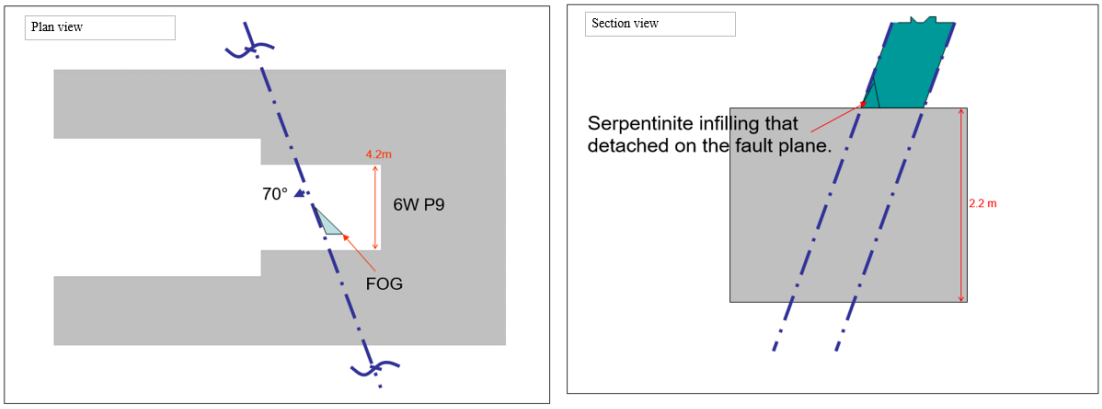

Figure 2-11. Plan view and section view of a FOG that occurred from a serpentinised fault zone (van Rensburg, 2007)

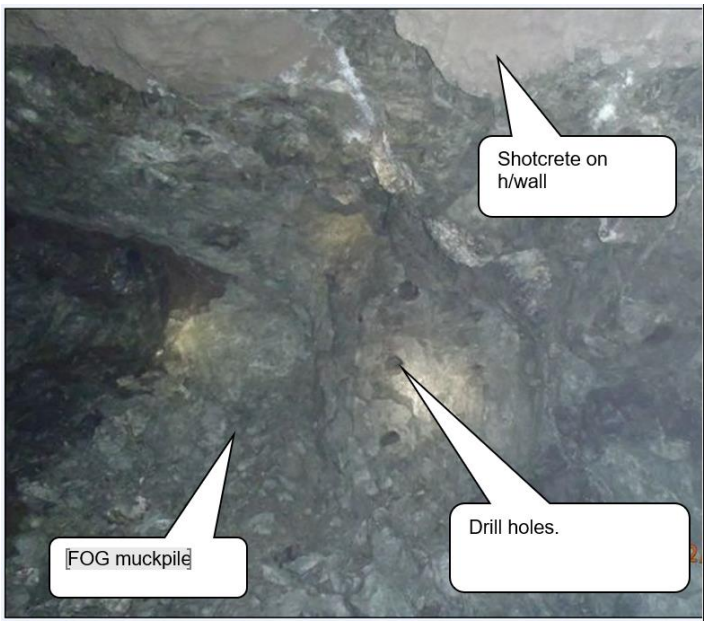

Figure 2-12. FOG from the Hex River fault zone (Sibanda, 2012)

2.2.3 Discussion on the FOG trends

Chromitite layers at normal positions, sub-vertical joints and veins and blasting induced fractures are the only triggers to take into account under normal

ground conditions (i.e. T1 conditions). FOGs occur as a result of insufficient barring or incorrect barring procedure for T1 conditions. Beam conditions can change into blocky conditions, or shallow dipping structures may be present in the hangingwall, or the position of the chromitite layers might change. The hangingwall beam would then have a combination of the structural patterns shown in Figure 2-13, which is what the FOG analyses showed. It is various discontinuities with different properties that result in beam instability. Serpentinite joint and a chromitite parting have different properties for instance. The combination of structural patterns with the structures having different properties presents a challenge at assessing the behaviour of rock mass.

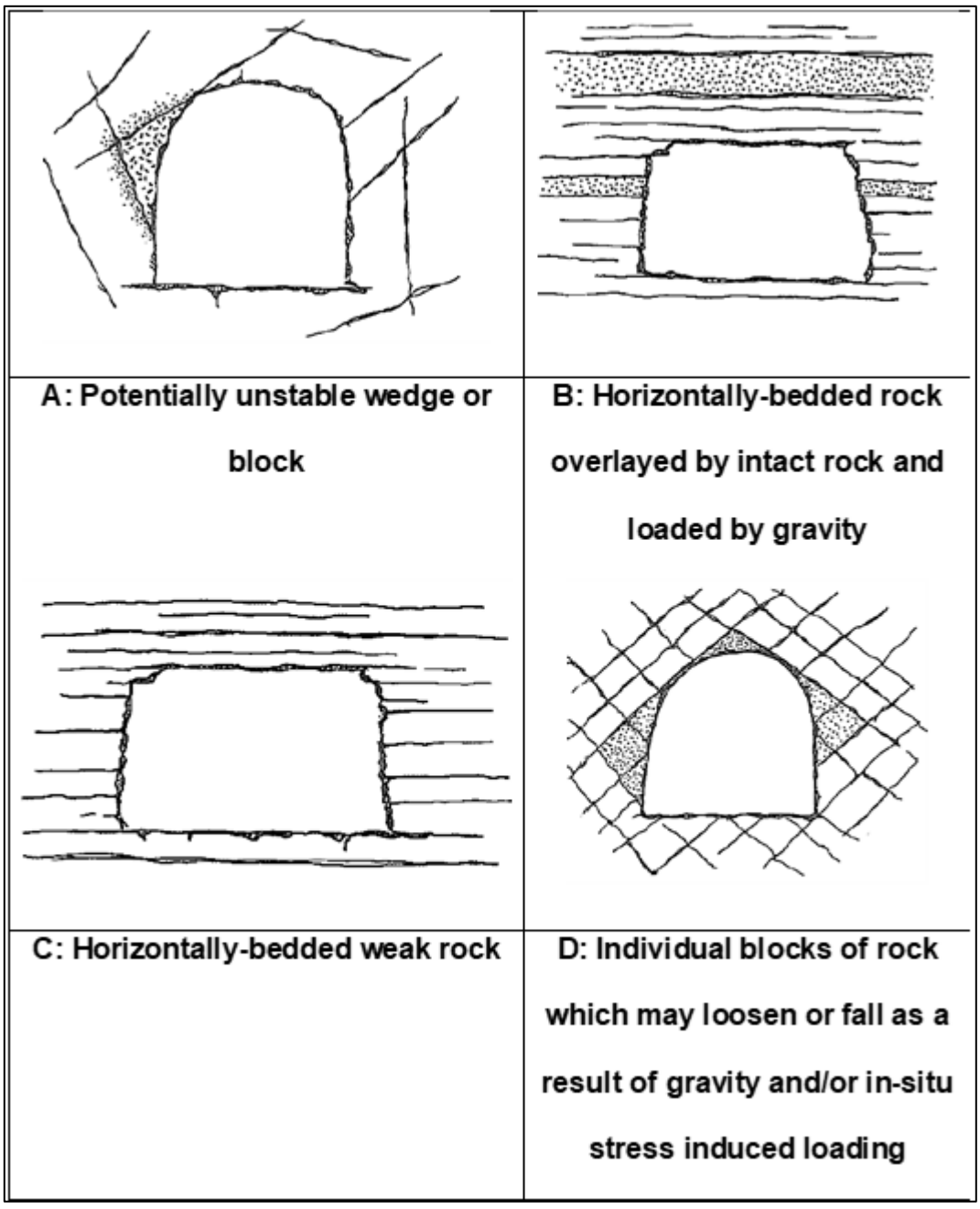

Figure 2-13. Various structural patterns (Stillborg, 1994:47)

It would be advantageous if there was confinement from abutment around the face area as this might contribute to the stability of the face area. However, According to Jager and Ryder (1999), generation of horizontal dilational

stresses is not possible due to virtual absence of face fracturing in shallow mines. The presence of such stresses would allow for the hangingwall to be knit into a coherent self-supporting beam (Jager & Ryder, 1999:31). Rock fragments can therefore slide out from natural or induced discontinuities from blasting under the action of gravity alone in the absence of sufficient compressive stresses (Budavari, 1983: 81). Photos provided in Figure 2-14 to Figure 2-16 of the FOGs from different triggers suggest zero confinement in the areas of the FOGs. The hangingwall unravelled up to the face or sidewalls in each case.



Figure 2-14. A photo of a FOG that resulted from unravelling of Iron-Rich Replacement Pegmatoids (Gloster, 2016)



Figure 2-15. Photo of FOG that resulted from multiple shallow dipping structures and vertical joints (Dube, 2015)

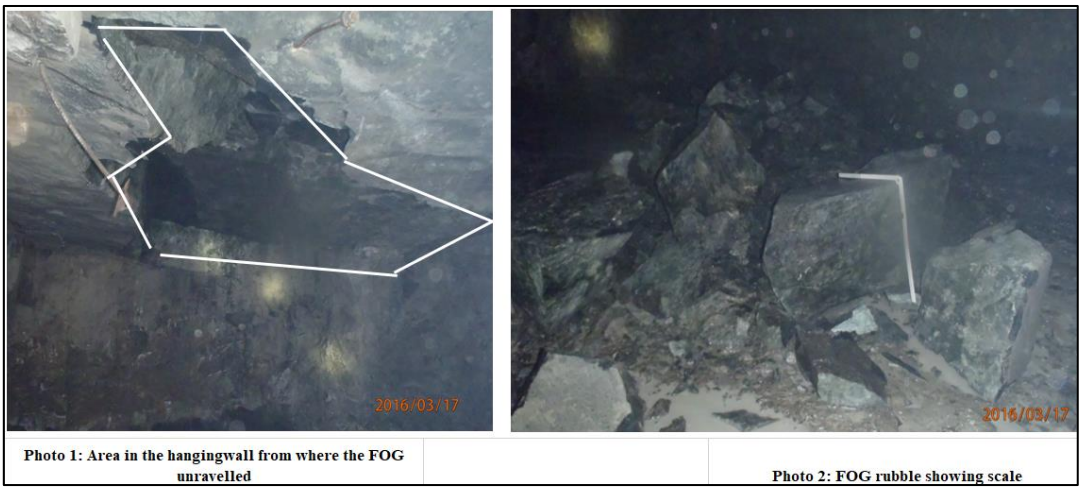

Figure 2-16. Photo of FOG that resulted from chromitite parting, vertical joints and water (Matsobane, 2016b).

Figure 14 shows a face area where hangingwall unravelled from Iron-Rich Ultramafic Replacement Pegmatoids (IRUP). Hangingwall unravelled from multiple shallow dipping structures in Figure 2-15 and the primary surface plane of the FOG in Figure 2-16 is a chromitite layer. Figure 2-17 shows the orientations of joints in a shallow stope with respect to the stope-face. It can be noted from Figure 2-17 that the joints intersect the stope face. The zone of influence of the stope face is limited to the wedges delineated by the joints because of the low horizontal clamping stresses. The joint sets control the zone of influence. The horizontal stresses are insufficient to clamp adjacent blocks and hence the blocks need to be supported individually. It is recommended that zero zone of influence be assumed for a conservative design (Daehnke et. al, 2002:40-41).

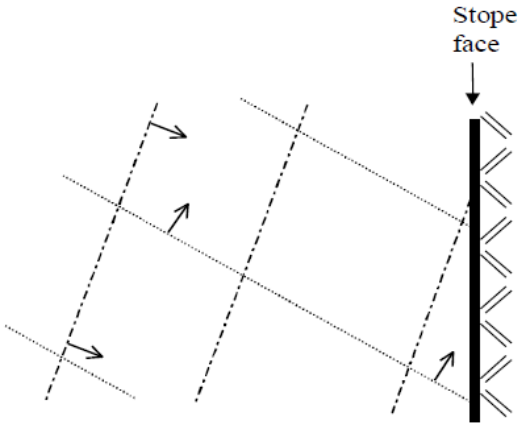

Figure 2-17. Zone of influence associated with stope face in a shallow mining environment (Daehnke, Roberts & Squelch, 2002)

According to Budavari (1983:81), the FOGs would be occurring from low stress or tensile zones and this is irrespective of depth or size of opening. This might explain the FOGs that involved a hangingwall layer. Based on the FOG data, hangingwall beam intersected by parting planes above 1 m within the face area should remain stable provided the planes are not intersected by shallow dipping structures. This is also in agreement with the work completed by Watson and Gerber (2018) which showed that in the absence of shallow dipping discontinuities, the chromitite partings control the fallout thickness and rockfalls occur within the vertical tensile zone (VTZ). Furthermore, the beam is self-supporting at specific span. Hangingwall failure in this case might be through beam buckling.

The potential for beam instability increases with an increase in size of tunnel and with decreasing depth below surface (Budavari, 1983:81). For instance, a 10 m bord at 400 m below surface may be more stable compared to a 10 m bord at 100 m below surface. The potential for instability is a function of the extent of the tensile zone, relative to the spacing between weaknesses (Budavari, 1983:81). A trend with regards to influence of bord span could not be identified in the FOG analysis. It is appreciated, though, that the number of FOG samples may not be sufficient to formulate trends. It was a challenge to use combined data from Bathopele and Kroondal operations because of the significant differences between the data that was captured.

The FOG analysis showed that the largest FOGs were as a result of shallow dipping structures. Such structures contributed to 32 % of all the FOGs. Watson and Gerber (2018) conducted numerical modelling exercises using UDEC modelling program to determine stable span in the UG2 mechanized bord and pillar environment. The influence of shallow dipping structures on beam stability was the primary objective of the exercise. The results of the model are provided in Figure 2-18, which shows potential instability without support installation at various bord spans.

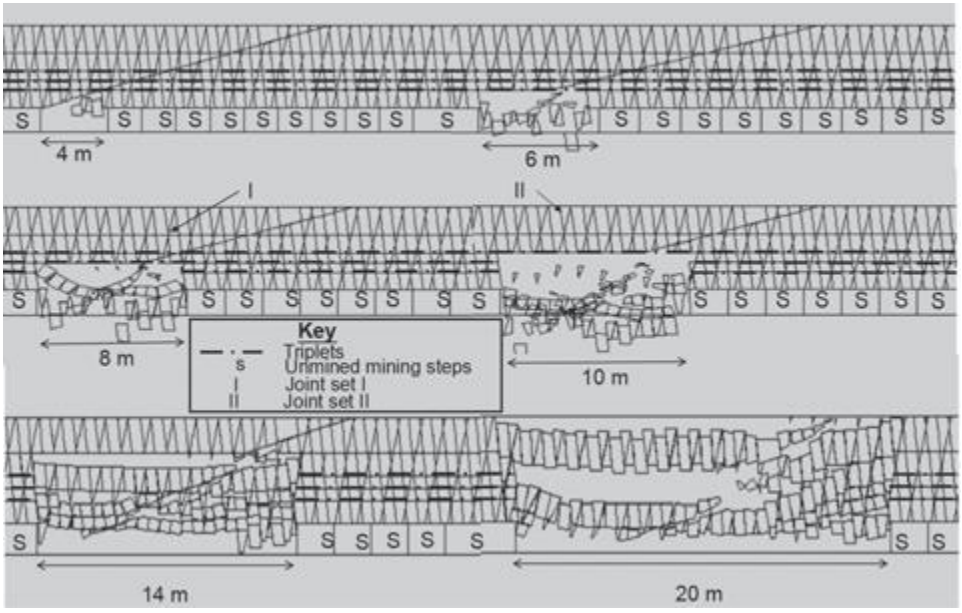

Figure 2-18. Unsupported model (Watson & Gerber, 2018)

In the presence of shallow dipping structures, the height of the VTZ is irrelevant. Fallout height is controlled by the extent of the shallow dipping discontinuities in the hangingwall. FOGs will occur at every tunnel width in the absence of

support from as little as 4 m span. The difference is the fallout thickness of the FOGs. This is in agreement with the FOG analysis shown in Table 2-5 for a FOT at specific span range for FOGs that involved shallow dipping structures. For instance, Watson and Gerber's model showed that failure up to 1.3 m can be anticipated at 6 m span however at 10 m span, failure would be up to 2.7 m. The point to take note of is that, the study looked at the worst-case scenario where the entire bord is on the weaker side of the thrust faults. Therefore, depending on the exposed surface of the thrust faults within the face area, conditions might be stable or the FOT may be smaller.

Table 2-5. Fall out thickness for a specific bord span range for FOGs that were caused by shallow dipping structures

Span range	FOT range	Comment
4 m - 6 m	None	
6.1 m - 7 m	0.04 m - 0.5 m	
7.1 m - 8 m	1.3 m - 1.6 m	
8.1 m - 9 m	0.5 m - 4.5 m	None
9.1 m - (>10 m)	0.4 m	FOG was a result of a minor curved joint emanating from a vein (Rajpal, 2011)

2.2.4 The effectiveness of the last row of support

The influence of the last line of support could not be established because data regarding the support is missing. However, because the FOGs are structurally controlled and there appears to be zero confinement from abutments, the

influence of the last row of support is limited and this can be seen by the FOGs depicted in Figures 2-14 up to 2-16 and Figure 2-19. The FOGs involved different triggers. Even though the bords in Figure 2-14 to 2-16 and Figure 2-19 were heavily supported with resin bolts and long cable anchors prior to blast, it would appear that the support had little influence on stability of the unsupported face area.

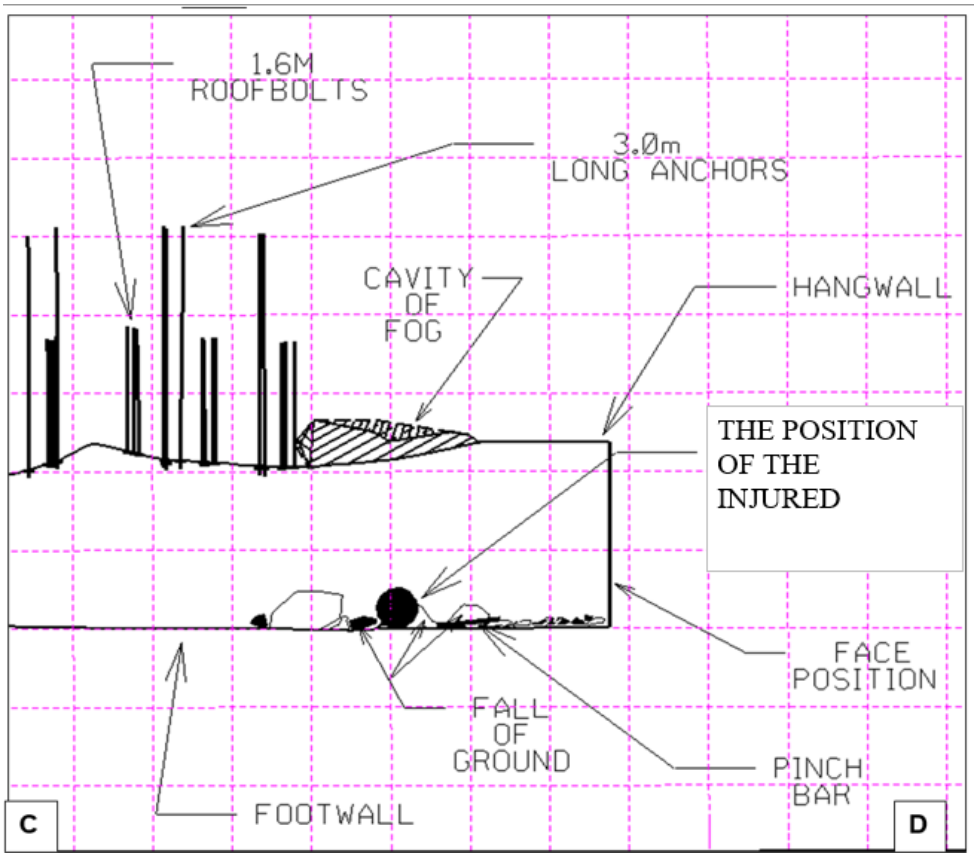

Figure 2-19. Long section of a FOG that was bounded by a single shallow dipping fault and a vertical pegmatite vein, showing zero influence of the last line of support (van Rooyen, 2011).

The issue of the zone of influence of a support unit in a form of bolts has been discussed by Stillborg, (1994: 67,43). In grouted bolts, the load distribution as transferred from the grout to the rock is done over a limited distance (Stillborg, 1994:43,67) and this is illustrated in Figure 2-20.

Figure 2-20 shows an example of very limited zone of influence in terms of load distribution from the bolt to the surrounding rockmass for a pre-tensioned bolt. According to Stillborg (1994:67), load carried by bolts is small compared to the loads acting in the rock and hence bolts enable the rock mass to be self-supporting, except in the case of supporting the deadweight of wedges or individual blocks. For wedge failure under the influence of gravity, the bolt must carry the deadweight of the wedge. Stillborg's statements explain the lack of influence of the last row of support on the stability of the unsupported face area for the FOGs depicted in Figure 2-14 to 2-16 and Figure 2-19.

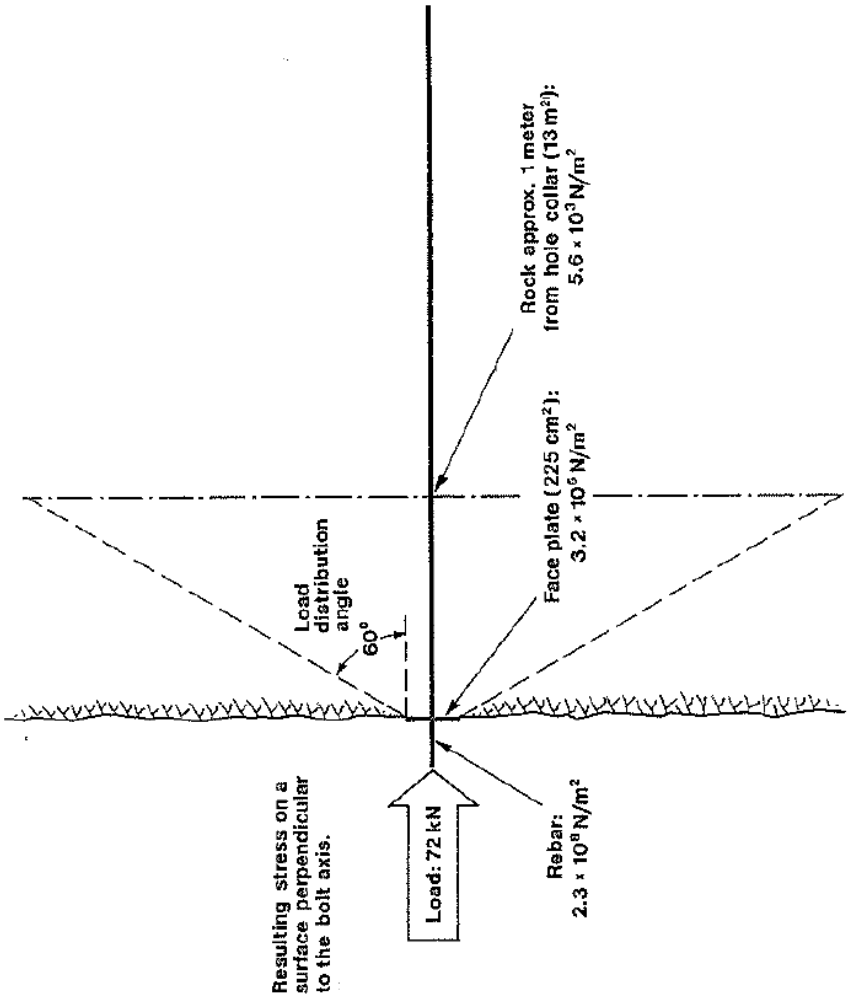

Figure 2-20. A schematic illustration of the load distribution into the rock as a result of rockbolt pre-tensioning (Stillborg, 1994: 43)

Watson and Gerber's 2018 UDEC model results concluded that distance of support to the face does influence the occurrence of FOGs within the face area. According to Stillborg (1994), for blocky ground conditions, the zone of influence is determined by the block sizes. Therefore, determining block sizes

and identifying potentially unstable blocks during EEE may be crucial for Bathopele. Watson and Gerber's model was only a 2-D model and the details of the blocks are not specified in the report. But from the diagrams of the models, it can be observed that the spacing of the sub-vertical joints used in the model was at least 1 m.

2.2.5 Summary of the FOG analysis

The main conclusions that can be drawn from the FOG analysis and the discussion is that the face area should be stable at Bathopele under T1/normal ground conditions provided mining and barring are done correctly. The non-existence of confinement within the face area is evident from the FOGs. The limited zone of influence of support units is also apparent. The need to support individual blocks or wedges in anomalous ground conditions is therefore a requirement which is in agreement with literature.

The bord span does have an influence on stability of the excavation for shallow dipping structures, in terms of potential FOT thickness according to literature. Furthermore, in the case where the position of the chromitite partings deviate from normal, for instance in reef rolls and potholes, the mining span and hence the VTZ, and the presence of other structures would play a role according to the literature. The relationship between span and FOT for FOGs due to parting planes could not be established from the FOG database. For IRUPs, thick shear zones and fault zones, further analysis may be required.

Collection and understanding of structural data become critical for Bathopele. The block size, which is a function of persistence and the spacing of structures, and orientation of the structures is the type of data that should be collected.

2.3 Applicable Methods of Analysis

Hoek et al (1993), Stacey (2001), Stacey and Swart (2001), Brady and Brown (2004) and Murphy et al (2016) discuss the problem of structural instability. Since failure occurs in a form of wedges or blocks falling under gravity, it becomes imperative to identify the potential wedges in a mining excavation. For the purpose of this study of which the objective is to assess stability taking into account both the width and the length of a bord, the methods applicable are JBlock, Unwedge and Potvin's stability method. Using multiple methods ensures that most ground conditions are covered because each method has its limitations. The different methods also can be used as a check against each other.

The ERF method was mentioned in Section 1.4.2 in comparison to the hydraulic radius. The EFR method was developed for complex geometry. The hydraulic radius is suitable for two-dimensional rectangular surfaces (Andrews & Barsanti, 2008). The area under assessment in the project is the face area of a bord and pillar layout which has a very simple surface geometry and hence the use of hydraulic radius.

On the issue of establishing the vertical tensile zone, Murphy et al (2016) used Map3D to determine the VTZ. Large spans of 14 m at shallow depth of 500 m and 6 m for depth of 1000 m were modelled in the handbook. The extension strain criterion was used. Conclusion was that the results agreed with observations and data obtained during the site visits. However, the criterion is applicable to stress related failure. There have been no stress related FOGs at Bathopele and, the depths and spans are not similar to those at Bathopele. Therefore, the VTZ was determined analytically in this project using the following equation:

$$\frac{Z_o}{S} \approx \left[\frac{8H}{S} - 6\right]^{-\frac{1}{2}}$$ ***Equation 2-1***

Where: Z_0 is the height of the tensile zone (m)

S is the span in of the bord (m)

H is depth below surface (m) (Ryder & Malan, 2002)

A brief description of each of the methods are provided below. Potvin's Modified stability graph method was discussed in detail in the previous chapter and hence only JBlock and Unwedge are discussed.

2.3.1 JBlock

JBlock is a computer program that uses a probabilistic method to determine potential keyblocks (Esterhuizen and Streuders, 1998). A JBlock flow chart is provided in Figure 2-21 and Esterhuizen and Streuders (1998) discuss the method in detail. In summary, the program uses joint orientation and spacing statistics to rapidly determine the probability of keyblock failure. The probabilities of failure are compared by varying excavation size and orientation, support types and support layouts.

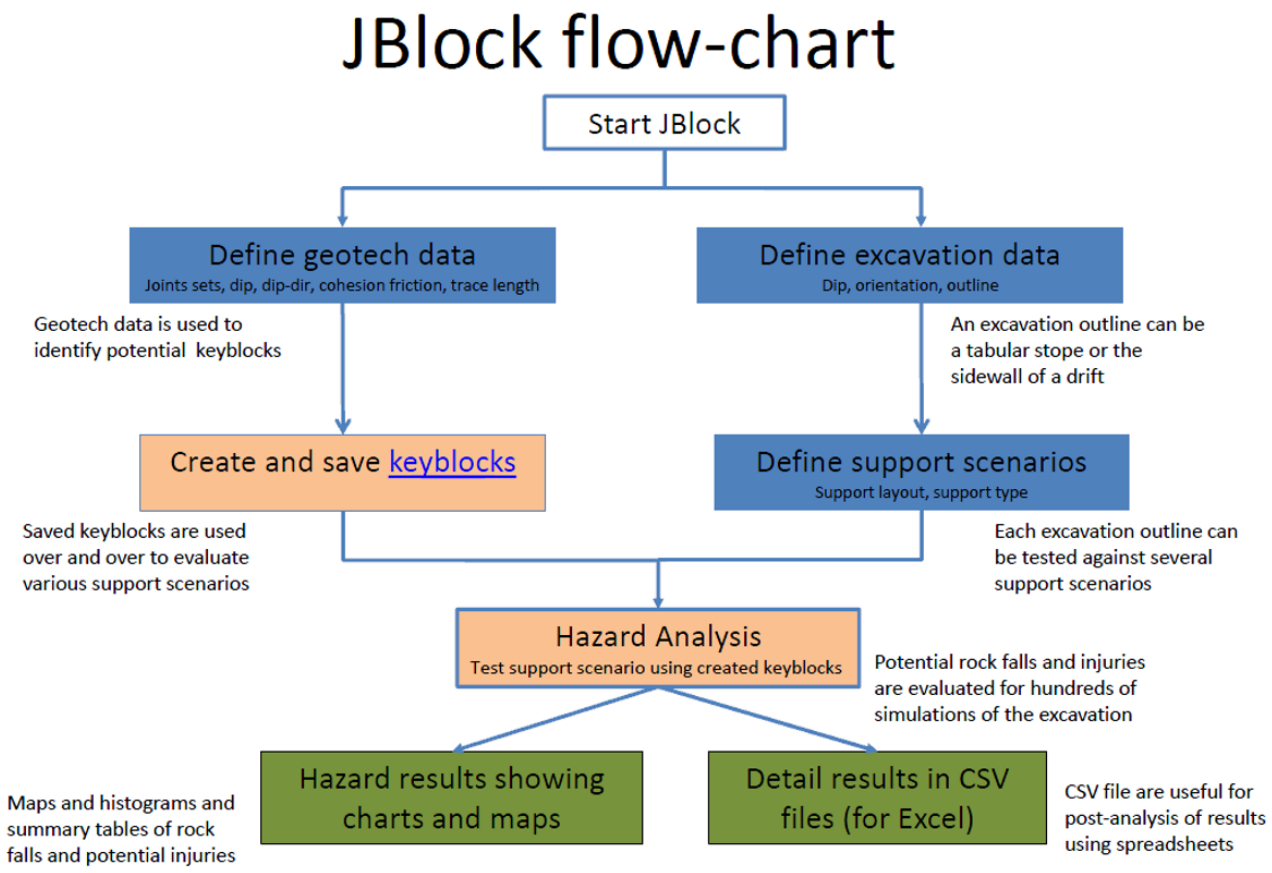

Figure 2-21. JBlock flow chart (Kotze, 2012)

The following information is required to simulate rockfalls in JBlock:

i. Excavation dip and dip direction,

ii. Mean and standard deviation of dip and dip direction of each joint set,

iii. Mean, minimum, and maximum of spacing and trace lengths of each joint set,

iv. Mean and standard deviation of friction angles for each joint set. These can be determined using Barton's (2002) equation, and

v. Mean and standard deviation of parting planes parallel to the hangingwall. The planes may be prominent bedding planes above reef such as chrome stringers. These planes can be determined from boreholes drilled into the hangingwall (Joughin et al, 2012).

The above information must be collected by mapping the joints in underground excavations and the data should represent a GCD (Joughin et al, 2012).

The data used in JBlock is processed using Rocscience software DIPS. The raw data collected is captured in DIPS to determine the joints sets. Once the joints sets are determined, the frictional properties and spacing of the joints may be determined.

It must be emphasized at this stage that absolute solutions cannot be reached using JBlock. JBlock may be used to compare different support scenarios to establish the most favourable scenario or to determine behaviour of a specific parameter under different conditions.

2.3.2 Unwedge

There are various possibilities of blocks that can be formed in the hangingwall as a result of discontinuities, depending on their orientations. Typical wedges that have been observed at Bathopele are shown on plan view in Figure 2-22. The legend for the geological structures shown in Figure 2-22 is provided in

Figure 2-23. For the wedges depicted in Figure 2-22, some might fail and others may not, for example the stable wedges shown in Figure 2-22 are similar to those in Figure 2-24 but those in Figure 2-24 actually failed.

Unstable wedges may fall or slide under their own weight. The recommended method of analysis of the stability/instability of wedges is Hoek and Brown stereonet analysis (Daehnke, Salamon & Roberts, 2000). An example of stereonet projections for stable and unstable wedges is provided in Figure 2-25. It becomes evident that in order to complete a wedge analysis, orientation of structures is required but frictional properties are required as well.

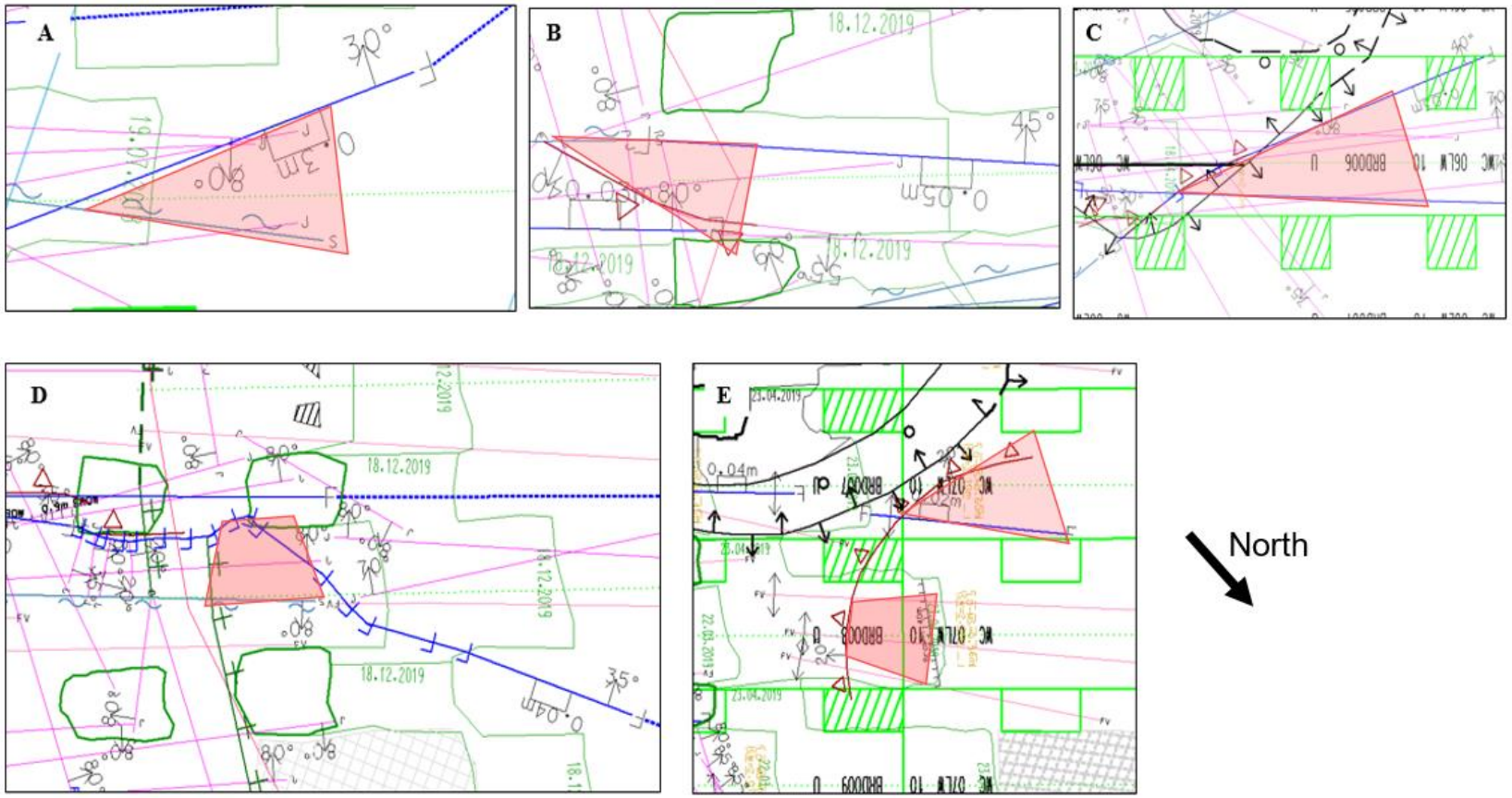

Figure 2-22. Various wedge shapes depicted on plan view

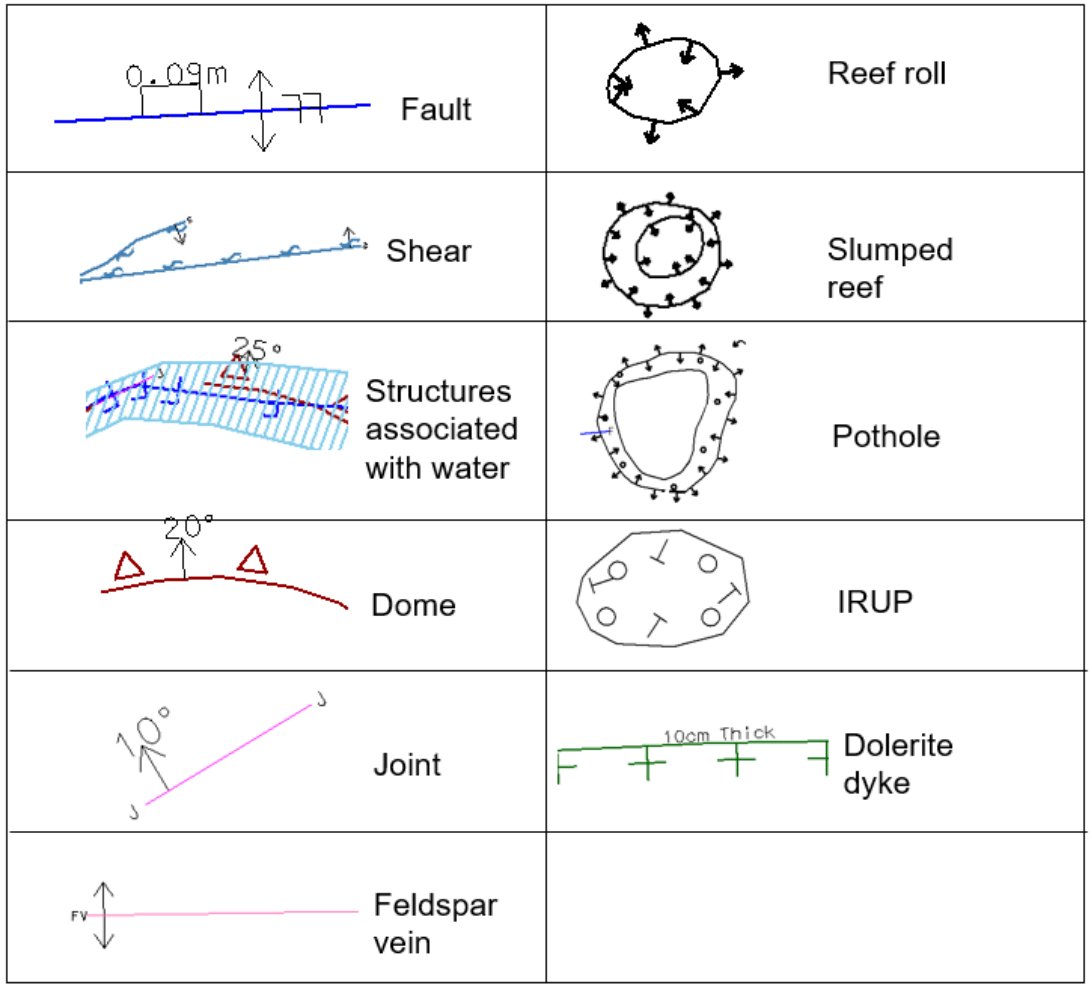

Figure 2-23. Bathopele geology legend

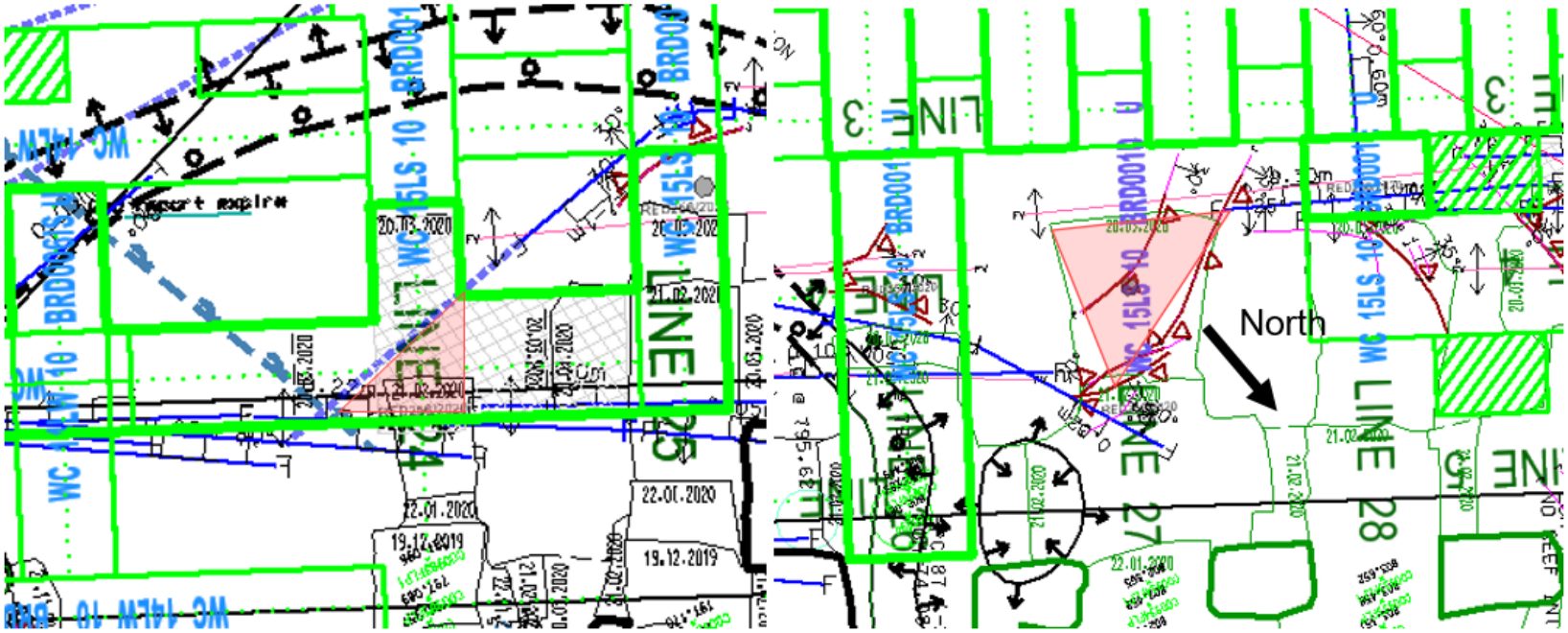

Figure 2-24. Wedges that failed under the action of gravity

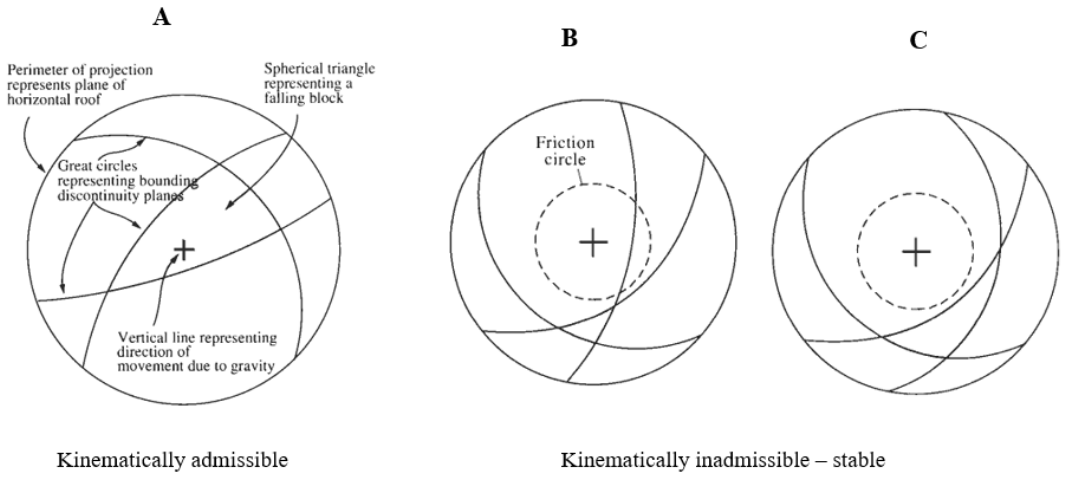

Figure 2-25. Examples of stereonet plots for an unstable and stable wedge (Hudson & Harrison, 1997)

The stereonet analysis can be performed in DIPS or Unwedge. In addition to the structural analysis in terms of orientation of discontinuities, the size of the wedges can be calculated in Unwedge. Unwedge is a Rocscience programme and it applies the Goodman and Shi (1985) block theory (as cited in Dunn et al, 2008). Wedge failure around hard rock conditions can be analysed using the software. The software is suited to conditions where discontinuities are persistent and where failure induced by stress does not occur (Dunn et al, 2008).

One of the limitations of Unwedge is that only three discontinuity planes can be analysed at one time. It therefore becomes necessary to conduct multiple

analyses on combinations of planes for cases where more than three discontinuities are present. For instance, Figure 2-22 B, D and E would require at least two combined analyses. Furthermore, the wedge analysis of those depicted in D and E would have to be an approximation because of the strike of the fault, and the dome that curves. The other limitation of Unwedge is that the wedge being analysed cannot be placed at a specific location in the excavation.

2.4 Chapter Summary

A brief description of the design process applicable to rock engineering was provided in this chapter. The purpose of considering and following the design process was to ensure that the correct data and valid processing of data is done in the chapters that follow. It was emphasized that it is crucial to understand the likely behaviour of the rock mass to ensure that the correct methods of analyses are used.

It was concluded that the FOGs in the Bathopele database are structurally controlled and gravity induced. JBlock, Unwedge and Potvin's modified stability graph were found to be the best methods of analyses for such failure mechanisms. The type of data required in order to complete the analyses is orientation, persistence and shear strength properties of the structural discontinuities. The next chapter discusses data that was collected and

provides the properties of the discontinuities present at Bathopele for the purpose of stability analyses.

3 DATA COLLECTION AND PROCESSING

The data required in order to complete this project is discussed in this chapter. The sections that follow discuss how the data was collected and the processing thereof.

3.1 Details of the Excavation to be Assessed

The assessment of hangingwall stability in the face area was done for the western side of Central shaft. The western side of Central shaft is mining on dual seam and the mining direction is roughly towards west at 294°. Mapping was done in strikes 5W, 7W, 8W, 9W, 10W and 14W sections. A plan view of the sections is provided in Figure 3-1. Plan view of the project site in relation to the rest of the Mine is provided in Figure 3-2. The dip of the excavation is approximately 9°, which is the dip of the reef. The dip direction of the excavation is approximately 24°.

The legend for the geological structures plotted is provided in Appendix B.

There are several possibilities of ‘face areas’ some of which are illustrated in Figure 3-3. This study is a first for Bathopele and therefore it is best to start with a simple model and confirm if the method of analysis and results are appropriate. Therefore, this study concentrates on the face area shown in diagram “A” only.

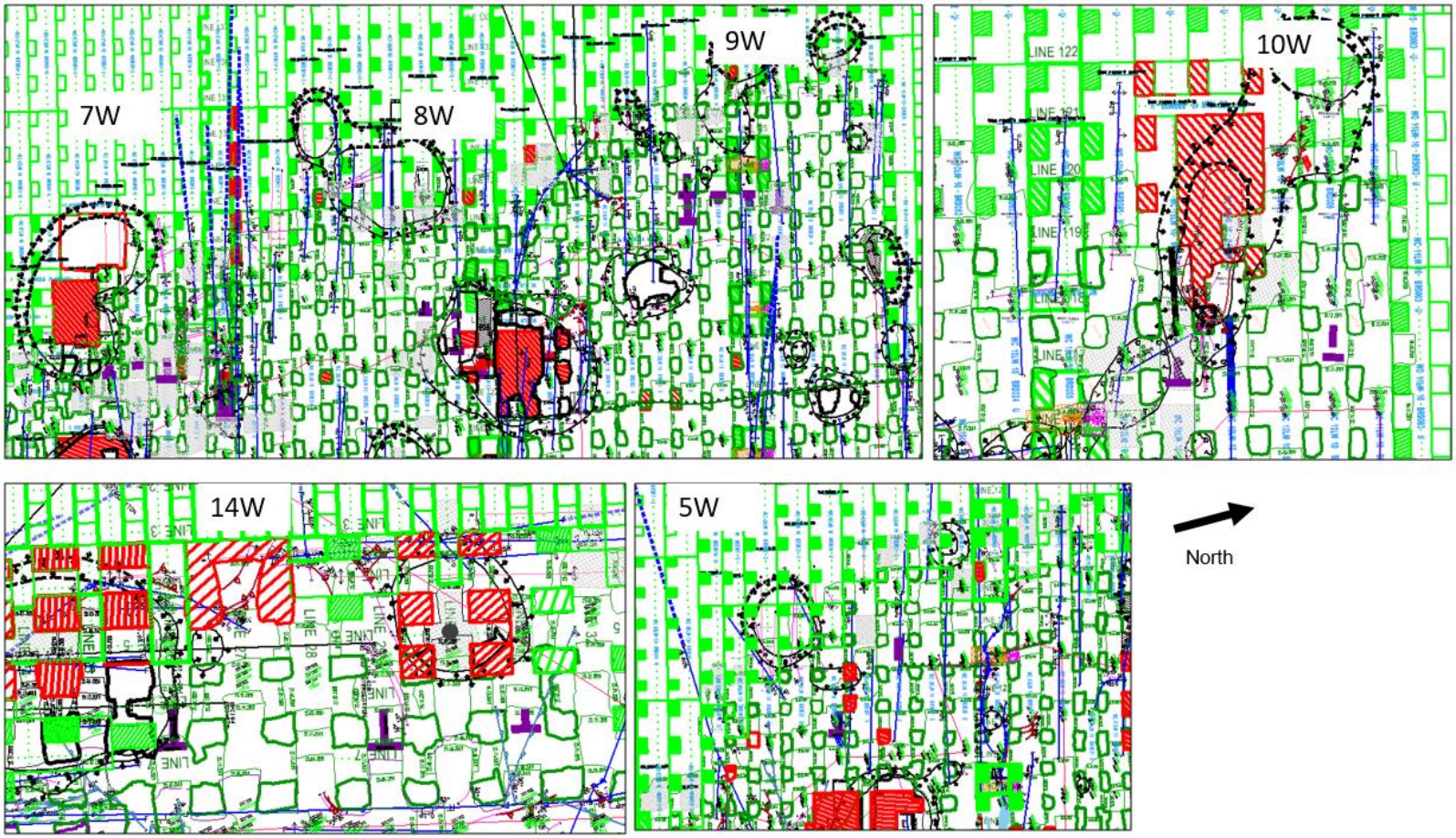

Figure 3-1. Plan view of the western side of Central shaft showing sections where mapping was done.

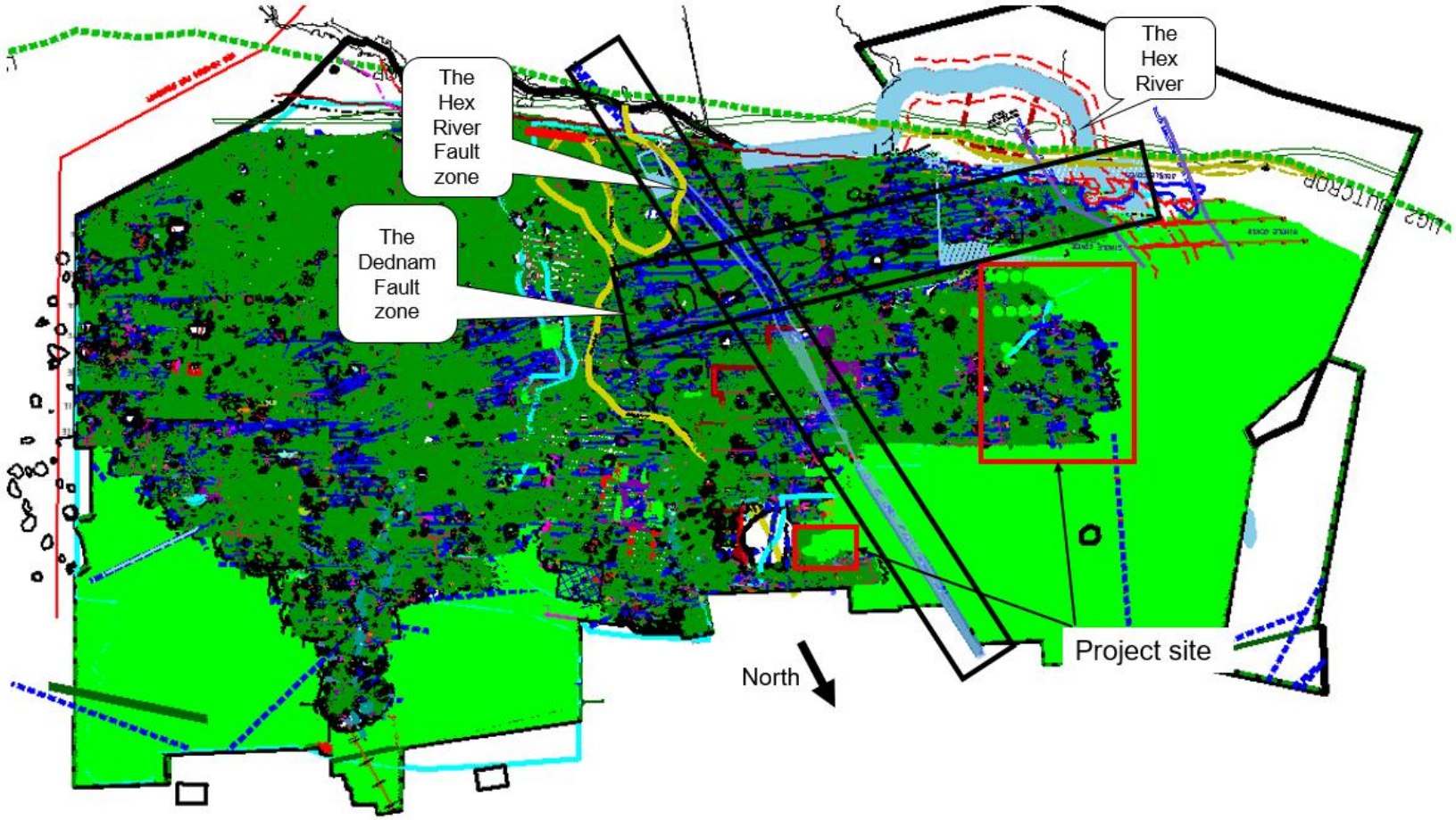

Figure 3-2. Plan view of Bathopele Mine showing the area where the investigation was done and major geological structures.

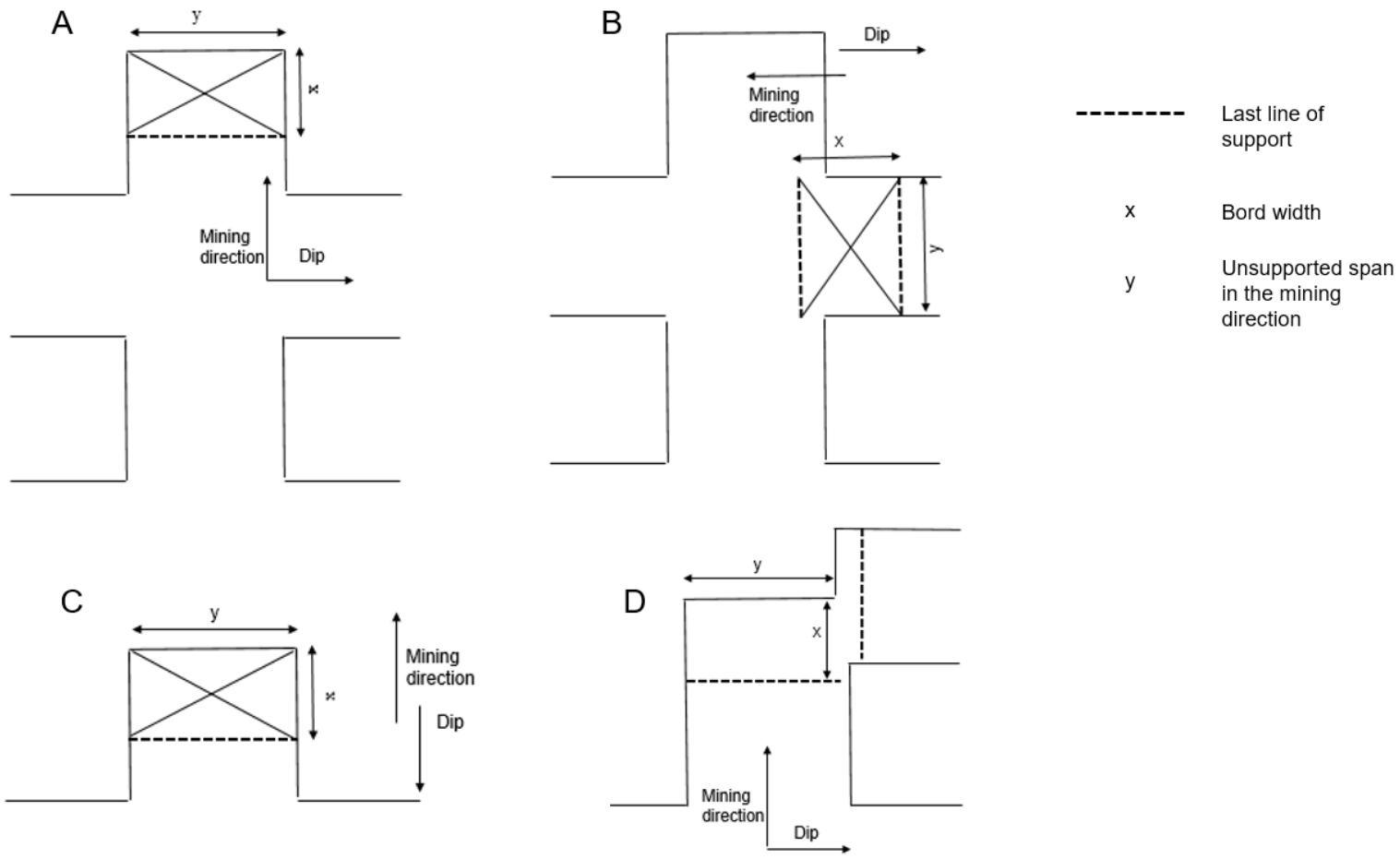

Figure 3-3. Various face area possibilities with respect to mining direction.

3.1 Orientation, Persistence and Shear Strength Properties of the Discontinuities

JBlock is the primary method of analysis in this research. According to Kemeny and Post (as cited by Nezomba, 2012), the recommended method of collection of data for JBlock analysis is scanline mapping. The scanline mapping technique is described in the literature by many authors including Brady and Brown (2004). Scanline mapping is associated with four main types of sampling bias, namely; orientation bias, size bias, truncation bias and censoring bias. The rationale and methods used in minimising sampling bias are included in the discussions that follow.

3.1.1 Data on hangingwall layers

Two scanlines perpendicular to each other (one on dip and the other on strike) and a borehole drilled into the hangingwall are recommended to reduce the orientation bias (Nezomba, 2012). Although an extensive borehole database is available at Bathopele, the data was not collected at the exact locations where scanline mapping was done during this project.

The borehole data was processed in 2016 from 3514 boreholes in Central shaft to determine the trend of the chromitite layers above the hangingwall. It was concluded, in 2016, that the height of the potential parting planes, above the hangingwall, at Bathopele does not change except in potholes and slump areas (Matsobane, 2016c). It is for this reason that the current Company procedure

requires boreholes to be drilled only in areas with a change in hangingwall composition to confirm the positions of chromitite layers.

It was also observed that depending on the type of camera being used, only prominent structures with discernible separation and/or infill can be identified during borehole inspections. Taking into account that borehole inspection is a point inspection, it is also difficult to establish the type, orientation and persistence of the features identified in the hole. It was for these reasons that the orthogonal scanlines and the data of prominent partings already available from borehole inspections in nearby areas were considered to be sufficient to complete the research.

A summary of the borehole data that was compiled in 2016 is provided in Table 3-1 and a scatter plot of the position of the triplets is provided in Figure 3-4, showing the average position of the triplets in Central shaft. In normal ground conditions away from potholes and reef rolls, triplets are 4.5 m above the leader seam and the double chrome stringers, 1 m below the triplets. Therefore, the mean height of 3.7 m for triplets is influenced strongly by the high number of potholes.

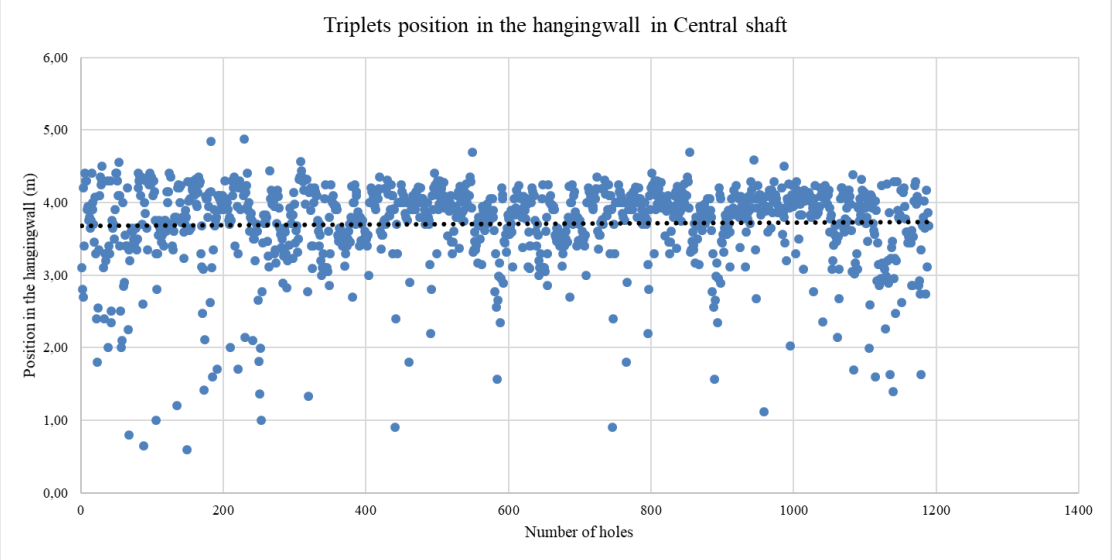

Figure 3-4. Position of triplets as observed from borehole inspections.

Table 3-1. Position of parting planes as observed from borehole inspections.

Parting	Parting plane data	
	Average (m)	Std Dev (m)
Triplets	3.7	0.57
Single chrome stringer	3.2	0.99
Double chrome stringers	3.45	0.57

3.1.2 Joint data collection

A log of the scanlines mapped during this research is provided in Appendix C.1 and the joint data is provided in Appendix C.2. A total of 49 scanlines were mapped for this project, comprised of 26 scanlines on dip and 23 on strike. The total length of the scanline amounts to 377.4 m.

A plan view of the portion of the mine that was mapped by geologists is provided in Figure 3-5. The pink lines represent joints and veins and the blue lines represent faults. The numbers with the letter ‘W’ are strike sections and those are the sections where mapping was conducted. It can be noted from Figure 3-5 that the major joint sets strike as follows: ESE-WNW, W-E and S-N. It was therefore easy to confirm the integrity of the mapping because of the extensive mapping done by the geology department. Based on the known orientation of the structures, it was concluded that all prominent joint sets will be captured within the two orthogonal scanlines and therefore alleviating the orientation bias.

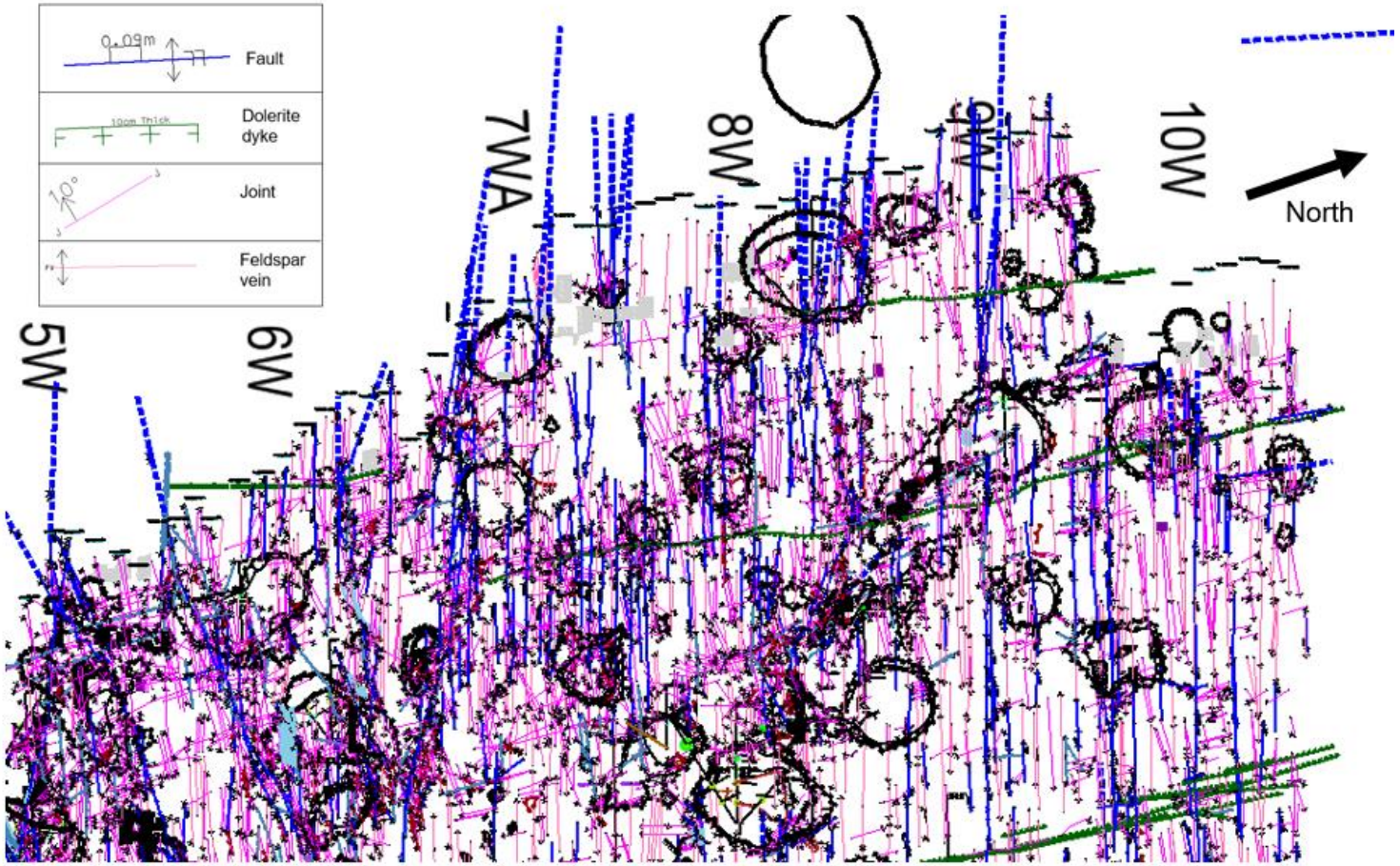

Figure 3-5. A plan view of Central shaft sections showing geology mapped by the geology department.

Blasting fractures and structures with a trace length of less than 0.5 m were not mapped. Even though 33 % of the FOGs within the face area had a width of less than 0.5 m, only three of those were in the dual seam section. From observations, such structures can be easily identified and addressed by barring or areal coverage support where required, provided entry examination is conducted correctly. Furthermore, such structures are not considered prominent as per current COP and TARP procedure.

Another factor to consider is the trace length of the prominent discontinuities. It can be noted from the joint data that persistence was captured in terms of length range. Taking into consideration the maximum length of FOG at Bathopele of 14 m (average length of 2.5 m), bord width of 10 m and diagonal span of 14.5 m, trace length beyond 15 m should not be a concern at Bathopele, unless striking parallel to mining direction along the axis of the panel.

3.1.3 Joint data processing

The data collected was processed using DIPS. Joint sets can be clustered and analysed from a pole plot generated in DIPS. This was done by drawing a window set around the poles concentrated in a specific area to group data related to a specific joint set (Rocscience, 2002). Figure 3-6 depicts a pole and

contour plot from DIPS. Orientation, true spacing, trace lengths and friction angles were calculated from data related to specific joint sets. A summary of the joint data is provided in Table 3-2. The data is also presented on plan view in Figure 3-7.

The location of the structures along the scanline captured during mapping were used to calculate the joint spacing. However, the joint spacing calculated from the locations is not true spacing unless the structure is perpendicular to the scanline (Figure 3-8). The true spacing for joints sets was calculated using the off-set angle captured during mapping and the following equation:

$$\boldsymbol{d = l\,sin\theta} \qquad \textbf{\textit{Equation 3-1}}$$

Where: d is the true joint spacing,

l is the apparent spacing, and

θ is the offset angle (°).

Using the range of the trace length captured under the 'persistence' column, the average for each persistence range for each structure was calculated. The data provided in Table 3-2 was determined from the calculated averages.

The Barton (2002) model was used to calculate friction angle of the joints. The values used to calculate the angles are provided in Table 3-3. The handbook on Using the Q-system by NGI was used to establish the joint roughness and joint alteration numbers (Barton, 2015). The following formula was used to calculate the friction angle:

$$\Phi = tan^{-1}\frac{j_r}{j_a} \qquad \textit{Equation 3-2}$$

Where: Φ is the friction angle

j_r is the joint roughness number, and

j_a is the joint alteration number.

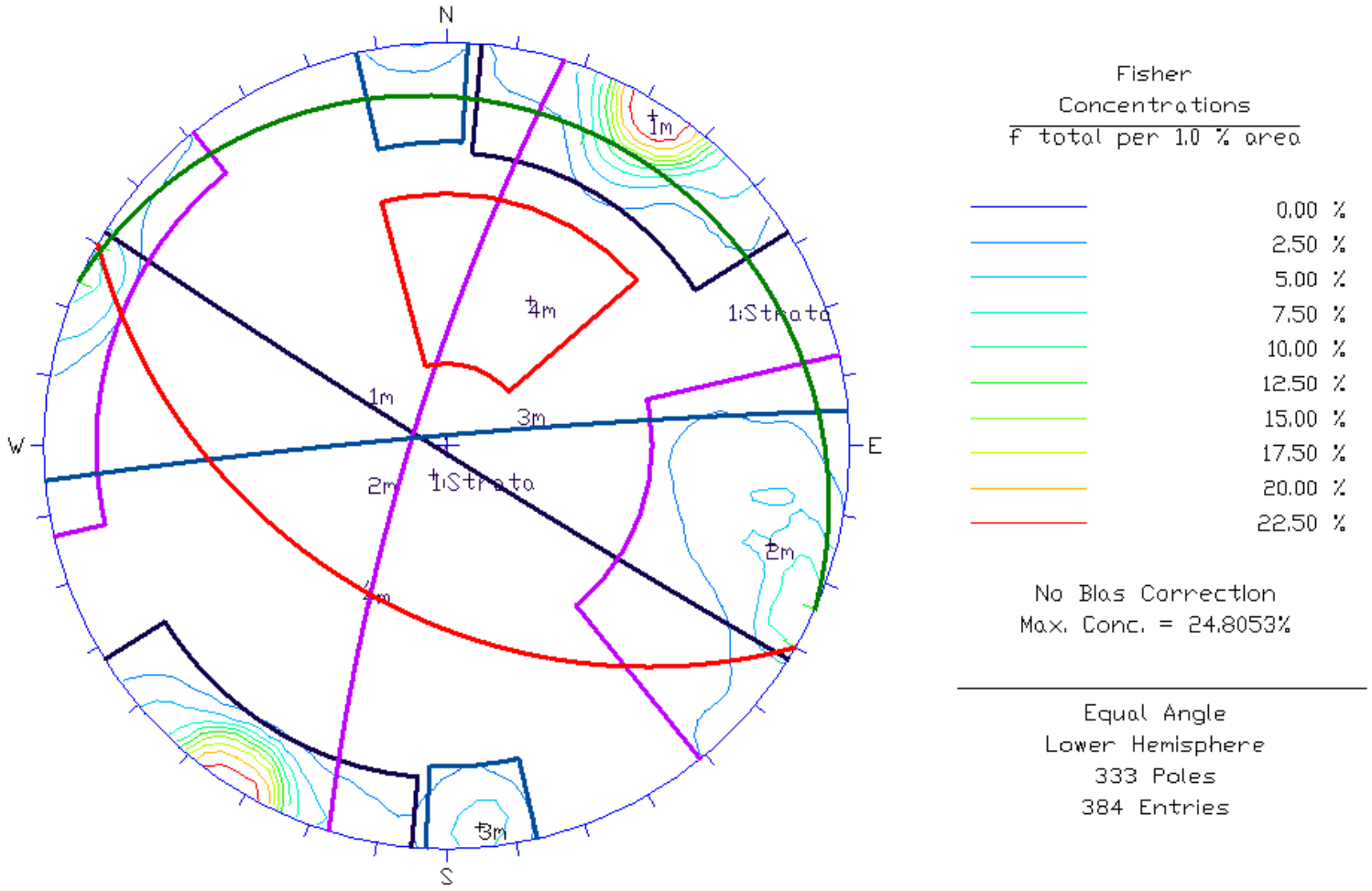

Figure 3-6. Stereographic pole contour plot of mapped discontinuities.

Table 3-2. Summarised joint properties.

Set	Orientation (°)				Friction angle (°)		Spacing (m)			Length (m)		
	Dip		Dip direction									
	Mean	Std Dev	Mean	Std Dev	Mean	Std Dev	Min	Ave	Max	Min	Ave	Max
J1	86.67	4.37	203.59	9.60	23.85	15.07	0.040	0.73	5.32	1.00	14.94	30.00
J2	79.78	10.20	284.73	14.25	27.21	15.08	0.060	1.09	10.74	1.00	10.65	30.00
J3	83.51	8.13	312.39	28.45	21.52	14.39	0.020	0.51	1.69	1.00	11.03	30.00
R1	45.00	14.14	199.00	13.36	14.97	6.37	0.050	1.29	3.04	7.50	15.00	30.00

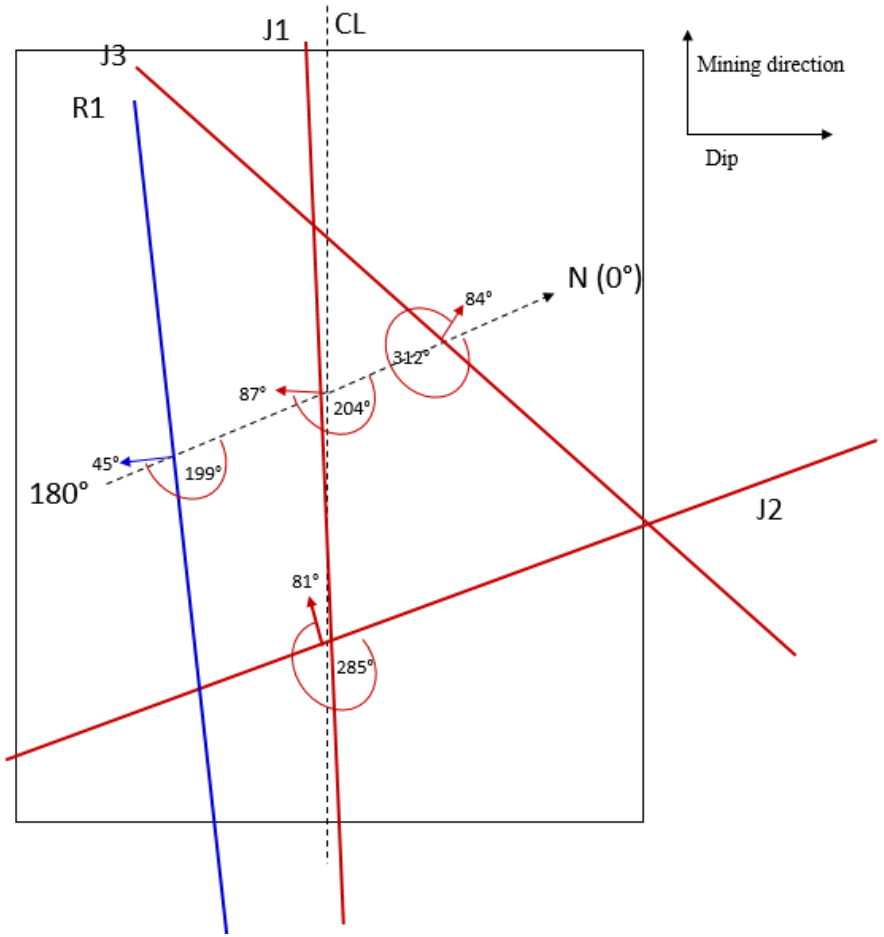

Figure 3-7. Mapped joints on plan as established from scanline mapping.

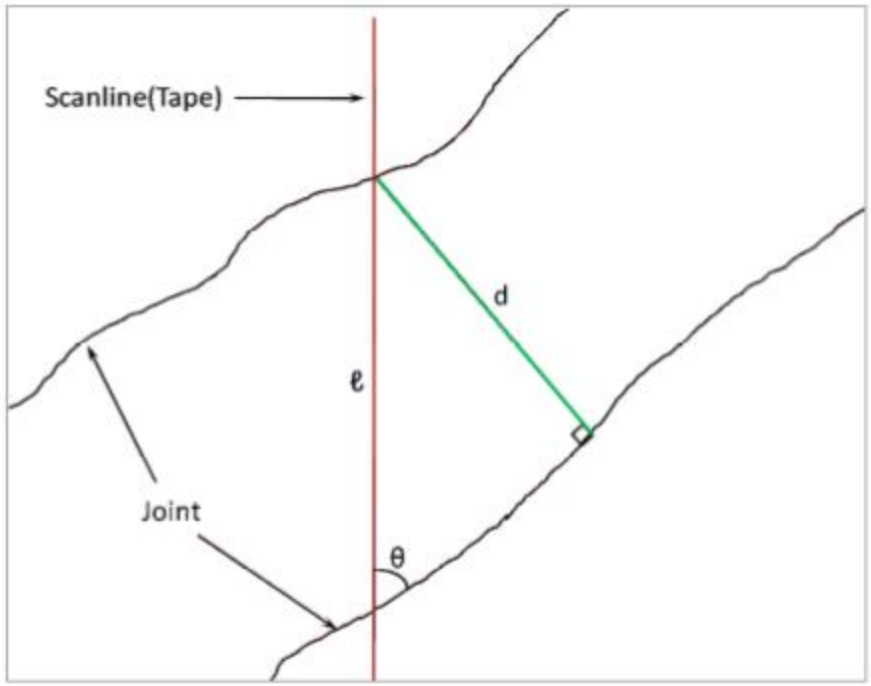

Figure 3-8. Correction for joint spacing error (Nezomba, 2012).

Table 3-3. Values used to calculate friction angle.

Infill type	Thickness	Jr	Ja
Serpentinite	<3 mm	*	4
	>3 mm	1	8
Pegmatite/calcite	<10 mm	*	3
	>10 mm	1	3
Surface staining	None	*	1
No infill	n/a	*	1
* Use surface shape and surface roughness description e.g. rough and planar = 1.5 and smooth and planar = 1			

3.2 Support Units Details

1.6 m resin bolts are used at Bathopele as primary support and 3 m coupling bolts are used as secondary support. Cable anchors are used to supplement coupling bolts where required. The spacing of the primary support for normal ground conditions at Bathopele is 1.2 m x 1.5 m, with 1.2 m in the mining direction. The tolerance on support spacing as specified in the COP is 0.2 m.

The primary aim of this research is to assist TARP members in addressing TARP triggers and as such, the ground conditions are those that would have not been anticipated in most cases. The majority of bords at Bathopele are TP2 bords as shown in Figure 3-9. The common practice is to support TP2 panels with 1.6 m resin bolts at 1 m x 1 m spacing. TP3 panels at Bathopele are normally supported at 1 m x 1 m in addition to 3 m coupling bolts, which are installed only in a specific portion of the panel. It is for these reasons that the support units to be used in the models are 1.6 m resin bolts at a spacing of 1 m x 1 m. Laboratory tests and pull tests results are provided in

Appendices D.1, D.2, D.3 and D.4 for the support used in the models. The pull tests show that, given proper mixing of resin and correct installation, over 14 t can be achieved from only 250 mm length of the bolt.

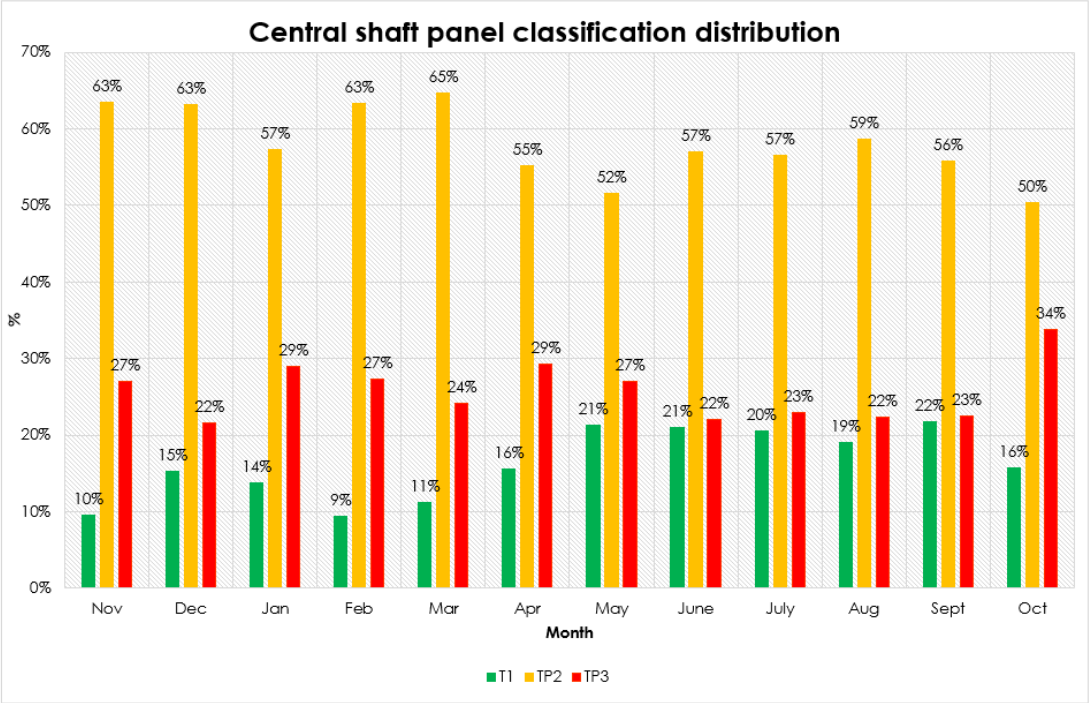

Figure 3-9. Central shaft panel classification distribution for 2018-2019 Oct (Sephaphathi, 2019).

3.3 Chapter Summary

Data collection and processing methods are discussed in this chapter. The data required to carry-out the face area analysis is presented. Using the methods discussed in Chapter 2 and the data presented in this chapter, Chapter 4 is about the actual modelling to determine behaviour.

4 MODELLING SET-UP AND RESULTS

There were various modelling methods used to achieve the objective of this research as discussed in Chapter 2. The model set-up, input parameters and results from each method are provided in the sections that follow.

The following points were considered prior to, and during, model set-up:

i. Ground conditions made up of vertical joints are stable. It is only when the block sizes decrease due to decreased joint spacing, and exposure due to over-breaking, where failure occurred on the periphery of the excavation, and between support units. These blocks are usually small and can be accommodated by barring or areal coverage support. The models involving these kind of ground conditions serve as a base model.

ii. Parting planes 1 m above the hangingwall are stable in the presence of vertical joints. Modelling partings planes at normal positions as shown in Table 4-1 would be pointless.

iii. Large falls are expected in the models where shallow dipping structures are included according to the literature and FOG analysis.

Table 4-1. Position of parting planes as observed from borehole inspections.

Parting	Parting plane data	
	Average (m)	**Std Dev (m)**
Triplets	3.70	0.57
Single chrome stringer	3.2	0.99
Double chrome stringers	3.45	0.57

Table 4-2 shows the various ground conditions that have resulted in FOGs within the face area. Those ground conditions were considered in this project. Ground conditions with IRUPS are excluded from the list because an appropriate method of assessing IRUPS could not be established. The letters A to J or the dip direction of the ramp structures were used in the models instead of giving full description of the ground conditions.

Table 4-2. Ground conditions considered during the project and their references.

<table>
<tr><th>Ground conditions reference</th><th colspan="2">Ground conditions considered</th></tr>
<tr><td>A</td><td colspan="2">Normal ground conditions with near vertical joints as determined from Dips data</td></tr>
<tr><td>B</td><td colspan="2">Normal ground conditions from Dips data plus Chromitite parting at <1 m in the hangingwall</td></tr>
<tr><td>C</td><td colspan="2">"A" ground conditions plus shallow dipping features as per Dips data (R1)</td></tr>
<tr><td>D</td><td rowspan="2">"A" ground conditions plus 45° shallow dipping feature in normal ground - sub parallel to mining direction</td><td>Dip direction same as the orebody, 45°, 024°</td></tr>
<tr><td>E</td><td>Dip direction opposite that of the orebody, 45°, 204°</td></tr>
<tr><td>F</td><td rowspan="2">"A" ground conditions plus 45° shallow dipping feature in normal ground - oblique to mining direction</td><td>Dip direction same as the orebody, 45°, 000°</td></tr>
<tr><td>G</td><td>Dip direction opposite that of the orebody, 45°, 180°</td></tr>
<tr><td>H</td><td rowspan="2">"A" ground conditions plus 45° shallow dipping feature in normal ground - perpendicular to mining direction</td><td>Dip direction same as the mining direction, 45°, 294°</td></tr>
<tr><td>I</td><td>Dip direction opposite that of the mining direction, 45°, 114°</td></tr>
<tr><td>J</td><td colspan="2">Shear zone</td></tr>
</table>

4.1 Assessment of Ground Conditions Using the Modified Stability Graph

The problem of the rockmass and the excavation can be addressed through the Modified Stability Graph Method by using the Modified Stability Number, N' (Hutchinson and Diederichs, 1996). As discussed in Chapter 1, N' is determined from Q', which is calculated from Barton's Q equation minus the last quotient in the equation. N' is determined as follows:

$$N' = Q' x\ A\ x\ B\ x\ C \qquad \textit{Equation 4-1}$$

Where:

$$Q' = \left({}^{RQD}/_{J_n}\right) x\ \left({}^{J_r}/_{J_n}\right) \qquad \textit{Equation 4-2}$$

RQD was calculated from the joint volume (J_v) collected with RMR data. J_v was also calculated from joint spacing using Palmström's joint spacing equation for comparison purposes, as follows:

$$RQD = 110 - 2.5J_V \qquad \textit{Equation 4-3}$$

for J_v between 4 and 44

$$J_v = \left({}^{1}/_{S_1}\right) + \left({}^{1}/_{S_2}\right) + \left({}^{1}/_{S_2}\right) \qquad \textit{Equation 4-4}$$

where S is the joint spacing (Palmström, 1982).

The average spacing as determined from scanline mapping analysis was considered in establishing the appropriate joint volume. The maximum J_v from RMC data was not used for further analysis because it is the worst-case scenario and it is usually localised to a small area from observations. The J_v average of 8.7 as shown in Table 4-3 was therefore used in the rest of the calculations.

Table 4-3. Calculation of joint volume from joint spacing and rock mass classification data.

	Minimum	Average	Maximum
Jv (From SL data)	91.66	4.25	0.87
RQD - SL		99.38	
Jv (From RMR data)	2	8.70	21.00
RQD - RMR		93.25	62.50

J_n, J_r and J_a were determined from Barton's Q tables. The selections are provided in Appendix E.1 and further details are shown below:

i. **J_n**: For a given area, the jointing at Bathopele based on RMC data is usually characterized by two joint sets plus random joints or 3 joint sets. The joint set number is therefore between 6 and 9. A value of 9 was selected for this analysis (Appendix E.1).

ii. **J_r**: The discontinuities at Bathopele are smooth and planar and therefore a value of 1 was selected. Occasionally, low angled structures may have slickensides. A value of 0.5 was considered for such structures (Appendix E.1).

iii. **J_a**: Softening, clay minerals that are less than 5 mm in thickness were used in the calculation. A value of 8 was therefore selected (Appendix E.1)

Hutchinson and Diederichs (1996) discuss in detail how to determine the A, B and C factors. The equations and the graphs used in determining the factors are provided in Appendix E.2 and Appendix E.3.

i. **Factor A**: The uniaxial compressive strength (UCS) of feldspathic pyroxenite (i.e. hangingwall) has been determined to be 156 MPa on average from rock laboratory tests (Chen, 2015). At a maximum depth of 510 m below surface, the maximum induced stress is less than 15 MPa. Therefore, factor A of 1 was used in the analysis (Appendix E.2).

ii. **Factor B**: the angle between the hangingwall and the dominating feature (i.e. α) was calculated using the equations provided in Appendix E.2. The calculation results are provided in Table 4-4.

iii. **Factor C:** The gravity adjustment factor C was determined to be 2 based on an average dip angle of 9° of the hangingwall (Appendix E.2).

Table 4-4. Calculation for factor B.

Factor B calculation								
	Hangingwall	**C**	**D**	**E**	**F**	**G**	**H**	**I**
Dip direction	24.00	199.00	24.00	204.00	0.00	180.00	294.00	114.00
Dip	9.00	45.00	45.00	45.00	45.00	45.00	45.00	45.00
Trend	204.00	19.00	204.00	24.00	180.00	360.00	114.00	294.00
Plunge	81.00	45.00	45.00	45.00	45.00	45.00	45.00	45.00
N_w	-0.14	0.67	-0.65	0.65	-0.71	0.71	-0.29	0.29
E_w	-0.06	0.23	-0.29	0.29	0.00	0.00	0.65	-0.65
D_w	0.99	0.71	0.71	0.71	0.71	0.71	0.71	0.71
w.j		0.59	0.81	0.59	0.80	0.60	0.70	0.70
α		0.94	0.63	0.94	0.64	0.93	0.80	0.80
		53.97	**36.00**	**54.00**	**36.92**	**53.32**	**45.70**	**45.70**
		0.70	0.30	0.70	0.30	0.70	0.50	0.50

The calculation results of N’ values are provided in Table 4-5 and 4-6 for cases where the low angled structures are slickensided and where the infill is only serpentinite.

Table 4-5. N' Calculation results for slickensided low angled joints.

N' calculation results with low angled features that are slickensided								
	From Dips	**Parallel to mining direction**		**Oblique to mining direction**		**Perpendicular to mining direction**		**Shear zone**
	C	D	E	F	G	H	I	J
	199	24	204	0	180	294	114	199
Jn	9	9	9	9	9	9	9	20
Jr	0.5	0.5	0.5	0.5	0.5	0.5	0.5	0.5
Ja	8	8	8	8	8	8	8	10
A	1	1	1	1	1	1	1	1
B	0.7	0.3	0.7	0.3	0.7	0.5	0.5	0.6
C	2	2	2	2	2	2	2	2
Q'	0.65	0.65	0.65	0.65	0.65	0.65	0.65	0.16
N'	0.91	0.39	0.91	0.39	0.91	0.65	0.65	0.19

Table 4-6. N' Calculation results for low angled joints with serpentinite infill only.

N' calculation results with low angled features with serpentinte infill only									
	From Dips	**Parting**	**From Dips**	**Parallel to mining direction**		**Oblique to mining direction**		**Perpendicular to mining direction**	
	Base line - A ground conditions	B	C	D	E	F	G	H	I
		Parting	199	24	204	0	180	294	114
Jn	9	9	9	9	9	9	9	9	9
Jr	1	1.5	1	1	1	1	1	1	1
Ja	4	5	8	8	8	8	8	8	8
A	1	1	1	1	1	1	1	1	1
B	1	0.3	0.7	0.3	0.7	0.3	0.7	0.5	0.5
C	2	2	2	2	2	2	2	2	2
Q'	2.59	3.11	1.30	1.30	1.30	1.30	1.30	1.30	1.30
N'	5.18	1.87	1.81	0.78	1.81	0.78	1.81	1.30	1.30

The problem of the excavation size is addressed through hydraulic radius. The hydraulic radius is calculated as follows (Hutchinson & Diederichs, 1996):

$$HR = {Area}/{Perimeter} = {(w\ x\ l)}/{2(w + l)} \qquad \textit{Equation 4-5}$$

The HR was calculated using the "*w*" and the "*l*" parameters shown in Figure 4-1. The "*w"* and the "*l"* in the calculation refer to the dimensions of a bord as shown in Figure 4-1. The "*w*" on the plan and in the calculation refers to the span of the bord on dip and it is varied from 4 m up to 10 m in the calculation of HR. The "*l*" on the plan refers to the length of the panel on strike. The "*l*" was varied from 2 m up to 30 m.

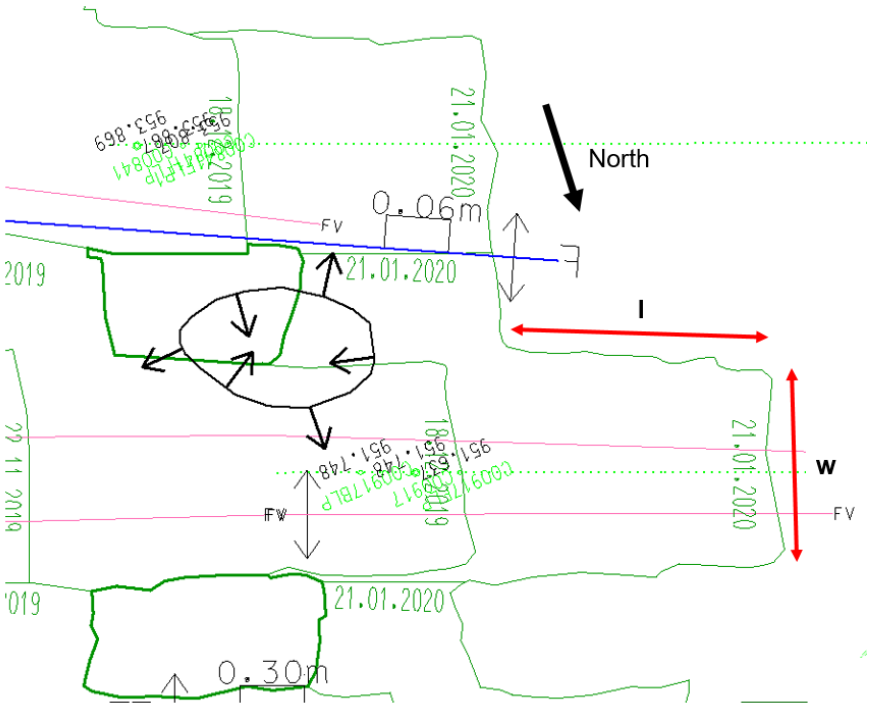

Figure 4-1. Hydraulic radius parameters.

The purpose of this exercise is to assess the face area which is limited to maximum 4.5 m in the mining direction and 10 m for the span of the excavation. Intersections are therefore excluded in this study. Due to ventilation constraints, ideally excavations must not be advanced to more than 15 m without a holing (P. J. du Toit 2020, pers. Comm., 19 May). The calculations were done up to 30 m because there are excavations that are mined beyond 15 m without a holing due to poor ground conditions and potholes. Such excavations are mined with ventilation ducts and fans (P. J. du Toit 2020, pers. Comm., 19 May). It is for this reason that the length of the panel i.e. "*l*" was cut-off at 30 m. The minimum length used was 2 m to account for situations where advance per blast may be reduced. The calculation results of the HR are provided in Table 4-7 and Figure 4-2.

Table 4-7. Calculation results for hydraulic radius for different mining span and length of panels.

Panel length	Hydraulic Radius (m)						
L (m)	**4m span**	**5m span**	**6m span**	**7m span**	**8m span**	**9m span**	**10m span**
2	0.67	0.71	0.75	0.78	0.80	0.82	0.83
3	0.86	0.94	1.00	1.05	1.09	1.13	1.15
4	1.00	1.11	1.20	1.27	1.33	1.38	1.43
4.5	1.06	1.18	1.29	1.37	1.44	1.50	1.55
5	1.11	1.25	1.36	1.46	1.54	1.61	1.67
6	1.20	1.36	1.50	1.62	1.71	1.80	1.88
7	1.27	1.46	1.62	1.75	1.87	1.97	2.06
8	1.33	1.54	1.71	1.87	2.00	2.12	2.22
9	1.38	1.61	1.80	1.97	2.12	2.25	2.37
10	1.43	1.67	1.88	2.06	2.22	2.37	2.50
11	1.47	1.72	1.94	2.14	2.32	2.48	2.62
12	1.50	1.76	2.00	2.21	2.40	2.57	2.73
13	1.53	1.81	2.05	2.28	2.48	2.66	2.83
14	1.56	1.84	2.10	2.33	2.55	2.74	2.92
15	1.58	1.88	2.14	2.39	2.61	2.81	3.00
16	1.60	1.90	2.18	2.43	2.67	2.88	3.08
17	1.62	1.93	2.22	2.48	2.72	2.94	3.15
18	1.64	1.96	2.25	2.52	2.77	3.00	3.21
19	1.65	1.98	2.28	2.56	2.81	3.05	3.28
20	1.67	2.00	2.31	2.59	2.86	3.10	3.33
21	1.68	2.02	2.33	2.63	2.90	3.15	3.39
22	1.69	2.04	2.36	2.66	2.93	3.19	3.44
23	1.70	2.05	2.38	2.68	2.97	3.23	3.48
24	1.71	2.07	2.40	2.71	3.00	3.27	3.53
25	1.72	2.08	2.42	2.73	3.03	3.31	3.57
26	1.73	2.10	2.44	2.76	3.06	3.34	3.61
27	1.74	2.11	2.45	2.78	3.09	3.38	3.65
28	1.75	2.12	2.47	2.80	3.11	3.41	3.68
29	1.76	2.13	2.49	2.82	3.14	3.43	3.72
30	1.76	2.14	2.50	2.84	3.16	3.46	3.75

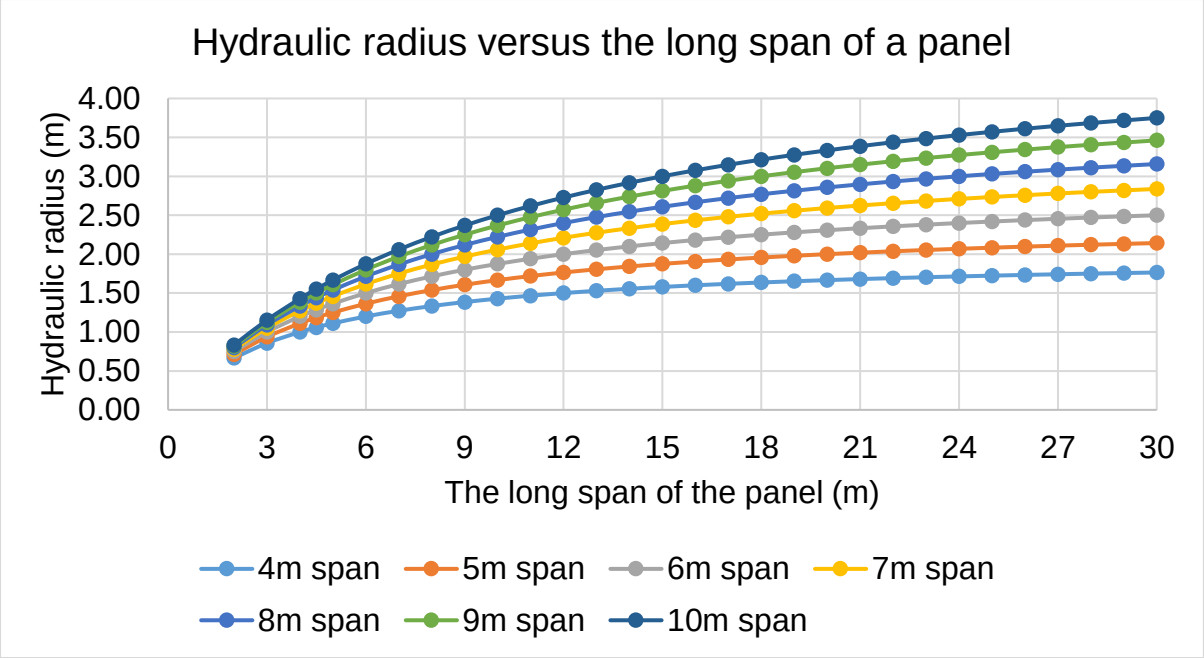

Figure 4-2. Hydraulic radius versus the long span of the panel.

The N' values were then plotted against the HR on the stability graph for both serpentinite and slickensided structures in Figure 4-3. The shaded rectangles in red and green in Figures 4-3 represent the minimum and the maximum values of the HR and N' values. The minimum and the maximum values of HR are those calculated in Table 4-7 and plotted in Figure 4-2. The minimum value of 0.83 m of the HR is included in the calculation and also on the graph in Figures 4-3 to check the effect of minimum length of bord on strike. This minimum length is a way of checking the effects of reducing advance per blast. The minimum and maximum values of N' represent normal ground conditions (i.e. maximum value of N') and very unfavourable ground conditions (i.e. minimum value of N'). The black vertical line represents HR at normal advance per blast of 4.5 m. Therefore, based on the geology at Bathopele, the advance per blast allowed and the maximum span of bords allowed (excluding bord intersections), the stability of the hangingwall can fall anywhere within the shaded rectangles in Figures 4-3.

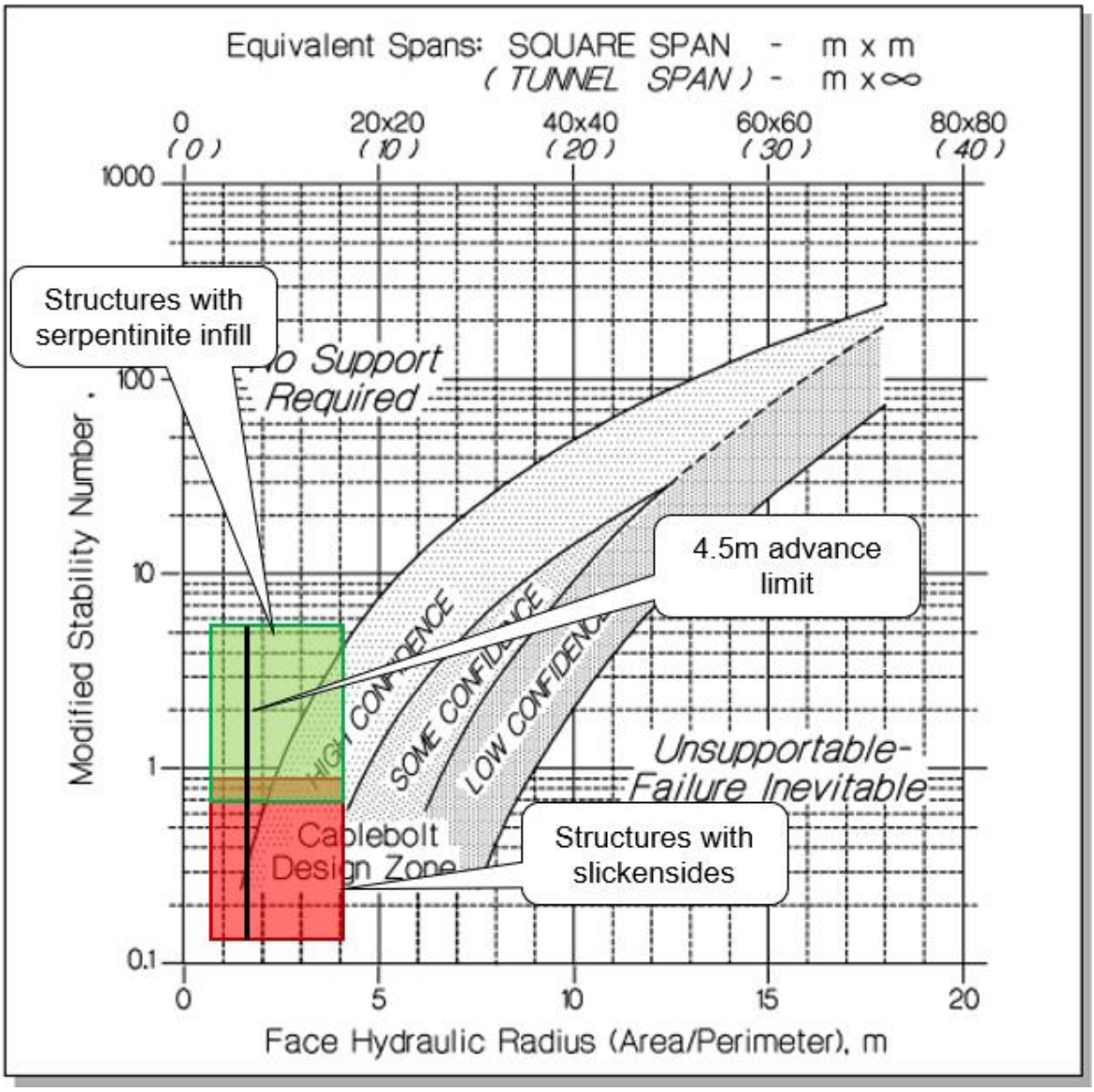

Figure 4-3. A plot of the calculated N' and hydraulic radius (After Hutchinson & Diederichs, 1996).

The purpose of this study is to analyse the face area, specifically the face area of a bord when mining is done on strike as illustrated in Figure 3-3. The analysis is to assist with TARP intervention. TARP is applied primarily in the face area. The assumption made in this study is that the ground conditions behind the face area have been adequately supported. The concern over the influence of the unsupported area on the last lines of support still remains.

To address this concern, consider “F” ground conditions (i.e. ground conditions with a shallow dipping structure striking obliquely to mining direction – Table 4-2) with N’ value of 0.78 (Table 4-6). The hangingwall should be stable upon intersection at 4.5 m advance as shown in Figure 4-4 but as the face advances, the support has to be sufficient to maintain hangingwall stability. However, if the shallow dipping structure has slickensides, hangingwall may be unstable. A reduction in advance per blast and reduction in excavation span would result is stable ground conditions. Therefore, stability of unsupported face area and the effectiveness of the last line of support would depend on the span of the excavation, the length of the excavation, the joint wall conditions, the orientation of the structure and the adequacy of the support in the back area.

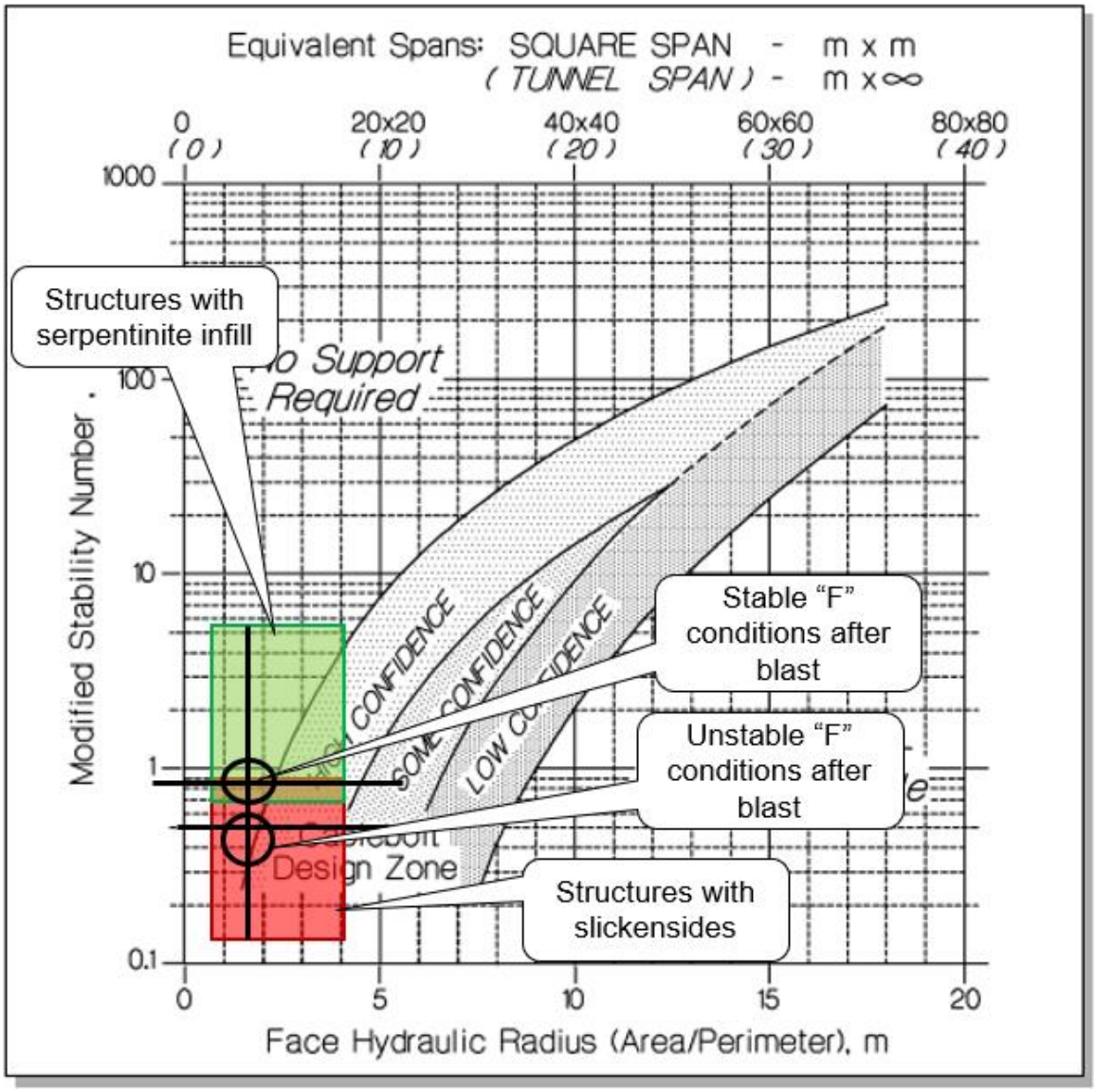

Figure 4-4. Assessment of "F" ground conditions using stability graph method showing the major influence of joint wall conditions and size of excavation (After Hutchinson & Diederichs, 1996).

The stability graph overall shows that:

i. Normal ground conditions in the face area at Bathopele are stable without support at 10 m span. However, as the density of the joints increases and the conditions of the joints become unfavourable, then the likelihood of instability increases. For ventilation purposes, the face should ideally not advance more

than 15 m without a holing at Bathopele. Taking this into consideration, then the maximum length of a 10 m wide panel would be 15 m and the hydraulic radius would be 3 m. Bearing the minimum HR of 3 m in mind, ground conditions with N' less than unity, in 10 m wide panels, require cablebolting (Figure 4-4). The analyses also suggest cablebolts as secondary support. At Bathopele, coupling bolts are used as substitute for cable bolts. The support resistance provided by coupling bolts is sufficient for the prevailing ground conditions.

ii. The likelihood of instability increases with an increase in panel span and length because the hydraulic radius is influenced by both dimensions, particularly at smaller lengths. A reduction in advance per blast would therefore be beneficial for poor ground conditions at smaller span.

iii. The influence of hangingwall layers on stability is evident, indicating that bolts are required.

iv. The influence of orientation of the low angled structures and joint wall condition is remarkable. Structures striking perpendicular to mining direction, irrespective of dip direction appear to be relatively less stable than those striking obliquely and sub-parallel to mining direction. It must be noted that alpha (as calculated in Table 4-4) is the same for structures striking perpendicular to mining direction irrespective of the dip direction.

v. Structures striking obliquely and sub-parallel to mining direction and dipping in the same direction as the hangingwall appear to be relatively more unstable

than structures striking perpendicular to mining direction and dipping in the opposite direction to the hangingwall

The explanation behind this may be that when the structure is dipping in the same direction as the hangingwall, the angle between the structure and the hangingwall is reduced as illustrated in Figure 4-5. Generally, the smaller the angle between the hangingwall and joint, the smaller the B factor as indicated in Appendix E.3.

vi. Rock mass conditions including a shear zone would fall on the minimum value of N' in Figure 4-4. Failure of a shear zone is likely at 10m span. This is also in agreement with the falls of ground that have occurred on shear zones and major fault zones at Bathopele where such geological structures tend to self-mine and require immediate support upon exposure.

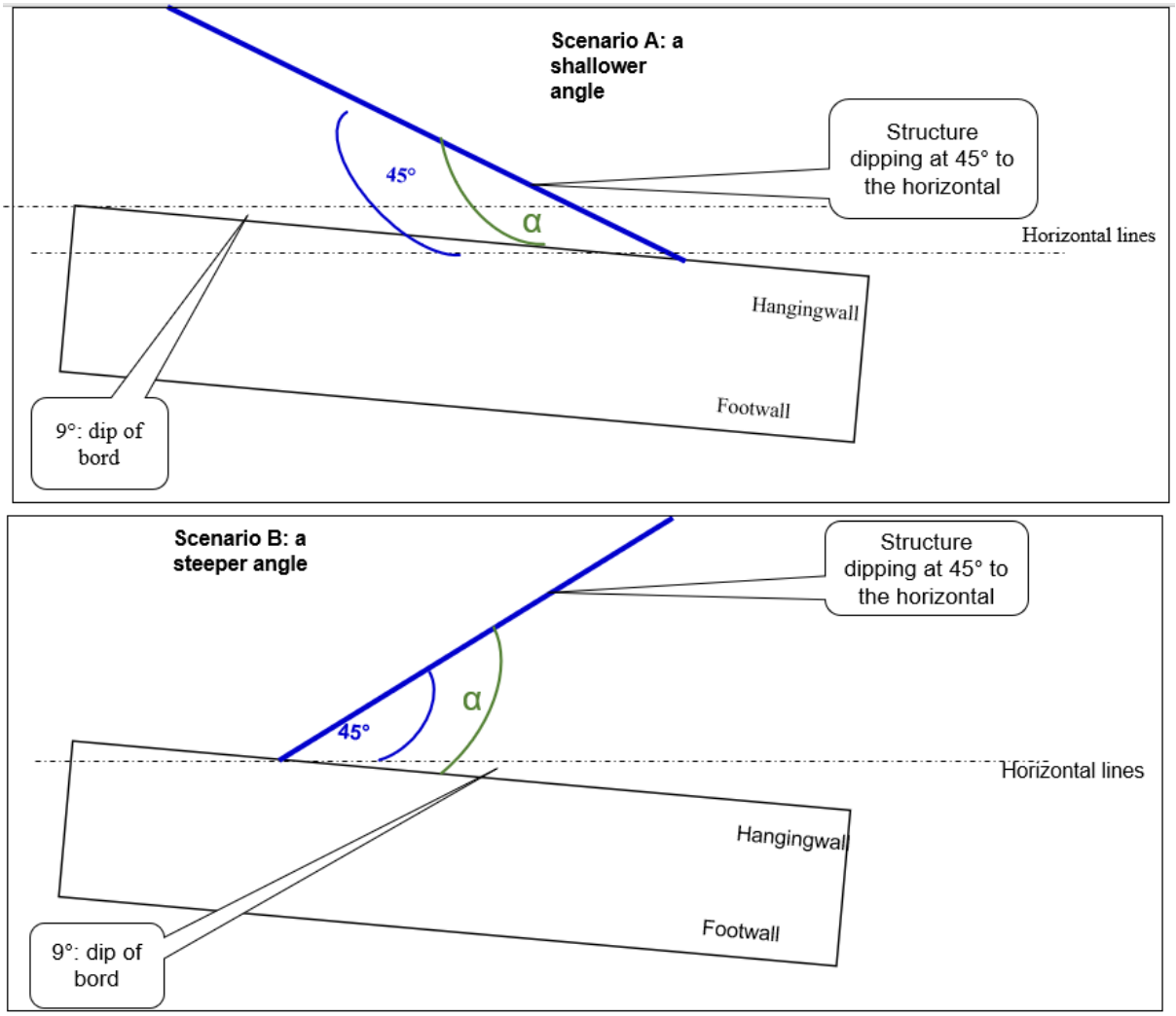

Figure 4-5. A demonstration of the influence of dip direction of low angled structures on the calculation of α.

The limitation of the stability graph method is that the assessment does not take into account the persistence of the structures and the position of the structures in the excavation. The assessment shows that certain shallow dipping structures may be more unstable than others but the presence of other geological structures on the weaker side of a shallow dipping structure is not explicitly taken into account. The presence of such structures might result in a wedge of unfavourable size depending on the angle of the low angled structure and its position in the hangingwall. To illustrate

this limitation, consider “A”, “B” and “C” scenarios in Figure 4-6. According to the Stability graph method, scenario “C” is unfavourable compared to scenario “A”. However, if the shallow dipping structure is positioned 1 m from the pillar, the scenario may be more favourable than scenario “A”. The method does not differentiate between scenario “B” and “C”.

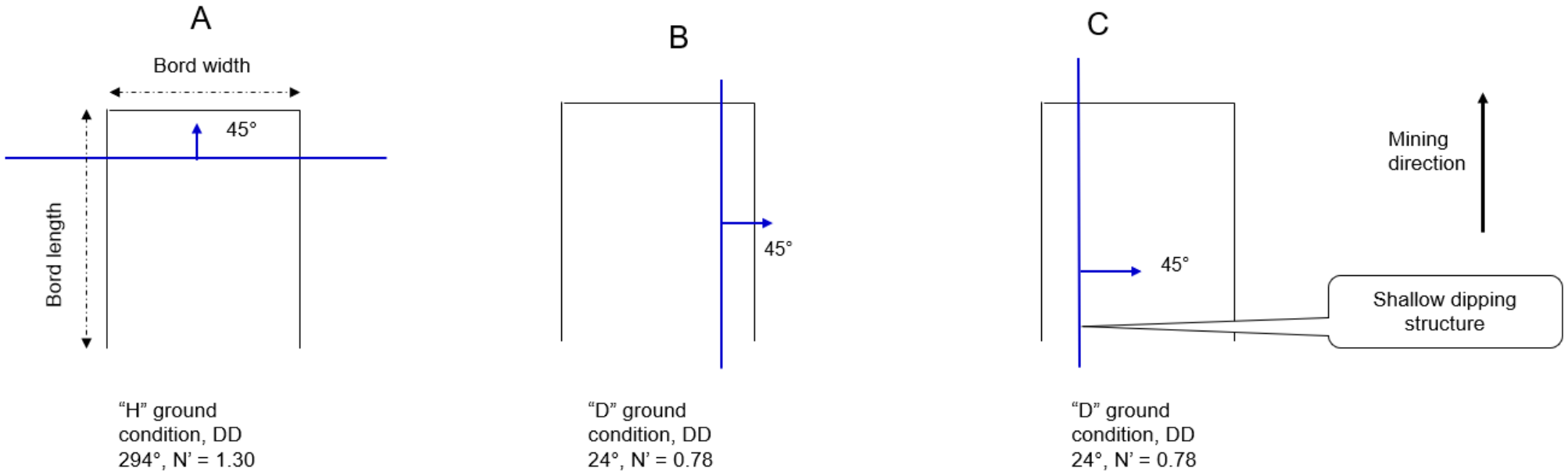

Figure 4-6. Illustration of the limitation of the Modified Stability Graph in terms of position of pervasive structures in a mining excavation.

The other limitation is that it does not address the position of the parting planes above the hangingwall. That is, the stability assessment results for a parting plane positioned at 2 m above the hangingwall would be the same as the results for a parting plane positioned at 4 m above the hangingwall.

4.2 Assessment of Ground Conditions Using JBlock

4.2.1 JBlock set-up and input parameters

Potential keyblocks are generated based on the geotechnical file and an excavation file. The geotechnical file describes the ground conditions to assess. Information regarding the size of the excavation, mining direction and advance per blast is captured in the excavation file. The advance per blast at this stage does not have an influence on the formation of keyblocks. The next step is to create a support scenario. At this stage, in addition to specification of the support in terms of spacing and capacity and type of support, the clamping force should be specified.

The geotechnical file was created using the joint data provided in Chapter 3. The rest of the geotechnical input values are provided in Table 4-8. The excavation file is as provided in Figure 4-7 and the input values for support unit parameters are shown in Figure 4-8. The aspect ratio and the mid-height clamping values were determined from the fall of ground database using the method recommended by Enslin and Spies (n.d.). The aspect ratio (i.e. width to height ratio) allowed in the model was based on the maximum FOT recorded at Bathopele in relation to the minimum allowable support spacing in terms of tendon support. According to Enslin and Spies (n.d.), Mid height = maximum thickness/2 and height to face area ratio = thickness/face area$^{1/2}$. Simulated

keyblocks were compared against actual FOGs to establish clamping stress at Bathopele, as follows:

i. The entire FOG database was considered instead of the FOGs that occurred within the face area;
ii. Outliers in terms of the larger sizes were not included in the analysis because these usually occurred on major fault zones or in areas with mixed support units;
iii. The Geotechnical file generated in JBlock was of similar ground conditions as those selected in the FOG database; and
iv. Only the FOGs where the source was in the hangingwall were used.

Table 4-8. Input parameters and values used in JBlock modelling.

Input parameter	Value	Units
Clamping stress	6	kPa
Minimum friction angle	10	°
Maximum friction angle	60	°
Minimum volume	0.001	m^3
Maximum volume	445	m^3
Aspect ratio	4.5	-
Mid height clamping	2.25	-
Height to face area ratio	1.9	-
Rock density	3200	Kg/m^3

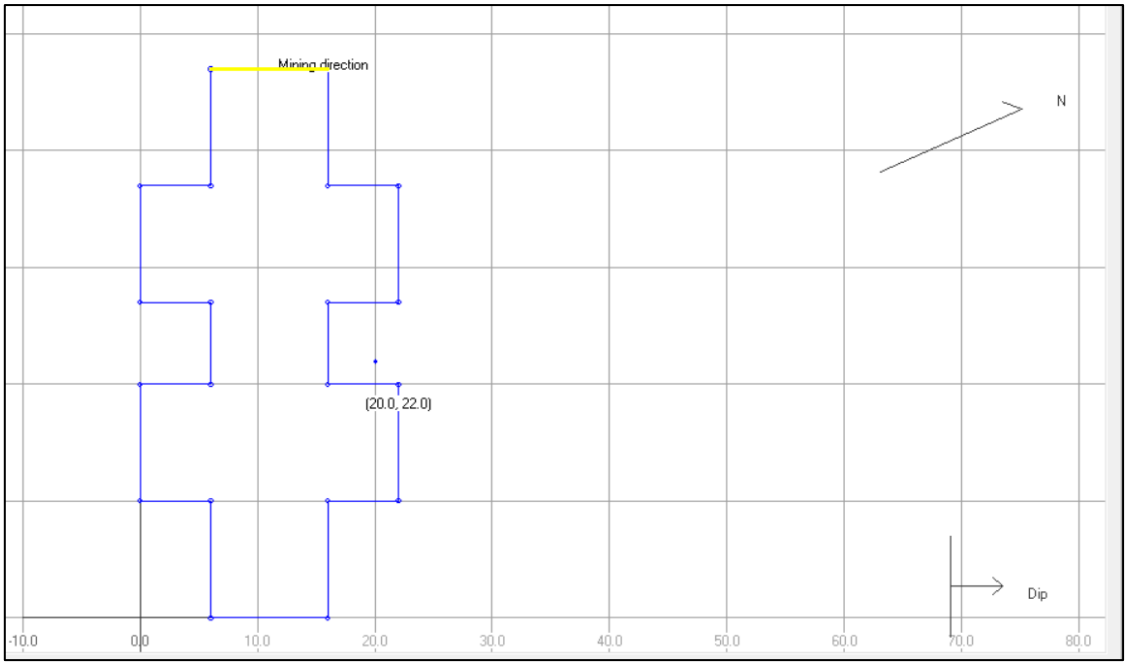

Figure 4-7. Excavation file in JBlock.

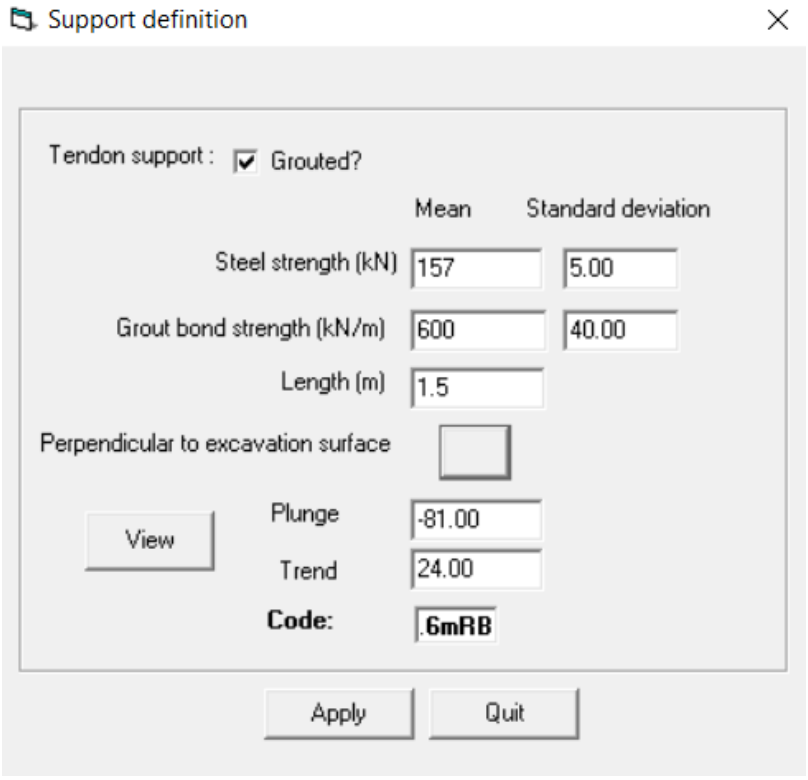

Figure 4-8. Support parameters and values used in JBlock.

10 000 keyblocks were generated. The results of the correlation exercise are provided in Figure 4-9. 6 kPa appears to have the best correlation to actual falls of ground,

except for the large falls. None of the clamping stresses correlated well for the large falls, but the majority of the falls of ground in reality are below about 80 m^2.

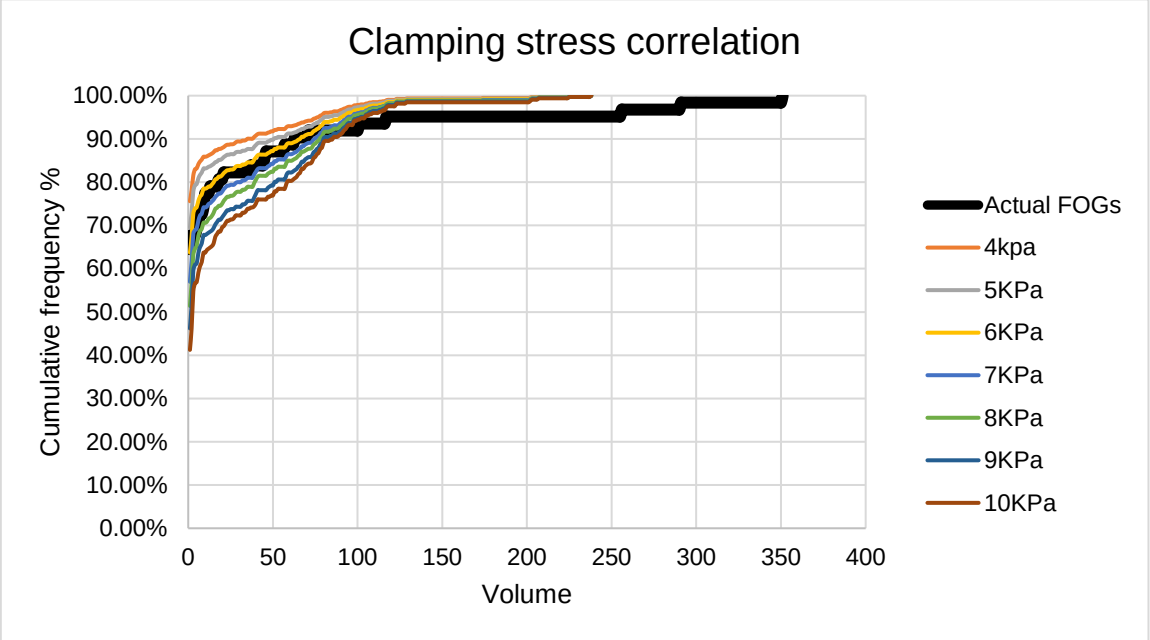

Figure 4-9. Clamping stress correlation.

4.2.2 JBlock results

The purpose of this project is to establish guidelines for TARP members when presented with ground conditions that have just been exposed after blast. It was for this reason that 'a cleaning shift' with support at 4 m behind the face (i.e. 3 m advance per blast), was simulated for the support scenario. The assessment initially was for ground conditions at 10 m span (i.e. current layout).

JBlock results are in a form of excel workbook containing data regarding keyblock dimensions, keyblock failure mode, support failure and cause of support failure. The keyblock dimensions are described in terms of the maximum edge, height, face area and volume of keyblocks. The maximum edge is the longest length of the keyblock in any direction (G. Kotze 2020, pers. Comm., 25 January). The face distance of the

keyblocks is also part of the results. The problem with the face distance is that it is the distance of the nearest corner of a keyblock to the face according to Joughin et al (2013). This is illustrated in Figure 4-10. For keyblocks that result in support failure, the support unit can be anywhere in the keyblock, i.e. cantilever effects are not considered.

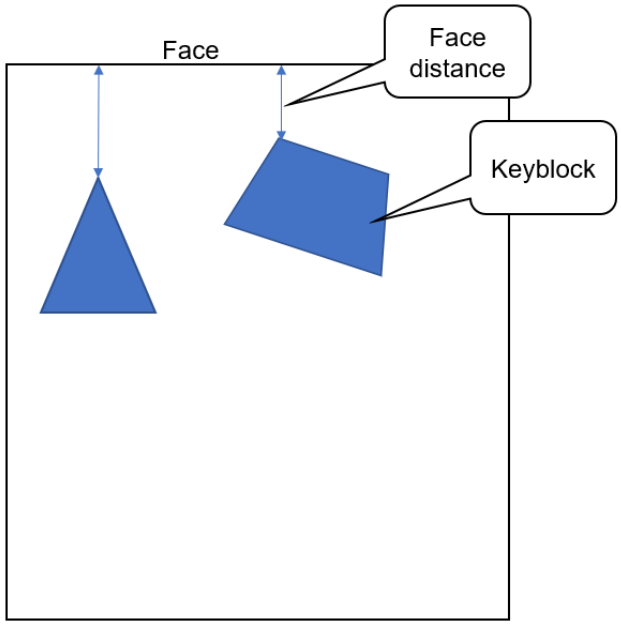

Figure 4-10. Demonstration of the meaning of face distance results from JBlock.

4.2.2.1 Assessment of normal ground conditions

The model was run with only joints sets 1 to 3. The maximum FOT was capped at 1.3 m. The results for normal ground conditions are summarized as follows and the graphs are provided in Figure 4-11 to 4-13 and Table 4-9:

i. The majority of the keyblocks occur within the face area peaking at 2.5 m-3 m from the face as shown in Figure 4-12. This may be attributed to lack of support

in the area. However, the keyblocks are small and smaller than the support spacing of 1 m^2 – (Figure 4-11, graph C).

ii. There are blocks that have the longest edges of 1.5 m and 2 m which is larger than support spacing. But the longest edge is in any direction and upon further analysis of the results data, the blocks are associated with height of no less than 0.96 m as shown in Figure 4-13.

iii. The keyblocks do not result in any support failure close to the face. Support failure is predicted at ±12 m from the face (Table 4-9).

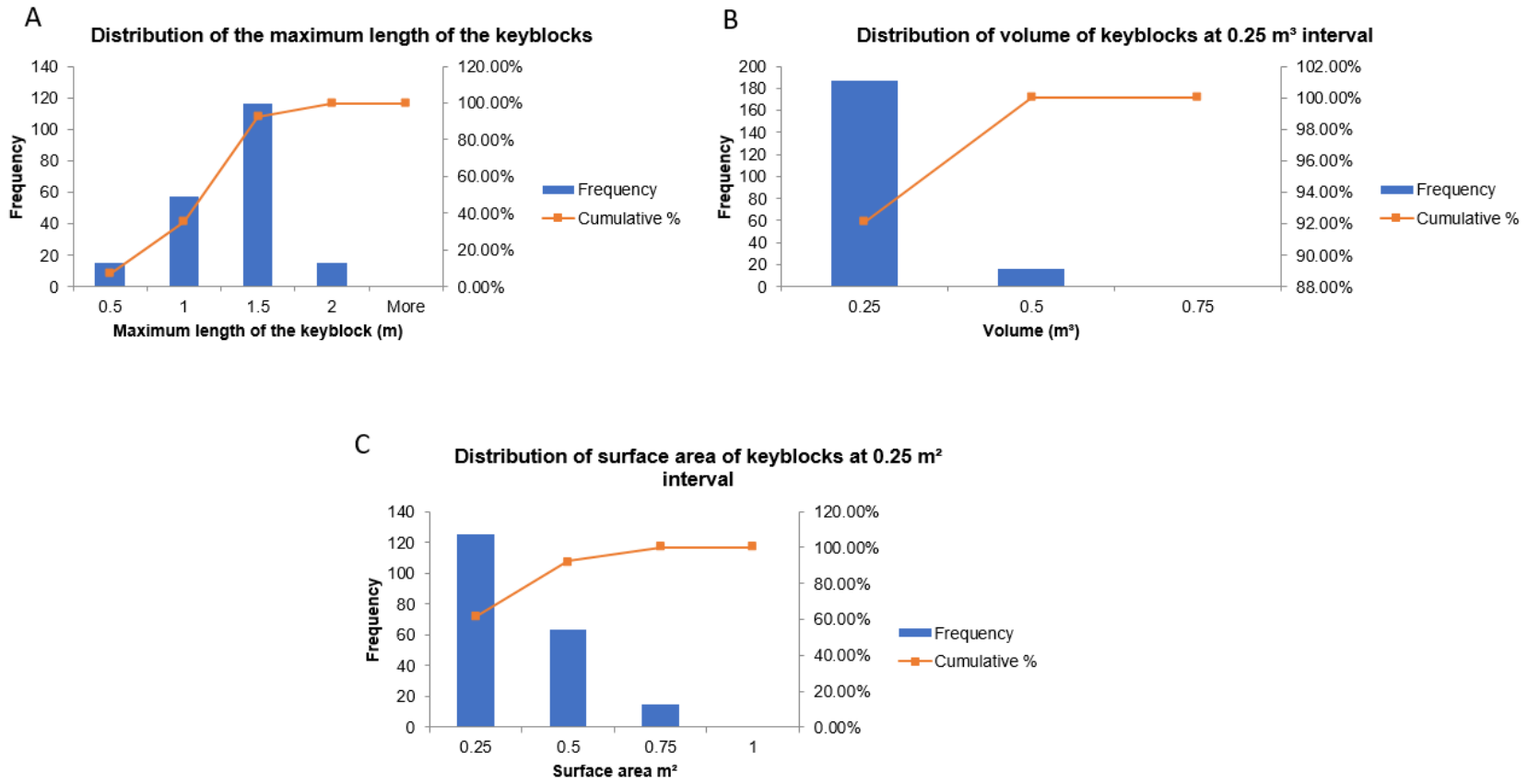

Figure 4-11. JBlock results for normal ground conditions with FOT at 1.3 m.

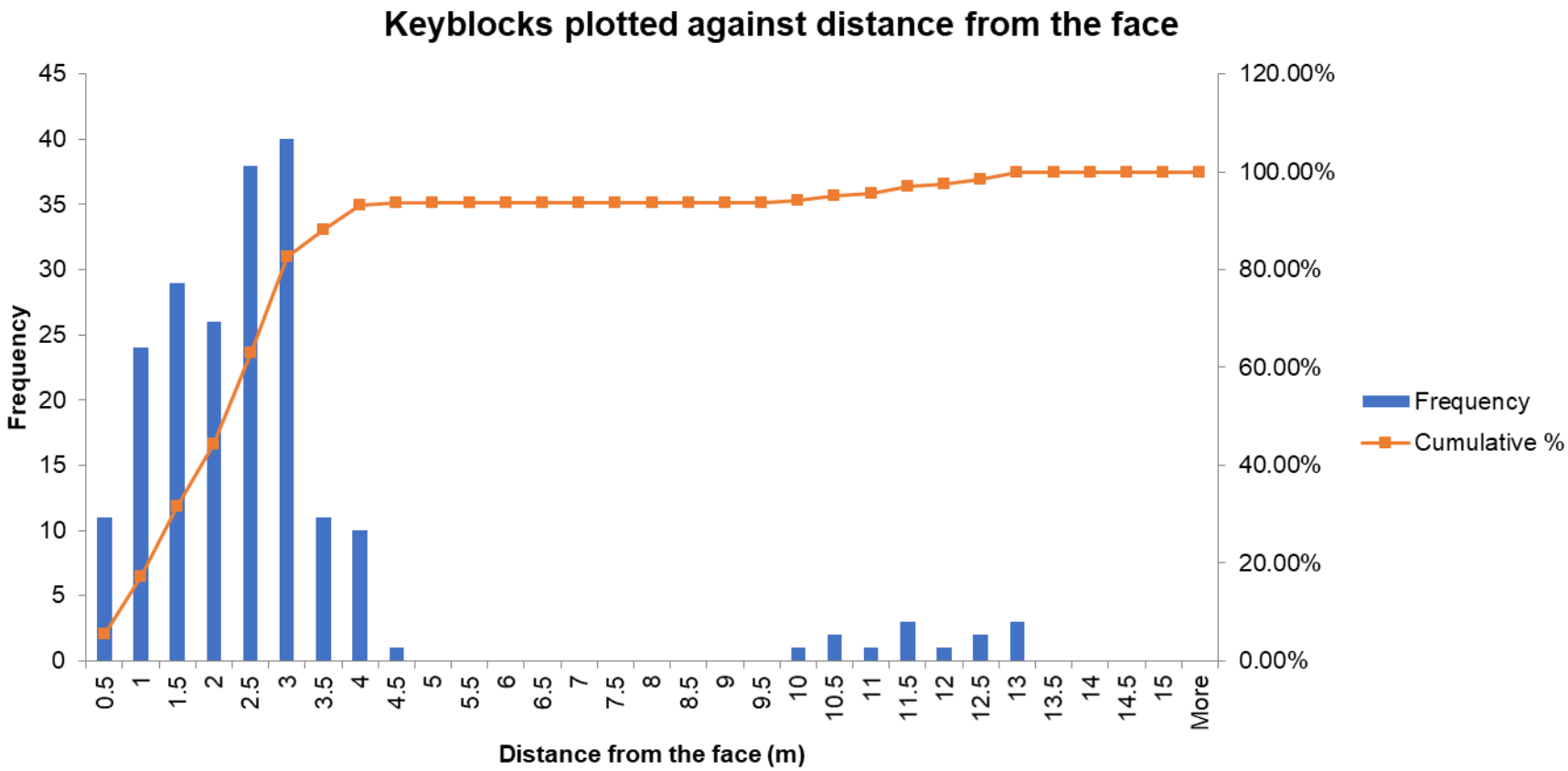

Figure 4-12. Frequency of keyblocks plotted against distance from the face for normal ground conditions.

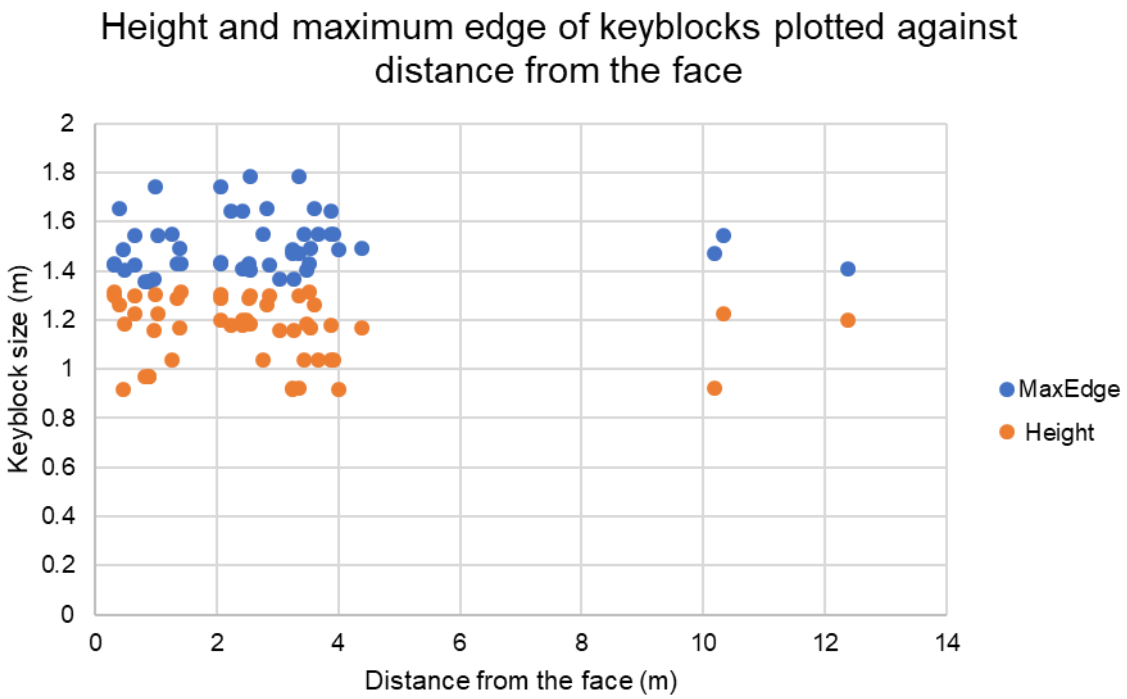

Figure 4-13. Height and maximum edge of keyblocks plotted against distance from the face.

Table 4-9 Support failure results from JBlock for normal ground conditions.

Height	Volume	FaceArea	Parting?	Sim No.	Fall?	Mode	BlockType	No.Bolts	No.tooShort	No.longEnuf	No.Bondfail	No.Steelfail	FaceDist
0.61304	0.03789	0.139	N	66	1	1	J	1	1				12.78
1.17036	0.16229	0.284	N	80	1	1	J	1	1				11.59

4.2.2.2 Ground conditions with a parting plane above the hangingwall

The results for the model with J1 to J3 and a parting plane with zero cohesion, similar to triplets with cavities and in some instances water-bearing, are provided in Figure 4-14 to 4-16 and Tables 4-10 and 4-11. The parting plane was positioned at 1 m above the hangingwall, with a standard deviation of 0.2 m. The results are summarized as follows:

i. The majority of the rockfalls occur within the face area. This may be attributed to lack of support in the area (Figure 4-14).
ii. The closest edge of keyblock that results in support failure is at approximately 6.5 m from the face in Figure 4-15.
iii. 99% of keyblocks failed in between support units (Table 4-10). The 1% of keyblocks failed as a result of either the support being too short or due to steel failure. The majority of support failure was due to steel failure at 86.67%. The steel failure as indicated in Table 4-10 is as a result of large blocks due to large surface area (Table 4-11).
iv. Compared to base model (i.e. normal ground conditions), ground conditions with a parting plane above the hangingwall require that the back area be sufficiently supported to allow for safe access to the face area. The support units installed must provide enough support resistance.

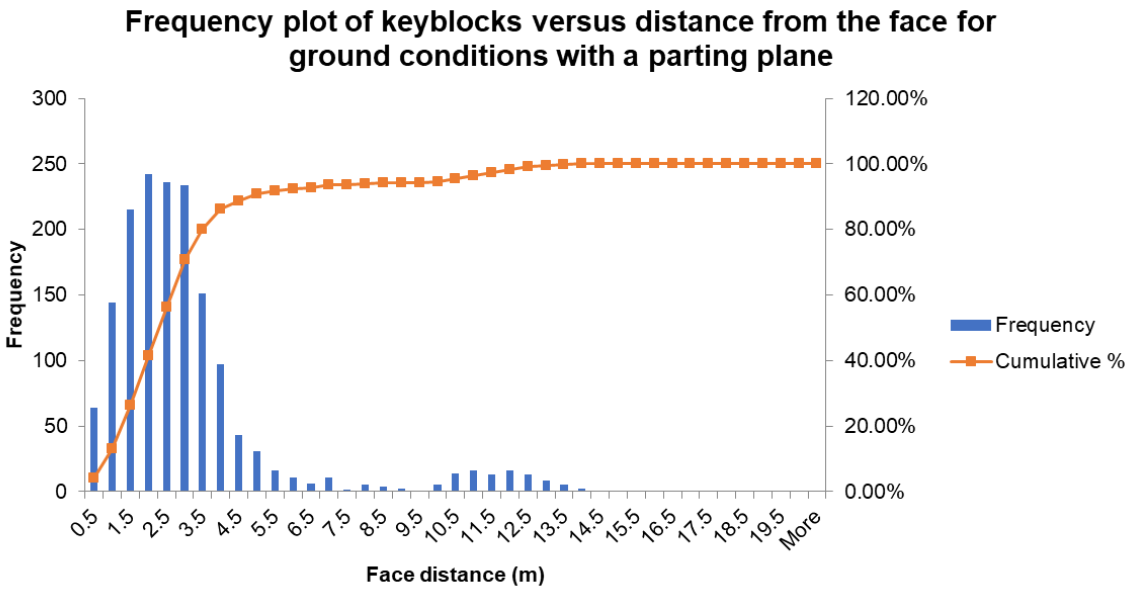

Figure 4-14. Frequency plot of keyblocks versus distance from the face for ground conditions with a parting plane.

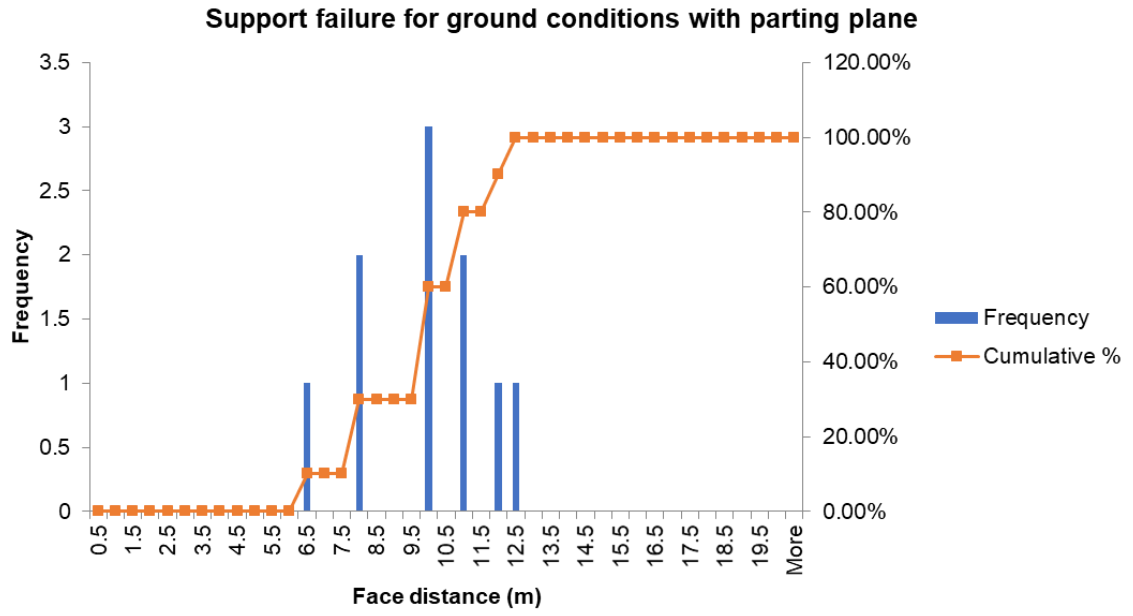

Figure 4-15. Support failure plot for ground conditions with parting plane.

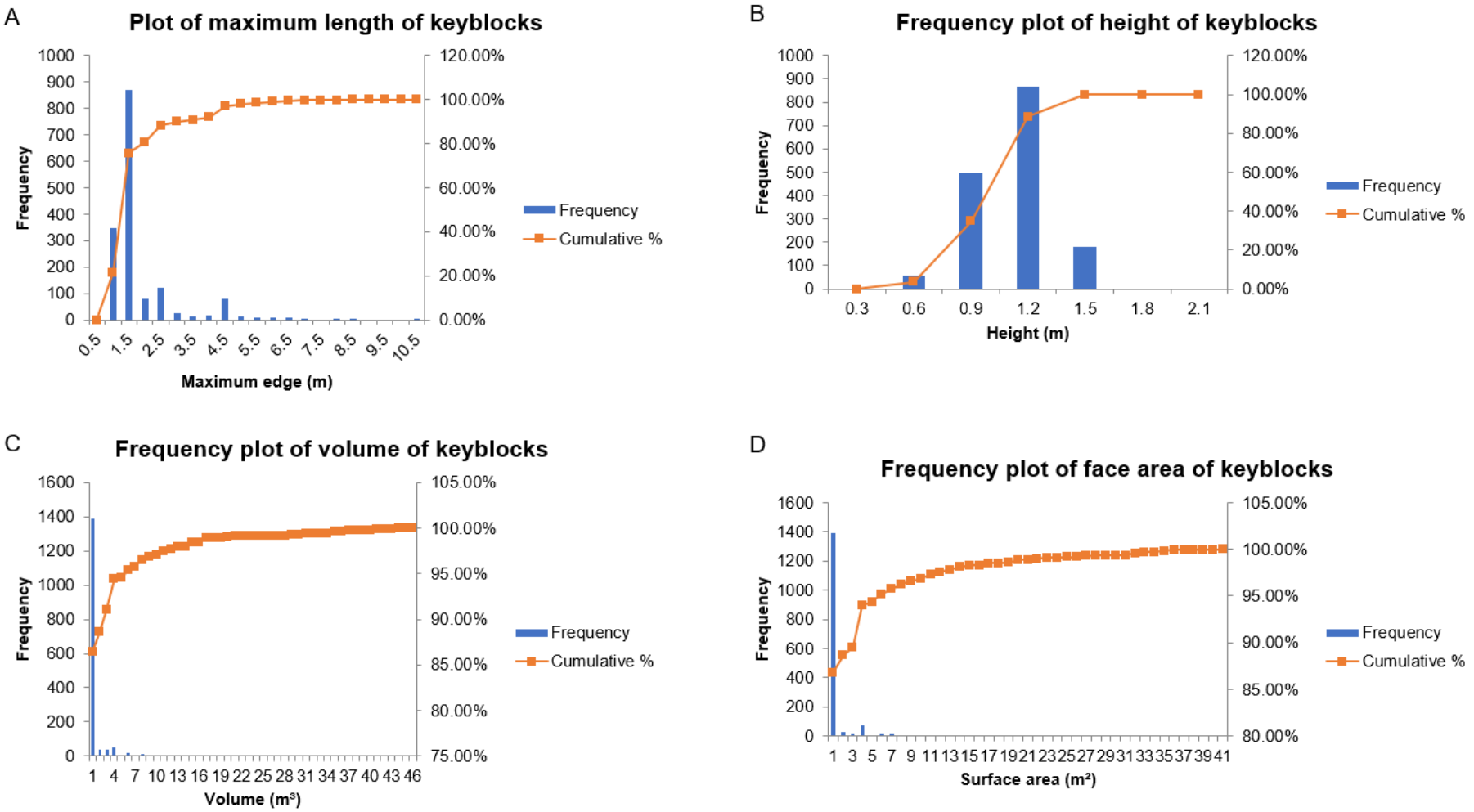

Figure 4-16. Distribution plots of the dimensions of the keyblocks with ground conditions with a parting plane.

Table 4-10. Summary of failure mode and failed support for ground conditions with a parting plane.

Support failure results for ground conditions with a parting with a cut-off at 1.3m

Failure mode			Support failure				
Failed support	**Failed between support**	**Failed by rotation**	Total number of bolts	Short bolts	Long enough	Bond failure	Steel failure
9	1595	1	15	2	13	0	13

Failure mode			Support failure		
Failed support	**Failed between support**	**Failed by rotation**	Short bolts	Bond failure	Steel failure
1%	99%	0%	13.33%	0.00%	86.67%

Table 4-11. Height, volume, face area and distance from the face of the keyblocks that resulted in support failure (large face area for blocks with FOT less than 1.2 m).

Height (m)	Volume (m³)	FaceArea (m²)	FaceDist (m)
1.05052	0.12382	0.22	10.91
1.08777	34.74645	32.65	9.95
1.08777	34.74645	32.65	9.73
1.09188	43.80377	40.684	9.58
1.1669	40.28661	35.385	6.13
1.1669	40.28661	35.385	10.84
1.1828	36.37555	31.506	7.79
1.1911	30.59207	26.283	7.56
1.21229	0.19208	0.334	12.4
1.27991	0.18454	0.377	11.75

4.2.2.3 Ground Conditions with low angled structures

The results provided in this section are of ground conditions that have low angled structures as the fourth joint set as determined from the mapping exercise and ramp structures. Ground conditions from D to I (Table 4-12) were modelled as ramp structures in the model. R1 in Table 4-12 refers to shallow dipping joint set as determined from Dips from mapped data (Table 3-2). The results for the mode of failure, support failure and cause of support failure are provided in Table 4-13. Unlike with base model, low angled structures result in support failure. There is support that fails due to bond and steel failure but the primary cause of support failure is the bolts being too short (Table 4-13). The cause is the height of the blocks that is more than the length of primary support (Figure 4-17).

It is evident that the majority of failures occur between support units, and the unsupported face area probably contributed to this high percentage. The incidence of

support failure is relatively higher for low angled structures with a dip direction of 204° and 294° (Table 4-13).

Table 4-12. Ground conditions considered during the project and their references.

Ground conditions reference	Ground conditions considered	
A	Normal ground conditions with near vertical joints as determined from Dips data	
B	Normal ground conditions from Dips data plus Chromitite parting at <1m in the hangingwall	
C	"A" ground conditions plus shallow dipping features as per Dips data (R1)	
D	"A" ground conditions plus 45° shallow dipping feature in normal ground - sub parallel to mining direction	Dip direction same as the orebody, 45°, 024°
E		Dip direction opposite that of the orebody, 45°, 204°
F	"A" ground conditions plus 45° shallow dipping feature in normal ground - oblique to mining direction	Dip direction same as the orebody, 45°, 000°
G		Dip direction opposite that of the orebody, 45°, 180°
H	"A" ground conditions plus 45° shallow dipping feature in normal ground - perpendicular to mining direction	Dip direction same as the mining direction, 45°, 294°
I		Dip direction opposite that of the mining direction, 45°, 114°
J	Shear zone	

Table 4-13. Summary of failure mode and failed support for ground conditions with low angled structures.

Low angled feature	Failure mode			Block type		Support failure		
	Failed support	Failed between support	Failed by rotation	Normal block	Ramp block	Short bolts	Bond failure	Steel failure
R1	1.97%	97.87%	0.16%	100.00%	0.00%	87.18%	2.29%	10.53%
0°	7.44%	92.51%	0.06%	83.31%	16.69%	86.66%	2.41%	10.93%
24°	4.68%	95.15%	0.17%	78.14%	21.86%	93.36%	1.11%	5.54%
114°	3.75%	95.97%	0.28%	86.44%	13.56%	82.45%	3.27%	14.29%
180°	5.07%	94.88%	0.05%	68.76%	31.24%	85.19%	3.27%	11.54%
204°	13.22%	86.49%	0.29%	77.67%	22.33%	90.01%	1.80%	8.19%
294°	13.27%	86.68%	0.05%	93.61%	6.39%	92.02%	1.55%	6.43%

More results on support failure and keyblocks are provided in Figures 4-18 to 4-21. The closest edge of the keyblocks that failed support is 0.5 m from the face (Figure 4-18) for structures with dip direction of 24°, 180°, 294° and 114°. Figure 4-19 shows that most of the blocks fail between 1.5 m and 3.5 m from the face. There is a higher incidence of failed blocks with joint set 4 (JS4/R1). This is likely due to the spacing of the joint set. However, looking at the rest of the results, the dimensions of the keyblocks for JS4 are smaller in terms of surface area and volume (compare Figure 4-20 and 4-21).

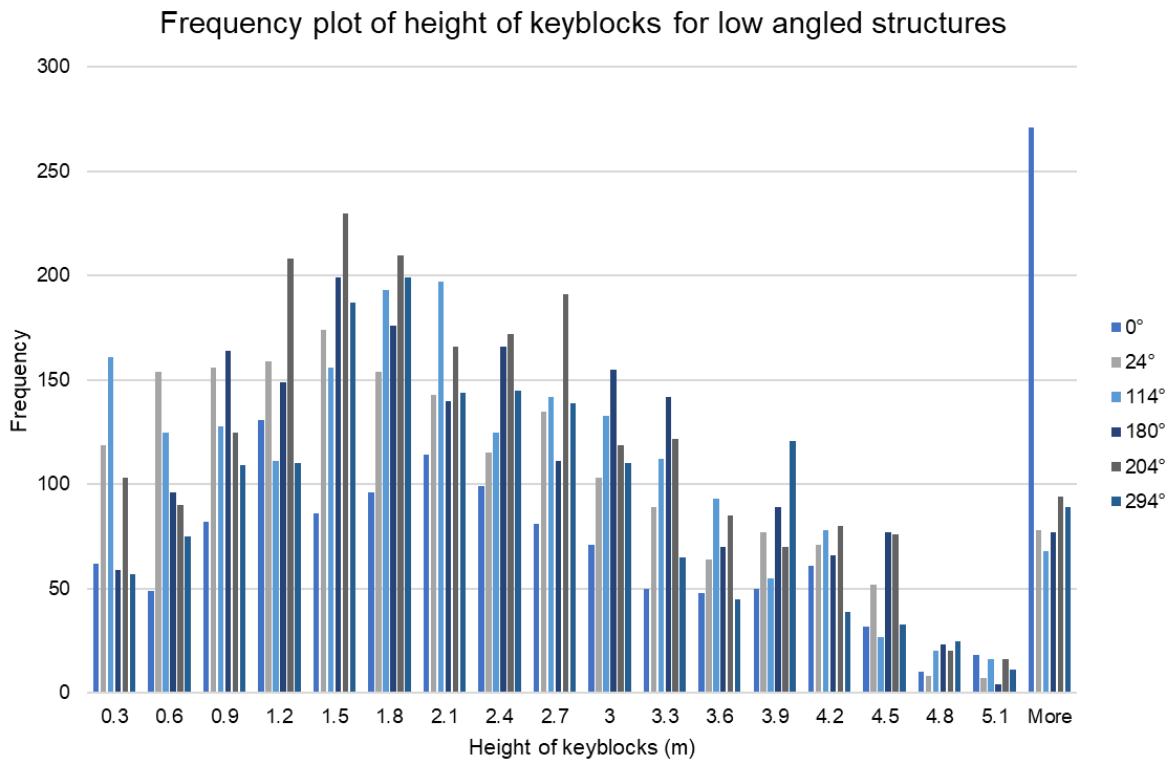

Figure 4-17. Frequency plot of the height of the keyblocks of low angled structures (excluding JS4).

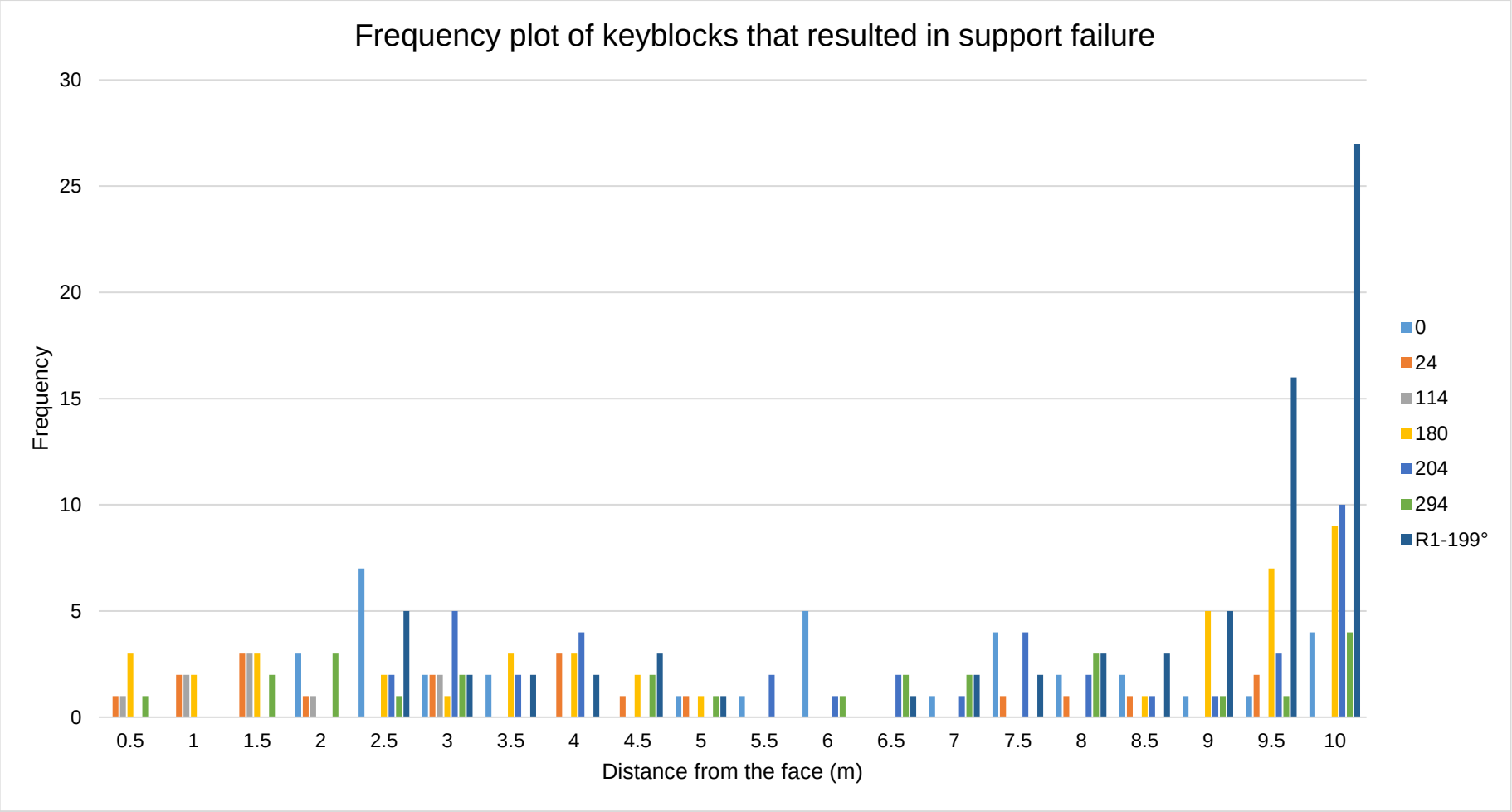

Figure 4-18. Keyblocks that resulted in support failure for ground conditions with low angled structures.

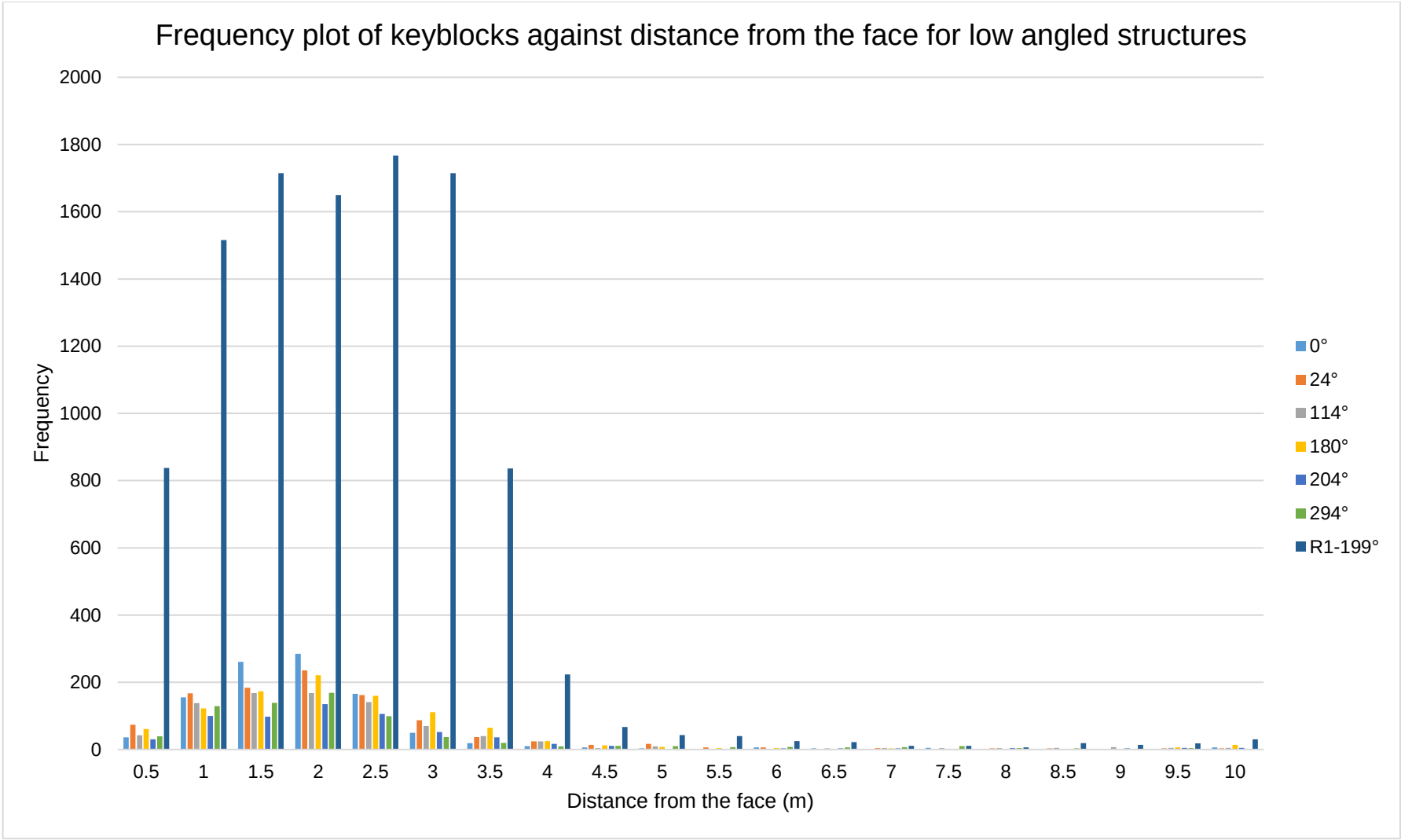

Figure 4-19. A plot of all the keyblocks with ground conditions with low angled structures.

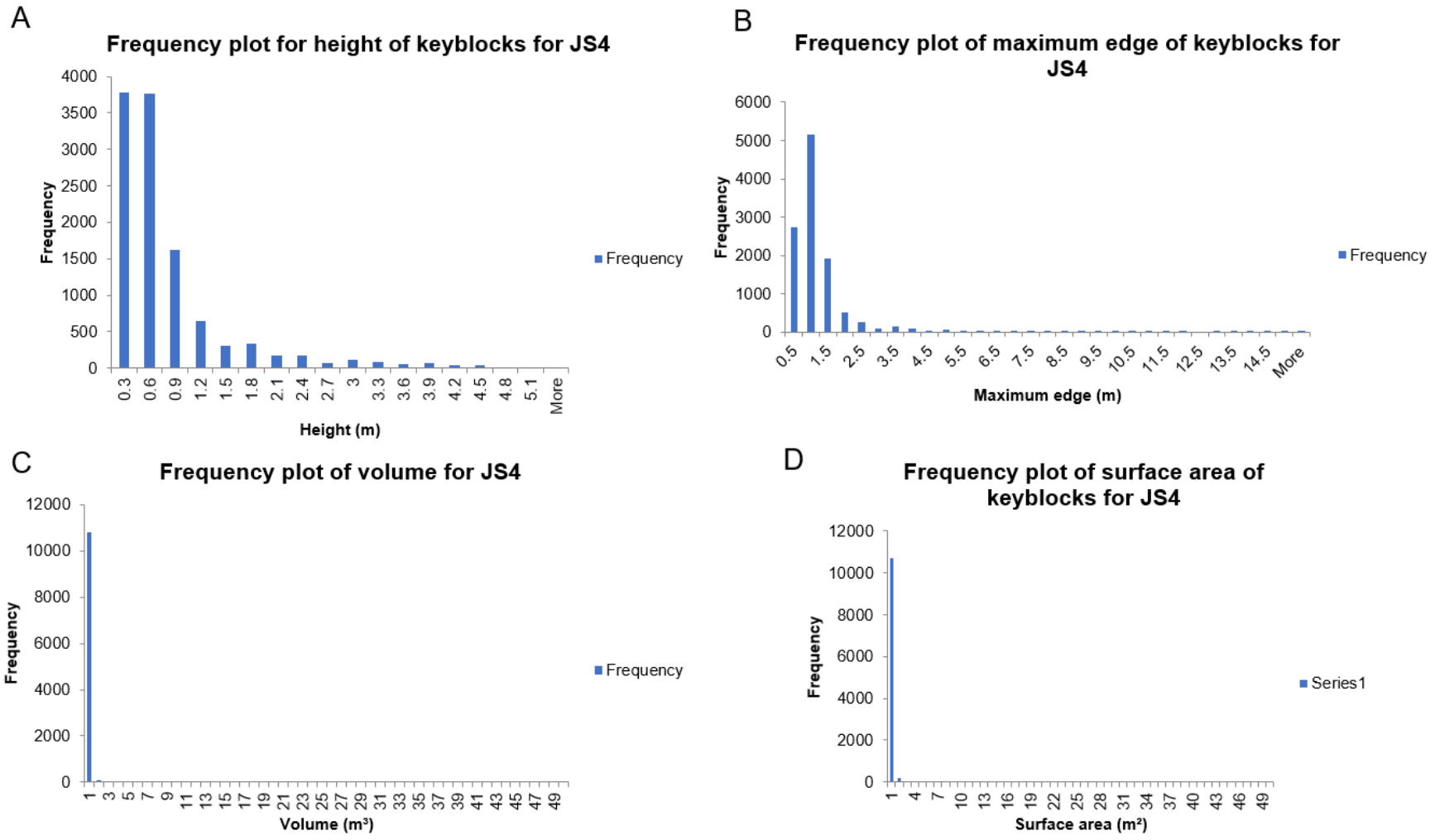

Figure 4-20. Dimensions of the keyblocks with joint set 4 (R1) included in the model.

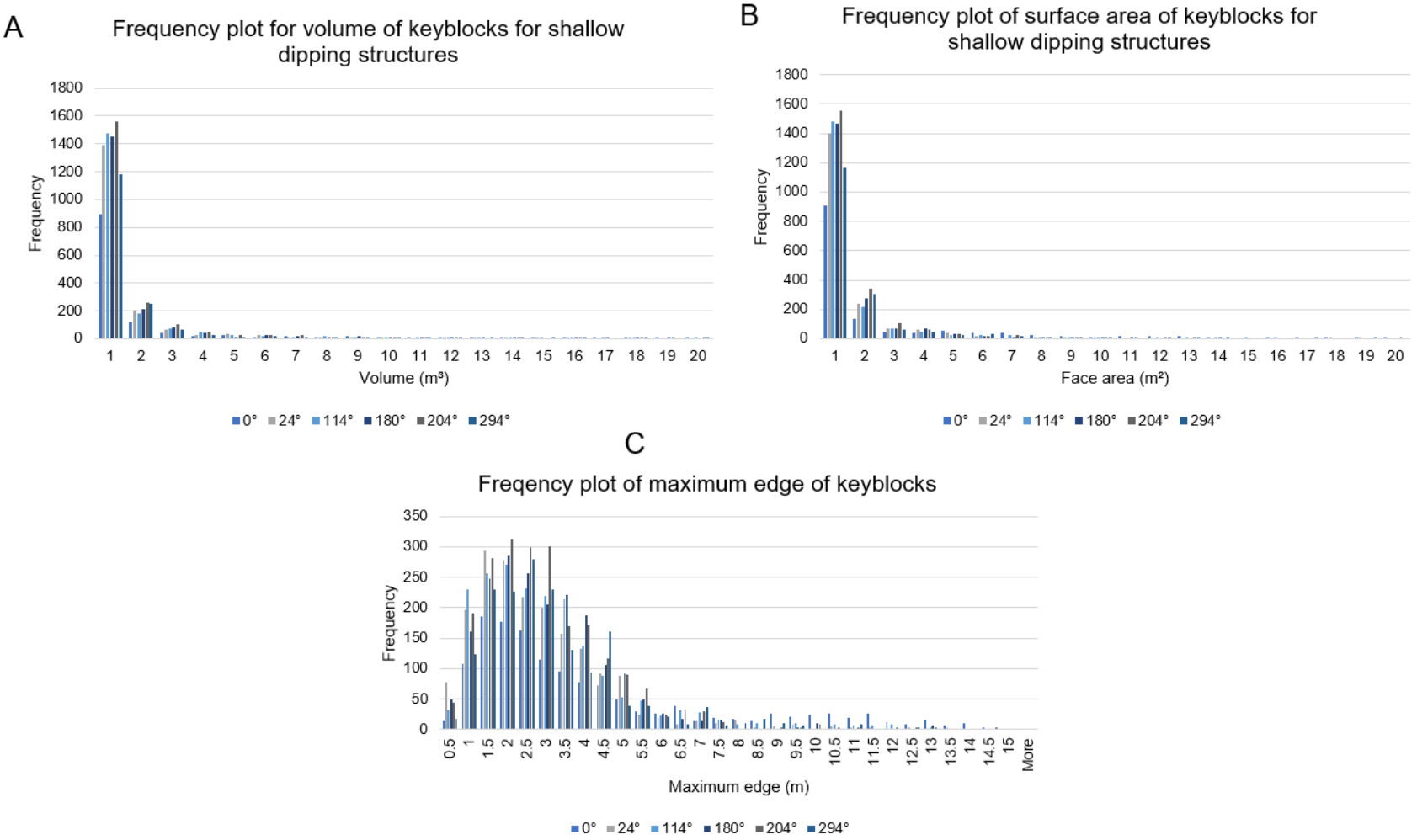

Figure 4-21. Frequency plots of dimensions of ground conditions with low angled ramp structures (excluding R1).

Figure 4-22 is a scatter plot of face distance versus height of keyblocks for JS4. The keyblocks with smaller height are concentrated within the unsupported face area but there are also blocks with FOT bigger than bolt length right along the position of last line of support. The same applies to ground conditions with a ramp structure striking perpendicular to mining direction in Figure 4-23. However, the numbers of keyblocks with excessive height are relatively less.

Ground conditions with a single ramp structure tend to result in a smaller number of keyblocks compared to ground conditions with multiple structures. But large keyblocks have much more severe consequences. The difference in keyblock dimensions are discussed above and can be seen in Figures 4-20 and 4-21. Severe consequences can be seen in Table 4-13 where support failure for JS4/R1 is only at 1.79 % and up to 13 % for ramp structures.

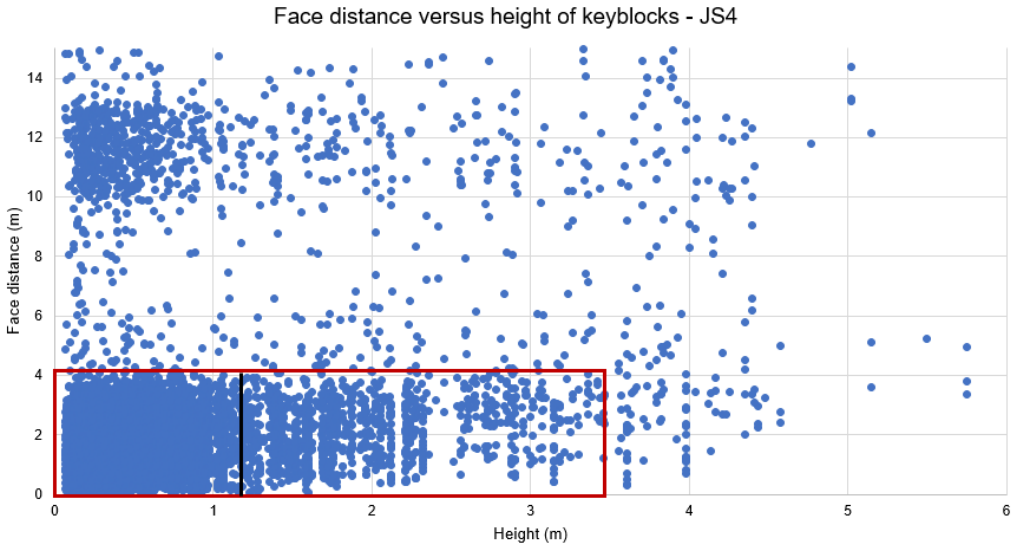

Figure 4-22. Plot of face distance versus height of keyblocks for JS4.

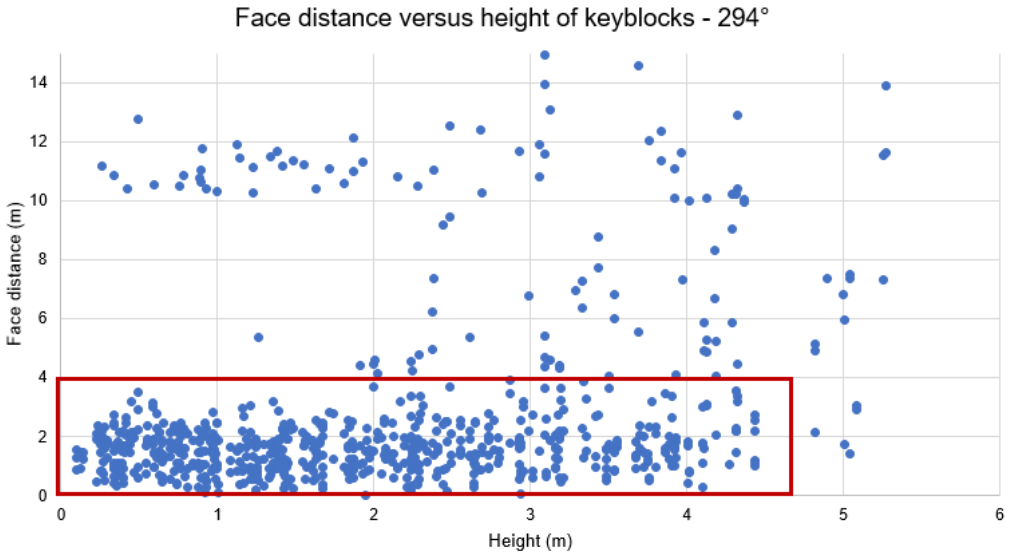

Figure 4-23. Plot of face distance versus height of keyblocks for ramp structure with 294° dip direction.

4.3 The Influence of Reduction in Span for Ground Conditions with Low Angled Structures

Support failure is not a concern for normal ground conditions and conditions with a parting plane. Therefore, no further analysis using JBlock was done for those ground conditions. This is provided the area behind the face is adequately supported. And even though support failure in the back area is predicted in the presence of a parting plane, failures with parting plane above 1.2 m above the hangingwall have never occurred at Bathopele in the absence of low angled structures in the face area.

As mentioned previously, support failure is mainly due to insufficient length of the bolts for ground conditions with low angled structures. Such failure is as a result of excessive FOT created by the low angled structures. The literature shows that conditions with low angled structures will fail irrespective of span of the panel as discussed in Chapter 1 and 2. However the smaller the span, the smaller the potential FOT. The smaller the FOT, the lower the likelihood of failure of support as a result of short bolts. Further assessments were done to check the influence of reduction in span.

The span was varied from 6 m to 9 m. The smallest span was chosen as 6 m because mining span at less than 6 m is possible but over a very short distance. Smaller panels present a loading challenge and limit the clearance between sidewalls and machines. The models with reduction in span were run with no

change in position of last line of support and advance per blast. The results are shown in Figure 4-24. The full results are provided in Appendix F. Mined out area and details regarding the number of short bolts are generated for each simulation in JBlock. The number of short bolts was normalized over the 2000 m^2 for the different spans for comparison purposes.

A reduction in span seems to be beneficial for structures with a dip direction of 204° and 199°. There are anomalies on the graph (e.g. 9m span for R1). Statistical nature of JBlock might be the reason for such anomalies. The results are inconclusive for other structures. Figure 2-25 and 2-26 show results for face distance versus height of keyblocks for JS4. The results show that reducing span does reduce the FOT especially at 6m span for JS4. These results show that the length of bolts required at 10 m span does not necessarily need to be the same as the length required at smaller span.

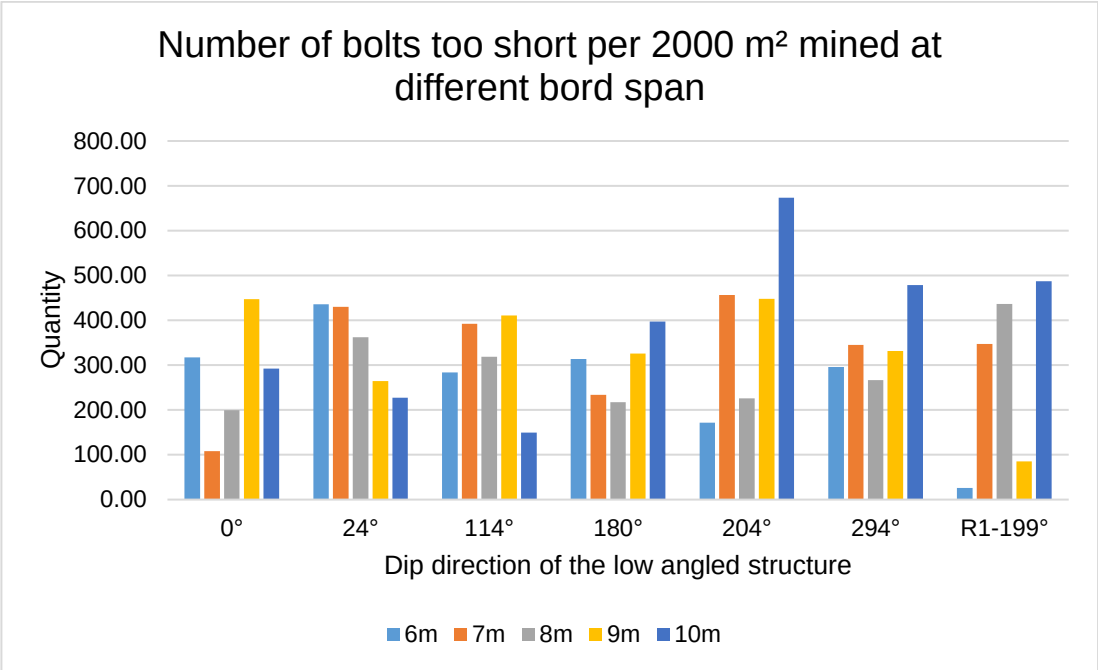

Figure 4-24. Number of bolts too short per 2000 m² mined at different bord span.

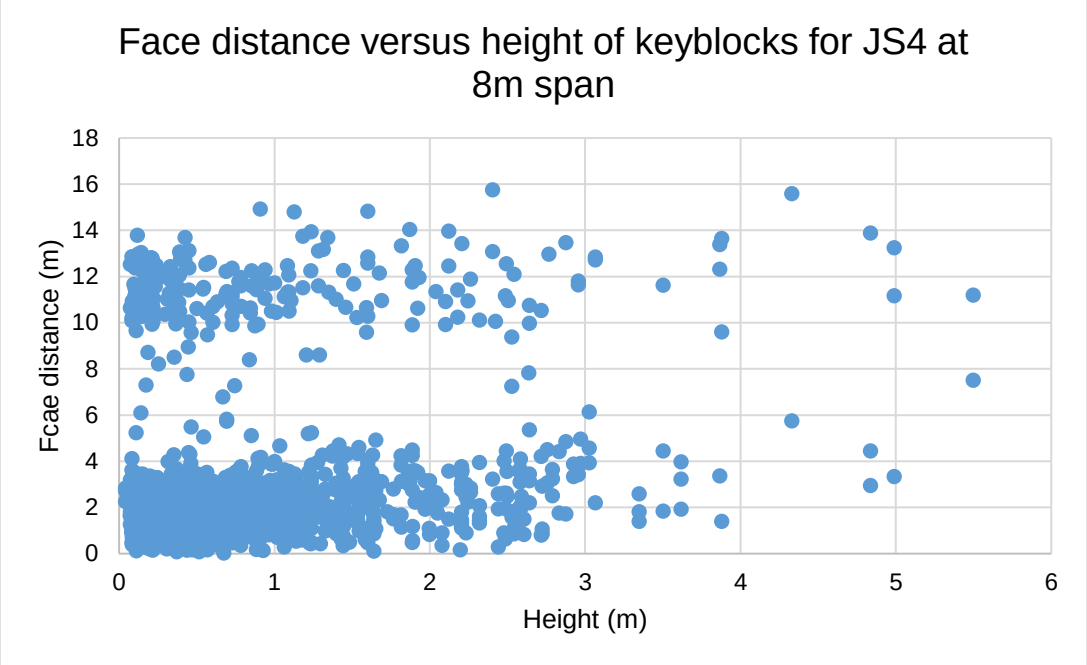

Figure 4-25. Face distance versus height of keyblocks for JS4 at 8m span.

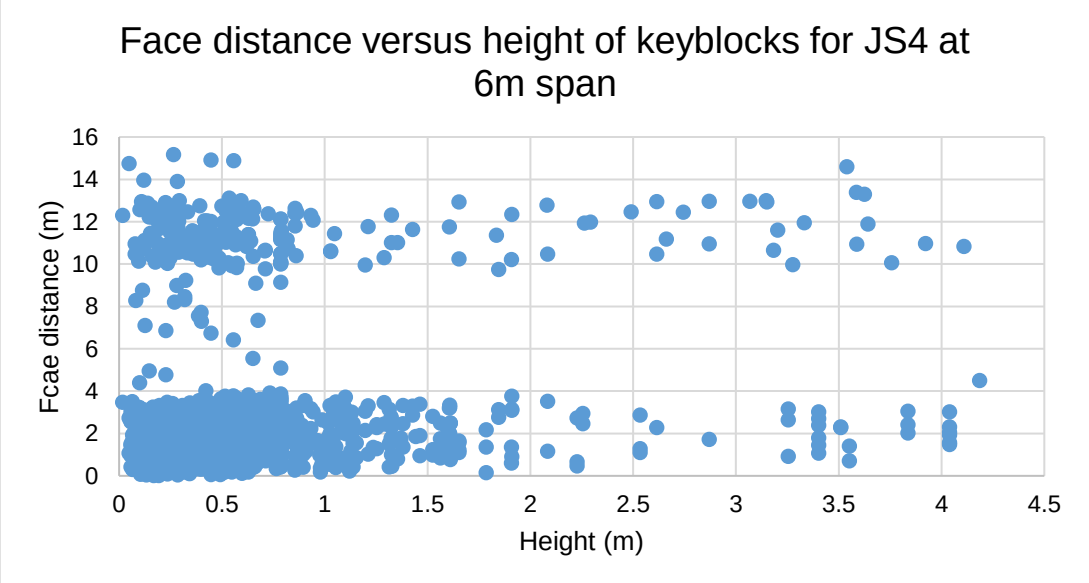

Figure 4-26. Face distance versus height of keyblocks for JS4 at 6m span

4.4 The Influence of Reduction in Advance per Blast for Ground Conditions with Low Angled Structures

The results of the influence of reduction in advance per blast are provided in Figure 2-27 up to Figure 2-29. It was discussed in Section 4.2 that the cause of support failure is the excessive height of keyblocks. Therefore, even in this section, the factor that was analysed was the number and percentage of short bolts for various low angled structures.

The advance per blast was reduced from 3 m to 2 m for both 10 m span and 8 m span. The results show that reduction in advance per blast is favourable especially at 10 m span for all ground conditions (Figure 2-27). The benefit of reducing advance per blast for 8 m span seems to be beneficial for some of the ground conditions (Figure 2-28). The results in Figure 2-28 and Figure 2-29 show results in terms of percentage of failed bolts due to length of bolts. However, when the quantity is normalised over 2000 m² area, the reduction in advance per blast is beneficial for structures with a dip direction of 180°, 204° and 294°.

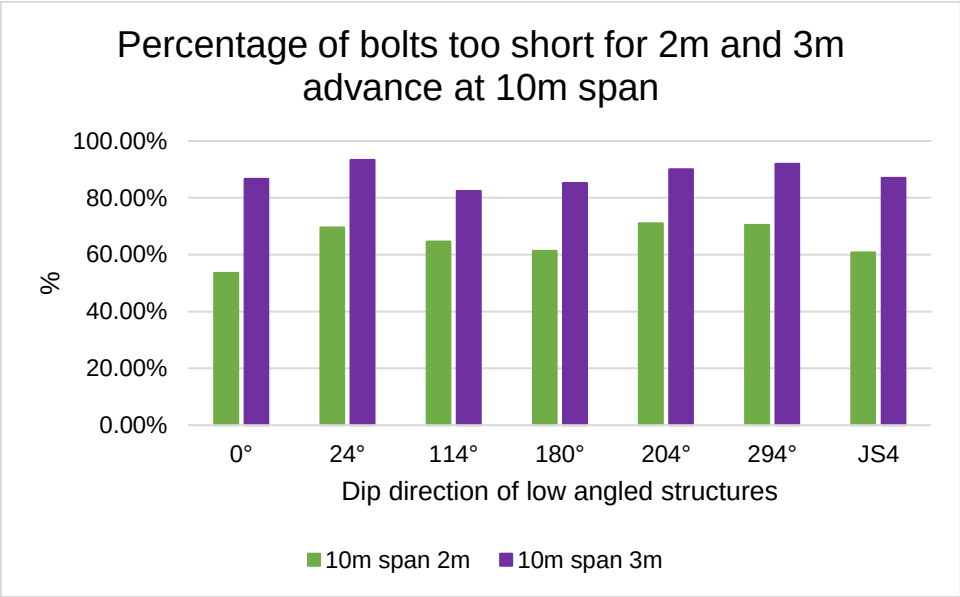

Figure 4-27. Percentage of bolts too short for 2m and 3m advance at 10m span.

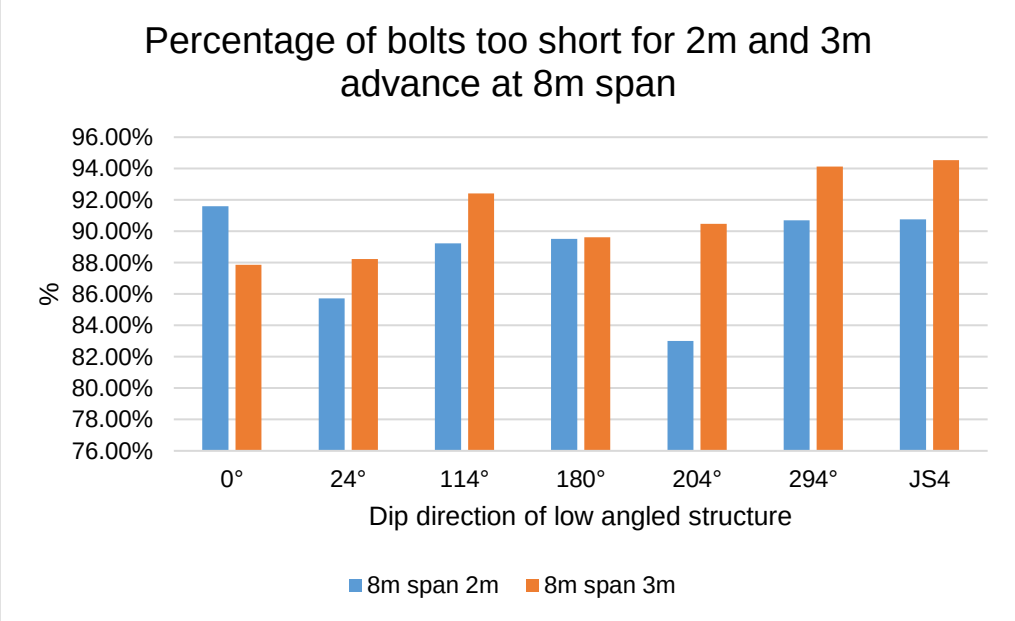

Figure 4-28. Percentage of bolts too short for 2m and 3m advance at 8m span.

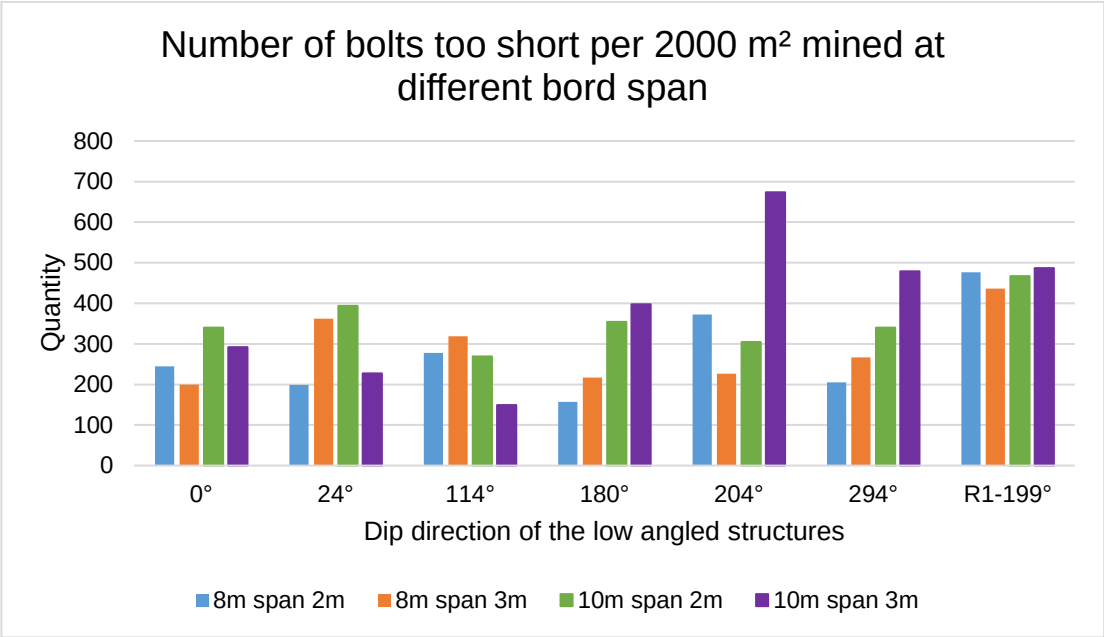

Figure 4-29. Number of bolts too short per 2000 m² mined at different bord span.

Figure 4-30 shows the results for JS4 with reduced advance per blast. It is evident that a smaller advance would result in fewer keyblocks. A smaller number of keyblocks is preferable because it translates into a reduction in likelihood of injuries. A reduction in advance per blast is beneficial in that it reduces the exposed area that requires support and therefore the risk of FOG.

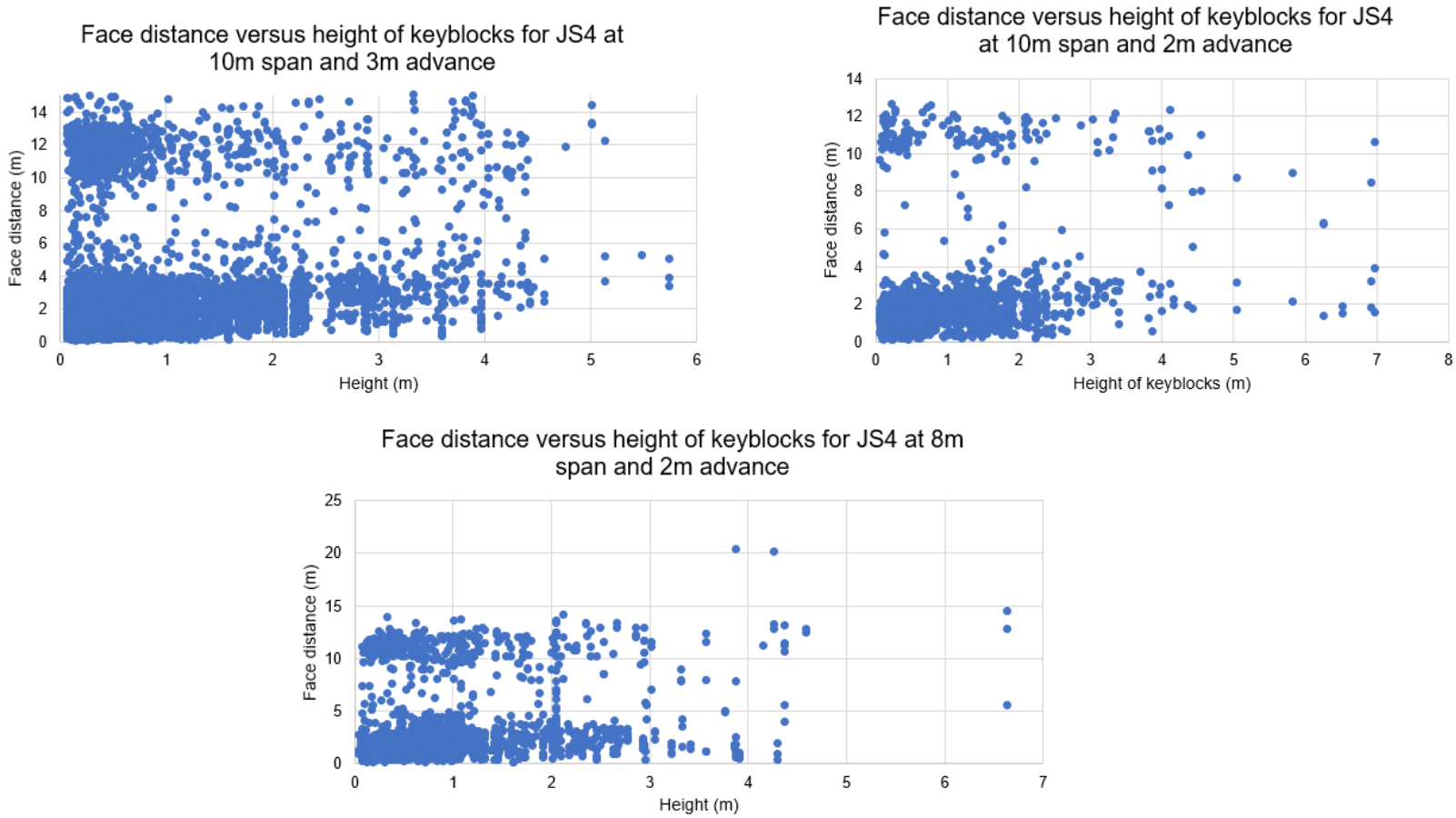

Figure 4-30. JBlock results for JS4 with reduced advance per blast.

4.5 Assessment Using Unwedge

The purpose of using Unwedge in this project was to confirm the instability of some of the potential wedges without support. Furthermore, the exercise was done to determine the required capacity of the support and then compare that against the capacity of existing support units at Bathopele. The input values for orientation of discontinuities are as provided in Table 4-1. The friction angles used for all low angled joints were those of JS4 as determined in Chapter 3. Figure 4-31 depicts the stereonet plot. The excavation outline was constructed at 10 m span.

The results are provided in Table 4-14. There were many other possible wedges that have been omitted from the table provided. The potential wedges considered are those that were considered in the previous assessments. The calculations in Unwedge assume that the structures can occur anywhere in the rockmass (Hoek, 2006).

The results are summarised as follows:

i. Joint set 3 is the most unfavourable when intersecting with either JS1 or JS2. In terms of an acceptable Factor of Safety (FOS), 114° dip direction is the most unfavourable. In terms of potential size of wedge, 199° is the most unfavourable.

ii. The biggest wedges are formed mainly by low angled structures striking obliquely to mining direction

iii. Given the capacity of primary support at Bathopele of at least 14 t/250 mm, the bolts would be strong enough to carry the deadweight of all formed keyblocks, given the correct support spacing. However, as proven by JBlock model, the issue is the bolts being too short. The required capacity of 9.6 t/m² can also be met by camlock jacks (temporary support) if the jacks are included in the support strategy.

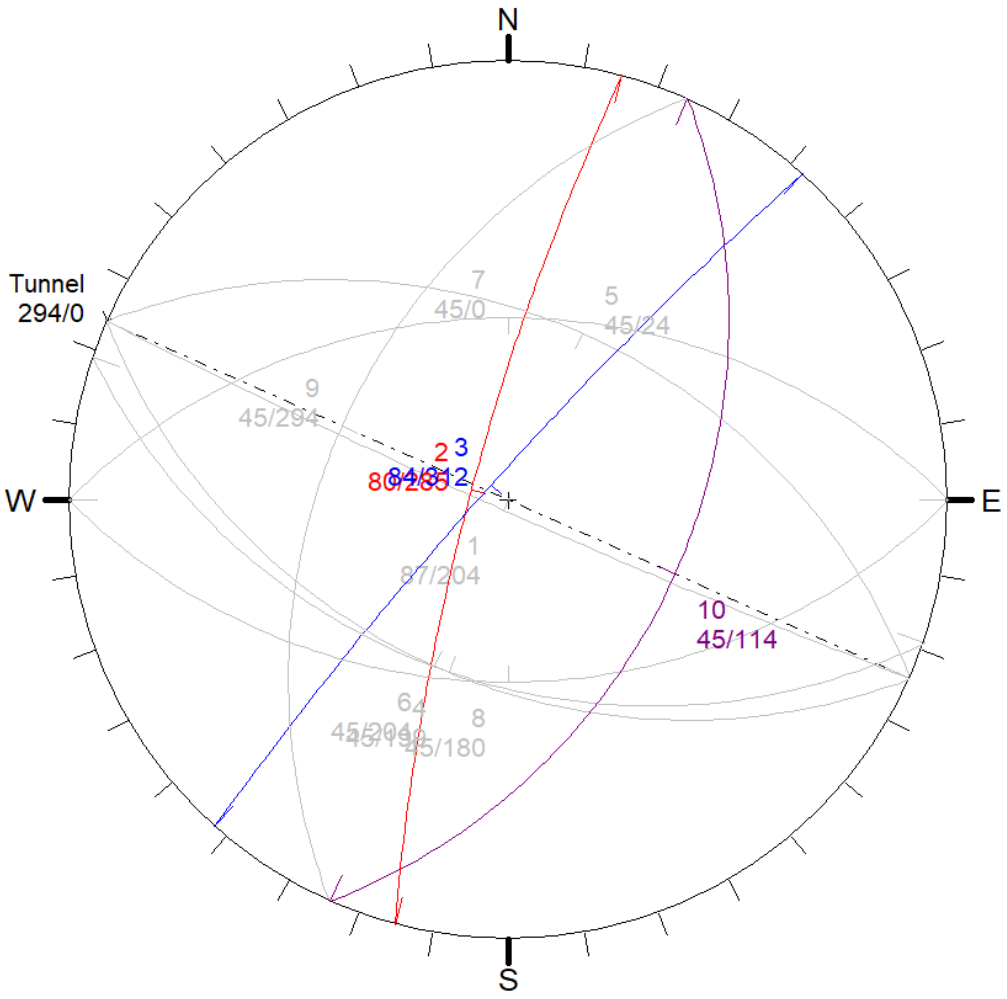

Figure 4-31. A stereonet plot of the major near-vertical joints sets and low angled structures.

Table 4-14. Unwedge results for potential wedges.

Unwedge results for potential wedges										
Combination	**Joint_A**	**Joint_B**	**Joint_C**	**Required support pressure (t/m²)**	**Factor of safety**	**Wedge weight (t)**	**Wedge volume (m³)**	**Excavation area (m²)**	**Number of wedges below FOS of 1.5**	**Joint C dip direction (°)**
6	2	3	7	9.6	0.074	82.64	25.825	12.91	3	0
9	1	3	7	9.6	0.074	359.577	112.368	56.18	3	0
11	2	3	5	9.6	0.074	656.001	205	102.5	3	24
12	1	2	7	9.6	0.123	277.371	86.679	43.34	3	0
14	2	3	6	9.6	0.453	41.109	12.847	6.42	1	204
18	2	3	4	9.47	0.453	41.684	13.026	6.64	1	199
19	2	3	8	9.46	0.453	60.842	19.013	9.72	1	180
34	1	2	4	7.24	0.037	1214.554	379.548	274.59	1	199
35	1	3	4	7.23	0.037	1257.93	393.103	284.66	1	199
36	1	2	8	7.23	0.037	302.75	94.609	68.6	1	180
61	1	3	10	4.61	0	49.937	15.605	16.25	2	114
63	1	3	9	4.41	0.159	68.383	21.37	25.55	1	294
73	1	2	9	3.05	0.123	16.124	5.039	7.92	2	294
84	2	3	9	2.02	0.123	7.167	2.24	5.32	2	294
89	1	2	10	1.51	0.037	12.829	4.009	14.26	1	114
90	2	3	10	1.47	0	5.23	1.634	5.32	2	114
99	1	2	5	No wedges formed						24
100	1	2	6							204
101	1	3	5							24
102	1	3	6							204

4.6 Calculation of Vertical Tensile Zone

As discussed in chapter 2 and 3, the height of the vertical tensile zone should be determined. This is for the purpose of confirming failures involving hangingwall layers. Tensile zone is defined as “the region above an isolated stope where the absolute vertical stress is tensile in nature, and thus conducive to bed separation and hangingwall instability in shallow and intermediate depth mining” (Ryder & Malan, 2002:15-16) and can be calculated using equation 1. The results are in Table 4-15.

According to Ryder and Malan (2002), for multiple pillar protected stopes with an extraction ratio of 85%, the VTZ is usually 20% less than the value calculated using the equation above. And hence, there is a column that has been added to indicate such VTZ.

The benefit of reducing the span is evident with the tensile zone being less at smaller spans. Shallower areas have a much larger VTZ. The VTZ is almost 4 times larger at 50 m below surface compared to 500 m below surface. This is also in accordance with the statements by Budavari (1983), as discussed in Section 2.2.3.

Although this calculation is for stopes and the span or S in the equation is meant for distance between regional pillars, the calculation does work as a check for the VTZ. It is still two dimensional similar to the Voussoir solution.

Furthermore, the Voussoir solution gives conservative results. Elastic beam analysis does not apply at Bathopele because the beams are cut by geological discontinuities.

Table 4-15. Calculation results of VTZ at different depths below surface and mining span.

Depth below surface (m)	**10 m span**		**9 m span**		**8 m span**		**7 m span**		**6 m span**	
H (m)	Z_0 (m)	Z_0 20% less (m)	Z_0 (m)	Z_0 20% less (m)	Z_0 (m)	Z_0 20% less (m)	Z_0 (m)	Z_0 20% less (m)	Z_0 (m)	Z_0 20% less (m)
50	1.71	1.37	1.45	1.16	1.21	0.96	0.98	0.78	0.77	0.62
100	1.16	0.93	0.99	0.79	0.83	0.66	0.67	0.54	0.53	0.43
150	0.94	0.75	0.80	0.64	0.67	0.53	0.54	0.44	0.43	0.34
200	0.81	0.64	0.69	0.55	0.57	0.46	0.47	0.38	0.37	0.30
250	0.72	0.57	0.61	0.49	0.51	0.41	0.42	0.33	0.33	0.27
300	0.65	0.52	0.56	0.45	0.47	0.37	0.38	0.31	0.30	0.24
350	0.60	0.48	0.52	0.41	0.43	0.35	0.35	0.28	0.28	0.22
400	0.56	0.45	0.48	0.39	0.40	0.32	0.33	0.26	0.26	0.21
450	0.53	0.43	0.45	0.36	0.38	0.30	0.31	0.25	0.25	0.20
500	0.50	0.40	0.43	0.34	0.36	0.29	0.29	0.24	0.23	0.19

5 ANALYSIS AND DISCUSSION OF RESULTS

The following chapter discusses the results from each method of analysis described in Chapter 4. The literature review and investigated falls of ground are also discussed.

The important learning from the modelling exercises conducted is that a single method does not take into consideration everything. What is more important is the way the different methods feed into each other i.e. the results from one method can be used in another. The limitations of the methods also come through in the results and the format of the results.

Table 5-1 shows a summary of the results from each method of assessment discussed in Chapter 4. The shallow dipping structures are ranked in terms of the most unfavourable to the more favourable starting at the top of the table. The comparison in the table can be interpreted as follows:

i. A shallow dipping structure with a dip direction of 24° (D conditions) is the least favourable in terms of N' rating compared to a shallow dipping structure dipping at 180° (G conditions) according to the Modified stability graph analysis. Therefore, it will be more beneficial to reduce bord dimensions and advance per blast in D conditions compared to G conditions.

ii. A shallow dipping structure with a dip direction of 199° is the least favourable in terms of the wedge created compared to a shallow dipping structure dipping at 294° according to Unwedge analysis.

iii. Shallow dipping structures with a dip direction of 204° are the most influenced by a reduction in span and advance per blast more than other structures.

Table 5-1. A summary of results, with shallow dipping structures ranked from the least favourable to favourable.

Modified stability graph	Unwedge	JBlock					Colour key	
In terms of N' value	In terms of largest wedge created	In terms of overall failed support	In terms of supprt failure due to short bolts	The most influenced by reduction in span	The most influenced by reduction in advance per blast - normalised data	The most influenced by reduction in advance per blast (% @ 8m span)		Striking oblique to mining direction, dipping in the same and almost the same direction as the hangingwall, dipping opposite J1 and almost the same as J3
24°	199°	294°	24°	204°	204°	204°		Striking oblique to mining direction, dipping in the same and almost the same direction as the hangingwall, dipping opposite J3 and almost the same as J1
0°	24°	204°	294°	199°	294°	199°		
294°	0°	0°	204°	294°	180°	294°		Striking perperndicular to mining direction, intersected from weaker side, dipping the same as J2
114°	180°	180°	199°	180° (statistic anomaly acknowlegded)	199°	114°		
199°	294°	24°	0°			24°		Striking perperndicular to mining direction, intersected from stronger side, dipping opposite J2
204°		114°	180°					
180°		199°	114°					

The modified stability graph is very good at assessing the influence of the size of the excavation on stability. It is also good at assessing the influence of intensity of jointing and the condition of the joints on stability. Overall, normal ground conditions were found to be stable at 10 m span. This is confirmed by the FOG database in which the FOGs were only a result of poor or incorrect barring. The FOG boundaries were joints and blasting fractures or a hangingwall parting plane in a case of poor mining. Although JBlock results predicted FOGs within the face area, the blocks were small and can be addressed by barring.

The stability graph method seems to also indicate the adverse effect on stability of parting planes parallel to the hangingwall. The limitation is that the method does not take into account how far the parting planes are above the hangingwall. It would be best to consider if the parting planes are within the tensile zone, and if not, then other discontinuities would be driving instability.

Depending on the span, ground conditions with parting planes in the hangingwall will require support according to the stability graph. The analytical solution showed that the shallower the mining depth, and the larger the span, the longer the bolts required. The findings from JBlock show that instability will depend on the presence of other structures. If the parting plane is intersected by other structures in the panel, irrespective of the angle of those structures, a potentially unstable block will be created. If the block is large enough, and the

capacity of the bolts do not meet the demand of the block, steel failure will most likely occur.

Actual FOGs were taken into account with regards to the stability of parting planes. Looking at FOG photos in Figure 2-16 and Figure 5-1, the parting planes were intersected by other joint sets in the panels. The FOG in figure 5.1 was bounded by at least 3 pegmatite veins plus multiple joints. The multiple joints are proven by the FOG rubble instead of a single intact block.

Comparing FOT to the calculation of the VTZ, there are some discrepancies. According to the VTZ calculation, no bed separation should occur above 0.6 m for 188 m mining depth at a 9 m span or less. However, failure did occur at 1 m for FOG number 1 in Table 5-2. The span was most likely 9 m or less because the FOG occurred in the year 2010, during which the layout was designed at 9 m at Bathopele. The same discrepancy can be observed with FOG number 4. These FOGs also prove the limitation of the Voussoir solution because a 0.7 m beam should be stable at a span of 4.7 m. These results prove that stability is structurally controlled.



Figure 5-1. Central shaft 10w panel 4 FOG within the face area (Macebele, 2019).

Table 5-2. Thickness and depth for FOGs involving chromitite stringers.

FOG number	Shaft	Report Number	Date	Working Place	Mining span	Mining direction	Depth (m)	Thickness	6.FOG Boundaries
1	Central	591	2010-12-10	6wwinze2	$	$	188	1	Chromitite stringer+ normal J1 & J2 jointing
2	Central	167	2016-03-16	3WBRD8	8	Strike	67	0.3	The fall boundaries were chromitite stringers (exposed due to pothole) and vertical joints.
3	Central	$	2016-04-08	7WBRD4 RSE	$	$	184	0.15	Double chrome stringers and vertical serpentinized joint
4	Central	772	2019-10-10	10W BRD4	4.7	Strike	212	0.7	Joints striking perpendicular to the face, double chrome stringers and two sub-vertical veins on the contact of both sidewalls

The Modified stability method is also good at assessing ground conditions with shallow dipping structures. The limitation with this method is that it does not explicitly take into account the potential creation of wedges whereas JBlock and Unwedge do.

Shallow dipping structures striking obliquely and near-parallel to mining direction were found to be most unfavourable with the stability graph method, Unwedge and JBlock (Table 5-1). The FOG reports confirm these modelling results (Rademan 2006, van Rooyen, 2010, van Rooyen, 2011, Rajpal, 2011, Sibanda, 2013, Handley, 2013, Sephaphathi, 2017a, Sephaphathi, 2017b, Mukwevho, 2018). The plan views of the FOGs as taken from the FOG reports are provided in Appendix G.1.

Structures striking near perpendicular to mining direction give rise to instability of the hangingwall in conditions where the hangingwall is intersected by multiple structures (Matsobane, 2011, Dube 2015, Matsobane, 2016a). The plan views of the FOGs as taken from the FOG reports are provided in Appendix G.2. The occurrence of such FOGs is less than of those with FOG boundaries striking parallel and obliquely to mining direction. Table 5-1 does show that structures striking perpendicular to mining direction can be unfavourable. A dip direction of 294° is more unfavourable than 114°, however, these structures result in smaller wedges as shown by Unwedge analysis. The

smaller wedges are expected because the persistences of the structures striking parallel to the face of the panel are limited by the width of the panel.

The stability graph method results show that ground conditions with shallow dipping structures do not necessarily mean inevitable failure but do require support depending on the size of the excavation and the conditions of the shallow dipping structures. JBlock results showed that the support required is longer bolts. It was found in Unwedge that the support capacity of bolts required was actually not excessive and the demand can be satisfied with the existing support units. The maximum capacity required was found to be 9.6 t/m^2 to meet a FOS of 1.5.

According to Hoek (2006), a wedge can fail as soon as its base is fully exposed in the excavation by mining. Therefore, rockbolts must be installed before the entire base of the wedge has been exposed. The East shaft, 8E P4 FOG confirms this statement. Plan view of the FOG location is provided in Figure 5-2. The wedge collapsed only after the tip of the wedge close to the face was finally exposed.

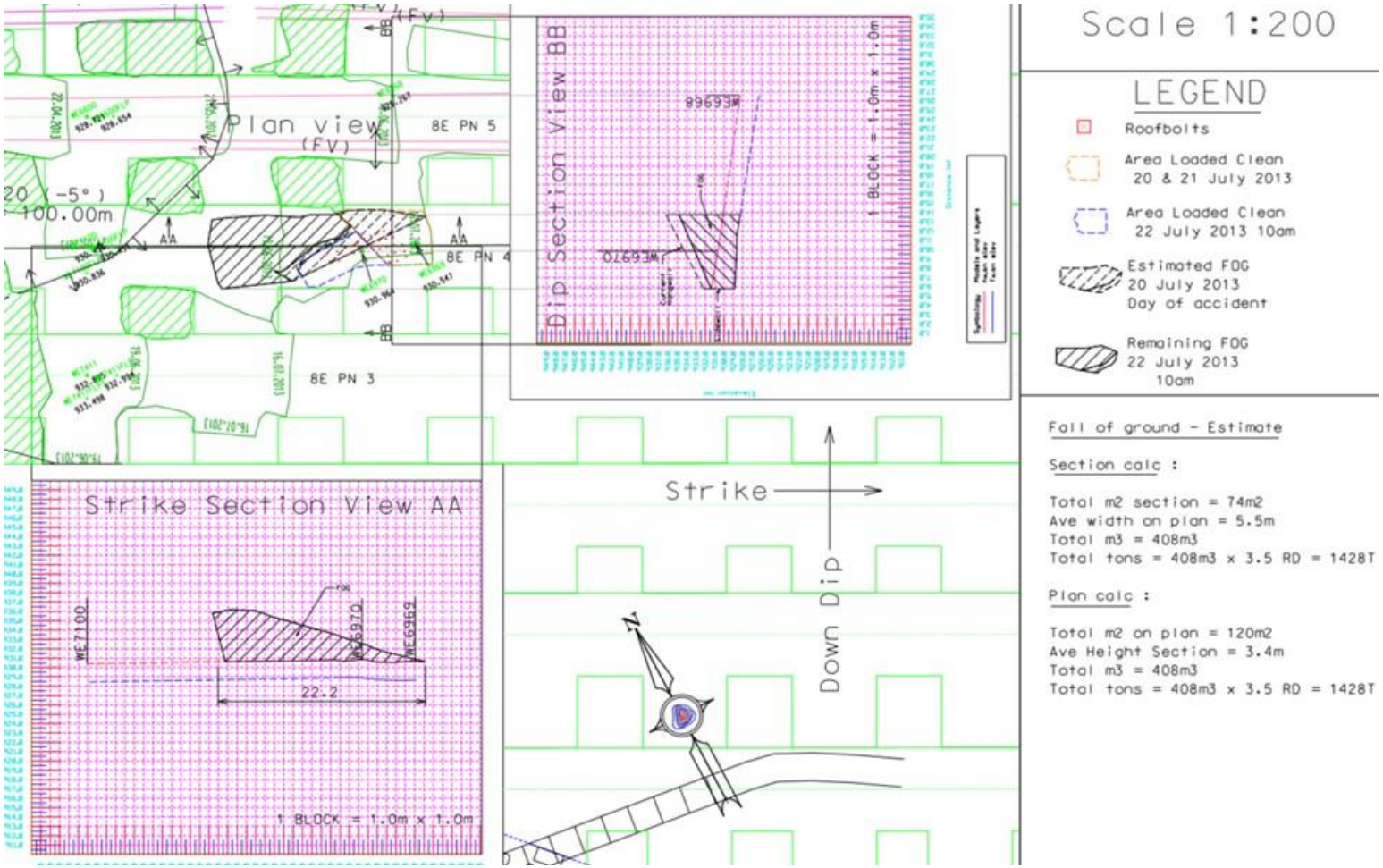

Figure 5-2. East shaft 8E P4 FOG plan (Bathopele Survey dept., 2013).

JBlock is a probabilistic-design based program and this is very clear on the difference of the keyblock distribution of those involving ramp structures and those with JS4. Furthermore, features cannot be placed in specific areas within the excavation for the purpose of assessment. The challenge is JBlock places the ramp structures randomly around the excavations per specified frequency. And hence, the frequency distribution for JS4 in terms of dimensions of the keyblocks and support failure are much *smoother* as compared to those involving ramp structures.

The hypothesis that the effectiveness of last line of support is limited by the geological structures is proven by the investigated FOGs. In addition to the FOGs discussed in Chapter 2, further evidence is shown in Figure 5-3. The FOG occurred at K6 shaft and the boundaries were pegmatite veins and a flat dipping fault striking obliquely to mining direction (Mukwevho, 2018). The bolts were very close to the boundary of the FOG.

In the case of wedges that may fall under the influence of gravity, support units no longer serve the purpose of reinforcing the rockmass (Stillborg, 1994), their purpose is to carry the deadweight of the wedges. Therefore, if the last line of support is carrying the deadweight of a wedge above its capacity, the bolts will most likely fail. The attempt to assess the last line of support with JBlock shows that the effectiveness of the support is controlled by the keyblock sizes in the hangingwall. In the case of shallow dipping structures for instance, the support

closer to the face would fail due to insufficient length and insufficient capacity for larger blocks. Results show that reducing the mining span in such ground conditions would result in less likelihood of failure of the last line of support because of the smaller height of keyblocks.

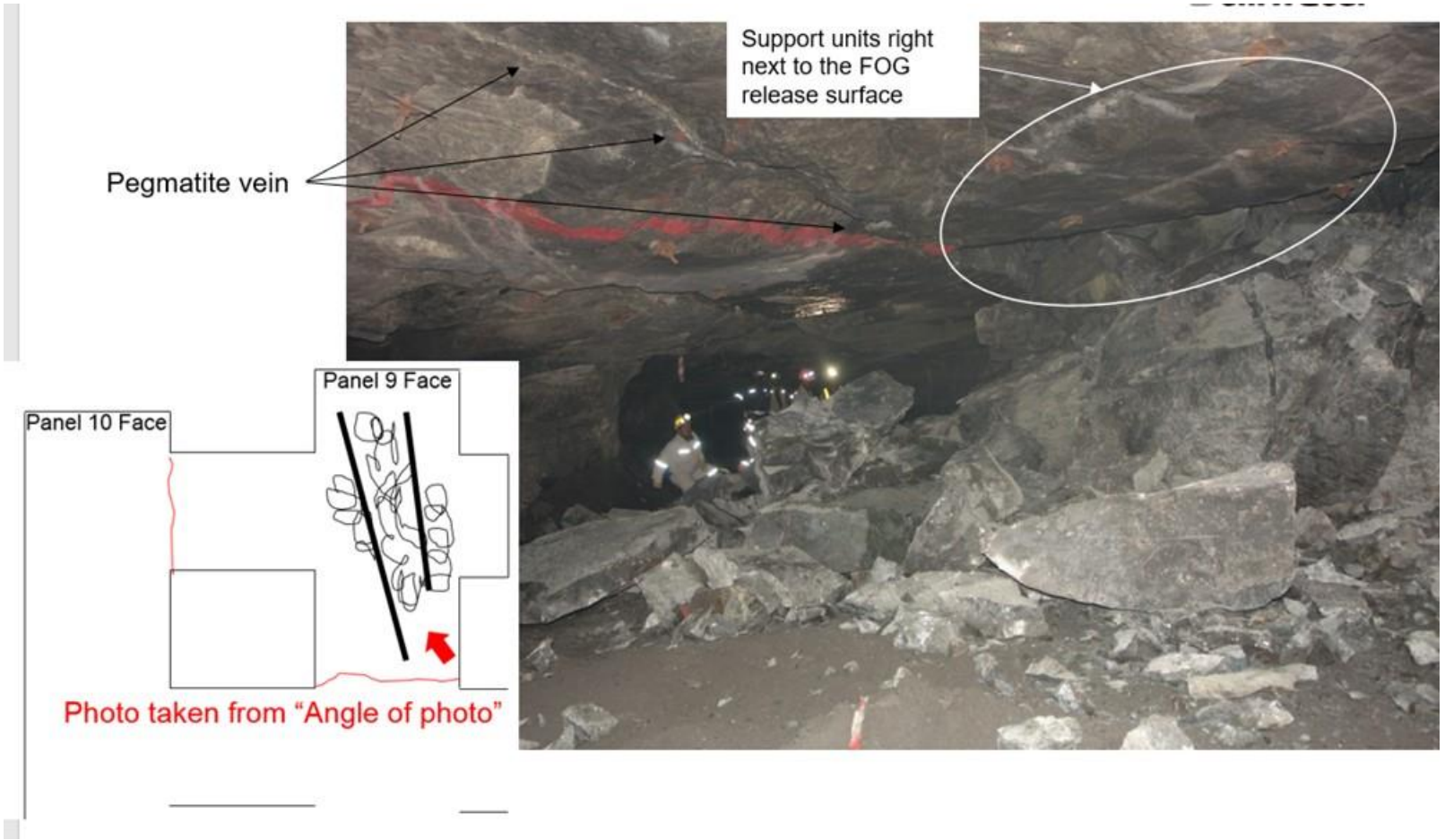

Figure 5-3. K6 large FOG plan and photo (K6, 2018).

Based on the fact that wedges only fail when the perimeter is fully exposed, a reduction in advance per blast and span should be implemented strategically. For example, a span can be reduced to clamp one of the structures that create the wedge, or advance per blast can be reduced to expose only a portion of a wedge for the purposes of installing support. Obviously both strategies can be implemented simultaneously.

Based on the FOGs that formed part of this research, pegmatite veins seem to be a problem for Bathopele and Kroondal operations. This may be due to the thin serpentinite infill on either side of the pegmatoid material and the altered joint walls. Presence of low friction biotite plates contained within the pegmatoid veins could also be a contributing factor (Watson, 2002). This phenomenon is shown in Figure 5-4. Additionally, pegmatite veins are fairly pervasive across the mining lease area.

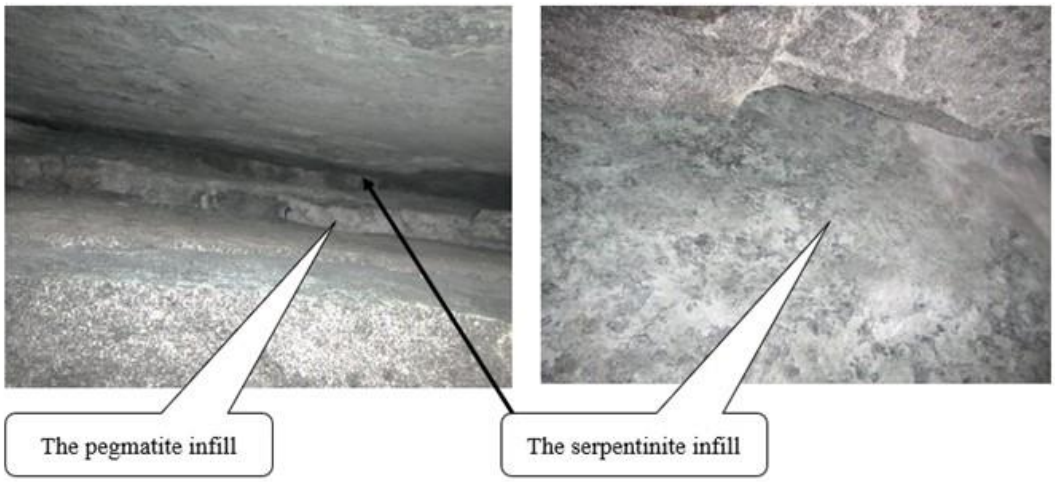

Figure 5-4. Pegmatite vein with serpentinite infill/coating on the sides.

6 TARP GUIDELINES

Guidelines for addressing TARP triggers assessed in the preceding sections are discussed in this chapter. The guidelines are for addressing parting planes, shear zones and shallow dipping structures.

6.1 Overall Ground Conditions

It was discussed in Chapter 2 and shown in Chapter 4, through the Modified stability graph method and JBlock that: ground conditions characterised by vertical structures only, are stable. It must be noted however that the intensity of jointing must be considered for such ground conditions. Failure is most likely to occur in between rockbolts. The higher the intensity of the jointing, the greater the need for areal coverage support. Considering the size of the blocks that are most likely to fail, reducing support spacing for rockbolts may be unnecessary. If good blasting practice is done, barring should be able to address most unstable blocks between support units.

Table 6-1, Table 6-2 and Table 6-3 show a summary of the guidelines for the ground conditions assessed in the previous chapters. The conditions are discussed in more detail in the sections that follow.

Table 6-1. TARP Guidelines for ground conditions A, B and J.

Ground conditions assessed		Fall of ground analysis	Jblock analysis	Guidelines		
				Advance per blast	**Reduction in span**	**Effectiveness of last line of support**
Normal ground conditions	A	Based on the 10 FOGs that resulted from vertical joints and blasting fractures, the maximum area of FOG was 0.56 m² with an average of 0.1 m²	Small rockfalls concentrated in the face area, starting at 4.5 m and peaking at 3m from the face. No support failure	Full blast acceptable	Unnecessary	Last line of support is effective - smaller blocks between support units must be barred
Parting plane	B	Based on the 18 FOGs that resulted from HW layer, the maximum area of FOG was 17.4 m² (in the smallest bord in terms of span) with an average of 4 m², the maximum thickness was 1 m. bord span ranged between 4.7m and 9.6m. Vertically inclined veins unfavourable in these conditions	Support failure due to steel failure as a result of large blocks with a large surface area.	Dependent on block sizes, however based on support resistance calculation, a ≤2 m advance per blast is recommended and bolts must be installed as close to the face as practically possible before blast i.e. ≤0.5 m.	Reducing span should be aimed at bracketing prominent structures such as veins, otherwise a reduction in span through these conditions should be on the basis of reducing the FOG risk by reducing the overall area mined given that there is no reef is such ground conditions i.e. mining through a pothole at full span carries an unnecessary risk.	Dependent on block sizes, maximum tributary area is 3.4 m² at a factor of safety of 1.1 and 2.5 m² for FOS of 1.5. A smaller span would reduce the likelihood of large blocks and therefore reduce the likelihood of support failure as a result of steel failure
Vertically inclined shear	J	Failure occurs only within the shear zone, even at small spans, confirmed cases of unravelling of hangingwall from shear zones occurred at a span of 6.7 m and 4.2 m. Failure also occurred after application of shotcrete as indicated in Figure 6-5. Mining done successfully through a shear zone with shotcrete, mesh and trusses - Figure 6-6.	Not assessed	Based on FOG experience, of which the results are confirmed by the Modified stability graph assessment, the minimum practical advance per blast and span through the shear zone is recommended. Blasting must only be done when support units and required equipment are available on site because immediate support installation is required. Blasting must be done regularly to mine through the zone as quickly as possible. Full blasts can be accommodated depending on the orientation of the shear zone, zone thickness and the shotcrete machine available. For instance, a shear zone striking parallel to the face with a thickness of <1.5m can be exposed in a single blast - with enough hose length and compressed air from the shotcrete machine, shotcrete can applied from a supported area. Mesh and trusses can follow afterwards.		Last line of support is not effective - a shear zone must be supported with areal coverage support such as mesh anchored with trusses in addition to shotcrete. Any support that is installed beyond the shear zone will not be effective. Presence of other discontinuities within the vicinity of the shear zone must also be taken into account.

Table 6-2. TARP Guidelines and recommendations for shallow dipping structures.

Ground conditions assessed		Fall of ground analysis	Jblock analysis	Unwedge analysis	Guidelines
				Maximum required support pressure t/m²	Advance per blast
C	199°	Based on the 18 FOGs that resulted from shallow dipping structures, highest FOT is 4.5 m (at 9 m span), bord span ranges from 5.8 m to 9.4 m, largest falls were in bords mined at 8 m-9.4 m. FOT higher than 1.3 m was in mining span wider than 7.5 m.	Support failure due to short bolts resulted from excessive height of keyblocks - % of bolts that failed as a result of insufficient length are between 85% and 94%	9.47	No significant difference in reducing advance per blast based on JBlock analysis
D	24°			9.6	A smaller advance per blast coupled with a smaller span would be beneficial based on JBlock analysis e.g. given 8m span, 396 bolts per 2000 m² would fail at 3m advance compared to 199 short bolts per 2000 m² for 2m advance.
E	204°			9.6	A reduction in span is more beneficial based on JBlock analysis but smaller advance per blast is beneficial - there's a reduction of 55% in failed bolts from 10m panel at 3m advance to a 10m panel at 2m advance
F	0°			9.6	A reduction in advance per blast does not make a difference based on JBlock analysis
G	180°			9.46	A reduction in advance per blast very beneficial based on JBlock analysis, especially coupled with a smaller span.
H	294°			4.4	A reduction in advance per blast very beneficial based on JBlock analysis, especially coupled with a smaller span.
I	114°			4.61	A reduction in advance per blast does not make a difference based on JBlock analysis

Table 6-3. TARP Guidelines and recommendations for shallow dipping structures.

Ground conditions assessed		Guidelines		
		Reduction in span	**Effectiveness of last line of support**	**Overall comments**
C	199°	6m span recommended based on support failure as a result of insufficient length of bolts based on JBlock analysis	Influenced by block sizes. Jblock analysis shows that 1.6 m resin bolts installed in the last line of support will fail primarily due to insufficient length of the bolts. Using the nomogram, assumining a 45° dip angle and taking into account the dip direction of the shallow dipping structures with respect to the hangingwall, 1.6m resin bolts are effective only up to 1.2m from the structure for C, E, G, H and I structures and the bolts are effective up to 1.7m for structures D and F. For an area that's already mining though the shallow dipping structures, given sufficient bolt length, maximum tributary area is 2.3 m² at a FOS of 1.1 and 1.7 m² for FOS of 1.5 for 3m bolts. Using the nomogram, assumining a 45° dip angle and taking into account the dip direction of the shallow dipping structures with respect to the hangingwall, 3m resin bolts are effective only up to 2m from the structure for C, E, G, H and I structures and the bolts are effective up to 3.7m for structures D and F . It is recommended in this case the TARP member consider the surface area of potential wegde created by shallow dipping structure.	Based on the span reduction results from JBlock, FOG analysis and literature, an 8m span seems to be the optimum span in terms of potential FOT. At 8m span, FOT was up to 2m according to Watson and Gerber (2018) and this is a height that can safely be supported by 3m bolts. Futhermore, the maximum height recorded is 2m for GCD F as shown by the FOG analysis. However, if the shallow dipping structures have slickensides or the structures are in a set (i.e. C conditions) a span of ≤6m is highly recommended. Structures C, D, E, F and G can be safely managed if treated immediately upon exposure. Structures H and I are different because the entire structure is exposed within one blast. This results in the entire hangingwall being on the weaker side of the structure. However, the potential size of the wedge for H and I conditions is small based on Unwedge analysis. **Overall, a reduction in advance per blast and mining span would be favourable because of less exposed area of the hangingwall that require support, however, these strategies should be employed where they would be of benefit.**
D	24°	A span of 6 m to 8 m is recommended based on the height of keyblocks generated in JBlock.		
E	204°	A span of 6 m or 8 m is recommended based support failure for as a result of insufficient length of bolts from JBlock analysis		
F	0°	A span of 6 m or 8 m is recommended based support failure for as a result of insufficient length of bolts from JBlock analysis		
G	180°	A span of 6 m or 8 m is recommended based support failure for as a result of insufficient length of bolts from JBlock analysis		
H	294°	Recommendation is to bracket structures that may intersect the ramp structure perpendicularly when reducing the bord span - the potential size of wedge is small though based on Unwedge		
I	114°	Recommendation is to bracket structures that may intersect the ramp structure perpendicularly when reducing the bord span - the potential size of wedge is small though based on Unwedge		

6.2 Potholes, Slumps and Reef Rolls

Instability when mining through potholes, slumps and reef rolls is primarily due to the following:

i. Poor hangingwall conditions due to absence of a layer over which hangingwall can be mined. The top contact of the leader seam in dual seam GCD and the chrome stringer above the main seam in single seam GCD provide a near-smooth layer for the hangingwall in normal ground conditions. The elevation of these layers changes or disappears in potholes, slumps and reef rolls resulting in poor hangingwall conditions.
ii. Increased jointing,
iii. presence of parting planes such as triplets close to the hangingwall; and,
iv. wedge formation as chromitite layers cut through the hangingwall

Poor hangingwall conditions and blocky ground conditions due to increased jointing can be addressed as discussed above through barring and areal coverage. Wedges created by chromitite layers may be addressed similar to any other shallow dipping, persistent structure.

The issue of parting planes above the hangingwall was discussed in Sections 2.2.2, 4.2.2.2 and 4.6. The FOG database shows that, within the face area at Bathopele, FOGs involving parting planes do not have a FOT higher than 1 m.

However, for a FOG to occur, the parting planes have to be intersected by other prominent structures, such as pegmatite veins and shallow dipping structures. JBlock analysis showed that instability occurs when the support installed is not strong enough to carry the weight of the blocks bounded by the parting planes.

The first step in addressing this type of ground conditions is to determine position of parting plane above hangingwall. It is recommended that borehole camera or Ground Penetrating Radar (GPR) be used in such cases to determine the position of the parting planes. Furthermore, it is recommended a marker be used as a way of determining when to drill an instrumentation hole.

A strategy of using a marker in a pothole or slump, is illustrated in Figure 6-1. For such a scenario, the message to production personnel should be that as soon as the main seam dips into the footwall, a borehole or instrumentation hole must be drilled close to the face before advancing the panel. For a 2.2 m mining height, when the main seam disappears into the footwall, the doublets would be approximately 2.1 m above the hangingwall. The borehole must be drilled approximately 1 m from the face in supported area. In this way, the triplets would still be far enough to be stable (i.e. 3.1 m above the hangingwall) but close enough to know what to do within the next blast depending on the ground conditions.

Keyblocks created by parting planes above the hangingwall will result in support failure when the blocks are too big. Large blocks may increase demand on last line of support due to cantilever effects. A support resistance calculation was done to determine the maximum block sizes that may be carried by existing support units using an acceptable FOS. A 1.2 m height was used. Effective length of 1.6 m resin bolts is 1.5 m and 30cm of bond length is required above the parting plane. The results are shown in Figure 6-2.

The support information used in the calculation is provided in Table 6-4. The calculation shows that when a TARP member is presented with pothole conditions, where a parting plane is a concern, there is a risk that the blocks closer to the unsupported face area may cantilever. This concern is applicable if the surface area of the blocks exceeds 3.4 m^2.

Identification of structures that may form FOG boundaries becomes important during inspections. Potentially unstable blocks may be identified this way thereby assisting with determining where to start with support installation. Structures such as pegmatite veins that usually cause FOGs when intersected by parting planes can be stabilised by reducing the span.

This guideline is valid provided complex ground conditions do not exist such as the presence of shallow dipping structures within the potholes. In the case of a

destructive pothole, where the reef pinches and/or disappears, a borehole may be drilled upon immediate disappearance/pinching of reef.

Reef elevation merely changes in slumps and the middling between the layers does not change at Bathopele (J. Mcunlwane 2020, pers. Comm., 17 February). Ground conditions in the UG2 are predictable in reef rolls and slumps because the chromitite layers remain at a constant distance from the reef. Regional differences in parting plane heights (from the reef) are captured on the mine isopach plans. Borehole inspections should be used to track any changes over the smaller scale and the isopach plans updated accordingly.

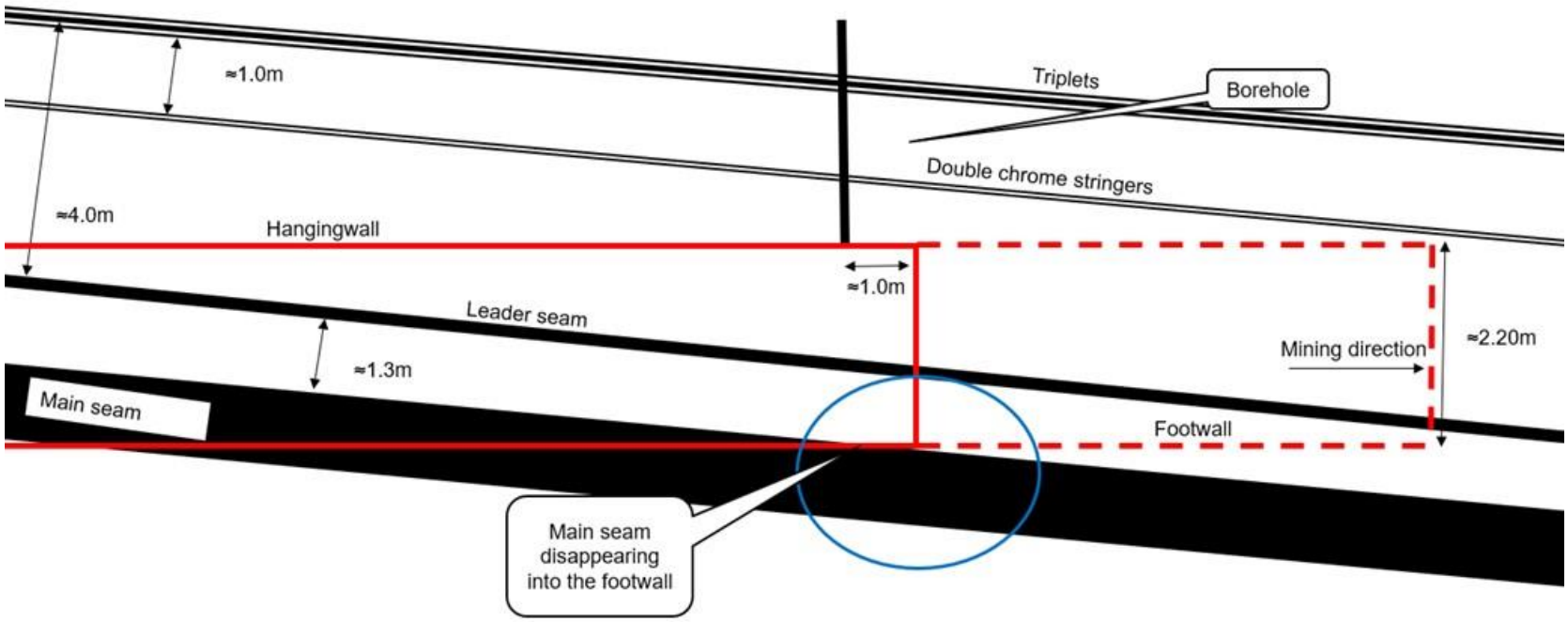

Figure 6-1. Position of chromitite layers with respect to the main seam for a typical reef roll or slumps.

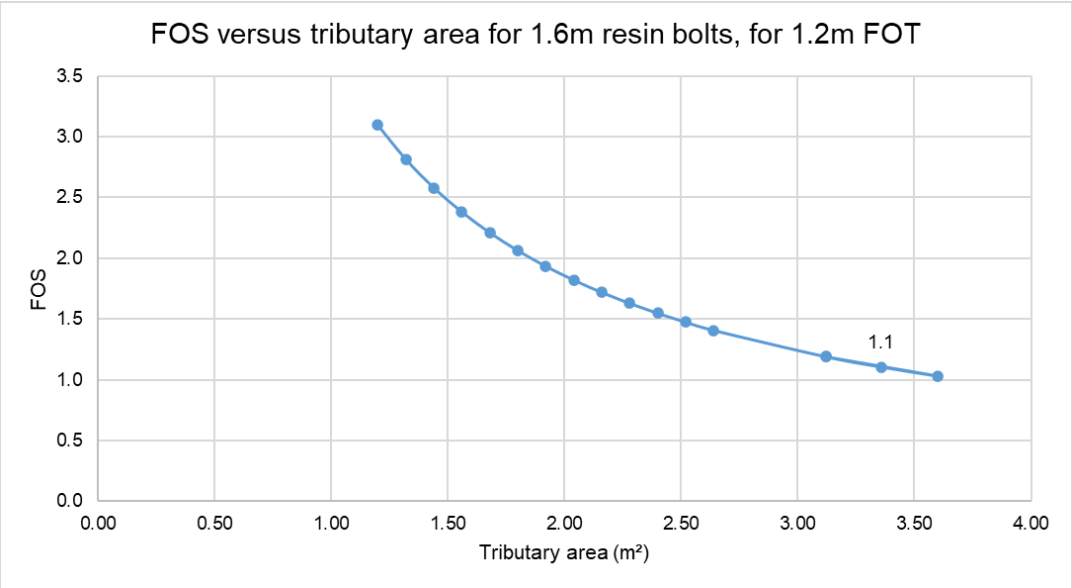

Figure 6-2. Factor of safety versus tributary area for 1.6m resin bolts.

Table 6-4. Support resistance calculation parameters and values for calculation of FOS calculation for 1.6 m resin bolts.

Support Resistance Calculations		
Known Variables:	**Value**	**Units**
Fallout height	1.20	m
Rock Density hangingwall	3.20	t/m³
Gravitational constant	9.81	m/s²
Support Resistance Required (kN/m²)	**37.67**	**kN/m²**
Bolt parameters:		
Steel Strength	550.00	MPa
Diameter	18	mm
Area	0.00025447	m²

6.3 Vertically Inclined Shear Zones

A photo of a shear zone and its position on a plan, is provided in Figure 6-3. Shear zones have a low rating of N' and will fail based on the Stability graph at a span of 10 m. The FOG database shows that shear zones unravel at as little as 4.5 m span. Therefore, a minimum practicable span is recommended for shear zones. A smaller advance means that support such as shotcrete can be applied effectively up to the face whilst the person applying the shotcrete is under supported area.

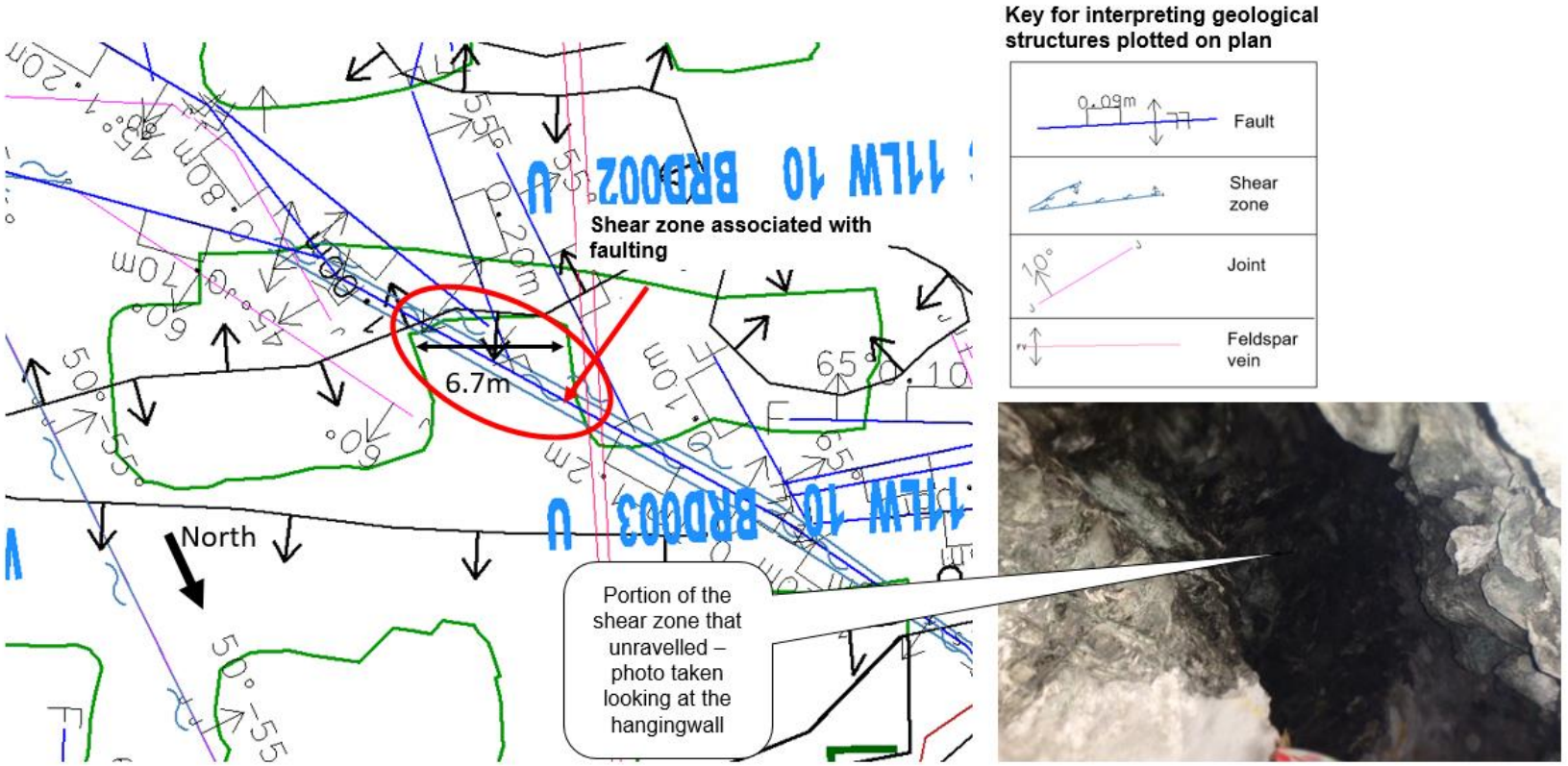

Figure 6-3. Plan view of location of an FOG due to shear zone and a photo of where the shear zone unravelled (Matsobane, 2017).

Immediate complete support is required for such ground conditions. Areal coverage requirements can be determined through RMR charts as described by Stacey (2001) as shown in Figure 6-4. For ground conditions with N' value of 0.19 (as calculated in Table 4-6), SRF of 2.5 and J_w of 1 for dry conditions, Q-value would be approximately 0.1. This would require close to 100 mm thick shotcrete at 6-8 m span.

Field observations show that the bond strength of shotcrete or Thin Spray Liners (TSL) to friable ground and slickensided features is weak. An example of such a case is shown in Figure 6-5 where the shear zone failed even after application of shotcrete. Therefore, once the shotcrete is applied, installation of support units such as mesh with trusses or straps anchored on either side of the shear zone must follow immediately. Figure 6-6 is a plan view of a panel that successfully mined through a shear zone associated with water by applying the aforementioned support strategy. The shotcrete in this case is used as a temporary support in a mechanised mine such as Bathopele where the use of nets and camlock jacks presents bolting challenges.

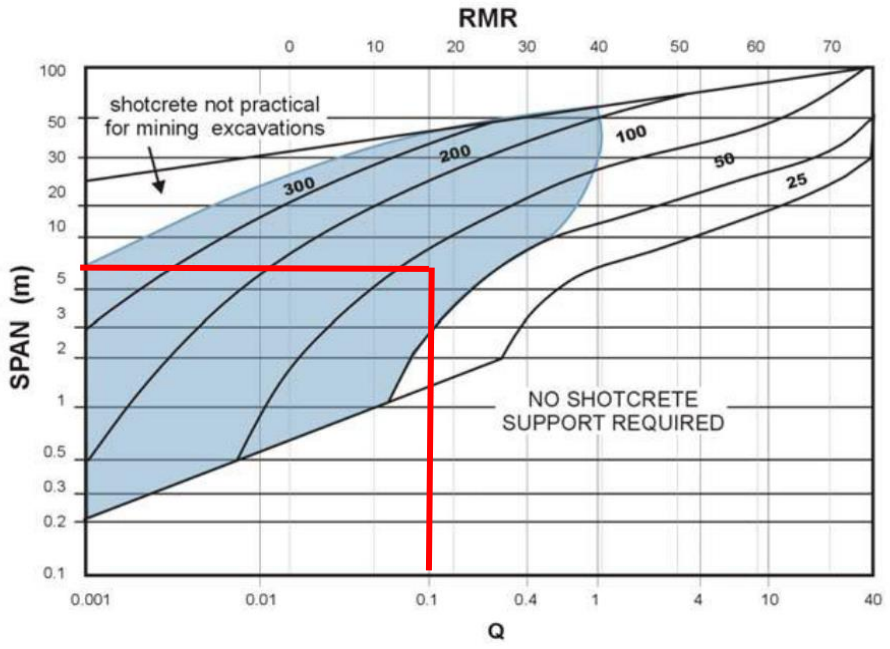

Figure 6-4. Selection of shotcrete thickness (Stacey, 2001).

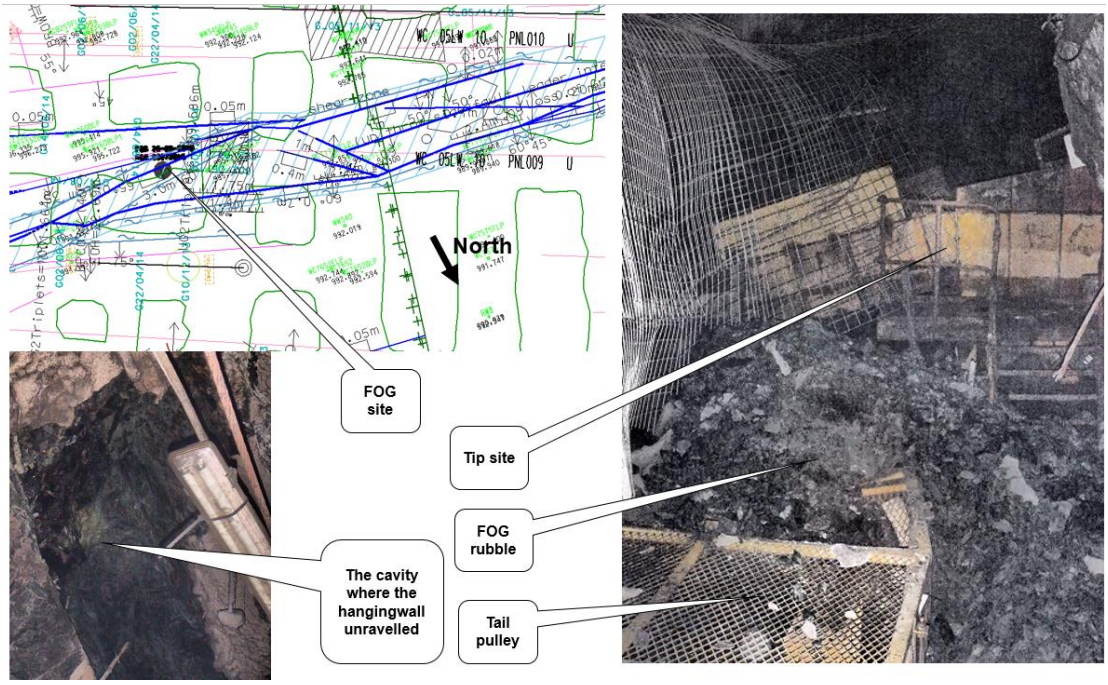

Figure 6-5. FOG that occurred from a vertically inclined shear zone at Central shaft strike 5W bord 5 (Matsobane, 2016d).

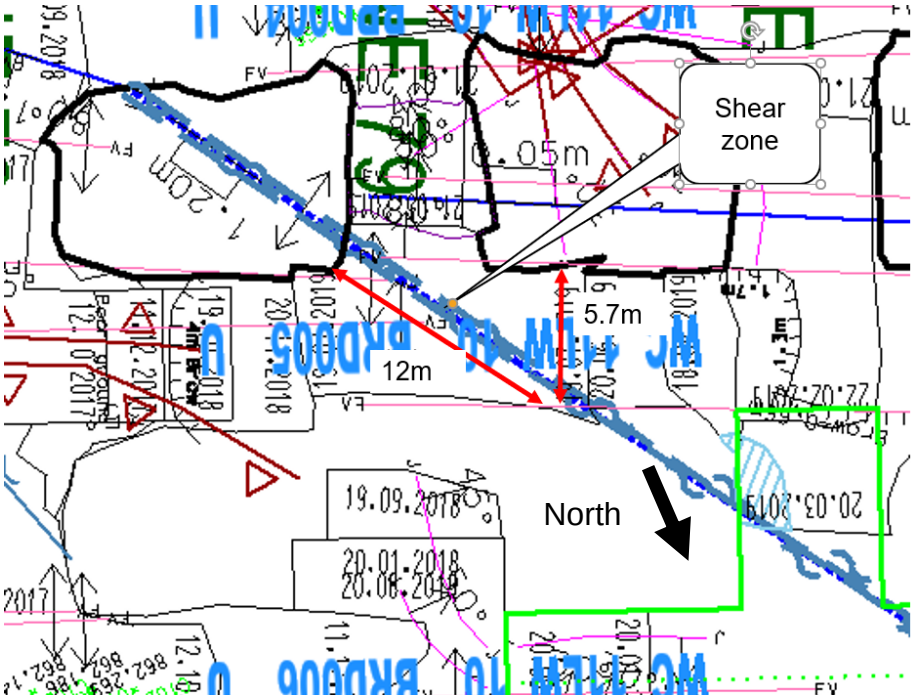

Figure 6-6. A shear zone that was successfully mined through at Central shaft strike 11W bord 5.

6.4 Shallow Dipping Structures

The Modified Stability Graph method shows that shallow dipping structures may cause hangingwall instability under the action of gravity due to their orientation with respect to the hangingwall. JBlock and Unwedge analysis show that shallow dipping structures cause instability because of their orientation with respect to JS1 to 3 and hangingwall. The intersection of the shallow dipping structures and those of JS 1 to 3 result in large wedges when compared to normal ground conditions (compare Figure 6-7 and Figure 6-8). Shallow dipping structures also result in FOT in excess of the length of primary support (Appendix F shows these results). As a result, bolts primarily fail because they

are of insufficient length. Bond and steel failure account for 12% of bolt failure in the analysis. Capacity of support in relation to demand is therefore still a concern.

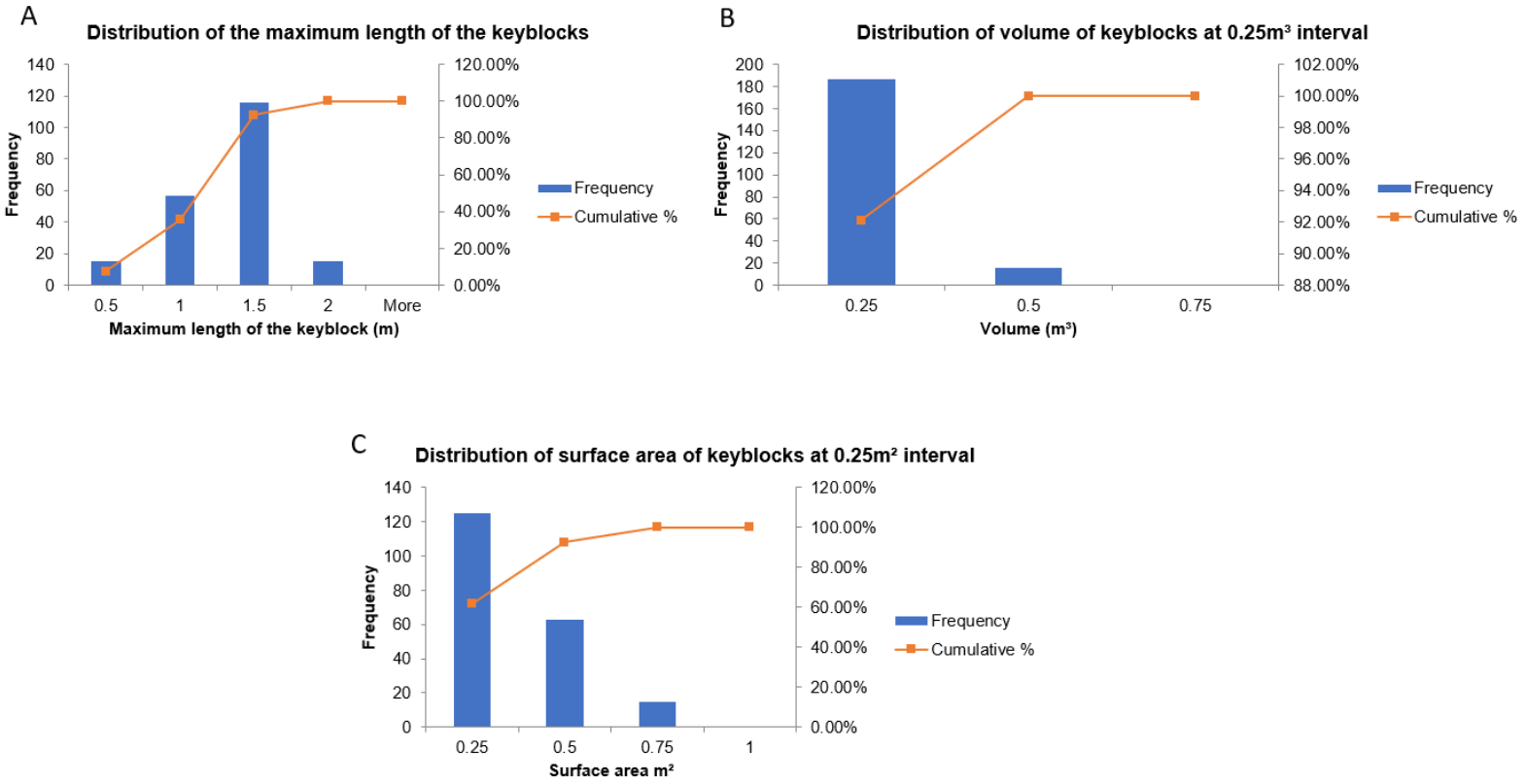

Figure 6-7. JBlock results for normal ground conditions with FOT at 1.3m.

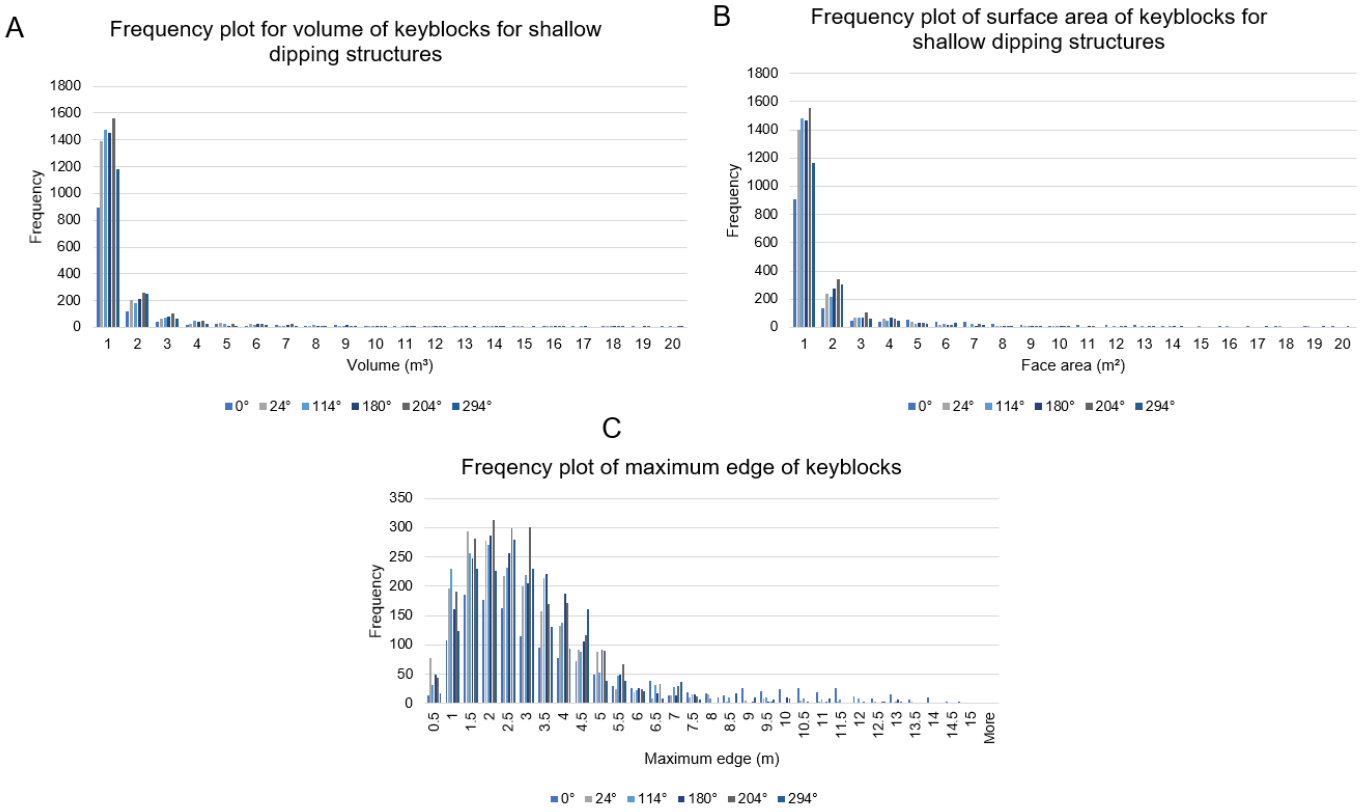

Figure 6-8. Frequency plots of dimensions of ground conditions with low angled ramp structures (excluding R1).

The strategy for addressing shallow dipping structures should therefore be aimed at a reduction in potential FOT or increase in support length and support capacity. The different strategies can be implemented simultaneously. The steps outlined in Figure 6-9 can be followed in addressing shallow dipping structures together with the guidelines provided in Table 6-2 and Table 6-3.

The issue of bond and steel failure can be addressed by increasing the support capacity or density. For instance, 3 m long coupling bolts can be installed at 1.2 m x 1.2 m spacing instead of 1. 5 m x 1.2 m spacing. However, the spacing of these bolts cannot exceed a tributary area of 2.3 m^2 to achieve at least a FOS of 1.1 as shown in Figure 6-10 for a FOT of 2.6 m. The parameters used in calculating the FOS in Figure 6-10 are provided in Table 6-5.

The position at which 1.6 m or 3 m bolts must be installed on the weak side of the shallow dipping structures can be determined using the nomogram in Figure 6-11. In order to effectively support shallow dipping structures, at least 30 cm of bond length is required above the plane of the shallow dipping structure into the hangingwall. This is to ensure that the wedges created by the structures are anchored beyond the plane of the structures into the solid.

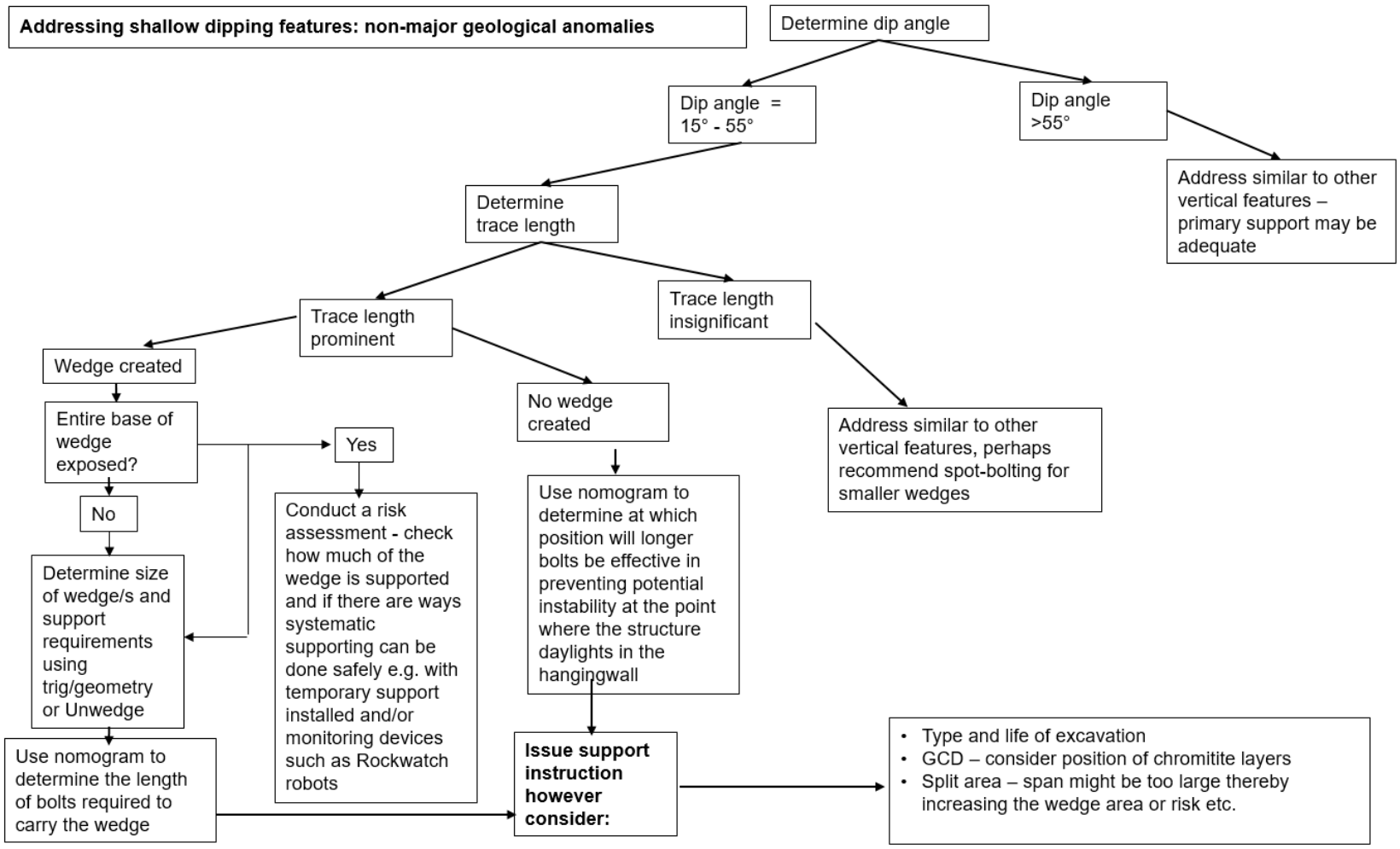

Figure 6-9. Recommended guidelines for addressing shallow dipping structures.

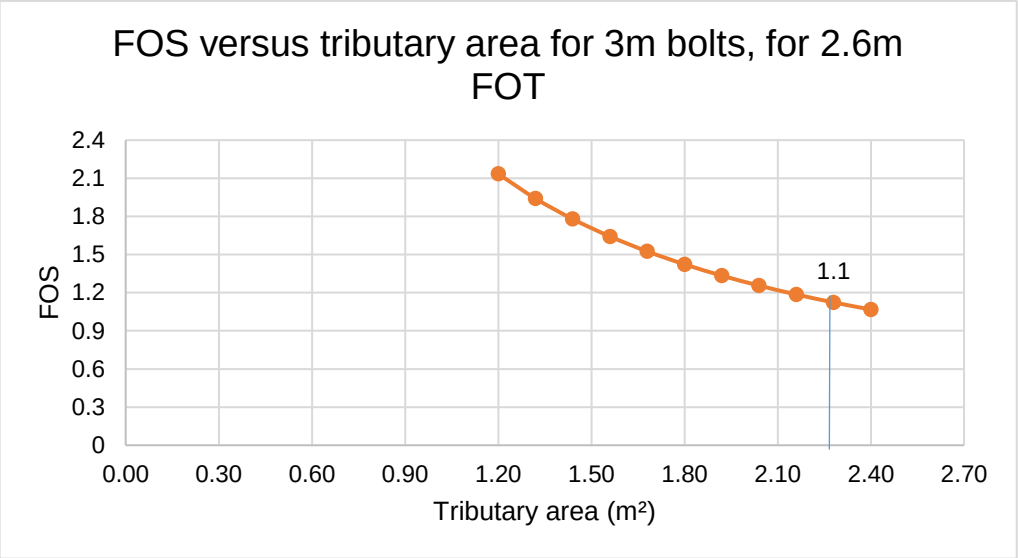

Figure 6-10. Factor of safety versus tributary area for 3m bolts for 2.6m fallout thickness.

Table 6-5. Support resistance calculation parameters and values for calculation of FOS for 3 m resin bolts.

Known Variables:	**Value**	**Unit**
Fallout height	2.60	m
Rock Density hangingwall	3.20	t/m³
Gravitational constant	9.81	m/s²
Support Resistance Required (kN/m²)	**81.62**	**kN/m²**
Bolt parameters:		
Steel Strength	550.00	MPa
Diameter	22	mm
Area	0.00038013	m²

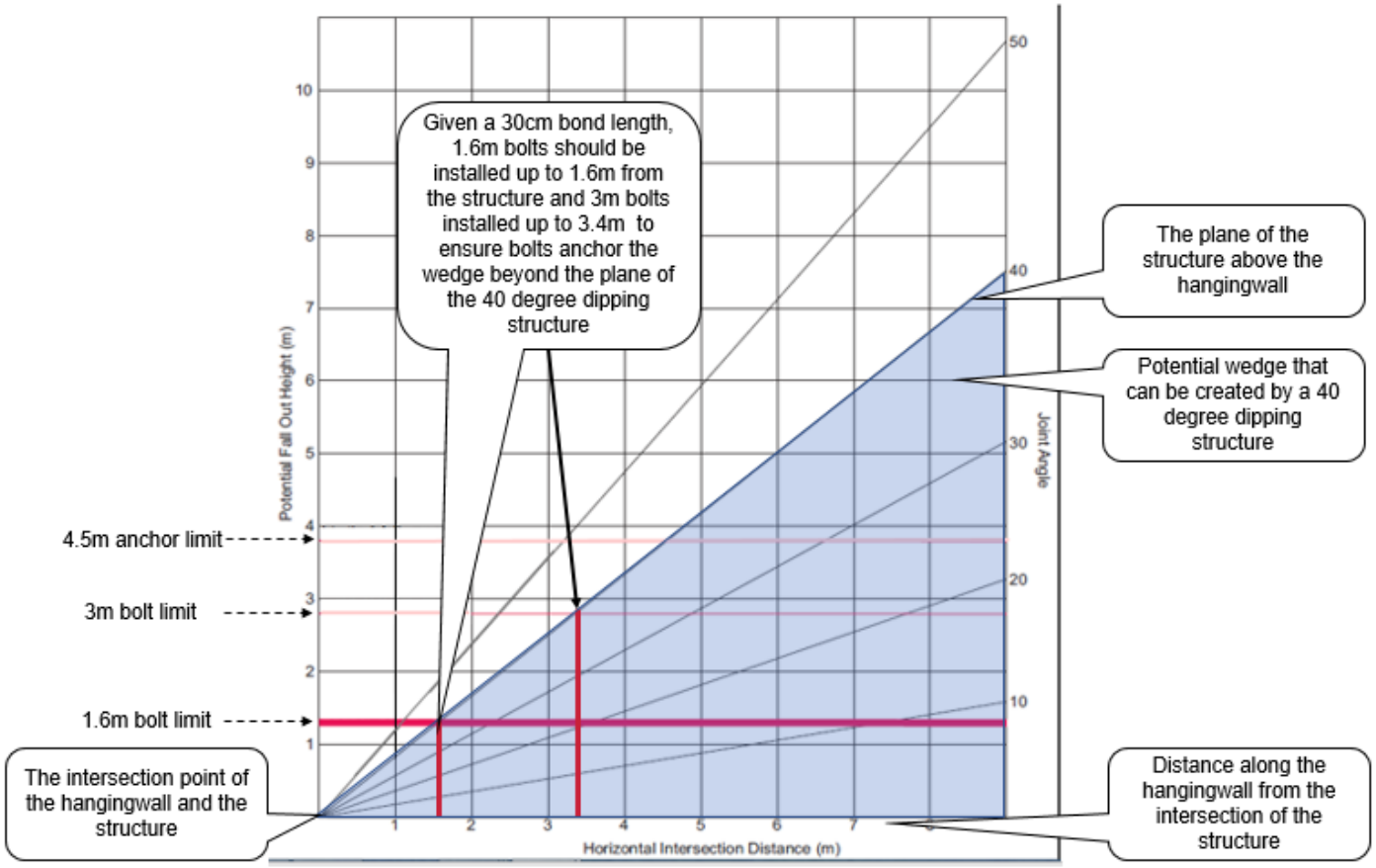

Figure 6-11. Nomogram for determining effective length of bolts and determining the point at which the bolts become ineffective (After Carstens, 2013).

It is clear that there is benefit to reducing the span and advance per blast but taking into consideration the limitations of the methods of assessment in this study as discussed in Chapter 4 and 5, the position of structures within the excavation is important. Therefore, given the option, the reduction in span should be strategic. The strategic reduction in panel span is illustrated in Figure 6-12.

Two possible solutions to addressing the 30° dipping fault are presented in Figure 6-12. A shallow dipping structure can either be bracketed or the span can be reduced in order to minimize the potential FOT. The bord can be mined at bottom portion of the panel, thereby bracketing the fault as shown in diagram B. If no other structures are intersected and there are no parting planes, with this strategy mining can safely continue with 1.6 m resin bolts.

The second option is to mine the top portion of the panel (see diagram C in Figure 6-12). If the shear persists as the face advances, the shear would be bracketed with this option. This option would also result in a decrease in diagonal span on the weak side of the fault. Sometimes the function of the excavation and the general mining and ventilation strategy of the section might influence the support recommendation from TARP members and hence it is best to consider various options. If the shear and the fault have slickensides, then the reduction of span can be accompanied by a reduction in advance per blast.

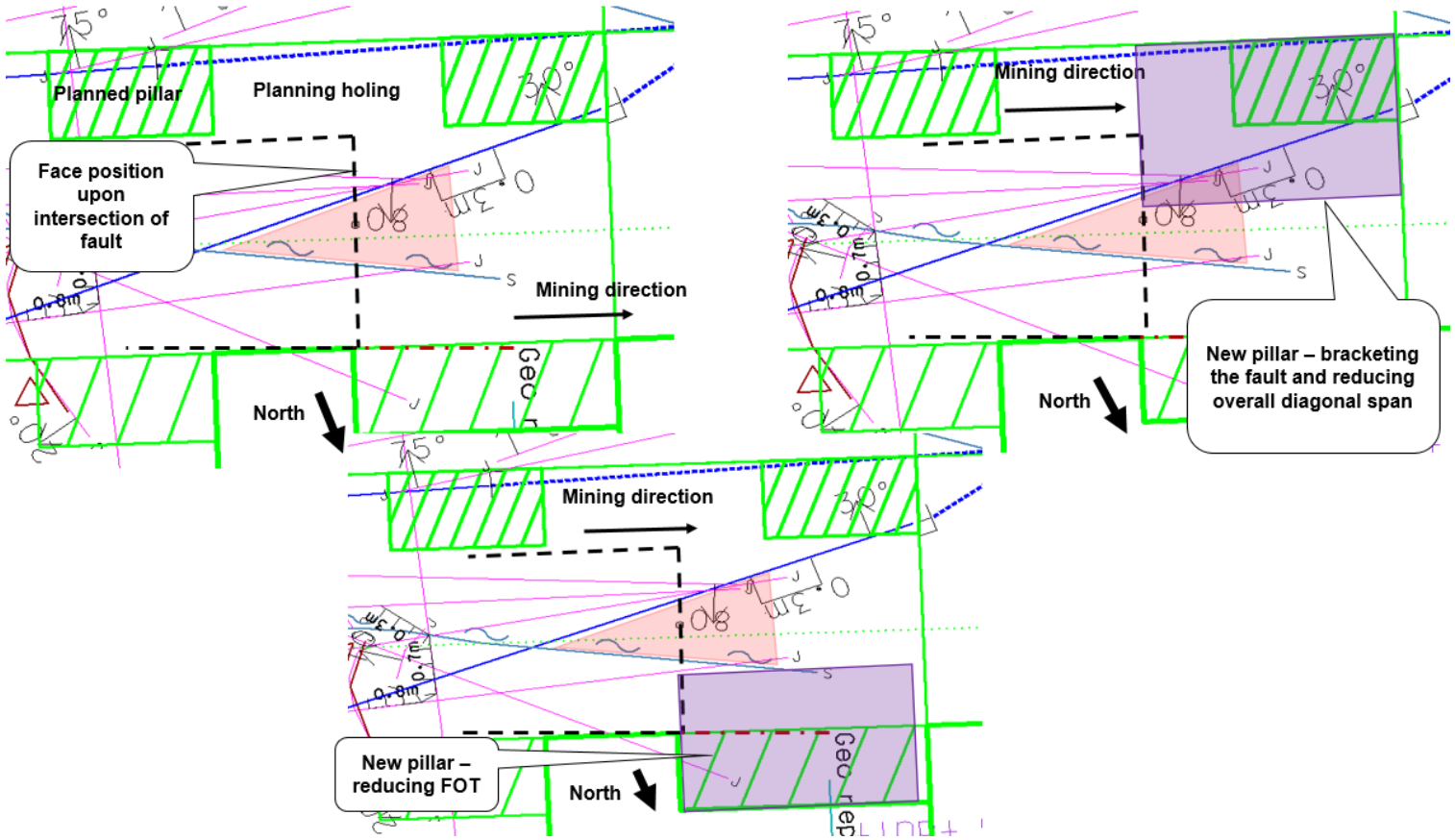

Figure 6-12. Strategic application of reducing panel span for dealing with shallow dipping structures.

The inherent hurried nature of a mining operation due to production targets dictates that proper support instruction be made available as soon as practically possible. As such, it is recommended that a design and support recommendation tool be made available to TARP members. For instance, the nomogram can be printed, cut and pasted on inside covers of field books and instruction books. Having such a tool readily available underground can assist with issuing of timeous support instructions.

Workplaces can be stopped temporarily underground until such time that appropriate support instructions are issued. A TARP member can quickly and easily enter information into an excel spreadsheet and support requirements can be known immediately. Following which, support instructions can be issued within the same shift using an instruction book whilst a formal report is being drafted.

Examples of excel tools are provided in Figure 6-13 and Figure 6-14. Figure 6-13 is for a rectangular block where instability due to parting plane is a concern. Figure 6-14 is for a tapered wedge.

Support data	Units	Value
1,6m resin bolt capacity		
Mass	t	14
Weight	kN	137.34
3m coupling bolt capacity		
Mass	t	20
Weight	kN	196.2
Cable anchor		
Mass	t	25
Weight	kN	245.25
	t	38
	kN	372.78

In-put data	Units	Value
Gravitational force (g)	m/s^2	9.81
Rock density	kg/m^3	3200
FOS	_	1.2
h	m	1.3
F	kN	48.97152
	m^2	2.8044872
Support spacing	m	1.6746603

Figure 6-13. An example of an excel tool that can be used to determine support requirements for rectangular wedges.

In-put data	Units	Value
Gravitational force (g)	m/s^2	9.81
Rock density	t/m^3	3.2
FOS (man-made)	_	1.2
FOS (natural)	_	1.5
θ (b)	°	40
a	m	5
b	m	10
c	m	7
h1	m	4
h2	m	3.356399
B	m^2	20
Volume	m^3	22.37599
Mass	t	85.9238
Weight	kN	842.9125
Number of 3m bolts required	_	4.29619

Support data	Units	Value
1,6m resin bolt capacity		
Mass	t	14
Weight	kN	137.34
3m coupling bolt capacity		
Mass	t	20
Weight	kN	196.2
Cable anchor		
Mass	t	25
Weight	kN	245.25
	t	38
	kN	372.78

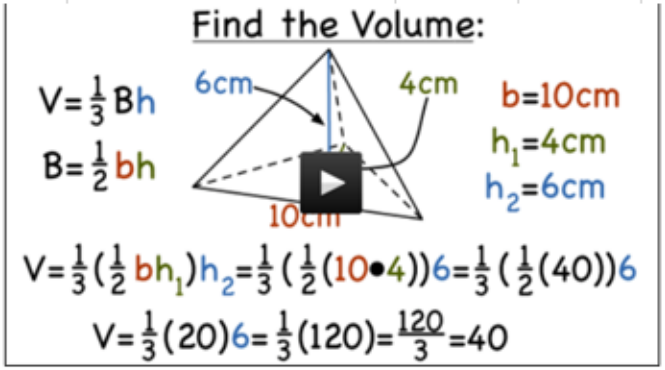

Figure 6-14. An example of an excel tool that can be used to determine support requirements for tapered wedges.

Secondary learnings during the project are summarised as follows:

i. In order to use a fall of ground database for support assessment or design purposes, the database should have geotechnical data. Most of the information during this project had to be collected from the FOG reports however, such information should be readily available in a FOG database. During compilation of this report, the FOG database was reviewed and Sibanye Stillwater operations will use the same database across the operations with minor differences between the bord and pillar operations and the breast stoping operations.
ii. Collection of joint data should be one of the functions of the rock engineering department. It was included in the rock engineer's performance contract only starting in 2019. Rock engineering personnel are being used for functions that should be addressed by legally appointed production personnel and safety department and the technical rock engineering functions are neglected in the process.
iii. With enough data, further analysis on other factors that influence stability such as change in mining direction may be assessed.
iv. Training and coaching using a set of guidelines on joint mapping should be done to avoid large difference in data. The guidelines should be site specific based on the FOGs and perhaps local experience.

v. Immediate stoppage of panels upon intersection of abnormal ground conditions must be done. Mining through geological structures without stopping should not be tolerated. It presents a risk of instability during supporting of the panels at a later stage.

vi. Training of production personnel on hazard identification is critical to the success of TARP. Both computer aided and practical training is required. Importantly, people should be held accountable for non-compliance. If proper training is done, then people can be held accountable.

vii. The importance and compliance of TARP recommendations at a mining operation cannot be overemphasized.

7 CONCLUSIONS

Assessment of hangingwall stability in the face area was necessitated by FOGs that have occurred in the face area following the provision of support recommendations by TARP members. FOG analyses show that the majority of FOGs at Sibanye Stillwater bord and pillar mining operations occur in the face area. Given that the TARP system is applied primarily to the face area, it then followed that the face area should be assessed. The aim of the assessment of the face area was to provide TARP members with guidelines when presented with various ground conditions to make informed decisions. The informed decisions can be made based on experience, empirical data and numerical modelling. This project was about establishing the guidelines.

The previous and current support design at Bathopele was reviewed to determine if the information contained in the design can be used in establishing guidelines. The main shortcoming of the current support design is that it does not address all ground conditions. In particular, the effects of advance per blast and the contribution of the last line of support are not clearly defined.

A literature review was done to determine what information is available, which could be added to the guidelines. The FOG database was analysed to determine the FOG mechanisms at Bathopele. The results of the investigation were used to determine appropriate methods of assessment. It was found that the FOGs are structurally controlled and gravity induced,

with very low clamping stresses. From the initial investigations, it was apparent that the most appropriate methods of assessment were JBlock, modified stability graph method and Unwedge.

A site was selected on the western side of Central shaft for the investigation. Joint data was collected within this area. The data was processed using DIPS in order to determine major joint sets. Various ground conditions were assessed using the Potvin's stability graph, JBlock, Unwedge and analytical vertical tensile zone solutions. The ground conditions that were assessed are:

- ground conditions with vertically inclined structures only and without partings;
- ground conditions with vertically inclined structures and a parting plane 1.0 m above the hangingwall (the nearest stratification plane is never closer than 1 m above the reef hangingwall except adjacent to potholes); and
- conditions influenced by a shear zone and ramp structures.

The dip direction of the ramp structures was varied to account for most of the orientations of the structures encountered at Bathopele.

The primary factors that were analysed are maximum unsupported length of bord for various ground conditions, the influence of shallow dipping structures and parting planes on hangingwall stability. Abnormal conditions

were compared to normal ground conditions. The stabilizing influences of reduction in mining span and advance per blast were investigated.

It was determined that the current 10 m bord spans can be safely accommodated at Bathopele for normal ground conditions. The zone of influence of the last line of support is subject to the size of the keyblocks, which was generally small due to the number of vertically inclined discontinuities. However, the FOGs that can be anticipated with vertically inclined discontinuities are smaller than the support spacing. Generally, such small rocks are addressed by systematic barring.

Parting planes are generally only problematic when intersecting potholes and slumps. In these instances, capacity of bolts versus the demand of the blocks created by partings is crucial, for which the demand is dependent on the keyblock sizes. Identifying potential keyblocks is priority when presented with these particular triggers.

The best method for addressing shear zones is immediate support installation, although the smallest span practicable is recommended. A reduction in advance per blast and panel span depends on the orientation of the shear zone, zone thickness, other discontinuities intersecting the shear zone and the secondary support equipment available.

FOGs that occur on shallow dipping structures are primarily due to insufficient bolt lengths. Therefore, strategies for shallow dipping structures

should be aimed at addressing this cause of failure, i.e. reducing the mining span and advance per blast in order to reduce the potential FOT. It should be noted that the analysis showed the mining span to have the greatest influence on stability where there are shallow dipping structures.

Addressing TARP triggers should be systematic and strategic. It should be systematic in that TARP members should first determine if exposed unsupported area is safe for support installation, then determine what is most likely to contribute to instability. The strategy should then be aimed at addressing the factor most likely to cause failure.

8 REFERENCES LIST

Andrews, P. G. & Barsanti, B. J. (2008). Results of the Radius Factor Stability Assessment Method for Design and Pillar Extraction at the Conqueror Mine, St Ives Gold Mine, Perth: Australian Centre for Geomechanics. [online] Available at: https://papers.acg.uwa.edu.au/p/808_06_Andrews/, Accessed 20 July 2021

Aquarius Platinum (SA) (Pty) Ltd. (2016). Mandatory Code of practice to Combat Rockfall and Rockburst Accidents in Tabular Metalliferous Mines - Underground: Stope support strategy and design guidelines for Kroondal and Marikana Platinum Mines, Rustenburg: Sibanye Stillwater, Reference no. *AQPSA-COP-018.1*

Barton, N. (2002). 'Some new Q-value correlations to assist in site characterisation and tunnel design', *International Journal of Rock Mechanics & Mining Sciences*, 39: 185-216.

Barton, N., (2015). Using the Q-system: Rock mass classification and support design. Retrieved from https://www.ngi.no/eng/content/download/4014/431191/version/1/inLanguage/nor-NO/file/Handbook%20The%20Q-system%20mai%202015%20nettutg.pdf.

Bathopele Survey dept. (2013). East shaft 8E P4 FOG investigation documents. Internal documents. Rustenburg: Sibanye Stillwater

Bathopele Mine (2019). 2019 FOG register, Rustenburg: Sibanye Stillwater

Brady, B. H. G., & and Brown, E.T. (2004). *Rock Mechanics for*

underground mining (3rd ed.). Retrieved from: https://www.researchgate.net/publication/49184303_Rock_Mechanics_For_Underground_Mining

Budavari, S. (1983). *Rock Mechanics in mining practice*. 1st ed. Johannesburg: The South African Institute of Mining and Metallurgy.

Carstens, R. (2013). Angle nomogram, Potential fall out thickness nomogram for Bathopele Mine. Rustenburg, Sibanye Stillwater.

Chen, J. F., (2015). Results of rock properties tests, sampling site: Bathopele mine, Rustenburg, Sibanye Stillwater. Internal Report, Reference number: *2015-Rustenburg-Platinum-Mines-01*

Daehnke, A., Roberts M. K., and Squelch A. P. (2002). Support of mine excavations, in J.A. Ryder and A. J. Jager (eds), *Rock mechanics for tabular hard rock mines* (1st ed). Johannesburg: The Safety in Mines Research Advisory Committee (SIMRAC).

Daehnke, A., Salamon, M. D., & Roberts, M. K. (2000). 'Quantifying stable hangingwall spans between support units', *The journal of The South African Institute of Mining and Metallurgy*, 375-388. https://www.saimm.co.za/Journal/v100n06p375.pdf

Dube, S. (2015). Investigation into fall of ground accident – Bathopele mine East shaft. Rustenburg, Sibanye Stillwater. Internal report. Report reference number: *bat_sd_476_20150811_East_shaft_13EP2_FOG_report.*

Dunn, M. J., Earl, P. J., and Watson, J. (2008). Support design using probabilistic keyblock methods. *Proceedings of the 6th International*

Symposium on Ground Support in mining and civil engineering construction, SAIMM, SANIRE and ISRM, Cape Town, pp. 623-636.

Enslin, Q. & Spies, P. (unknown). JBlock Training Presentation. OHMS Consultancy Division

Esterhuizen, A. (2014). 'Unique fall-of-ground prevention strategy implemented at Two Rivers Platinum Mine', *The Journal of The Southern African Institute of Mining and Metallurgy*. 114: 785-790

Esterhuizen, G. S., & Streuders, S. B. (1998). 'Rockfall hazard evaluation using probabilistic keyblock analysis', *The Journal of The Southern African Institute of Mining and Metallurgy.* 59-64.

Fourie, W. (2020). Bathopele Mine Visitors Induction 2020 presentation. Sibanye Stillwater.

Gieling, J. (2018). Short Encapsulation Pull Test (SEPT). Rocbolt Technologies for Sibanye Stillwater (Bathopele Mine). Internal Report

Gloster, C. (2016). Investigation into fall of ground accident. Rustenburg: Sibanye Stillwater. Internal report. Report reference number: *bat_cg_036_20160116_East#_15EP4_FOG_Report.*

Godden, S. (2010). Instability Risk & Hangingwall Support Design, Kroondal & Marikana, Rustenburg: Aquarius platinum. Internal report.

Gouvea, J. P. (2013). Sensitivity of key block formation to variations in shallow dipping joint set properties and effectiveness of primary support, Rustenburg: Sibanye Stillwater. Report reference number: *JP/20130913/AP01*

Handley, M.F. (2013). Report on independent rock engineering assessment of fall of ground at Bathopele mine on 20 July 2013. Rustenburg, Sibanye Stillwater. Internal Report, Reference number: *REP2013/003/MFH*

Hoek, E. (2006). *Practical rock engineering*. North Vancouver: Evert Hoek Consulting Engineer Inc.

Hoek, E., Kaiser, P. K., & Bawden, W.F. (1993). *Support of underground excavations in hard rock.* Retrieved from https://www.researchgate.net/publication/37408005_Support_of_Underground_Excavation_in_Hard_Rock

Hudson, J. A., & Harrison, J. P. (1997). *Engineering Rock Mechanics: An Introduction to the Principles* (1st ed). Oxford, Elsevier Science.

Hutchinson, D. J. & Diederichs, M. S. (1996). *Cablebolting in underground mines.* Richmond: BiTech Publishers.

Itasca (2017). FLAC3D Version 6.0, manual and user guides. Accessed on May. 29, 2020. [Online] Available: https://www.itascacg.com/software/downloads/flac3d-downloads, Itasca Consulting Group, Inc.

Jager, A. J. & Ryder, J. A. (1999). *Rock engineering practice for tabular hard rock rock mines.* Johannesburg: The Safety in Mines Research Advisory committee (SIMRAC)

Johnson, R. A., & Noble, K. (2002). Geotechnical aspects – Waterval stope design. Rustenburg, Anglo Platinum. Report reference number: *JR-003rev2-08-2002*

Joughin, W. C., Jager, A., Nezomba, E. & Rwodzi, L. (2012). 'A risk evaluation model for support design in Bushveld Complex underground mines: Part I-Description of the model', *The Journal of Southern African Institute of Mining and Metallurgy*, 112, 83-94.

Joughin, W. C., Nezomba, E., Rwodzi, L., & Jager, A., (2013). Rockfall Elimination Track B A Risk Based Approach to Enhancing Support Design in Bushveld Underground Mines Volume I, Safety in Mines Research Advisory Committee, SIM 060201 Track B.

K6, (2018). K6 Shaft FOG Incident presentation, Rustenburg, Sibanye Stillwater. Internal presentation.

Kotze, G. (2012). JBLOCK Training Course presentation. OHMS: Geotechnical Modelling Unit.

Le Bron, K. S. & Piper, P. S. (2015). Geotechnical assessment of stability between pillars for Bathopele Mine using UDEC software, Johannesburg: Groundwork. Report reference number: *CR462_Bathopele_UDEC_Modelling_RS244_May2015_Rev5*

Louw, G. (2007) Waterval shaft Rustenburg Section - FOG 4W Panel, Central Shaft, Rustenburg: Sibanye Stillwater. Internal report. Report reference number: *gl_wv_red444_20070903_FOG_report_Central#_4WP9*

Macebele, N. L. (2019). Fog report central shaft 10w brd 4, Rustenburg: Sibanye Stillwater. Internal report. Report reference number: *bat_nm_772_20191010_central_shaft_10W_P4_FOG_report*

Machuca, L., Sutton, M., Grow, R. & Andrews, B. (2015). Geotechnical approach to stope and pillar optimisation at Granny Smith Mine, Perth: Australian Centre for Geomechanics. [online] Available at: https://www.researchgate.net/publication/301629189_Geotechnical_approach_to_stope_and_pillar_optimisation_at_Granny_Smith_Mine, Accessed 20 July 2021

Matsobane, J. M. (2011). Immediate FOGM Report Bathopele Mine Central Shaft Section 8E Panel 4. Rustenburg, Sibanye Stillwater. Internal Report, Reference number: *bat_jm_475_20110822_Immediate_FOG_Report_CentralShaft_8EP4*

Matsobane, J. (2016a). Investigation into fall of ground accident. Rustenburg: Sibanye Stillwater. Internal report. Report reference number: *bat_jm_166_20160317_FOG_report_c#_3w_brd3.*

Matsobane, J. (2016b). Investigation into fall of ground accident. Rustenburg: Sibanye Stillwater. Internal report. Report reference number: *bat_jm_167_20160317_FOG_report_c#_3w_brd8*.

Matsobane, J. (2016c). Instrumentation procedure review. Rustenburg: Sibanye Stillwater. Internal report.

Matsobane, J. (2016d). Investigation into fall of ground accident. Rustenburg: Sibanye Stillwater. Internal report. Report reference number: *bat_jm_592_20160927_c#_5w_p11_FOG_report*.

Matsobane, J. (2017). FOG report Central shaft 11WP3UD. Rustenburg: Sibanye Stillwater. Internal report. Report reference number:

bat_jm_387_20170607_Central_Shaft_11WP3updip_FOG_Report.

Matsobane, J. M. (2019). Bathopele Mine: Mine support design. Rustenburg: Sibanye Stillwater. Internal report. Report reference number: *bat_jm_427_20190613_Bathopele_mine_support_design_document_v4*

Milne, D. M. (1997). Underground design and deformation based on surface geometry, Vancouver: The university of British Columbia. [online] Available at: https://open.library.ubc.ca/cIRcle/collections/ubctheses/831/items/1.0081050 Accessed 30 March 2019

Mukwevho, G. (2018). K6 # - Section 1BM2 FOG Accident. Rustenburg: Sibanye Stillwater. Internal report. Report reference number: *GM_K6_383_26072018_FOG_incident Report_08LS_PNL9_Sect.1BM2.*

Murphy, S. K., Joughin, W. C., Walls, E. J. & Zermatten, C. (2016). A handbook on practical design methodology for spans (bord widths) in bord and pillar mining on platinum and chrome mines in the Bush Veld Complex, Johannesburg: Mine Health and Safety Council. [online] Available at: http://mhsc.org.za/site/sites/default/files/public/research_documents/SIM%20150201%20Handbook_0.pdf Accessed 30 March 2019

Nezomba, E. (2012). Use of joint trace data to evaluate stability of mining excavations, and validation against underground observations. Dissertation, University of the Witwatersrand, Johannesburg.

Palmström, A. (1982). The volumetric joint count - a useful and simple measure of the degree of rock mass jointing. Proceedings of IV congress international association of engineering geology, Research Gate, New Delhi, pp. 221-228.

Palmström, A. (1995). A rock mass characterization system for rock engineering purposes. PhD thesis, Oslo University, Norway. Retrieved from http://www.rockmass.net/articles/rmi/phd_thesis_on_rmi.html

Peake, A. V., & Ashworth, S. G. E. (1996). Factors influencing the detection of unsafe hangingwall conditions. CSIR: Division of Mining Technology. Project No. GAP 202.

Potgieter, G., (2017) Bathopele Procedure Sweepings and Vampings, Rustenburg: Sibanye Stillwater. Reference number: *SSZAPGM's-PRO-MIN-BAP-0976*

Rademan, J. (2006). Fall of ground incident at W6P5 on Central shaft. Rustenburg, Sibanye Stillwater. Internal Report, Reference number: *jr_wv_RED044_20060215_FOG_Incident_W6P5*

Rajpal, Y. (2011). Immediate FOG Report Bathopele Mine East Shaft Section 10W Panel 4. Rustenburg, Sibanye Stillwater. Internal Report, Reference number: *bat_yr_553_20110920_Immediate_FOG_Report_EastShaft_10WP4_DMR*

Rocscience (2002). Dips User's guide.

Ryder, J. A., & Malan, D. F. (2002). 'Analytic elasticity and inelasticity', in

J. A. Ryder and A. J. Jager (eds), A Textbook on Rock Mechanics for Tabular Hard Rock Mines (1st ed). Johannesburg: The Safety in Mines Research Advisory Committee (SIMRAC)

Sephaphathi, T. (2017a). FOG Report Central Shaft 15w P6. Rustenburg, Sibanye Stillwater. Internal Report, Reference number: *bat_ts_838_20171127_C#_15W_Bord_6D_FOG_Report*

Sephaphathi, T. (2017b). FOG Report East Shaft 12E P10. Rustenburg, Sibanye Stillwater. Internal Report, Reference number: *bat_ts_709_20171005_East_shaft_12EP10face_FOG_Report*

Sephaphathi, T. (2019). HSE presentation, Rustenburg, Sibanye Stillwater. Internal presentation, report reference number: *bat_tm_846_20191030_HSE_November_Presentation*

Sibanda, S. M. (2012). Immediate FOGM report – Bathopele Mine, Central Shaft, 8W Panel 7. Sibanye Stillwater: Bathopele Mine. Internal report, reference number: *bat_fs_533_20121207_central_#_8W_P7_immediate_FOG_report.*

Sibanda, S.M. (2013). Bathopele Mine East Shaft 10E P9 Immediate FOGM Report. Rustenburg, Sibanye Stillwater. Internal Report, Reference number: *bat_fs_069_20130212_East#_10E_P9_immediate_FOG_report1.docx*

Sibanda, S. M. (2018). Mechanized operations group mandatory code of practice combat rock fall and rock burst accidents, Rustenburg: Sibanye Stillwater. Reference number: *SS-ZA-PGM's-MCOP-MTS-RE-1001*

Sibanda, S. M. (2019a). Mine technical services Kroondal and Rustenburg operations procedure: TARP system, Rustenburg: Sibanye Stillwater. Reference number: *SS-ZA-PGM's-PRO-MTS-RE-1006*

Sibanda, S. M. (2019b). Mine technical services trackless operations standard: Ground Control Districts and associated bord and pillar support, Rustenburg: Sibanye Stillwater. Reference number: *SS-ZA-PGM's-STD-MTS-RE-100*

Sibanda, S. M. (2019c). Rock Engineering 2019 FOG accidents and analysis, Presentation, Rustenburg: Sibanye Stillwater.

Stacey, T. R. (2001). Best practice rock engineering handbook for "other" mines. Braamfontein: The Safety in Mines Research Advisory Committee (SIMRAC).

Stacey, T. R. (2004). 'The link between the design process in rock engineering and the code of practice to combat rock fall and rockburst accidents', *The Journal of Southern African Institute of Mining and Metallurgy*, 29-34.

Stacey, T. R. (2009). The importance of engineering design with regard to safety in mining. Hard Rock Safe Safety Conference 2009: A Sense of Safety Urgency. *The Southern African Institute of Mining and Metallurgy*. Sun City, North West, South Africa.

Stacey, T. R., & Swart, A. H. (2001). Booklet: Practical Rock Engineering Practice for Shallow and Opencast Mines. Braamfontein: The Safety in Mines Research Advisory Committee (SIMRAC).

Stillborg, B. (1994). Professional users handbook for rock bolting (2nd ed.). Clausthal-Zellerfeld: Trans tech publications.

Van Rensburg, W. J. (2007). Rock engineering FOG report. Rustenburg, Sibanye Stillwater. Internal report, reference number: *wvr_wv_829_FOG_Injury_report_6WP9*

Van Rooyen, D. (2002) Waterval Business Unit Area Resource Department Rock Engineering, Rustenburg: Sibanye Stillwater. Internal report. Report reference number: *dv_1806_20021122_east_stoping_east_section1&2 doc*

Van Rooyen, L. (2010). FOG Report: Central shaft 6W P12. Rustenburg, Sibanye Stillwater. Internal Report, Reference number: *Bat_lvr_383_20100908_Central_Shaft_6W Panel 12*

Van Rooyen, L. (2011). Investigation into fall of ground accident Bathopele mine East shaft section 8e panel 1. Rustenburg, Sibanye Stillwater. Internal Report, Reference number: *bat_lvr_122_20110219_Detailed_FOG_report_East_Shaft_ Section_8E_Panel_1*

Watson, B. P., (2002). The feasibility of using rock mass ratings for the design of panel spans and support requirements in the shallow to intermediate depth Bushveld complex mines. Dissertation, University of the Witwatersrand, Johannesburg.

Watson, B. P., (2004). 'A Rock Mass Rating System for Evaluating Stope Stability on the Bushveld Platinum Mines.' *The journal of The South*

African Institute of Mining and Metallurgy, 104, 229-238.

Watson, B. P. & Gerber, R., (2018). ‘Determination of stable spans in UG2 excavations.’ *The journal of The South African Institute of Mining and Metallurgy*, 118, 493-50

A. Bathopele Fall of Ground Database (Bathopele Mine, 2019)

Shaft	Report Number	Date	Working Place	Activity	GCDG	GCDD	GCDE	GCDF	TARP classification	Mining span	Mining direction	Dist to face [m]	Location	Between face and first line of support	Depth (m)	Source	Length	Width	Thickness	Area of FOG (m^2)	Volume (m^3)	Mass [kg]	Support to Std.	correct Cut	6.FOG Boundaries
Central	0879	2002/07/09	RW3 strike 2	Barring	Y				TP3	$	Dip	$	F	Y	79	H	1,20	1,00	0,14	1,20	0,17	588	$	$	20° joint, gash vein with 50mm pegmatite infill and 1mm serpentinite infill on boundary
East	1806	2002/11/22	E1P1	$	Y				TP3	$	Strike	0,0	F	Y	$	H	$	$	$	$	$	$	$	$	Serpentinised jointing
East	0005	2003/01/02	e1p5	U	Y				TP3	$	Dip	$	F	$	57	H	5	3	2	15,00	30	102 000	N	U	Low angled jointing,dyke,pegmatite vein.
East	0169	2003/04/03	E3P4	Loading	Y				T1	$	Strike	$	F	$	$	H	2,5	2,5	0,2	6,25	1,25	4 000	Y	U	Fell along poorly exposed LT stringer
Central	0195	2003/04/24	e1p2	$	Y				TP3	$	Strike	$	F	$	$	H	$	$	$	$	$	$	N	$	Low angled joint+pegmatite vein
Central	0079	2004/02/17	Strike 8 P4	Support installation	Y				TP2	6,00	Strike	0,0	F	Y	67,5	H	0,33	0,25	0,1	0,08	0	17	Y	Y	3 intersecting joints
East	0147	2004/05/05	sec 2 p3	U	Y				TP3	6,00	Dip	0,0	F	Y	71		6	4	1,3	24,00	31,2	109 200	N	U	Low angle joint+leader seam+vein
East	0213	2005/07/28	w4p10	Hand lashing			Y		T1	$	Dip	$	F	Y	132	H	0,2	0,2	0,1	0,04	0	14	Y	U	Jointing
Central	0236	2005/08/29	w6p1	Hand lashing			Y		T1	$	Strike	0,0	F	Y	164	F	0,2	0,2	0,2	0,04	0,01	21	Y	U	Jointing
East	0316	2005/11/11	e5p3	Barring			Y		$	$	Strike	5,0	F	$	143	H	0,2	0,1	0,1	0,02	0	4	N	U	Fault and jointing

Shaft	Report Number	Date	Working Place	Activity	GCDG	GCDD	GCDE	GCDF	TARP classification	Mining span	Mining direction	Dist to face [m]	Location	Between face and first line of support	Depth (m)	Source	Length	Width	Thickness	Area of FOG (m^2)	Volume (m^3)	Mass [kg]	Support to Std.	correct Cut	6.FOG Boundaries
Central	0044	2006/02/11	w6p5				Y		TP3	9,00	Strike		F	$	174	H	5	3	2	15,00	30	20 000	Y	U	Fault + jointing
Central	0435	2006/12/20	6wp7	Support installation				Y	T1	8,60	Strike	1,0	F	Y	175	H	2,00	1,50	0,23	3,00	0,69	2 208	Y	Y	Joint + serpentinized trc
Central	0105	2007/01/24	3wp6	Barring	Y				T1	8,60	Strike	1,8	F	Y	95	S	0,20	0,20	0,05	0,04	0	4 100	Y	Y	Blast fractures + trc
East	0361	2007/07/05	3ep9	Support installation			Y		TP2	5,60	Dip	2,5	F	Y	105	F	1,40	0,90	0,27	1,26	0,34	1 089	Y	Y	Blast fractures + trc of leader seam
Central	0829	2007/12/19	6wp9	Barring		Y			TP3	4,20	Strike	2,2	F	Y	173	H	0,7	0,55	0,2	0,39	0,08	250	Y	Y	Fault
Central	0095	2008/01/23	5wp8	Drilling face			Y		TP2	6,10	Dip	2,5	F	Y	150	F	1,50	0,90	0,30	1,35	0,41	1 460	Y	N	Joints (J1) and leader seam
Central	0649	2008/11/06	3wp4	Support installation	Y				TP2	6,00	Dip	1,8	F	Y	78	H	0,40	0,40	0,15	0,16	0,02	78	Y	Y	Layering
Central	0671	2008/11/13	CDSr/w 1	Barring			Y		T1	6,70	Dip	1,7	F	Y	270	H	0,10	0,05	0,05	0,01	0	1	Y	N	Blasting fractures
East	0310	2009/09/14		Painting roof bolts			Y		T1	$	$	0,0	F	Y	217	h	0,50	0,35	0,08	0,18	0,01	42	y	y	jointing
Central	0060	2010/03/05	4wp7					Y	T1	$	$	0,0	F	Y	115	F	0,84	0,83	0,19	0,70	0,13	424	Y	Y	veins/joints
Central	383+398	2010/08/23	6wp12	Barring				Y	TP3	6,00	Strike	3,0	F	Y	175	S	0,30	0,20	0,05	0,06	0	10	Y	Y	Jointing
Central	0591	2010/12/10	6wwinze2	Blasting + loading operations				Y	TP2	$	$	0,0	F	N	188	H	5,00	3,00	1,00	15,00	15	21 600	Y	Y	Chromitite stringer+ normal J1 & J2 jointing

Shaft	Report Number	Date	Working Place	Activity	GCDG	GCDD	GCDE	GCDF	TARP classification	Mining span	Mining direction	Dist to face [m]	Location	Between face and first line of support	Depth (m)	Source	Length	Width	Thickness	Area of FOG (m^2)	Volume (m^3)	Mass [kg]	Support to Std.	correct Cut	6.FOG Boundaries
East	0085	2011/02/01	8EP9	None			Y		TP2	8,70	Dip		F	Y	225	H	3,70	2,80	0,20	10,36	2,07	6 216	N	Y	Jointing
East	0118	2011/02/14	8EP1	Barring			Y		TP3	6,50	Strike	1,0	F	Y	208	H	0,20	0,70	0,50	0,14	0,07	210	Y	Y	Reverse faulting plane with vertical pegmatoidal vein
East	0222	2011/04/12	6EP7	Support installation			Y		TP2	8,70	Strike	N/A	F	Y	168	H	0,17	0,07	0,06	0,01	0	2	Y	N/A	Fall was bounded by three joint sets one on strike and two on dip.
Central	0262	2011/05/07	7wap6e w0	Support installation		Y			TP2	7,20	Dip	0,9	F	Y	187	H	0,48	0,38	0,15	0,18	0,03	S	Y	NA	Four joints, two on dip, one on strike and one striking oblique to face. The joints had serpentinite/calcite infill <2mm thick
Central	0338	2011/06/21	9e rse	None			Y		TP2	7,10	Dip	1,3	F	Y	237	H	1,20	0,50	0,40	0,60	0,24	768	N	Y	Jointing
East	0434	2011/08/01	3EP13	Loading	Y				TP2	9,00	Strike	1,5	F	Y	96,2	H	2,00	1,70	0,35	3,40	1,19	4 403	Y	Y	Leader Seam, blocky ground
Central	0449	2011/08/02	5wp7	Barring				Y	TP2	9,00	Strike	3,0	F	Y	142	H	0,15	0,10	0,05	0,02	0	2	N	Y	65° faults and vertical joints
Central	0475	2011/08/19	8ep4	After blast				Y	TP3	9,00	Strike	0,0	F	N	217	H	6,00	2,00	0,50	12,00		19 200	Y	Y	A dome with an average dip angle of 30°, near vertical joints with pegmatite infill and joint set 1 with a dip angle of ±60° and serpentinite infill.

Shaft	Report Number	Date	Working Place	Activity	GCDG	GCDD	GCDE	GCDF	TARP classification	Mining span	Mining direction	Dist to face [m]	Location	Between face and first line of support	Depth (m)	Source	Length	Width	Thickness	Area of FOG (m^2)	Volume (m^3)	Mass [kg]	Support to Std.	correct Cut	6.FOG Boundaries
East	0553	2011/09/16	10W BRD4	After blast			Y		TP3	9,40	Strike	1,0	F	Y	255	H	2,30	1,30	0,40	2,99		3 827	Y	Y	Vertical dipping pegmatite vein and curved joint associated with the vein.
East	0554	2011/09/16	9W P3	After blast			Y		TP3	6,50	Dip	0,8	F	Y	235	H	1,50	0,50	0,30	0,75		720	Y	Y	Flat dipping joints coupled with a steep dipping fault.
East	0656	2011/12/07	Roadway 5	Loading			Y		T1	6,60	Dip	0,0	F	N/A	304	F	0,83	0,33	0,14	0,27	0,04	134	Y	Y	Top contact of UGS main seam and associated jointing.
East	0089	2012/02/24	8E P1	After blast			Y		TP3	8,80	Dip	0,0	F	Y	205	H	4,20	3,30	0,50	13,86		20 790	Y	Y	Low angle/dome structure coupled with low angled fault.
Central	0533	2012/12/07	8W P7	While drilling face		Y			TP3	6,00	Strike	0,0	F	Y	205	F	2,80	2,10	2,00	5,88	11,8	35 280	Y	Y	Portion of serpentinised fault infill. (Fault infilling is ~2.5m in total and 2.1m of that came out)
East	0069	2013/02/08	10E P9	Support installation			Y		TP3	6,60	Strike	3,5	F	Y	273	H	0,28	0,29	0,04	0,08	0	11	N	N	Low angle joint and vertical joint
Central	0094	2013/03/05	13W P8	Drilling face				Y	TP2	9,20	Strike	0,9	F	Y	332	H	0,35	0,35	0,07	0,12	0,01	27	Y	Y	The fall was bounded by 3 joints and blasting fractures. The top surface was a blasting fracture. The joints are from the same set, trending parallel to mining direction, with a vertical dip angle and serpentinite coating.
East	0120	2013/03/15	13W P6	Barring			Y		T1	7,00	Strike	0,0	F	Y	327	H	3,50	2,90	0,38	10,15	3,81	11 419	Y		2 intersecting joints and 1 blast fracture (top release surface)

Shaft	Report Number	Date	Working Place	Activity	GCDG	GCDD	GCDE	GCDF	TARP classification	Mining span	Mining direction	Dist to face [m]	Location	Between face and first line of support	Depth (m)	Source	Length	Width	Thickness	Area of FOG (m^2)	Volume (m^3)	Mass [kg]	Support to Std.	correct Cut	6.FOG Boundaries
East	$	2013/07/20	8E P4	Support installation			Y		TP3	9,00	Strike	4,0	F	N	208	H	14,00	7,00	4,50		441	1 300 000	N	N	Low angle joint and vertical fault.
Central	0691	2013/11/21	8W P7	Face preparation				Y	TP2	8,40	Strike	1,0	F	N	215	S	0,34	0,19	0,14	0,10	0,01	29	Y	N	Blasting fractures, a joint and a faulted vein.
Central	0770	2013/12/10	10E P3	None			Y		TP3	>25 m	Strike	0,0	F	N	264	H	10,00	6,00	1,50	33,00	90	256 500	Y	Y	35° fault, ±85° faulted vein and Joints
East	0413	2014/06/17	12EP1	Face preparation			Y		T1	9,10	Strike	0,0	F	Y	296	F	0,80	0,70	0,30	0,56	0,17	538	Y	N	FOG was top bounded by the LT stringer and 80 degree dipping joints on the sides. The side parallel to the face was bounded by a blasting fracture.
East	0008	2015/01/05	11EP10	identified during start-			Y		TP2	6,30	Strike	0,0	F	Y	289	H	1,80	1,20	0,15	2,20	0,32	342	N	Y	Top contact of leader seam to pyroxenite, vertical jointing
East	0476	2015/08/10	13E P2	None			Y		TP3	8,40	Strike	0,0	F	Y	315	H	6,50	3,00	1,10	12,90	21,5	11 440	Y	Y	35 degree dipping domal joint and vertical joints
Central	0538	2015/09/08	BDS 15EP5	Drilling			Y		TP2	6,00	Strike	3,0	F	No	373	S	0,90	0,70	0,15	0,60	0,09	320	Y	Y	Pothole, IRUP
East	0036	2016/01/14	15E P4	Support installation			Y		TP2	8,90	Strike	0,0	F	y	359	H	4,00	3,00	0,50	12,00	6	5 584	Y	N	Iron replacement ultramafic pegmatite, multiple joints
East	0043	2016/01/18	8EP4	Support installation			Y		TP2	9,60	Dip	3,0	F	Y	207	H	1,00	0,30	0,10	0,50	0,03	96	Y	N	Bottom contact of leader seam and brow face
Central	0139	2016/03/10	8WP1	None			Y		TP3	$	$	0,0	F	Y	290	H	1,50	0,70	0,55	0,50	0,58	1 600	Y	Y	low angle joints + veins
Central	0166	2016/03/16	3WBR D3	None	Y				TP3	7,60	Strike	0,0	F	Y	50	H	7,30	2,30	1,60	8,40	26,9	14 327	N	Y	The fall boundaries were a shallow dipping joint, vertical joints and a shear zone.
Central	0167	2016/03/16	3WBR D8	None	Y				TP2	8,00	Strike	0,0	F	Y	67	H	3,00	2,00	0,30	6,00	1,8	5 760	Y	Y	The fall boundaries were chromitite stringers (exposed due to pothole) and vertical joints.

Shaft	Report Number	Date	Working Place	Activity	GCDG	GCDD	GCDE	GCDF	TARP classification	Mining span	Mining direction	Dist to face [m]	Location	Between face and first line of support	Depth (m)	Source	Length	Width	Thickness	Area of FOG (m^2)	Volume (m^3)	Mass [kg]	Support to Std.	correct Cut	6.FOG Boundaries
Central	$	2016/04/08	7WBR D4 RSE	None				Y	TP2	$	$	0,0	F	Y	184	H	2,80	3,00	0,15	8,40	1,26	4 032	Y	Y	Double chrome stringers and vertical serpentinized joint
East	0695	2016/11/04	10E P8	None			Y		TP3	$	$	0,0	F	Y	258	H	4,20	1,09	1,05	2,29	4,81	7 210	Y	Y	Vertical vein and low angle fault
Central	bat387	2017/06/07	11W P3 up dip	None				Y	TP2	6,40	Dip	0,0	F	Y	271	H	4,00	0,80	0,90	3,20	2,88	8 208	Y	Y	Vertical shear zone
East	bat709	2017/10/05	12E P10 face	Support installation			Y		TP2	5,80	Strike	2,5	F	Y	311	H	2,00	1,80	0,50	3,60	1,8	5 760	Y	Y	Fault, parting planes, vertical joints.
Central	0838	Unknown - 2017	15WBr d6D	None			Y		TP3	7,40	Intersection	0,0	f	n	348	h	10,00	6,50	1,30	65,70	84,5	272 960	n	y	Shallow dipping fault, lamp dyke and vertical faults and joints
East	0521	2018/07/20	15E BRD8	Drilling face			Y		TP3	6,70	Dip	0,0	F	Y	372	H	1,28	0,33	0,41	0,42	0,17	554	Y	Y	Shallow dipping fault, LT stringer and joint
Central	0167	2019/03/09	14E BRD13	Inspecting socket holes			Y		T1	9,80	Strike	0,0	F	Y	350	F	0,33	0,11	0,05	0,04	0	6	Y	Y	Blast fractures and joints
East	0746	2019/10/01	10E BRD5	Barring			Y		TP2	7,50	Strike	3,5	F	Y	245	H	$	$	$	$	$	$	Y	Y	Joints and horizontal parting plane
Central	0772	2019/10/10	10W BRD4	With blast and None				Y	TP2	4,70	Strike	0,0	F	Y	212	H	3,70	4,70	0,70	17,39	12,2	38 954	Y	N	Joints striking perpendicular to the face, double chrome stringers and two sub-vertical veins on the contact of both sidewalls
East	0840	2019/10/25	14W BRD9	Face preparation			Y		T1	6,80	Up dip	0,0	F	Y	350	F	0,32	0,25	0,55	0,08	0	14	y	y	Blasting fractures

B. Bathopele Geology Legend

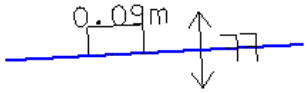 Fault	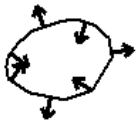 Reef roll
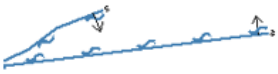 Shear	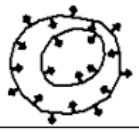 Slumped reef
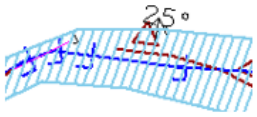 Structures associated with water	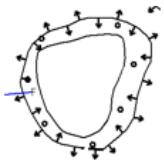 Pothole
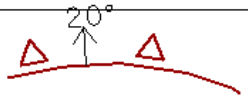 Dome	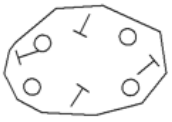 IRUP
 Joint	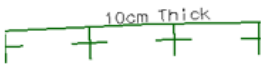 Dolerite dyke
 Feldspar vein	

C. Mapping Data

C.1 A log of the scanlines

Traverse ID in Dips	Scanline ID	Shaft	Mining distri	Sectio	Panel	Exact location of scanline	Dip (°)	Dip direction	Length (m)
11	SL011/2019	Central	Dual seam	9W	6	BLTT2986 + 29m	9	22.5	9.9
12	SL012/2019	Central	Dual seam	9W	1	WC9478 + 14,2m	9	22.5	6.6
13	SL013/2019	Central	Dual seam	10W	5	BLT2623 + 5,2m	9	22.5	6.7
16	SL016/2019	Central	Dual seam	6W	1A	C10720 + 66m	9	12	5.4
17	SL017/2019	Central	Dual seam	6W	1A	C10720 + 63,2m	0	132	7.2
18	SL018/2019	Central	Dual seam	5W	12	C00600 - 7,6m	0	112	5.5
21	SL021/2019	Central	Dual seam	6W	6	E000757 + 43,8m	9	24	9
22	SL022/2019	Central	Dual seam	6W	6	E000757 + 43,8m	0	114	10
23	SL023/2019	Central	Dual seam	6W	4	C10562 + 10,7m	9	24	8
24	SL024/2019	Central	Dual seam	6W	4	C10562 + 10,7m	0	114	10
25	SL025/2019	Central	Dual seam	7W	9	C10946 + 21,25m	9	24	9.9
26	SL026/2019	Central	Dual seam	7W	9	C10946 + 21,25m	0	114	10
27	SL027/2019	Central	Dual seam	10W	10	C00906 + 15m	0	114	6
28	SL028/2019	Central	Dual seam	10W	10	C00906 + 18m	9	24	6
29	SL029/2019	Central	Dual seam	8W	4	C00767 + 12,6m	8.5	4	6.3
30	SL030/2019	Central	Dual seam	8W	4	C00767 + 12,6m	0	114	5
31	SL031/2019	Central	Dual seam	8W	5	C00732 + 37m	8	19	6.7
32	SL032/2019	Central	Dual seam	8W	5	C00732 + 37m	0	114	7
33	SL033/2019	Central	Dual seam	8W	6	BLT1840 + 25m	8	14	5.5
34	SL034/2019	Central	Dual seam	8W	6	BLT1840 + 25m	0	99	10
35	SL035/2019	Central	Dual seam	10W	7	C00760 + 24m	0	114	7
36	SL036/2019	Central	Dual seam	10W	7	C00760 + 24m	9	24	7
37	SL037/2019	Central	Dual seam	5W	8	C10560 + 31,1m	9	24	6
38	SL038/2019	Central	Dual seam	5W	8	C10560 + 28,1m	0	114	9
39	SL039/2019	Central	Dual seam	7W	11	BLT1837 + 21,7m	9	34	9.4
40	SL040/2019	Central	Dual seam	7W	11	BLT1837 + 21,7m	0	114	10
41	SL041/2019	Central	Dual seam	8W	5	C00732 + 54,6m	9	24	5
42	SL042/2019	Central	Dual seam	8W	5	C00732 + 51,6m	0	114	5
43	SL043/2019	Central	Dual seam	9W	4	C00810 + 11,2m	9	29	10.5
44	SL044/2019	Central	Dual seam	9W	4	C00810 + 11,2m	0	114	14
45	SL045/2019	Central	Dual seam	7W	8	C00672 + 35,6m	10	24	5.4
46	SL046/2019	Central	Dual seam	11W	4	C00747 + 15,7m	9	24	8
47	SL047/2019	Central	Dual seam	11W	4	C00747 + 15,7m	0	114	10
48	SL048/2019	Central	Dual seam	14W	1H	C00860 + 24,5m	0	114	7.8
49	SL049/2019	Central	Dual seam	14W	1H	C00860 + 24,5m	8.5	24	5.2
50	SL050/2019	Central	Dual seam	14W	1F	C00789 + 21m	0	114	9.5
51	SL051/2019	Central	Dual seam	14W	1F	C00789 + 21m	9	24	10
52	SL052/2019	Central	Dual seam	14W	1C	C00780 + 23m	0	114	7
53	SL053/2019	Central	Dual seam	14W	1C	C00780 + 23m	9	24	10
54	SL054/2019	Central	Dual seam	9W	4	C00810 + 23,9m	9	24	8
55	SL055/2019	Central	Dual seam	9W	4	C00810 + 23,9m	0	114	10
56	SL056/2019	Central	Dual seam	9W	7	C00808 +26,5m	0	114	10
57	SL057/2019	Central	Dual seam	9W	7	C00808 +26,5m	9	24	9
58	SL058/2019	Central	Dual seam	7W	7	C00766 +25,9m	29	5	6.4
59	SL059/2019	Central	Dual seam	7W	7	C00766 +25,9m	0	114	4.6
60	SL060/2019	Central	Dual seam	9W	6	BLT2654 + 41,7m	8.5	24	5.8
61	SL061/2019	Central	Dual seam	9W	6	BLT2654 + 36m	0	114	5.3
62	SL062/2019	Central	Dual seam	9W	5	C00901 + 21m	8.5	24	7.6
63	SL063/2019	Central	Dual seam	9W	5	C00901 + 16,8m	0	114	4.2

C.2 Data of mapped discontinuities

Dip (°)	Strike	Dip direction (°)	Scanline ID	Off Set Angle (clockwise) (°)	Structure	Spacing (m)	Infill Type	Infill Thickness	Separation	Surface shape	Surface roughness	Persistance	Ends
85	112.5	202.5	11	90	Vein	1.00	Serpentinite	>30mm	Tight	Planar	Smooth	>30m	Both ends visible
85	112.5	202.5	11	90	Vein	0.10	Serpentinite	>30mm	Tight	Planar	Smooth	>30m	Both ends visible
85	257.5	347.5	11	35	Joint	1.50	Serpentinite	<1mm	Tight	Discontinuous	Smooth	1-3m	Both ends visible
85	212.5	302.5	11	80	Joint	0.00	Serpentinite	<1mm	Tight	Planar	Smooth	3-10m	One end visible
85	257.5	347.5	11	35	Joint	0.10	Serpentinite	<1mm	Tight	Discontinuous	Smooth	<1m	Both ends visible
85	257.5	347.5	11	35	Joint	0.10	Serpentinite	<1mm	Tight	Discontinuous	Smooth	<1m	Both ends visible
85	257.5	347.5	11	35	Vein	0.90	Serpentinite	10-30mm	<1mm	Planar	Smooth	3-10m	Both ends visible
85	257.5	347.5	11	35	Vein	0.50	Serpentinite	10-30mm	<1mm	Planar	Smooth	10-30m	One end visible
85	257.5	347.5	11	35	Vein	0.80	Serpentinite	1-3mm	Tight	Undulating	Smooth	10-30m	No ends visible
85	257.5	347.5	11	35	Joint	0.08	Serpentinite	<1mm	Tight	Discontinuous	Smooth	1-3m	Both ends visible
85	257.5	347.5	11	35	Joint	0.04	Serpentinite	<1mm	Tight	Discontinuous	Smooth	<1m	Both ends visible
85	257.5	347.5	11	35	Joint	0.58	Serpentinite	<1mm	Tight	Discontinuous	Smooth	<1m	Both ends visible
85	257.5	347.5	11	35	Joint	-0.40	Serpentinite	<1mm	Tight	Discontinuous	Smooth	3-10m	Both ends visible
85	257.5	347.5	11	35	Vein	1.30	Serpentinite	>30mm	Tight	Planar	Smooth	10-30m	One end visible
85	257.5	347.5	11	35	Vein	1.40	Serpentinite	10-30mm	Tight	Planar	Smooth	10-30m	Both ends visible
85	257.5	347.5	11	35	Vein	0.74	Serpentinite	10-30mm	Tight	Undulating	Smooth	1-3m	Both ends visible
65	257.5	347.5	11	35	Vein	0.36	Serpentinite	>30mm	1-3mm	Planar	Smooth	10-30m	One end visible
85	112.5	202.5	12	90	Vein	0.52	Serpentinite	>30mm	Tight	Planar	Smooth	>30m	One end visible
85	112.5	202.5	12	90	Joint	3.08	Serpentinite	<1mm	Tight	Discontinuous	Smooth	1-3m	Both ends visible
90	219.5	309.5	13	73	Joint	0.20	Serpentinite	<1mm	Tight	Discontinuous	Smooth	1-3m	Both ends visible
90	202.5	292.5	13	90	Joint	0.07	Serpentinite	<1mm	Tight	Discontinuous	Smooth	<1m	Both ends visible
90	202.5	292.5	13	90	Joint	0.53	No infill	None	<1mm	Discontinuous	Rough	1-3m	Both ends visible
85	202.5	292.5	13	90	Vein	0.10	Serpentinite	1-3mm	Tight	Planar	Smooth	>30m	Both ends visible
85	202.5	292.5	13	90	Vein	0.40	Serpentinite	1-3mm	Tight	Planar	Smooth	>30m	Both ends visible
90	202.5	292.5	13	90	Joint	0.80	Serpentinite	<1mm	Tight	Discontinuous	Smooth	1-3m	Both ends visible
90	202.5	292.5	13	90	Joint	0.40	Serpentinite	<1mm	Tight	Planar	Smooth	10-30m	Both ends visible
80	202.5	292.5	13	90	Joint	1.40	Serpentinite	<1mm	Tight	Planar	Smooth	10-30m	Both ends visible
90	202.5	292.5	13	90	Joint	1.80	Serpentinite	<1mm	Tight	Discontinuous	Smooth	1-3m	Both ends visible
90	202.5	292.5	13	90	Joint	0.75	Calcite	<1mm	Tight	Discontinuous	Rough	<1m	Both ends visible
85	213	303	14	90	Joint	0.10	Serpentinite	<1mm	Tight	Discontinuous	Smooth	1-3m	No ends visible

Dip (°)	Strike	Dip direction (°)	Scanline ID	Off Set Angle (clockwise) (°)	Structure	Spacing (m)	Infill Type	Infill Thickness	Separation	Surface shape	Surface roughness	Persistance	Ends
85	213	303	14	90	Joint	0.90	No infill	None	<1mm	Discontinuous	Rough	1-3m	Both ends visible
85	213	303	14	90	Joint	0.50	No infill	None	Tight	Discontinuous	Rough	1-3m	Both ends visible
85	213	303	14	90	Joint	0.40	No infill	None	<1mm	Discontinuous	Rough	1-3m	Both ends visible
85	213	303	14	90	Joint	0.20	No infill	None	<1mm	Discontinuous	Rough	1-3m	Both ends visible
85	218	308	14	95	Vein	0.70	Pegmatite	>30mm	Tight	Planar	Rough	>30m	No ends visible
85	233	323	14	110	Joint	1.80	No infill	None	<1mm	Discontinuous	Rough	1-3m	Both ends visible
85	213	303	14	90	Joint	0.10	No infill	None	<1mm	Planar	Rough	1-3m	Both ends visible
85	218	308	14	95	Vein	1.00	Pegmatite	1-3mm	Tight	Planar	Rough	3-10m	Both ends visible
85	218	308	14	95	Vein	0.50	Pegmatite	>30mm	Tight	Planar	Rough	>30m	One end visible
85	218	308	14	95	Vein	0.40	Pegmatite	>30mm	Tight	Planar	Rough	>30m	One end visible
85	218	308	14	95	Vein	1.50	Pegmatite	1-3mm	Tight	Planar	Rough	3-10m	Both ends visible
85	213	303	14	90	Joint	0.70	No infill	>30mm	Tight	Discontinuous	Rough	1-3m	Both ends visible
90	213	303	14	90	Joint	1.20	No infill	None	Tight	Discontinuous	Rough	1-3m	Both ends visible
75	212	302	15	90	Vein	0.80	Serpentinite	<1mm	<1mm	Planar	Smooth	>30m	No ends visible
75	212	302	15	90	Joint	0.10	Serpentinite	<1mm	<1mm	Planar	Smooth	>30m	No ends visible
80	212	302	15	90	Joint	0.20	Serpentinite	<1mm	<1mm	Planar	Smooth	1-3m	Both ends visible
40	222	312	15	80	Joint	0.30	Serpentinite	<1mm	<1mm	Undulating	Smooth	1-3m	Both ends visible
85	212	302	15	90	Joint	0.70	Serpentinite	<1mm	Tight	Planar	Smooth	>30m	No ends visible
85	212	302	15	90	Joint	0.10	Serpentinite	<1mm	Tight	Planar	Smooth	>30m	No ends visible
75	212	302	15	90	Joint	0.20	Serpentinite	<1mm	Tight	Discontinuous	Smooth	1-3m	Both ends visible
75	217	307	15	85	Joint	0.20	Serpentinite	<1mm	<1mm	Planar	Smooth	>30m	No ends visible
90	217	307	15	85	Joint	0.30	Serpentinite	<1mm	<1mm	Planar	Smooth	>30m	No ends visible
85	222	312	15	80	Joint	0.60	Serpentinite	<1mm	Tight	Planar	Smooth	>30m	No ends visible
90	217	307	15	85	Joint	0.94	Serpentinite	<1mm	Tight	Planar	Smooth	>30m	No ends visible
80	217	307	15	85	Joint	0.05	Serpentinite	<1mm	Tight	Planar	Smooth	>30m	No ends visible
70	202	292	16	80	Joint	0.50	Serpentinite	<1mm	Tight	Discontinuous	Smooth	1-3m	Both ends visible
85	182	272	16	100	Joint	1.00	Serpentinite	<1mm	Tight	Discontinuous	Smooth	1-3m	Both ends visible
67	242	332	16	40	Joint	0.60	Serpentinite	1-3mm	Tight	Undulating	Smooth	10-30m	One end visible
85	182	272	16	100	Joint	1.10	Serpentinite	1-3mm	Tight	Undulating	Smooth	10-30m	No ends visible
85	282	372	16	90	Joint	0.30	Serpentinite	1-3mm	Tight	Planar	Smooth	3-10m	No ends visible

Dip (°)	Strike	Dip direction (°)	Scanline ID	Off Set Angle (clockwise) (°)	Structure	Spacing (m)	Infill Type	Infill Thickness	Separation	Surface shape	Surface roughness	Persistance	Ends
85	172	262	16	110	Joint	0.50	Serpentinite	<1mm	Tight	Discontinuous	Smooth	<1m	Both ends visible
85	172	262	16	110	Joint	0.90	Serpentinite	<1mm	Tight	Discontinuous	Smooth	<1m	One end visible
85	313	403	17	80	Joint	0.60	No infill	None	Tight	Discontinuous	Rough	<1m	Both ends visible
85	348	438	17	45	Joint	0.30	No infill	None	Tight	Discontinuous	Rough	1-3m	Both ends visible
85	303	393	17	90	Joint	0.80	Serpentinite	<1mm	Tight	Planar	Smooth	3-10m	One end visible
85	298	388	17	95	Joint	0.70	No infill	None	Tight	Discontinuous	Rough	1-3m	Both ends visible
85	293	383	17	100	Joint	0.70	Serpentinite	<1mm	Tight	Planar	Smooth	3-10m	One end visible
85	303	393	17	90	Joint	0.20	Serpentinite	1-3mm	Tight	Planar	Smooth	3-10m	No ends visible
85	313	403	17	80	Joint	1.70	Serpentinite	1-3mm	Tight	Undulating	Smooth	10-30m	One end visible
85	363	453	17	30	Joint	0.90	Serpentinite	1-3mm	Tight	Planar	Smooth	3-10m	One end visible
85	293	383	17	100	Joint	0.30	No infill	None	Tight	Discontinuous	Rough	<1m	Both ends visible
85	298	388	17	95	Joint	0.16	Serpentinite	<1mm	Tight	Undulating	Smooth	1-3m	Both ends visible
85	298	388	17	95	Joint	0.29	Serpentinite	<1mm	Tight	Discontinuous	Smooth	<1m	Both ends visible
85	298	388	17	95	Joint	0.45	Serpentinite	<1mm	Tight	Undulating	Smooth	3-10m	One end visible
55	312	402	18	70	Joint	0.26	No infill	None	<1mm	Discontinuous	Rough	<1m	Both ends visible
55	312	402	18	70	Joint	0.01	No infill	None	<1mm	Discontinuous	Rough	<1m	Both ends visible
55	312	402	18	70	Joint	0.08	No infill	None	<1mm	Discontinuous	Rough	<1m	Both ends visible
55	312	402	18	70	Joint	0.30	No infill	None	<1mm	Discontinuous	Rough	<1m	Both ends visible
85	312	402	18	70	Joint	0.38	No infill	None	Tight	Discontinuous	Rough	<1m	One end visible
85	302	392	18	80	Joint	0.29	No infill	None	Tight	Planar	Rough	1-3m	One end visible
85	307	397	18	75	Joint	0.24	No infill	None	Tight	Planar	Rough	1-3m	Both ends visible
90	297	387	18	85	Joint	0.40	No infill	None	Tight	Discontinuous	Rough	<1m	Both ends visible
60	297	387	18	85	Joint	0.53	No infill	None	Tight	Undulating	Rough	3-10m	One end visible
85	317	407	18	65	Joint	0.00	No infill	None	Tight	Discontinuous	Rough	<1m	One end visible
85	292	382	18	90	Joint	0.22	No infill	None	<1mm	Discontinuous	Rough	<1m	One end visible
85	282	372	18	100	Joint	0.44	No infill	None	<1mm	Discontinuous	Rough	<1m	One end visible
85	282	372	18	100	Joint	0.36	No infill	None	Tight	Discontinuous	Rough	<1m	One end visible
85	282	372	18	100	Joint	0.07	No infill	None	Tight	Undulating	Rough	1-3m	One end visible
85	282	372	18	100	Joint	0.28	No infill	None	<1mm	Undulating	Rough	1-3m	One end visible
90	192	282	19	90	Joint	0.80	Serpentinite	<1mm	Tight	Planar	Smooth	1-3m	Both ends visible

Dip (°)	Strike	Dip direction (°)	Scanline ID	Off Set Angle (clockwise) (°)	Structure	Spacing (m)	Infill Type	Infill Thickness	Separation	Surface shape	Surface roughness	Persistance	Ends
85	257	347	19	25	Joint	0.40	Serpentinite	<1mm	Tight	Planar	Smooth	3-10m	Both ends visible
82	202	292	19	80	Vein	1.38	Serpentinite	1-3mm	Tight	Planar	Smooth	>30m	No ends visible
82	202	292	19	80	Vein	0.14	Serpentinite	1-3mm	Tight	Planar	Smooth	>30m	No ends visible
80	197	287	19	85	Joint	0.88	Serpentinite	<1mm	Tight	Planar	Smooth	3-10m	Both ends visible
80	197	287	19	85	Vein	0.30	Serpentinite	<1mm	Tight	Planar	Smooth	>30m	No ends visible
80	197	287	19	85	Vein	0.02	Serpentinite	<1mm	Tight	Planar	Smooth	>30m	No ends visible
85	187	277	19	95	Vein	0.48	Serpentinite	<1mm	Tight	Planar	Smooth	>30m	One end visible
90	187	277	19	95	Vein	1.00	Serpentinite	<1mm	Tight	Planar	Smooth	1-3m	Both ends visible
85	187	277	19	95	Vein	0.20	Serpentinite	<1mm	Tight	Planar	Smooth	3-10m	Both ends visible
90	192	282	19	90	Vein	0.20	Serpentinite	<1mm	Tight	Planar	Smooth	3-10m	One end visible
90	187	277	19	95	Vein	0.17	Serpentinite	<1mm	Tight	Planar	Smooth	3-10m	One end visible
90	187	277	19	95	Vein	0.63	Serpentinite	<1mm	Tight	Planar	Smooth	3-10m	One end visible
95	187	277	19	95	Vein	0.20	Serpentinite	<1mm	Tight	Planar	Smooth	10-30m	One end visible
90	267	357	20	15	Joint	0.70	Serpentinite	<1mm	Tight	Planar	Smooth	1-3m	One end visible
90	252	342	20	30	Joint	2.20	Serpentinite	<1mm	Tight	Planar	Smooth	3-10m	One end visible
65	177	267	20	105	Joint	0.90	No infill	None	Tight	Planar	Rough	1-3m	Both ends visible
65	177	267	20	105	Joint	0.30	Serpentinite	<1mm	Tight	Planar	Smooth	1-3m	Both ends visible
55	177	267	20	105	Joint	0.30	Serpentinite	<1mm	Tight	Planar	Smooth	1-3m	Both ends visible
82	167	257	20	115	Joint	0.90	Serpentinite	<1mm	Tight	Planar	Smooth	1-3m	Both ends visible
90	187	277	20	95	Vein	0.50	Serpentinite	<1mm	Tight	Planar	Smooth	1-3m	Both ends visible
90	187	277	20	95	Vein	0.70	Serpentinite	<1mm	Tight	Planar	Smooth	1-3m	Both ends visible
85	192	282	20	90	Vein	0.30	Serpentinite	<1mm	Tight	Planar	Smooth	1-3m	Both ends visible
90	202	292	20	80	Vein	0.70	Serpentinite	<1mm	Tight	Planar	Smooth	1-3m	Both ends visible
85	217	307	20	65	vein	0.30	Serpentinite	<1mm	Tight	Planar	Smooth	1-3m	Both ends visible
90	114	204	21	90	Joint	0.10	Calcite	1-3mm	Tight	Planar	Rough	3-10m	Both ends visible
90	114	204	21	90	Joint	0.10	Calcite	1-3mm	Tight	Planar	Rough	3-10m	Both ends visible
90	114	204	21	90	Joint	0.10	Calcite	1-3mm	Tight	Planar	Rough	3-10m	Both ends visible
90	114	204	21	90	Vein	1.10	Pegmatite	3-10mm	Tight	Planar	Rough	>30m	No ends visible
90	114	204	21	90	Joint	1.30	Serpentinite	1-3mm	Tight	Planar	Smooth	>30m	No ends visible
90	114	204	21	90	Joint	0.30	Serpentinite	1-3mm	Tight	Planar	Smooth	>30m	No ends visible

Dip (°)	Strike	Dip direction (°)	Scanline ID	Off Set Angle (clockwise) (°)	Structure	Spacing (m)	Infill Type	Infill Thickness	Separation	Surface shape	Surface roughness	Persistance	Ends
85	257	347	19	25	Joint	0.40	Serpentinite	<1mm	Tight	Planar	Smooth	3-10m	Both ends visible
82	202	292	19	80	Vein	1.38	Serpentinite	1-3mm	Tight	Planar	Smooth	>30m	No ends visible
82	202	292	19	80	Vein	0.14	Serpentinite	1-3mm	Tight	Planar	Smooth	>30m	No ends visible
80	197	287	19	85	Joint	0.88	Serpentinite	<1mm	Tight	Planar	Smooth	3-10m	Both ends visible
90	114	204	21	90	Vein	0.90	Pegmatite	1-3mm	Tight	Planar	Rough	3-10m	Both ends visible
80	104	194	21	100	Vein	0.70	Pegmatite	10-30mm	Tight	Planar	Rough	>30m	No ends visible
90	114	204	21	90	Joint	2.50	No infill	None	Tight	Planar	Rough	10-30m	One end visible
30	264	354	22	30	Joint	4.00	No infill	None	Tight	Planar	Rough	1-3m	Both ends visible
30	264	354	22	30	Joint	1.00	No infill	None	Tight	Planar	Rough	1-3m	Both ends visible
30	264	354	22	30	Joint	3.80	No infill	None	Tight	Planar	Rough	1-3m	Both ends visible
90	114	204	23	90	Vein	0.30	Pegmatite	10-30mm	Tight	Planar	Rough	>30m	No ends visible
90	114	204	23	90	Vein	4.10	Pegmatite	10-30mm	Tight	Planar	Rough	>30m	No ends visible
85	119	209	23	85	Joint	2.60	No infill	None	<1mm	Undulating	Rough	1-3m	Both ends visible
80	264	354	24	30	Joint	2.00	Surface staining	<1mm	Tight	Undulating	Smooth	3-10m	Both ends visible
85	264	354	24	30	Joint	1.80	Surface staining	<1mm	Tight	Undulating	Smooth	1-3m	Both ends visible
90	204	294	24	90	Joint	2.10	Serpentinite	1-3mm	<1mm	Undulating	Smooth	3-10m	Both ends visible
90	214	304	24	80	Joint	1.00	Serpentinite	1-3mm	1-3mm	Undulating	Smooth	3-10m	Both ends visible
90	204	294	24	90	Joint	1.40	Serpentinite	1-3mm	1-3mm	Undulating	Smooth	3-10m	Both ends visible
90	204	294	24	90	Joint	0.70	Serpentinite	1-3mm	1-3mm	Undulating	Smooth	3-10m	Both ends visible
90	204	294	24	90	Joint	0.70	Serpentinite	1-3mm	1-3mm	Undulating	Smooth	3-10m	Both ends visible
90	114	204	25	90	Vein	0.36	Serpentinite	1-3mm	Tight	Planar	Smooth	>30m	No ends visible
90	114	204	25	90	Vein	0.10	Serpentinite	1-3mm	Tight	Planar	Smooth	>30m	No ends visible
85	109	199	25	95	Joint	0.59	Serpentinite	<1mm	Tight	Planar	Smooth	3-10m	Both ends visible
85	109	199	25	85	Joint	0.24	Serpentinite	<1mm	Tight	Planar	Smooth	3-10m	Both ends visible
85	109	199	25	85	Joint	0.08	Serpentinite	<1mm	Tight	Planar	Smooth	3-10m	Both ends visible
85	109	199	25	85	Joint	0.25	Serpentinite	<1mm	Tight	Planar	Smooth	3-10m	Both ends visible
85	124	214	25	100	Joint	0.08	Serpentinite	<1mm	Tight	Planar	Smooth	3-10m	Both ends visible
75	144	234	25	120	Joint	0.44	Serpentinite	<1mm	Tight	Planar	Smooth	1-3m	Both ends visible
90	114	204	25	90	Joint	0.22	Serpentinite	<1mm	Tight	Planar	Smooth	1-3m	Both ends visible
85	109	199	25	85	Joint	0.80	Serpentinite	<1mm	Tight	Planar	Smooth	>30m	No ends visible
90	119	209	25	95	Joint	0.28	Serpentinite	<1mm	Tight	Planar	Smooth	3-10m	Both ends visible
90	124	214	25	100	Joint	0.25	Serpentinite	<1mm	Tight	Planar	Smooth	3-10m	Both ends visible
90	119	209	25	95	Joint	0.40	Serpentinite	<1mm	Tight	Planar	Smooth	3-10m	Both ends visible
90	114	204	25	80	Joint	0.21	Serpentinite	<1mm	Tight	Planar	Smooth	1-3m	Both ends visible

Dip (°)	Strike	Dip direction (°)	Scanline ID	Off Set Angle (clockwise) (°)	Structure	Spacing (m)	Infill Type	Infill Thickness	Separation	Surface shape	Surface roughness	Persistance	Ends
90	114	204	25	90	Vein	0.14	Serpentinite	1-3mm	Tight	Planar	Smooth	>30m	No ends visible
90	114	204	25	90	Vein	0.05	Serpentinite	1-3mm	Tight	Planar	Smooth	>30m	No ends visible
90	114	204	25	95	Joint	0.60	Serpentinite	<1mm	Tight	Planar	Smooth	3-10m	Both ends visible
90	114	204	25	90	Joint	0.22	Serpentinite	<1mm	Tight	Planar	Smooth	3-10m	Both ends visible
90	129	219	25	105	Joint	0.60	Serpentinite	<1mm	Tight	Planar	Smooth	10-30m	Both ends visible
90	114	204	25	90	Vein	0.60	Serpentinite	<1mm	Tight	Planar	Smooth	>30m	No ends visible
90	114	204	25	90	Vein	0.04	Serpentinite	<1mm	Tight	Planar	Smooth	>30m	No ends visible
90	114	204	25	90	Joint	1.31	Serpentinite	<1mm	Tight	Planar	Smooth	>30m	No ends visible
90	204	294	26	90	Joint	7.40	No infill	None	Tight	Discontinuous	Rough	3-10m	Both ends visible
90	209	299	27	95	Joint	6.00	Calcite	<1mm	Tight	Planar	Rough	1-3m	Both ends visible
90	89	179	28	115	Joint	2.10	Calcite	<1mm	Tight	Planar	Rough	3-10m	Both ends visible
90	114	204	28	90	Vein	1.50	Serpentinite	<1mm	Tight	Planar	Smooth	>30m	No ends visible
90	114	204	28	90	Vein	0.16	Serpentinite	<1mm	Tight	Planar	Smooth	>30m	No ends visible
90	114	204	28	90	Joint	1.74	Calcite	1-3mm	Tight	Planar	Rough	10-30m	One end visible
85	64	154	29	100	Joint	0.12	Serpentinite	<1mm	Tight	Planar	Smooth	3-10m	Both ends visible
85	84	174	29	95	Joint	0.38	Serpentinite	<1mm	Tight	Planar	Smooth	1-3m	Both ends visible
90	94	184	29	90	Joint	0.38	Serpentinite	<1mm	Tight	Planar	Smooth	10-30m	One end visible
90	94	184	29	90	Joint	0.34	Serpentinite	<1mm	Tight	Planar	Smooth	3-10m	Both ends visible
80	54	144	29	95	Joint	0.13	Serpentinite	<1mm	Tight	Planar	Smooth	3-10m	Both ends visible
90	99	189	29	90	Joint	0.25	Serpentinite	<1mm	Tight	Planar	Smooth	3-10m	Both ends visible
80	94	184	29	90	Vein	0.74	Pegmatite	10-30mm	Tight	Planar	Rough	>30m	One end visible
80	94	184	29	90	Vein	0.04	Pegmatite	10-30mm	Tight	Planar	Rough	>30m	One end visible
90	104	194	29	100	Vein	0.60	Serpentinite	<1mm	Tight	Planar	Smooth	>30m	No ends visible
90	104	194	29	100	Vein	0.32	Serpentinite	<1mm	Tight	Planar	Smooth	>30m	No ends visible
90	39	129	29	35	Joint	2.20	Serpentinite	<1mm	Tight	Planar	Smooth	3-10m	Both ends visible
90	224	314	30	110	Joint	1.18	Pegmatite	<1mm	<1mm	Planar	Rough	3-10m	Both ends visible
90	224	314	30	110	Joint	0.17	Pegmatite	<1mm	<1mm	Planar	Rough	3-10m	Both ends visible
90	199	289	30	85	Joint	0.06	Pegmatite	<1mm	<1mm	Planar	Rough	3-10m	Both ends visible
90	199	289	30	85	Joint	0.18	Pegmatite	<1mm	<1mm	Planar	Rough	3-10m	Both ends visible
90	199	289	30	85	Joint	0.54	Pegmatite	<1mm	<1mm	Planar	Rough	3-10m	Both ends visible

Dip (°)	Strike	Dip direction (°)	Scanline ID	Off Set Angle (clockwise) (°)	Structure	Spacing (m)	Infill Type	Infill Thickness	Separation	Surface shape	Surface roughness	Persistance	Ends
90	199	289	30	85	Joint	0.24	Pegmatite	<1mm	<1mm	Planar	Rough	3-10m	Both ends visible
90	199	289	30	85	Joint	0.64	Pegmatite	<1mm	<1mm	Planar	Rough	3-10m	Both ends visible
90	204	294	30	90	Joint	0.69	Pegmatite	<1mm	<1mm	Planar	Rough	3-10m	Both ends visible
70	159	249	31	40	Joint	0.93	Serpentinite	<1mm	Tight	Discontinuous	Smooth	1-3m	Both ends visible
50	154	244	31	45	Joint	2.41	Serpentinite	<1mm	Tight	Planar	Smooth	10-30m	Both ends visible
90	109	199	31	90	Vein	2.34	Serpentinite	1-3mm	Tight	Planar	Smooth	<1m	Both ends visible
90	109	199	31	90	Vein	0.18	No infill	None	Tight	Planar	Rough	<1m	Both ends visible
60	189	279	32	75	Joint	3.37	No infill	None	1-3mm	Undulating	Rough	>30m	No ends visible
40	199	289	32	85	Joint	1.50	No infill	None	1-3mm	Undulating	Rough	>30m	No ends visible
90	209	299	32	95	Joint	0.22	Surface staining	<1mm	1-3mm	Discontinuous	Smooth	3-10m	No ends visible
90	204	294	32	70	Joint	1.01	Surface staining	<1mm	1-3mm	Discontinuous	Smooth	3-10m	One end visible
90	204	294	32	75	Joint	0.75	Surface staining	<1mm	1-3mm	Discontinuous	Smooth	3-10m	One end visible
90	39	129	33	25	Joint	2.20	Serpentinite	<1mm	Tight	Planar	Smooth	3-10m	Both ends visible
90	39	129	33	25	Joint	0.70	Serpentinite	<1mm	Tight	Planar	Smooth	3-10m	Both ends visible
90	104	194	33	90	Vein	1.20	Pegmatite	3-10mm	<1mm	Planar	Rough	<1m	Both ends visible
90	104	194	33	90	Vein	0.15	Pegmatite	10-30mm	<1mm	Planar	Rough	>30m	One end visible
90	49	139	33	35	Joint	0.55	Serpentinite	<1mm	Tight	Planar	Smooth	1-3m	Both ends visible
90	169	259	34	65	Joint	0.25	Serpentinite	<1mm	Tight	Planar	Smooth	3-10m	Both ends visible
70	184	274	34	80	Joint	6.75	No infill	None	1-3mm	Planar	Rough	3-10m	Both ends visible
65	189	279	35	75	Joint	1.10	Calcite	<1mm	1-3mm	Planar	Rough	3-10m	One end visible
60	184	274	35	70	Joint	0.10	Calcite	<1mm	Tight	Planar	Rough	>30m	No ends visible
65	174	264	35	60	Joint	1.30	Calcite	<1mm	Tight	Planar	Rough	3-10m	One end visible
75	174	264	35	60	Joint	1.00	Calcite	<1mm	Tight	Planar	Rough	>30m	No ends visible
75	184	274	35	70	Joint	0.30	Calcite	<1mm	Tight	Planar	Rough	3-10m	One end visible
70	184	274	36	160	Joint	2.40	Calcite	<1mm	Tight	Planar	Rough	>30m	No ends visible
75	174	264	36	150	Joint	0.60	Calcite	<1mm	Tight	Planar	Rough	3-10m	One end visible
70	169	259	36	145	Joint	1.23	Calcite	<1mm	Tight	Planar	Rough	>30m	No ends visible
80	174	264	36	150	Joint	0.27	Calcite	<1mm	Tight	Planar	Rough	3-10m	Both ends visible
70	174	264	36	150	Joint	1.00	Calcite	<1mm	Tight	Planar	Rough	3-10m	Both ends visible
25	79	169	37	55	Fault	2.17	Serpentinite	10-30mm	Tight	Planar	Smooth	10-30m	Both ends visible

Dip (°)	Strike	Dip direction (°)	Scanline ID	Off Set Angle (clockwise) (°)	Structure	Spacing (m)	Infill Type	Infill Thickness	Separation	Surface shape	Surface roughness	Persistance	Ends
35	114	204	37	90	Joint	1.30	Serpentinite	<1mm	Tight	Planar	Smooth	3-10m	One end visible
30	114	204	37	90	Fault	3.04	Serpentinite	10-30mm	Tight	Planar	Smooth	10-30m	One end visible
25	254	344	38	140	Fault	9.00	Serpentinite	10-30mm	Tight	Planar	Smooth	10-30m	Both ends visible
90	134	224	39	100	Joint	0.50	No infill	None	<1mm	Planar	Rough	1-3m	Both ends visible
90	134	224	39	100	Joint	0.15	No infill	None	<1mm	Planar	Rough	1-3m	Both ends visible
90	134	224	39	100	Joint	0.15	No infill	None	<1mm	Planar	Rough	3-10m	Both ends visible
90	124	214	39	90	Vein	0.11	No infill	None	Tight	Planar	Rough	>30m	No ends visible
90	124	214	39	90	Vein	0.09	No infill	None	Tight	Planar	Rough	>30m	No ends visible
90	134	224	39	100	Joint	1.10	No infill	None	Tight	Planar	Rough	1-3m	Both ends visible
90	69	159	39	35	Shear	1.32	Serpentinite	<1mm	Tight	Planar	Smooth	10-30m	Both ends visible
80	144	234	39	110	Joint	0.38	Serpentinite	<1mm	Tight	Planar	Smooth	10-30m	Both ends visible
80	144	234	39	110	Joint	0.13	Serpentinite	<1mm	Tight	Planar	Smooth	10-30m	Both ends visible
90	74	164	39	40	Shear	1.40	Serpentinite	<1mm	Tight	Planar	Smooth	10-30m	Both ends visible
90	124	214	39	90	Vein	1.00	Serpentinite	<1mm	Tight	Planar	Smooth	>30m	No ends visible
90	124	214	39	90	Vein	0.55	No infill	None	Tight	Planar	Rough	>30m	No ends visible
80	194	284	40	110	Joint	0.30	Serpentinite	<1mm	Tight	Planar	Smooth	10-30m	Both ends visible
90	284	374	40	170	Joint	0.58	Serpentinite	<1mm	Tight	Planar	Smooth	10-30m	Both ends visible
80	189	279	40	105	Joint	0.95	No infill	None	Tight	Planar	Rough	3-10m	Both ends visible
80	194	284	40	100	Joint	0.60	No infill	None	Tight	Planar	Rough	3-10m	Both ends visible
80	194	284	40	100	Joint	0.09	No infill	None	Tight	Planar	Rough	3-10m	Both ends visible
80	179	269	40	115	Joint	0.70	No infill	None	Tight	Planar	Rough	3-10m	Both ends visible
65	179	269	40	115	Shear	0.46	Serpentinite	<1mm	Tight	Planar	Smooth	10-30m	Both ends visible
65	179	269	40	115	Shear	0.08	Serpentinite	<1mm	Tight	Undulating	Smooth	3-10m	Both ends visible
60	189	279	40	105	Joint	1.60	Serpentinite	<1mm	Tight	Planar	Smooth	3-10m	Both ends visible
60	189	279	40	105	Joint	0.22	Serpentinite	<1mm	Tight	Planar	Smooth	3-10m	Both ends visible
60	199	289	40	95	Joint	0.40	Serpentinite	<1mm	Tight	Planar	Smooth	3-10m	Both ends visible
70	199	289	40	95	Joint	0.43	Serpentinite	<1mm	Tight	Planar	Smooth	3-10m	Both ends visible
70	199	289	40	95	Joint	0.22	Serpentinite	<1mm	Tight	Planar	Smooth	3-10m	Both ends visible
70	199	289	40	95	Joint	0.22	Serpentinite	<1mm	Tight	Planar	Smooth	3-10m	Both ends visible
80	199	289	40	95	Shear	0.40	Serpentinite	1-3mm	Tight	Planar	Smooth	10-30m	Both ends visible

Dip (°)	Strike	Dip direction (°)	Scanline ID	Off Set Angle (clockwise) (°)	Structure	Spacing (m)	Infill Type	Infill Thickness	Separation	Surface shape	Surface roughness	Persistance	Ends
70	199	289	40	95	Joint	1.70	No infill	None	<1mm	Planar	Rough	3-10m	Both ends visible
50	179	269	41	25	Joint	2.79	Serpentinite	1-3mm	Tight	Planar	Smooth	1-3m	One end visible
75	174	264	41	30	Joint	1.21	Serpentinite	1-3mm	Tight	Planar	Smooth	3-10m	No ends visible
40	109	199	41	85	Joint	1.00	Serpentinite	1-3mm	Tight	Planar	Smooth	3-10m	Both ends visible
70	184	274	42	70	Joint	0.30	Serpentinite	1-3mm	Tight	Planar	Smooth	>30m	No ends visible
70	184	274	42	75	Joint	2.04	Serpentinite	1-3mm	Tight	Planar	Smooth	>30m	No ends visible
60	199	289	42	85	Joint	1.81	Serpentinite	1-3mm	Tight	Planar	Smooth	3-10m	One end visible
70	199	289	42	85	Joint	0.50	Serpentinite	1-3mm	Tight	Planar	Smooth	3-10m	One end visible
90	64	154	43	35	Joint	1.46	Serpentinite	<1mm	Tight	Planar	Smooth	3-10m	Both ends visible
90	124	214	43	95	Vein	5.34	Serpentinite	<1mm	Tight	Planar	Smooth	>30m	No ends visible
90	124	214	43	95	Vein	0.14	Serpentinite	<1mm	Tight	Planar	Smooth	>30m	No ends visible
65	174	264	43	35	Joint	0.30	No infill	None	<1mm	Discontinuous	Rough	1-3m	Both ends visible
65	174	264	44	120	Joint	1.00	Serpentinite	<1mm	Tight	Discontinuous	Smooth	3-10m	Both ends visible
90	224	314	44	110	Joint	1.46	Serpentinite	<1mm	Tight	Planar	Smooth	3-10m	Both ends visible
90	204	294	44	90	Joint	10.74	No infill	None	Tight	Undulating	Rough	3-10m	Both ends visible
80	89	179	45	65	Joint	0.37	Serpentinite	<1mm	Tight	Planar	Smooth	3-10m	Both ends visible
85	99	189	45	75	Joint	0.13	Serpentinite	<1mm	Tight	Planar	Smooth	1-3m	Both ends visible
90	109	199	45	85	Vein	0.70	Calcite	<1mm	Tight	Discontinuous	Rough	3-10m	Both ends visible
80	109	199	45	85	Joint	1.20	Serpentinite	<1mm	Tight	Planar	Smooth	3-10m	Both ends visible
75	109	199	45	85	Vein	0.95	Calcite	>30mm	Tight	Planar	Rough	>30m	Both ends visible
75	109	199	45	85	Vein	0.10	Calcite	>30mm	Tight	Planar	Rough	>30m	Both ends visible
85	129	219	46	75	Joint	0.40	Serpentinite	<1mm	<1mm	Undulating	Smooth	3-10m	Both ends visible
90	114	204	46	90	Vein	1.35	Pegmatite	3-10mm	Tight	Planar	Rough	>30m	No ends visible
90	114	204	46	90	Fault	0.10	Pegmatite	3-10mm	Tight	Planar	Rough	>30m	No ends visible
70	129	219	46	75	Fault	4.45	Serpentinite	<1mm	Tight	Planar	Smooth	10-30m	No ends visible
70	204	294	47	90	Joint	1.20	Serpentinite	1-3mm	1-3mm	Planar	Smooth	10-30m	No ends visible
70	204	294	47	90	Joint	0.20	Serpentinite	1-3mm	1-3mm	Planar	Smooth	10-30m	No ends visible
85	204	294	47	90	Joint	1.80	Serpentinite	<1mm	<1mm	Planar	Smooth	10-30m	No ends visible
50	204	294	47	90	Joint	1.30	Surface staining	None	<1mm	Discontinuous	Smooth	1-3m	One end visible
85	144	234	48	30	Joint	0.40	Serpentinite	<1mm	<1mm	Undulating	Smooth	1-3m	One end visible

Dip (°)	Strike	Dip direction (°)	Scanline ID	Off Set Angle (clockwise) (°)	Structure	Spacing (m)	Infill Type	Infill Thickness	Separation	Surface shape	Surface roughness	Persistance	Ends
90	199	289	48	85	Joint	0.35	Serpentinite	<1mm	<1mm	Undulating	Smooth	1-3m	One end visible
85	174	264	48	60	Joint	0.15	Serpentinite	<1mm	<1mm	Undulating	Smooth	1-3m	One end visible
80	169	259	48	55	Joint	0.30	Serpentinite	<1mm	<1mm	Planar	Smooth	>30m	No ends visible
80	194	284	48	80	Joint	0.40	Serpentinite	<1mm	<1mm	Undulating	Smooth	>30m	No ends visible
85	174	264	48	60	Shear	0.35	Calcite	10-30mm	<1mm	Planar	Rough	>30m	No ends visible
90	189	279	48	75	Joint	0.35	No infill	None	<1mm	Planar	Rough	<1m	No ends visible
85	199	289	48	85	Joint	0.10	Serpentinite	<1mm	Tight	Discontinuous	Smooth	3-10m	Both ends visible
80	184	274	48	70	Vein	0.40	Calcite	<1mm	<1mm	Planar	Rough	>30m	No ends visible
70	144	234	48	30	Shear	0.40	Surface staining	<1mm	<1mm	Undulating	Smooth	>30m	No ends visible
75	199	289	48	85	Joint	0.50	Serpentinite	<1mm	<1mm	Planar	Smooth	>30m	No ends visible
80	204	294	48	90	Joint	0.30	Serpentinite	<1mm	<1mm	Planar	Smooth	>30m	No ends visible
80	214	304	48	100	Joint	2.00	Serpentinite	<1mm	<1mm	Planar	Smooth	>30m	No ends visible
90	114	204	49	90	Joint	0.10	Serpentinite	<1mm	<1mm	Planar	Smooth	3-10m	One end visible
90	124	214	49	100	Joint	0.30	Serpentinite	<1mm	<1mm	Discontinuous	Smooth	3-10m	One end visible
90	114	204	49	90	Joint	1.10	Calcite	<1mm	<1mm	Planar	Rough	<1m	Both ends visible
85	119	209	49	95	Joint	0.50	No infill	None	<1mm	Planar	Rough	<1m	Both ends visible
90	124	214	49	100	Joint	0.05	Serpentinite	<1mm	<1mm	Planar	Smooth	>30m	No ends visible
90	114	204	49	90	Joint	0.85	Serpentinite	<1mm	<1mm	Planar	Smooth	>30m	No ends visible
85	114	204	49	90	Joint	0.40	Calcite	>30mm	<1mm	Planar	Rough	>30m	No ends visible
85	114	204	49	90	Joint	0.80	Calcite	>30mm	<1mm	Planar	Rough	>30m	No ends visible
75	114	204	49	90	Joint	0.35	Serpentinite	<1mm	<1mm	Planar	Smooth	>30m	No ends visible
80	134	224	49	110	Joint	0.60	Serpentinite	<1mm	<1mm	Planar	Smooth	>30m	No ends visible
90	204	294	50	90	Joint	5.00	No infill	None	Tight	Discontinuous	Rough	1-3m	Both ends visible
65	179	269	50	65	Joint	3.30	Serpentinite	<1mm	Tight	Planar	Smooth	10-30m	Both ends visible
90	114	204	51	90	Joint	0.50	Serpentinite	1-3mm	<1mm	Discontinuous	Smooth	3-10m	No ends visible
90	114	204	51	90	Joint	1.00	Serpentinite	<1mm	<1mm	Discontinuous	Smooth	3-10m	No ends visible
90	114	204	51	90	Vein	0.30	Pegmatite	10-30mm	Tight	Planar	Rough	3-10m	One end visible
85	114	204	51	90	Joint	1.40	Serpentinite	<1mm	<1mm	Undulating	Smooth	3-10m	No ends visible
85	114	204	51	90	Joint	0.80	Serpentinite	<1mm	1-3mm	Planar	Smooth	3-10m	One end visible
85	114	204	51	90	Joint	2.20	Serpentinite	<1mm	1-3mm	Planar	Smooth	3-10m	One end visible

Dip (°)	Strike	Dip direction (°)	Scanline ID	Off Set Angle (clockwise) (°)	Structure	Spacing (m)	Infill Type	Infill Thickness	Separation	Surface shape	Surface roughness	Persistance	Ends
90	114	204	51	90	Joint	0.50	Serpentinite	<1mm	1-3mm	Planar	Smooth	3-10m	No ends visible
90	114	204	51	90	Vein	1.90	Pegmatite	>30mm	Tight	Planar	Rough	10-30m	No ends visible
90	114	204	51	90	Vein	0.10	Pegmatite	>30mm	Tight	Planar	Rough	10-30m	No ends visible
90	114	204	51	90	Joint	0.70	No infill	<1mm	<1mm	Planar	Rough	3-10m	One end visible
90	114	204	51	90	Joint	0.40	Serpentinite	<1mm	<1mm	Planar	Smooth	3-10m	One end visible
80	194	284	52	80	Dome	1.50	Serpentinite	<1mm	1-3mm	Undulating	Smooth	10-30m	Both ends visible
80	194	284	52	80	Joint	0.20	Serpentinite	<1mm	1-3mm	Planar	Smooth	10-30m	One end visible
80	194	284	52	80	Joint	0.40	Serpentinite	<1mm	1-3mm	Planar	Smooth	10-30m	One end visible
90	204	294	52	90	Joint	1.60	Serpentinite	1-3mm	1-3mm	Planar	Smooth	3-10m	Both ends visible
35	199	289	52	85	Joint	0.80	Serpentinite	1-3mm	3-10mm	Planar	Smooth	3-10m	No ends visible
35	199	289	52	85	Joint	0.80	Surface staining	None	3-10mm	Undulating	Smooth	1-3m	Both ends visible
55	204	294	52	90	Joint	1.40	Serpentinite	1-3mm	3-10mm	Planar	Smooth	10-30m	No ends visible
90	114	204	53	90	Joint	0.60	No infill	<1mm	<1mm	Planar	Rough	3-10m	No ends visible
90	114	204	53	90	Joint	0.30	No infill	<1mm	<1mm	Planar	Rough	3-10m	One end visible
90	114	204	53	90	Joint	0.90	No infill	<1mm	Tight	Discontinuous	Rough	1-3m	Both ends visible
90	114	204	53	90	Joint	0.60	Serpentinite	<1mm	<1mm	Planar	Smooth	3-10m	Both ends visible
75	114	204	53	90	Joint	0.50	Serpentinite	<1mm	Tight	Discontinuous	Smooth	3-10m	Both ends visible
75	74	164	53	50	Joint	0.60	No infill	<1mm	<1mm	Discontinuous	Rough	3-10m	Both ends visible
80	89	179	53	65	Joint	0.70	No infill	<1mm	<1mm	Discontinuous	Rough	1-3m	Both ends visible
90	114	204	53	90	Vein	1.60	Pegmatite	3-10mm	Tight	Planar	Rough	10-30m	No ends visible
90	114	204	53	90	Vein	0.80	Pegmatite	>30mm	Tight	Planar	Rough	10-30m	No ends visible
90	114	204	53	90	Vein	0.10	Pegmatite	>30mm	Tight	Planar	Rough	10-30m	No ends visible
90	114	204	53	90	Joint	0.30	Serpentinite	<1mm	<1mm	Planar	Smooth	3-10m	One end visible
90	114	204	53	90	Joint	1.00	No infill	<1mm	<1mm	Planar	Rough	3-10m	One end visible
90	74	164	53	50	Joint	0.20	No infill	<1mm	<1mm	Planar	Rough	10-30m	No ends visible
85	79	169	53	55	Joint	0.20	Serpentinite	<1mm	<1mm	Planar	Smooth	10-30m	No ends visible
90	74	164	53	50	Joint	0.70	Serpentinite	<1mm	<1mm	Planar	Smooth	10-30m	No ends visible
80	104	194	54	80	Joint	2.50	Serpentinite	1-3mm	<1mm	Planar	Smooth	>30m	No ends visible
80	114	204	54	90	Vein	3.60	Pegmatite	10-30mm	<1mm	Planar	Rough	>30m	No ends visible
80	114	204	54	90	Fault	0.30	Pegmatite	10-30mm	<1mm	Planar	Rough	>30m	No ends visible

Dip (°)	Strike	Dip direction (°)	Scanline ID	Off Set Angle (clockwise) (°)	Structure	Spacing (m)	Infill Type	Infill Thickness	Separation	Surface shape	Surface roughness	Persistance	Ends
75	114	204	54	90	Joint	1.40	Serpentinite	<1mm	<1mm	Planar	Smooth	10-30m	No ends visible
0	204	294	55	90	Other	2.00	No infill	None	<1mm	Planar	Rough	<1m	Both ends visible
0	204	294	55	90	Other	1.50	No infill	None	<1mm	Planar	Rough	<1m	Both ends visible
0	204	294	55	90	Other	1.50	No infill	None	<1mm	Planar	Rough	<1m	Both ends visible
0	204	294	55	90	Other	2.00	No infill	None	<1mm	Planar	Rough	<1m	Both ends visible
0	204	294	55	90	Other	2.40	No infill	None	<1mm	Planar	Rough	<1m	Both ends visible
90	194	284	56	80	Joint	0.20	Surface staining	None	<1mm	Planar	Smooth	1-3m	Both ends visible
90	194	284	56	80	Joint	0.70	Surface staining	None	<1mm	Planar	Smooth	1-3m	Both ends visible
70	234	324	56	120	Shear zone	0.10	Serpentinite	10-30mm	3-10mm	Planar	Smooth	10-30m	No ends visible
90	204	294	56	90	Joint	1.40	No infill	None	Tight	Planar	Rough	3-10m	One end visible
90	204	294	56	90	Joint	6.60	Surface staining	<1mm	<1mm	Planar	Smooth	3-10m	Both ends visible
60	124	214	57	100	Dome	0.20	Serpentinite	<1mm	<1mm	Undulating	Smooth	3-10m	No ends visible
60	104	194	57	80	Joint	0.30	Serpentinite	<1mm	<1mm	Planar	Smooth	3-10m	One end visible
90	114	204	57	90	Vein	1.20	Pegmatite	<1mm	<1mm	Planar	Rough	>30m	No ends visible
90	114	204	57	90	Vein	0.10	Pegmatite	<1mm	<1mm	Planar	Rough	>30m	No ends visible
90	114	204	57	90	Vein	1.40	Pegmatite	<1mm	<1mm	Planar	Rough	>30m	No ends visible
90	114	204	57	90	Vein	0.10	Pegmatite	<1mm	<1mm	Planar	Rough	>30m	No ends visible
90	114	204	57	90	Joint	2.00	Surface staining	None	Tight	Planar	Smooth	3-10m	Both ends visible
90	114	204	57	90	Joint	1.80	Surface staining	None	<1mm	Planar	Smooth	1-3m	Both ends visible
80	109	199	58	80	Joint	0.50	Serpentinite	<1mm	Tight	Planar	Smooth	3-10m	Both ends visible
80	109	199	58	80	Joint	0.10	Serpentinite	<1mm	Tight	Planar	Smooth	3-10m	Both ends visible
90	109	199	58	80	Joint	0.10	Serpentinite	<1mm	Tight	Discontinuous	Smooth	3-10m	Both ends visible
80	119	209	58	90	Joint	0.40	Serpentinite	<1mm	Tight	Planar	Smooth	1-3m	No ends visible
75	124	214	58	95	Fault	0.25	Pegmatite	>30mm	Tight	Planar	Rough	>30m	No ends visible
75	124	214	58	95	Fault	0.07	Pegmatite	>30mm	Tight	Planar	Rough	>30m	No ends visible
80	119	209	58	90	Vein	2.58	Pegmatite	10-30mm	Tight	Planar	Rough	>30m	No ends visible
80	94	184	58	65	Joint	0.80	Serpentinite	<1mm	Tight	Discontinuous	Smooth	3m	No ends visible
80	99	189	58	70	Joint	0.50	Serpentinite	<1mm	Tight	Planar	Smooth	3-10m	Both ends visible
80	104	194	58	75	Joint	0.40	Serpentinite	<1mm	Tight	Planar	Smooth	3-10m	Both ends visible
85	89	179	58	60	Joint	0.30	Serpentinite	<1mm	Tight	Planar	Smooth	3-10m	Both ends visible

Dip (°)	Strike	Dip direction (°)	Scanline ID	Off Set Angle (clockwise) (°)	Structure	Spacing (m)	Infill Type	Infill Thickness	Separation	Surface shape	Surface roughness	Persistance	Ends
80	214	304	59	100	Joint	0.30	Serpentinite	<1mm	<1mm	Planar	Smooth	3-10m	Both ends visible
85	184	274	59	70	Joint	1.10	Serpentinite	<1mm	<1mm	Planar	Smooth	3-10m	Both ends visible
85	234	324	59	120	Joint	0.30	Serpentinite	<1mm	<1mm	Planar	Smooth	1-3m	Both ends visible
80	189	279	59	75	Joint	0.70	Serpentinite	<1mm	<1mm	Undulating	Smooth	3-10m	Both ends visible
90	224	314	59	110	Joint	0.20	Serpentinite	<1mm	<1mm	Planar	Smooth	3-10m	Both ends visible
80	194	284	59	80	Joint	0.35	Serpentinite	<1mm	<1mm	Planar	Smooth	1-3m	Both ends visible
75	204	294	59	90	Joint	0.95	Serpentinite	<1mm	<1mm	Planar	Smooth	>30m	No ends visible
80	204	294	59	90	Joint	0.45	Serpentinite	<1mm	<1mm	Planar	Smooth	3-10m	Both ends visible
75	114	204	60	90	Fault	2.45	Pegmatite	>30mm	1-3mm	Planar	Rough	>30m	No ends visible
55	114	204	60	90	Vein	2.70	Pegmatite	>30mm	<1mm	Planar	Rough	>30m	No ends visible
55	114	204	60	90	Vein	0.05	Pegmatite	>30mm	<1mm	Planar	Rough	>30m	No ends visible
80	209	299	61	95	Joint	0.30	Serpentinite	<1mm	<1mm	Planar	Smooth	1-3m	One end visible
65	174	264	61	60	Joint	1.60	No infill	None	Tight	Undulating	Rough	<1m	Both ends visible
75	184	274	61	70	Joint	3.20	No infill	None	Tight	Undulating	Rough	3-10m	One end visible
90	204	294	61	90	Joint	0.20	No infill	None	Tight	Undulating	Rough	3-10m	One end visible
90	94	184	62	70	Joint	0.40	No infill	None	Tight	Planar	Rough	>30m	No ends visible
90	114	204	62	90	Joint	0.60	No infill	None	Tight	Planar	Rough	>30m	No ends visible
75	109	199	62	85	Joint	0.20	No infill	None	Tight	Planar	Rough	>30m	No ends visible
90	114	204	62	90	Joint	0.30	No infill	None	Tight	Planar	Rough	>30m	No ends visible
80	114	204	62	90	Vein	0.25	Pegmatite	>30mm	<1mm	Planar	Rough	>30m	No ends visible
80	114	204	62	90	Vein	0.10	Pegmatite	>30mm	<1mm	Planar	Rough	>30m	No ends visible
80	114	204	62	90	Vein	3.75	Pegmatite	>30mm	<1mm	Planar	Rough	>30m	No ends visible
65	184	274	63	70	Joint	1.10	No infill	None	Tight	Planar	Rough	<1m	Both ends visible
60	189	279	63	75	Joint	2.92	Surface staining	<1mm	<1mm	Planar	Smooth	>30m	Both ends visible

D. Support product information

D.1 Laboratory Uniaxial Tensile Strength test certificate for 18mm rebar

VIDEX MINING PRODUCTS
A Division of videx wire products (pty)Ltd
(Registration Number: 1984/09466/07)

Certificate No :V1794289

REPORT No:V1794289
CUSTOMER:BATHOPELE
PRODUCT:1.6m Secura Resin Bolt Y18 Din 20 LH + DDE +
PRODUCT+:Ss + S/Pin Nut
CAST NUMBER:184202 (050219D1)
TORQUE TEST:Shearpin Breaks @90Nm
TESTED BY:DESMOND MDAKA
COMMENT:Nut Running Freely After Torque Test
Specification:Tension test
Test Date:2019/02/05
Test Time:08:09:20
Finish Date:2019/02/05
Finish Time:08:11:44

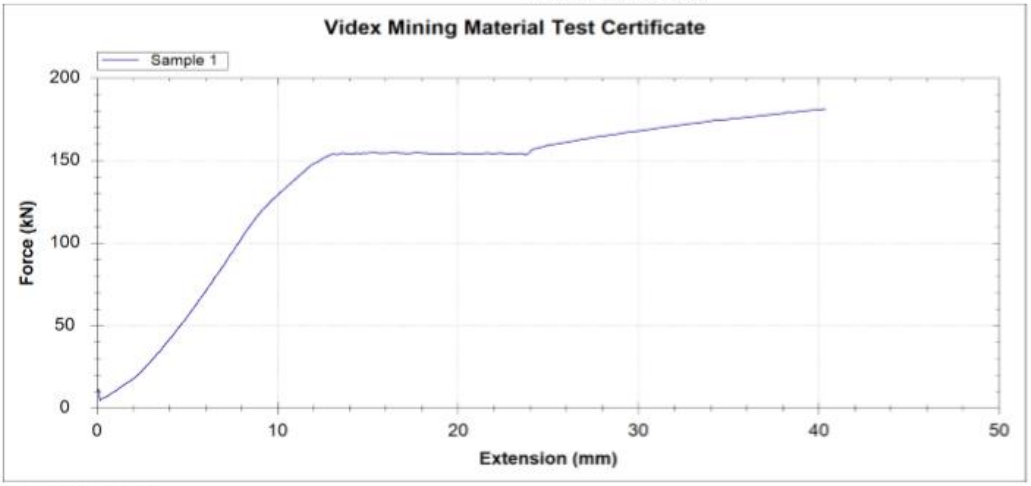

Test Results

Diameter	**18** mm
Peak Force	**181.30235** kN
MaxStress1	**712.473214732763** mpa
GaugeLength	**738** mm
Extension@140kN	**11.09** mm
Extension@150kN	**12.33** mm

D.2 Laboratory test certificate for 18mm rebar washer

VIDEX MINING PRODUCTS
A Division of videx wire products (pty)Ltd
(Registration Number: 1984/09466/07)

Certificate No :V1795719

REPORT No:V1795719
CUSTOMER:Inhouse
PRODUCT:DDE Washer C/Hole Dia 34mm
TESTED BY:Cliffort Mahoa
COMMENT:Pass
Specification:125mm DDE Washer 33.5mm x 4mm
Test Date:2019/03/08
Test Time:08:27:06
Finish Date:2019/03/08
Finish Time:08:28:06

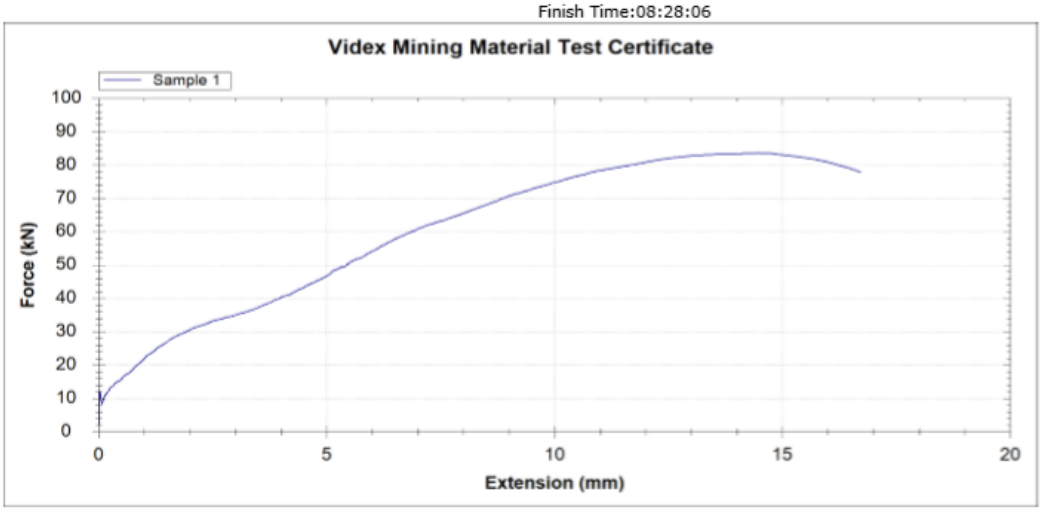

Test Results

Peak Force	**83.62027** kN
Diameter	**4** mm

D.3 Underground pull tests information on the 18mm bolts and results

Table D-1. Underground pull test information on encapsulated length and hole diameter (Gieling, 2018)

SEPT	Bolt length (18mm)	Drill Bid Size	Actual hole size (mm)	Hole lengths (mm)	Resin length (mm)
1	1600	28	30	1520	240
2	1600	28	30	1530	240
3	1600	28	30	1545	240
4	1600	28	30	1560	240
5	1600	28	30	1565	240

Table D-2. Underground pull test results on the 18mm bolts (Gieling, 2018)

Readings obtained underground.

Force	Displacement (mm)				
kN	SEPT 1	SEPT 2	SEPT 3	SEPT 4	SEPT 5
0	0.00	0.00	0.00	0.00	0.00
10	1.03	0.25	0.78	Could not Pull	Could not Pull
20	1.52	0.84	1.02		
30	1.89	1.25	1.48		
40	2.10	1.77	1.76		
50	2.54	2.34	2.28		
60	2.99	2.77	2.59		
70	3.46	3.16	3.10		
80	3.82	3.52	3.41		
90	4.11	3.72	3.69		
100	4.17	4.06	4.01		
110	4.42	4.25	4.51		
120	4.64	4.44	5.07		
130	4.85	4.51	5.52		
140	5.16	4.56	6.18		
150	5.55	4.68	6.94		
160	Stopped	Stopped	Stopped		

E. Q' system and N' tables (Barton, 2015)

E.1 Selection of joint roughness and joint alteration for calculation on N'

2	Joint set number	J_n
A	Massive, no or few joints	0.5-1.0
B	One joint set	2
C	One joint set plus random joints	3
D	Two joint sets	4
E	Two joint sets plus random joints	6
F	Three joint sets	9
G	Three joint sets plus random joints	12
H	Four or more joint sets, random heavily jointed "sugar cube", etc	15
J	Crushed rock, earth like	20

Note: i) For tunnel intersections, use 3 x J_n
ii) For portals, use 2 x J_n

3	Joint Roughness Number	J_r
a) Rock-wall contact, and b) Rock-wall contact before 10 cm of shear movement		
A	Discontinuous joints	4
B	Rough or irregular, undulating	3
C	Smooth, undulating	2
D	Slickensided, undulating	1.5
E	Rough, irregular, planar	1.5
F	Smooth, planar	1
G	Slickensided, planar	0.5
Note: i) Description refers to small scale features and intermediate scale features, in that order		
c) No rock-wall contact when sheared		
H	Zone containing clay minerals thick enough to prevent rock-wall contact when sheared	1
Note: ii) Add 1 if the mean spacing of the relevant joint set is greater than 3 m (dependent on the size of the underground opening)		
iii) J_r = 0.5 can be used for planar slickensided joints having lineations, provided the lineations are oriented in the estimated sliding direction		

4	Joint Alteration Number	Φ_r approx.	J_a
a) Rock-wall contact (no mineral fillings, only coatings)			
A	Tightly healed, hard, non-softening, impermeable filling, i.e., quartz or epidote.		0.75
B	Unaltered joint walls, surface staining only.	25-35°	1
C	Slightly altered joint walls. Non-softening mineral coatings; sandy particles, clay-free disintegrated rock, etc.	25-30°	2
D	Silty or sandy clay coatings, small clay fraction (non-softening).	20-25°	3
E	Softening or low friction clay mineral coatings, i.e., kaolinite or mica. Also chlorite, talc gypsum, graphite, etc., and small quantities of swelling clays.	8-16°	4
b) Rock-wall contact before 10 cm shear (thin mineral fillings)			
F	Sandy particles, clay-free disintegrated rock, etc.	25-30°	4
G	Strongly over-consolidated, non-softening, clay mineral fillings (continuous, but <5mm thickness).	16-24°	6
H	Medium or low over-consolidation, softening, clay mineral fillings (continuous, but <5mm thickness).	12-16°	8
J	Swelling-clay fillings, i.e., montmorillonite (continuous, but <5mm thickness). Value of J_a depends on percent of swelling clay-size particles.	6-12°	8-12
c) No rock-wall contact when sheared (thick mineral fillings)			
K	Zones or bands of disintegrated or crushed rock. Strongly over-consolidated.	16-24°	6
L	Zones or bands of clay, disintegrated or crushed rock. Medium or low over-consolidation or softening fillings.	12-16°	8
M	Zones or bands of clay, disintegrated or crushed rock. Swelling clay. J_a depends on percent of swelling clay-size particles.	6-12°	8-12
N	Thick continuous zones or bands of clay. Strongly over-consolidated.	12-16°	10
O	Thick, continuous zones or bands of clay. Medium to low over-consolidation.	12-16°	13
P	Thick, continuous zones or bands with clay. Swelling clay. J_a depends on percent of swelling clay-size particles.	6-12°	13-20

E.2 Graphs and equations used in calculating A and C factor and α, respectively (Hutchinson & Diederichs, 1996)

Determining A factor

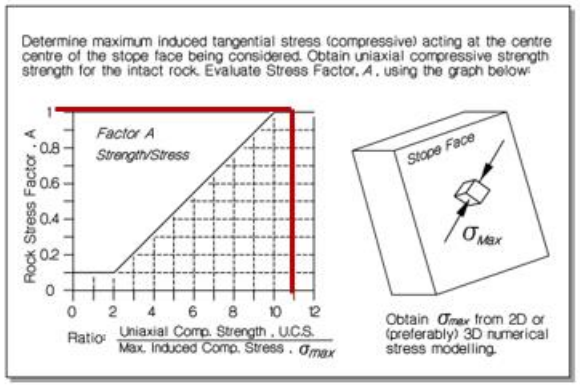

Determining C factor

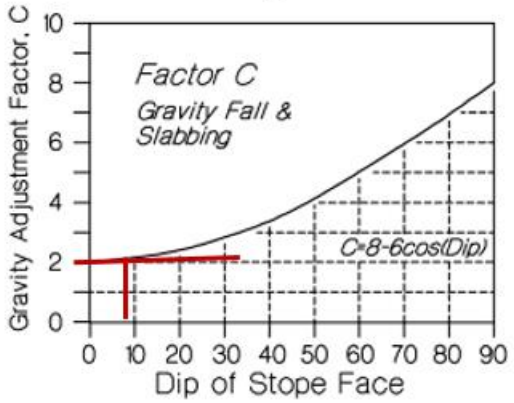

Equations for determining α

Given the *Dip* and the *Dip Direction* for a plane, the *Trend* and *Plunge* of the corresponding pole (normal vector) can be calculated:

$$T = Trend = Dip\ Direction + 180^\circ$$
$$P = Plunge = 90^\circ - Dip$$

For a stope wall plane, w, and a joint plane, j, the direction cosines with respect to the global coordinate grid (North, East, Down) are denoted by N, E and D respectively and are calculated as follows:

For the stope wall:

$$N_w = \cos(T_w) \cdot \cos(P_w)$$
$$E_w = \sin(T_w) \cdot \cos(P_w)$$
$$D_w = \sin(P_w)$$

For the joint plane:

$$N_j = \cos(T_j) \cdot \cos(P_j)$$
$$E_j = \sin(T_j) \cdot \cos(P_j)$$
$$D_j = \sin(P_j)$$

Next calculate the dot product, $\mathbf{w}\cdot\mathbf{j}$, between the wall face and the joint plane:

$$\mathbf{w}\cdot\mathbf{j} = N_w N_j + E_w E_j + D_w D_j$$

Finally, the true interplane angle, $\boldsymbol{\alpha}$, is given by:

$$\boldsymbol{\alpha} = \cos^{-1}(\mathbf{w}\cdot\mathbf{j}) = \text{acos}(\mathbf{w}\cdot\mathbf{j})$$

E.3 Graph used in establishing the B factor (Hutchinson & Diederichs, 1996)

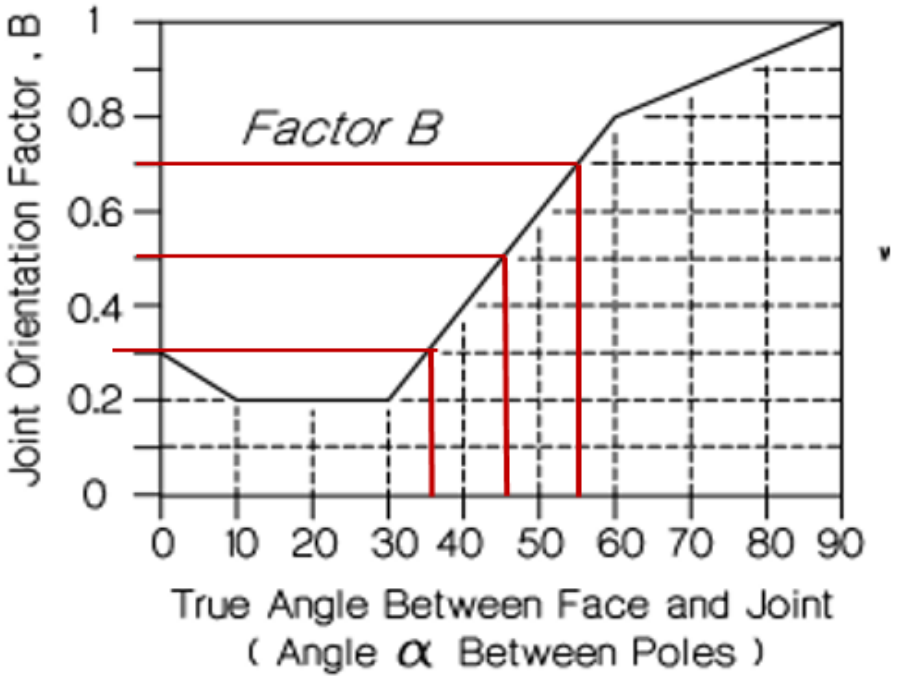

F. Frequency plots of dimensions of keyblocks for shallow dipping structures from JBlock models

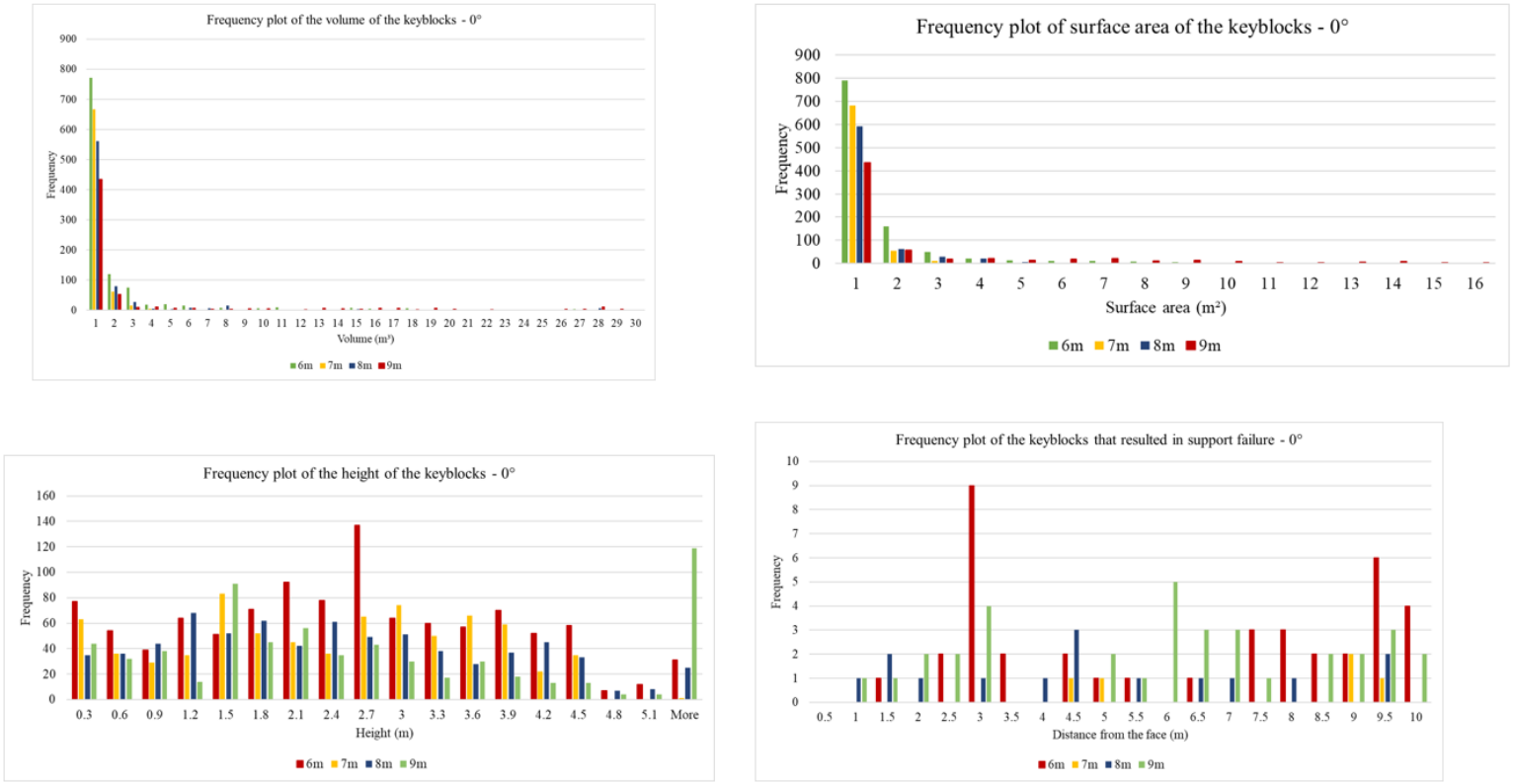

Figure F-1. Frequency plots of dimensions of keyblocks for shallow dipping structure with 0° dip direction at 6 m to 9 m span from JBlock models

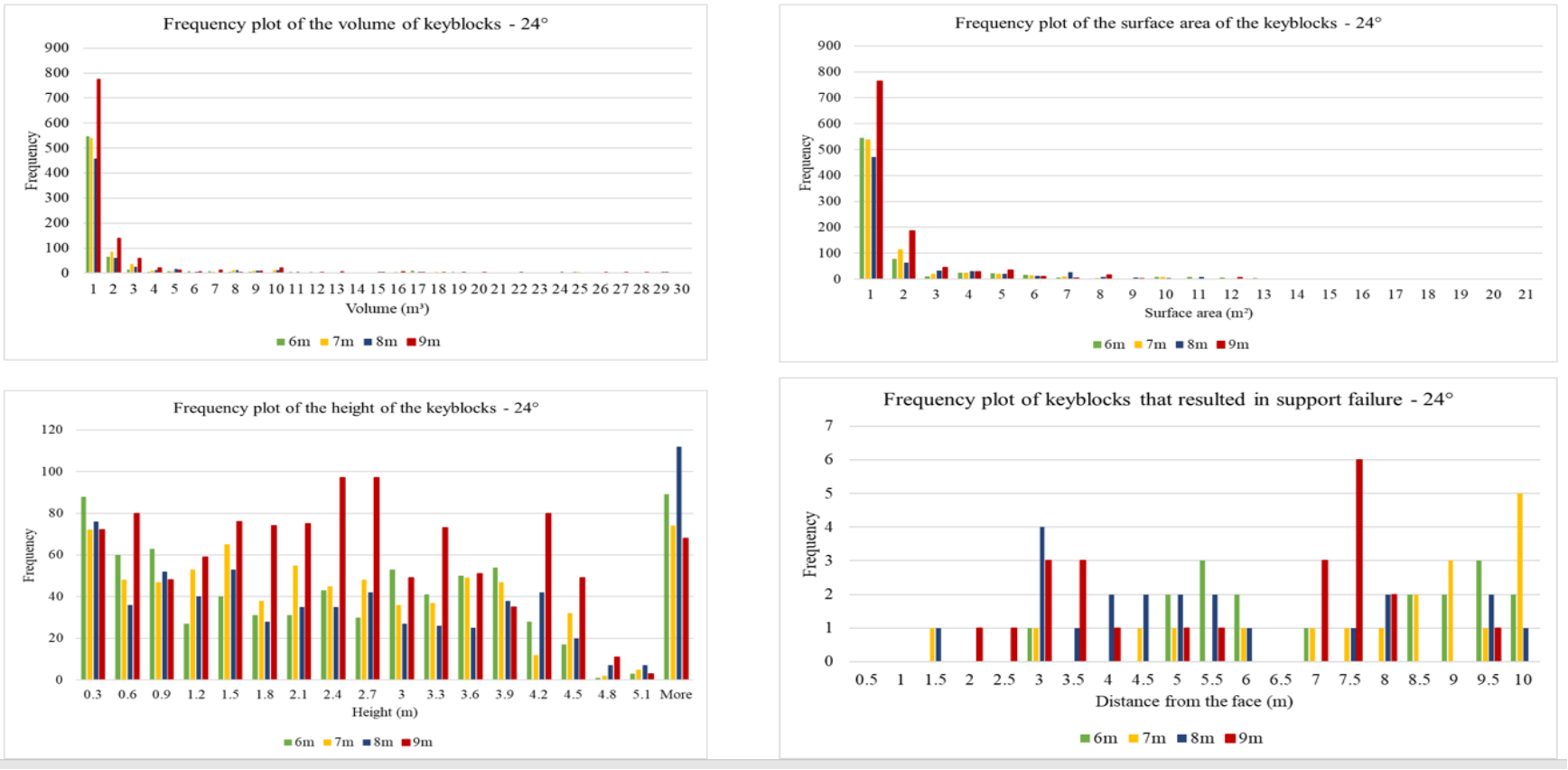

Figure F-2. Frequency plots of dimensions of keyblocks for shallow dipping structure with 24° dip direction at 6 m to 9 m span from JBlock models

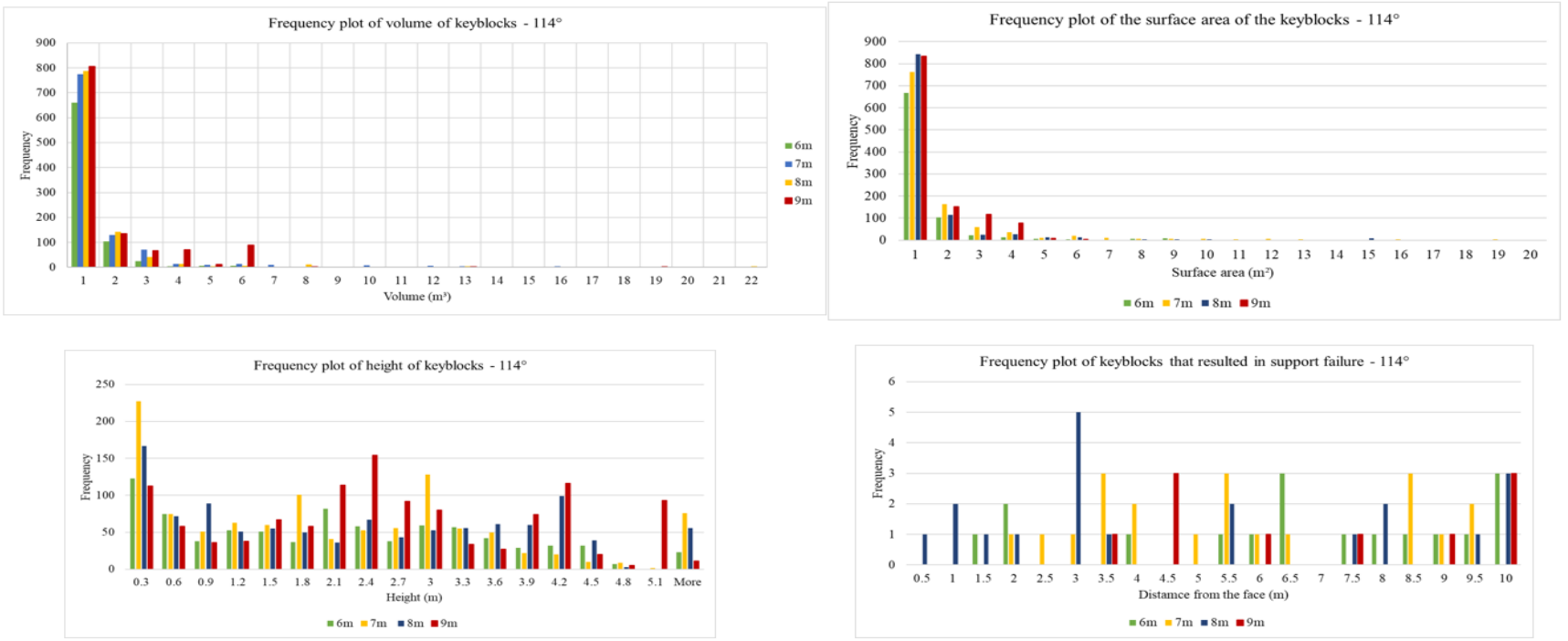

Figure F-3. Frequency plots of dimensions of keyblocks for shallow dipping structure with 114° dip direction at 6 m to 9 m span from JBlock models

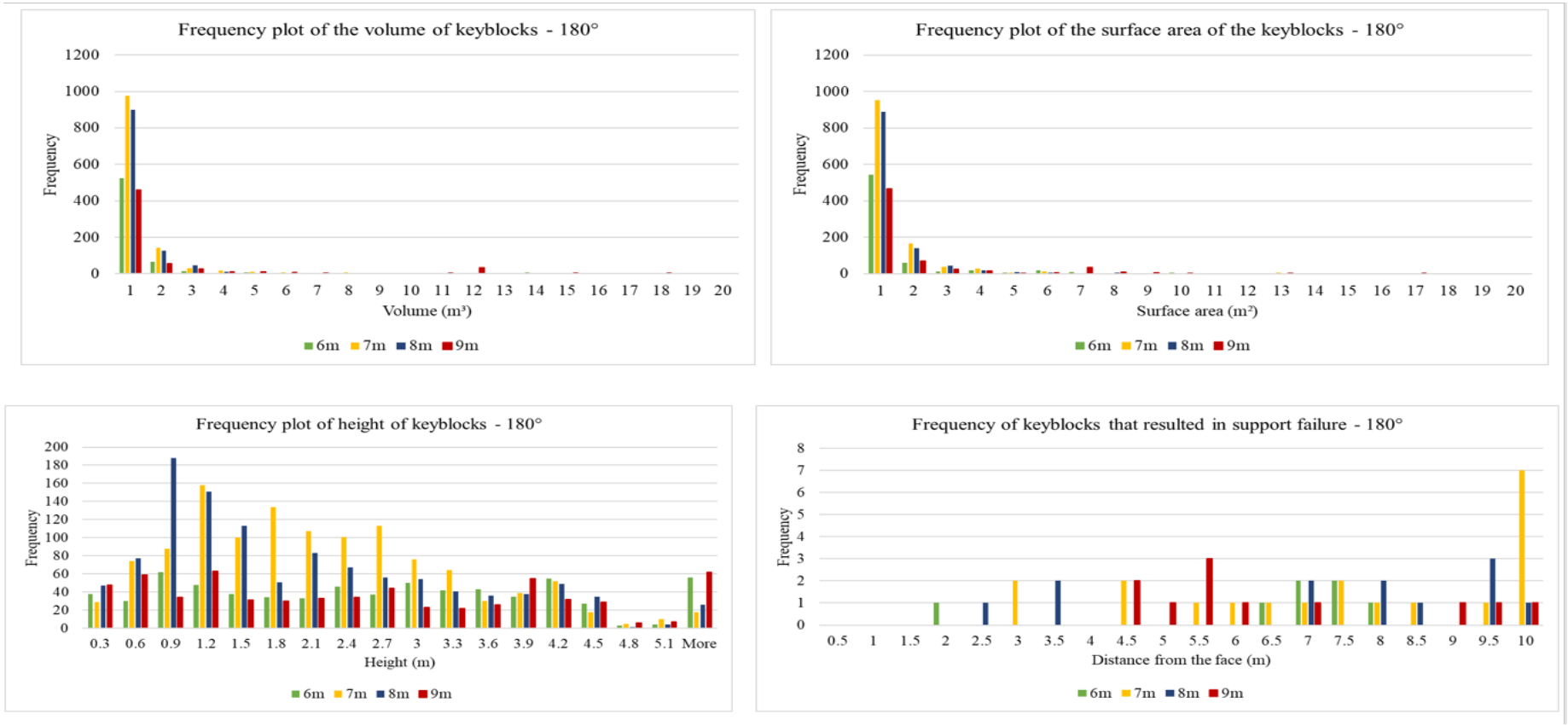

Figure F-4. Frequency plots of dimensions of keyblocks for shallow dipping structure with 180° dip direction at 6 m to 9 m span from JBlock models



Figure F-5. Frequency plots of dimensions of keyblocks for shallow dipping structure with 204° dip direction at 6 m to 9 m span from JBlock models

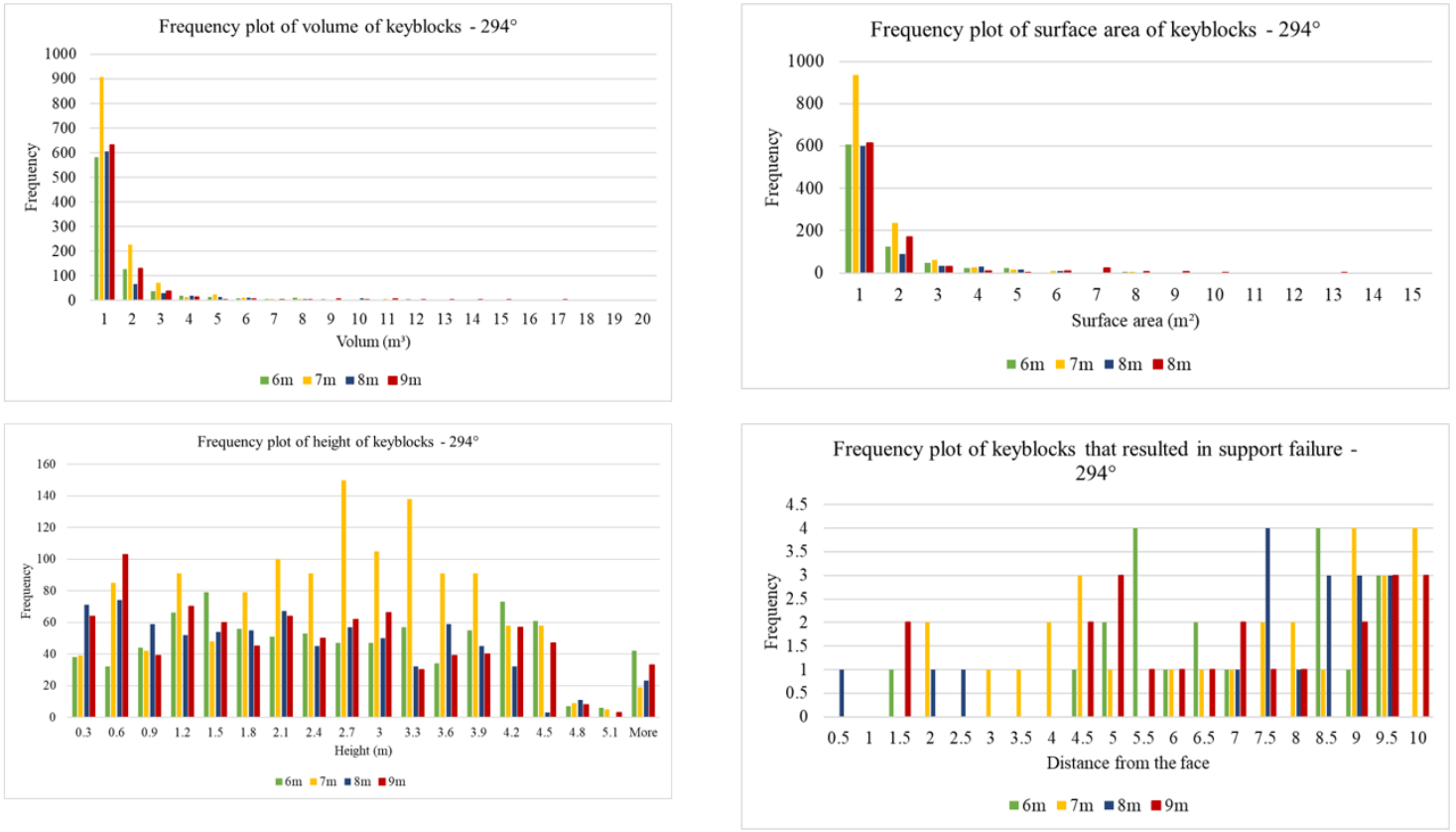

Figure F-6. Frequency plots of dimensions of keyblocks for shallow dipping structure with 294° dip direction at 6 m to 9 m span from JBlock models

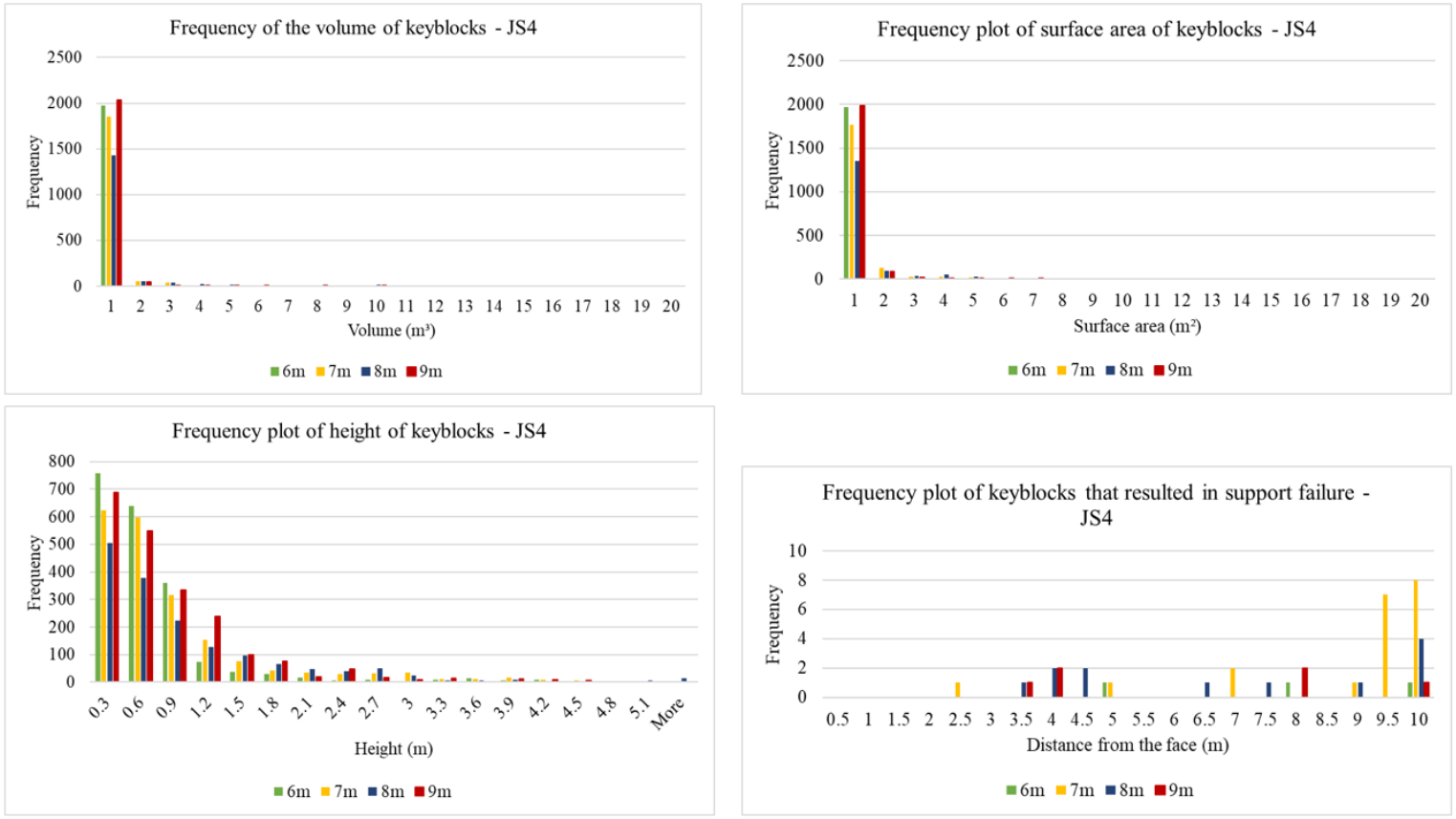

Figure F-7. Frequency plots of dimensions of keyblocks for shallow dipping structure with 199° (JS4/R1) dip direction at 6 m to 9 m span from JBlock models

G. Location of FOGs of plan view from FOG reports

G.1 FOGs that resulted from shallow dipping structures striking obliquely and near-parallel to mining direction

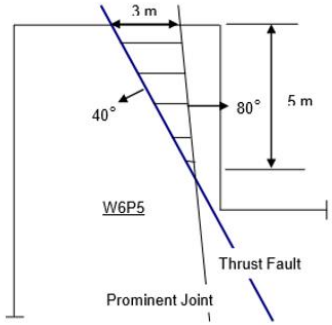

Central shaft 6W P5 FOG (Rademan, 2006)

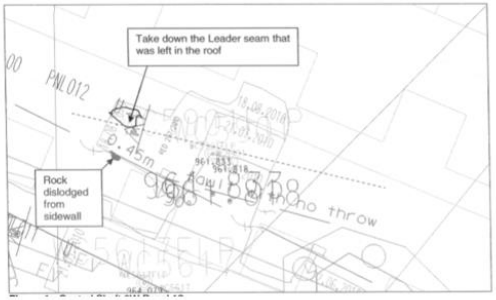

Central shaft 6W P12 FOG (Van Rooyen, 2010)

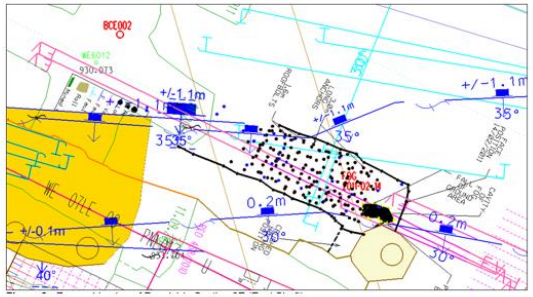

East shaft 8E P1 FOG (Van Rooyen, 2011)

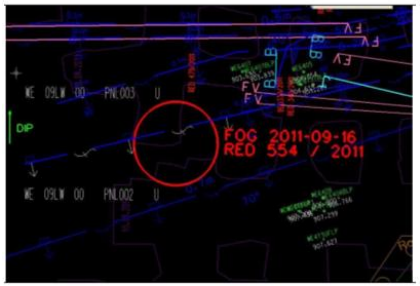

East shaft 10w P4 (Rajpal, 2011)

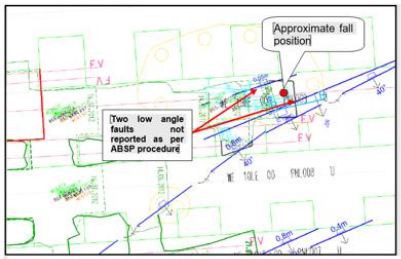

East shaft 10E P9, (Sibanda, 2013)

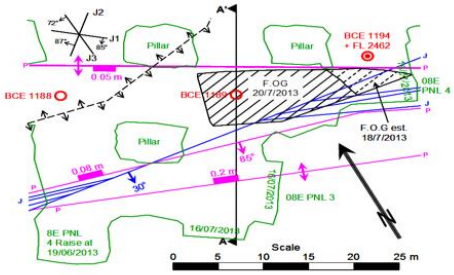

East shaft 8E P4 FOG (Handley, 2013)

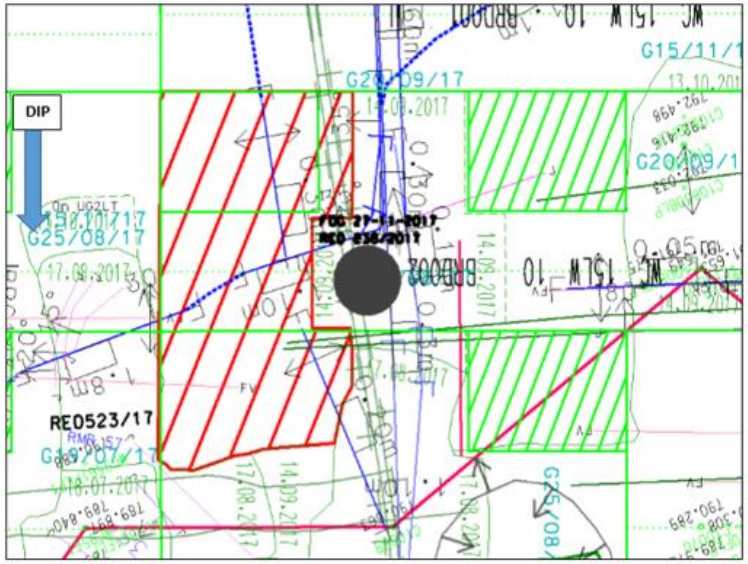

Central shaft 15W P2 & 6DS FOG (Sephaphathi 2017a)

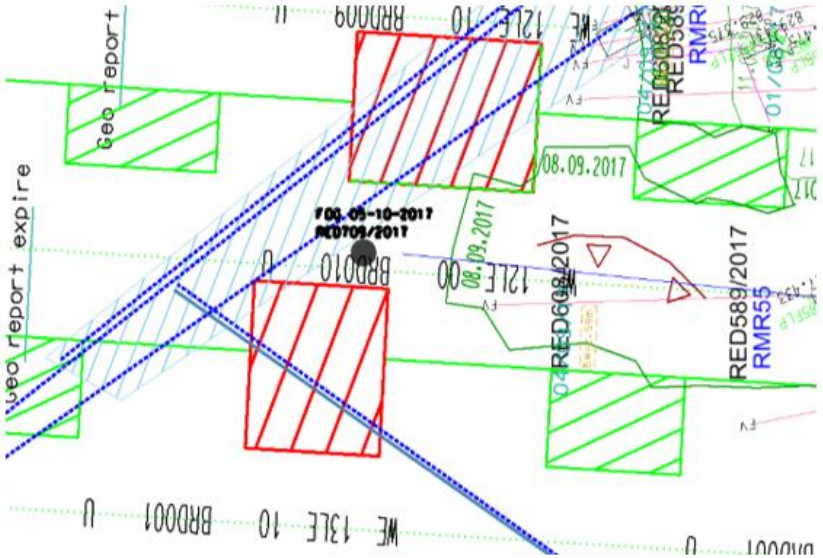

East shaft 12E P10 FOG (Sephaphathi 2017b)

G.2 FOGs that resulted from shallow dipping structures near-perpendicular to mining direction

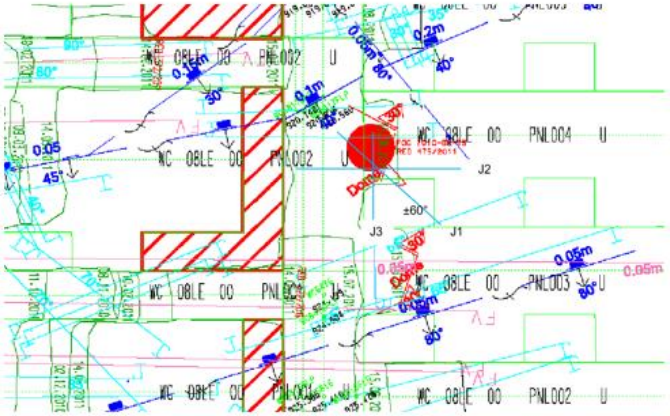

Central shaft, 8E P2 FOG, Matsobane, 2011

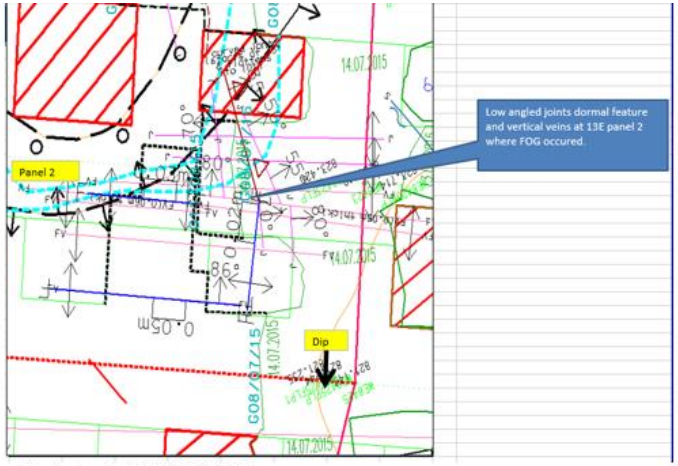

East shaft, 13E P2 FOG, Dube 2015

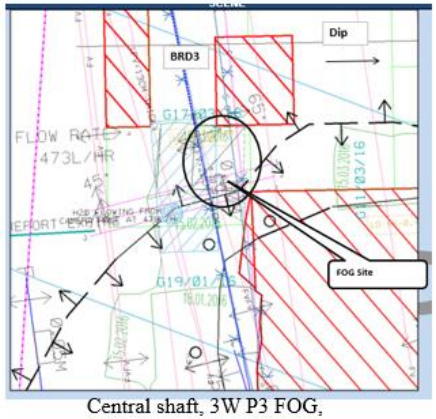

Central shaft, 3W P3 FOG, Matsobane, 2016a